USGS
science for a changing world

Prepared in cooperation with the California Geological Survey

The HayWired Earthquake Scenario—Earthquake Hazards

Scientific Investigations Report 2017–5013–A–H

U.S. Department of the Interior
U.S. Geological Survey

Cover. Oblique aerial image showing how the main active traces of the Hayward Fault (red lines) cut through the urban landscape of the east bay part of the San Francisco Bay area (north is to the upper right; fault is oriented northwest-southeast). The image is overlain on a "hillshade" (artificially illuminated from the northwest) to show fault-zone ground-surface features, such as a right-laterally offset stream channel in the foreground. The fault trace roughly bisects California Memorial Stadium at the University of California, Berkeley (O-shaped feature in the middle of the image). The stadium was renovated and seismically strengthened at an expense of $321 million (see http://news.berkeley.edu/2011/09/01/memorial-stadium-renovated-with-help-of-berkeleys-own/) as an engineered countermeasure against fault-rupture hazard from a future earthquake such as that modeled in the HayWired scenario. Similarly, beneath the viewpoint of this image, the East Bay Municipal Utility District (EBMUD) mitigated the Hayward Fault crossing of the Claremont water-transmission tunnel by constructing a bypass tunnel at an expense of $38 million (see http://www.geoprac.net/geonews-mainmenu-63/64-project-related/333-the-claremont-tunnel-designed-to-survive-fault-rupture-on-the-hayward-fault/). Although notable risk-reduction measures such as these have already been taken along the Hayward Fault, issues with more than 300 buildings (mostly homes) that are situated directly on the fault, and dozens of major lifelines that cross it, have not yet been addressed. (Fault mapping by J. Lienkaemper, U.S. Geological Survey, 2008, see https://pubs.usgs.gov/ds/2006/177/. Hillshade is based on EarthScope airborne light detection and ranging (lidar) data that covers the Hayward Fault and other important faults in northern California, http://opentopo.sdsc.edu/datasetMetadata?otCollectionID=OT.052008.32610.1.)

The HayWired Earthquake Scenario—Earthquake Hazards

Edited by Shane T. Detweiler and Anne M. Wein

Prepared in cooperation with the California Geological Survey

Scientific Investigations Report 2017–5013–A–H

U.S. Department of the Interior
U.S. Geological Survey

U.S. Department of the Interior
RYAN K. ZINKE, Secretary

U.S. Geological Survey
William H. Werkheiser, Acting Director

U.S. Geological Survey, Reston, Virginia: 2017

Suggested citation:
Detweiler, S.T., and Wein, A.M., eds., 2017, The HayWired earthquake scenario—Earthquake hazards: U.S. Geological Survey Scientific Investigations Report 2017–5013–A–H, 126 p., https://doi.org/10.3133/sir20175013v1.

ISSN 2328-0328 (online)

Foreword

The 1906 Great San Francisco earthquake (magnitude 7.8) and the 1989 Loma Prieta earthquake (magnitude 6.9) each motivated residents of the San Francisco Bay region to build countermeasures to earthquakes into the fabric of the region. Since Loma Prieta, bay-region communities, governments, and utilities have invested tens of billions of dollars in seismic upgrades and retrofits and replacements of older buildings and infrastructure. Innovation and state-of-the-art engineering, informed by science, including novel seismic-hazard assessments, have been applied to the challenge of increasing seismic resilience throughout the bay region. However, as long as people live and work in seismically vulnerable buildings or rely on seismically vulnerable transportation and utilities, more work remains to be done.

With that in mind, the U.S. Geological Survey (USGS) and its partners developed the HayWired scenario as a tool to enable further actions that can change the outcome when the next major earthquake strikes. By illuminating the likely impacts to the present-day built environment, well-constructed scenarios can and have spurred officials and citizens to take steps that change the outcomes the scenario describes, whether used to guide more realistic response and recovery exercises or to launch mitigation measures that will reduce future risk.

The HayWired scenario is the latest in a series of like-minded efforts to bring a special focus onto potential impacts when the Hayward Fault again ruptures through the east side of the San Francisco Bay region as it last did in 1868. Cities in the east bay along the Richmond, Oakland, and Fremont corridor would be hit hardest by earthquake ground shaking, surface fault rupture, aftershocks, and fault afterslip, but the impacts would reach throughout the bay region and far beyond. The HayWired scenario name reflects our increased reliance on the Internet and telecommunications and also alludes to the interconnectedness of infrastructure, society, and our economy. How would this earthquake scenario, striking close to Silicon Valley, impact our interconnected world in ways and at a scale we have not experienced in any previous domestic earthquake?

The area of present-day Contra Costa, Alameda, and Santa Clara Counties contended with a magnitude-6.8 earthquake in 1868 on the Hayward Fault. Although sparsely populated then, about 30 people were killed and extensive property damage resulted. The question of what an earthquake like that would do today has been examined before and is now revisited in the HayWired scenario. Scientists have documented a series of prehistoric earthquakes on the Hayward Fault and are confident that the threat of a future earthquake, like that modeled in the HayWired scenario, is real and could happen at any time. The team assembled to build this scenario has brought innovative new approaches to examining the natural hazards, impacts, and consequences of such an event. Such an earthquake would also be accompanied by widespread liquefaction and landslides, which are treated in greater detail than ever before. The team also considers how the now-prototype ShakeAlert earthquake early warning system could provide useful public alerts and automatic actions.

Scientific Investigations Report 2017–5013 and accompanying data releases are the products of an effort led by the USGS, but this body of work was created through the combined efforts of a large team including partners who have come together to form the HayWired Coalition (see chapter A). Use of the HayWired scenario has already begun. More than a full year of intensive partner engagement, beginning in April 2017, is being directed toward producing the most in-depth look ever at the impacts and consequences of a large earthquake on the Hayward Fault. With the HayWired scenario, our hope is to encourage and support the active ongoing engagement of the entire community of the San Francisco Bay region by providing the scientific, engineering, and economic and social science inputs for use in exercises and planning well into the future.

David Applegate

Acting Deputy Director
U.S. Geological Survey

Contents

Chapters

Conversion Factors

U.S. customary units to International System of Units

Multiply	By	To obtain
Length		
inch (in.)	2.54	centimeter (cm)
inch (in.)	25.4	millimeter (mm)
foot (ft)	0.3048	meter (m)
mile (mi)	1.609	kilometer (km)
Area		
square foot (ft^2)	0.09290	square meter (m^2)
square mile (mi^2)	2.590	square kilometer (km^2)
Cohesion		
pound per square foot (lb/ft^2)	0.04788	kilopascal (kPa)

International System of Units to U.S. customary units

Multiply	By	To obtain
Length		
centimeter (cm)	0.3937	inch (in.)
millimeter (mm)	0.03937	inch (in.)
meter (m)	3.281	foot (ft)
kilometer (km)	0.6214	mile (mi)
Area		
square meter (m^2)	10.76	square foot (ft^2)
square kilometer (km^2)	0.3861	square mile (mi^2)
Velocity		
centimeter per second (cm/s)	0.3937	inch per second (in./s)
centimeter per second (cm/s)	0.0223694	mile per hour (mi/hr)
meter per second (cm/s)	3.281	foot per second (ft/s)
meter per second (cm/s)	2.23694	mile per hour (mi/hr)

Datum

Vertical coordinate information is referenced to the North American Vertical Datum of 1988 (NAVD 88).

Horizontal coordinate information is referenced to the North American Datum of 1983 (NAD 83).

Abbreviations and Acronyms

3D	three dimensional
ABAG	Association of Bay Area Governments
BAREPP	Bay Area Regional Earthquake Preparedness Project
BART	Bay Area Rapid Transit
Cal OES	California Governor's Office of Emergency Services
Caltrans	California Department of Transportation
CAPSS	Citizens Advisory Panel on Seismic Safety
CDC	Centers for Disease Control and Prevention
CGS	California Geological Survey
CPT	cone penetration test
CSSC	California Seismic Safety Commission
DEM	digital elevation model
EBMUD	East Bay Municipal Utility District
EERI	Earthquake Engineering Research Institute
ESIP	Earthquake Safety Improvements Program
ETAS	epidemic-type aftershock sequence
FEMA	Federal Emergency Management Agency
F_v	site coefficient
g	acceleration due to gravity
GMPE	ground-motion prediction equation
LPI	liquefaction potential index
M	magnitude
Ma	mega-annum or millions of years ago
MMI	Modified Mercalli Intensity
M_W	moment magnitude
NAD83	North American Datum of 1983
NED	National Elevation Dataset
NGA-West2	Next Generation Attenuation Relationships for Western United States
NISEE	National Information Service for Earthquake Engineering
NRC	National Research Council
PEER	Pacific Earthquake Engineering Research Center
PDT	Pacific Daylight Time
PGA	peak ground acceleration

PGV	peak ground velocity
PSA or pSa	pseudo-spectral acceleration
PSA03	short-period (0.3-second) pseudo-spectral-acceleration response
PSA10	long-period (1-second) pseudo-spectral-acceleration response
PST	Pacific Standard Time
RMS	Risk Management Solutions
SA	spectral acceleration
SAFRR	U.S. Geological Survey Science Application for Risk Reduction project
SCEC	Southern California Earthquake Center
SHZ	seismic hazard zone
SPUR	San Francisco Bay Area Planning and Urban Research Institute
UCERF3	Uniform California Earthquake Rupture Forecast, version 3
USGS	U.S. Geological Survey
V_{S30}	time-averaged shear-wave velocity to a depth of 30 meters
WGS84	World Geodetic Survey 1984

The HayWired Earthquake Scenario—Earthquake Hazards
Edited by Shane T. Detweiler and Anne M. Wein
Scientific Investigations Report 2017–5013–A–H
[Also see https://doi.org/10.3133/sir20175013]

Chapter A

The HayWired Scenario—How Can the San Francisco Bay Region Bounce Back from or Avert an Earthquake Disaster in an Interconnected World?

By Kenneth W. Hudnut,[1] Anne M. Wein,[1] Dale A. Cox,[1] Suzanne C. Perry,[1] Keith A. Porter,[2] Laurie A. Johnson,[3] and Jennifer A. Strauss[4]

Introduction

The HayWired scenario is a hypothetical yet scientifically realistic and quantitative depiction of a moment magnitude (M_w) 7.0 earthquake (mainshock) occurring on April 18, 2018, at 4:18 p.m. on the Hayward Fault in the east bay part of the San Francisco Bay area, California. The hypothetical earthquake has its epicenter in Oakland, and strong ground shaking from the scenario causes a wide range of severe impacts throughout the greater bay region. In the scenario, the Hayward Fault is ruptured along its length for 83 kilometers (about 52 miles).

Building on a decades-long series of efforts to reduce earthquake risk in the San Francisco Bay region, the hypothetical HayWired earthquake is used to examine the well-known earthquake hazard of the Hayward Fault, with a focus on newly emerging vulnerabilities. After a major earthquake disaster, reestablishing water services and food-supply chains are, of course, top priorities. However, problems associated with telecommunication outages or "network congestion" will increase and become more urgent as the bay region deepens its reliance on the "Internet of Things."

Communications at all levels are crucial during incident response following an earthquake. Damage to critical facilities (such as power plants) from earthquake shaking and to electrical and telecommunications wires and fiber-optic cables that are severed where they cross a fault rupture can trigger cascading Internet and telecommunications outages, and restoring these services is crucially important for emergency-response coordination. Without good communications, emergency-response efficiency is reduced, and as a result, life-saving response functions can be compromised. For these reasons, the name Hay**Wired** was chosen for this scenario to emphasize the need to examine our interconnectedness and reliance on telecommunications and other lifelines (such as water and electricity) toward the goal of making the San Francisco Bay region more resilient in future earthquakes.

Earthquake risk in the San Francisco Bay region has been greatly reduced as a result of previous concerted efforts; for example, an as much as $50 billion investment in strengthening infrastructure was motivated in large part by the 1989 magnitude (M) 6.9 Loma Prieta earthquake (KQED, 2014). The earthquake hazard from the Hayward Fault remains high, however, and much work still needs to be done to ensure that the region is ready for a major earthquake like that modeled in the HayWired scenario. Already, there is a renewed commitment from the newly formed HayWired Coalition—consisting of numerous government, academic, utility-provider, and community stakeholders—to bring new and varied perspectives to bear on the problems that remain.

Similar to previous U.S. Geological Survey (USGS) Science Application for Risk Reduction project (SAFRR) led scenarios, the HayWired scenario earthquake is a natural-hazards incident, with additional cascading hazards of fault rupture, aftershocks (subsequent earthquakes), afterslip (subsequent movement on a fault), landslides, liquefaction (soils becoming liquid-like during shaking), and fire following earthquake (potentially widespread fires triggered by an earthquake) that can be as destructive and disruptive as powerful ground shaking in the mainshock. For the earthquake scenario, damages are calculated using engineering best practices combined with new basic research into building-code performance objectives, urban search and rescue, interactions between lifelines, self-protective actions, and other topics. This research provides new insight into expected physical and environmental damages from an event such as the earthquake modeled in the HayWired scenario, as well as into the restoration of structures, infrastructure, and lifelines and the addressing of environmental effects. Social and economic consequences, as well as topics for discussion of policy considerations, are also addressed in the scenario.

[1]U.S. Geological Survey.

[2]University of Colorado Boulder.

[3]Laurie Johnson Consulting.

[4]University of California Berkeley Seismological Laboratory.

Why the Name HayWired?—Internet and Interconnectedness

The scenario's name, Hay**Wired**, refers to the rupture of the Hayward Fault and speaks to the potential disruption to our wired and wireless world. California has not experienced a large earthquake in an urban environment since our society, culture, and economy have become intertwined with the Internet. Experience in recent Japan (2011 magnitude-9.1 Tohoku) and New Zealand (2011 magnitude-6.2 Christchurch) earthquakes suggest that Internet service outages tend to be localized and coinciding in duration with the loss of power service. Although designed to be robust because of its redundancy, the Internet is not immune to performance problems. More generally, "wired" represents interconnectedness at many levels—the interconnectedness of seismicity evidenced by afterslip and aftershocks, interdependencies of lifelines, social connectivity through technology (including earthquake early warning), and ripple effects of damages and disruption throughout an economy, encompassing especially the modern digital economy. The HayWired theme is particularly appropriate for the San Francisco Bay region, which is home to Silicon Valley and to world leaders in technology and digital communications.

The HayWired Coalition stakeholders are addressing implications of the scenario during the year from April 2017 through April 2018. The idea is that solutions will be devised and initial actions taken during this year to reduce the impacts of future damaging earthquakes in the San Francisco Bay region and elsewhere. Longer-term actions and outcomes also are hoped for and expected. Discussions, workshops, and exercises will focus on key themes not addressed as fully (or at all) in previous SAFRR earthquake scenarios—(1) the effects of aftershocks and afterslip, (2) performance objectives embedded in building codes, (3) complications of fire following earthquake, (4) anticipating environmental health issues, (5) urban search and rescue implications, (6) effects of lifeline interdependencies (including the Internet and digital economy), and (7) communities at risk for long-term recovery and rebuilding challenges. The scenario is intended to help communities improve their knowledge and use of earthquake-hazard, early warning, and aftershock and afterslip forecast information. Through community engagement, the HayWired scenario will help inform decisions about building-code-performance objectives, business-continuity planning, and empowering communities through capacity building.

USGS Scientific Investigations Report (SIR) 2017–5013, describing the HayWired scenario, is planned to be published as three volumes. As HayWired volumes are published, they will be made available at https://doi.org/10.3133/sir20175013. Ideally, the HayWired scenario volumes will help readers collectively improve their own and their community's resilience in future disasters.

The Hayward Fault

Most people living in the San Francisco Bay region understand that the threat of earthquakes is real and inescapable. Few other regions on Earth are as strongly associated with earthquakes. Photographers vividly depicted the aftermath of the 1906 *M*7.8 Great San Francisco earthquake and the fire that followed (fig. 1). The San Andreas Fault, the source of this earthquake (Lawson, 1908), runs along the Pacific Ocean side of the San Francisco Peninsula and then continues offshore of the City of San Francisco and the Golden Gate Bridge.

Scientists recognize another earthquake threat in the bay region, rivaling that of the San Andreas Fault, that is posed by the Hayward Fault along the east side of San Francisco Bay (fig. 2). The most recent large earthquake on the Hayward Fault was

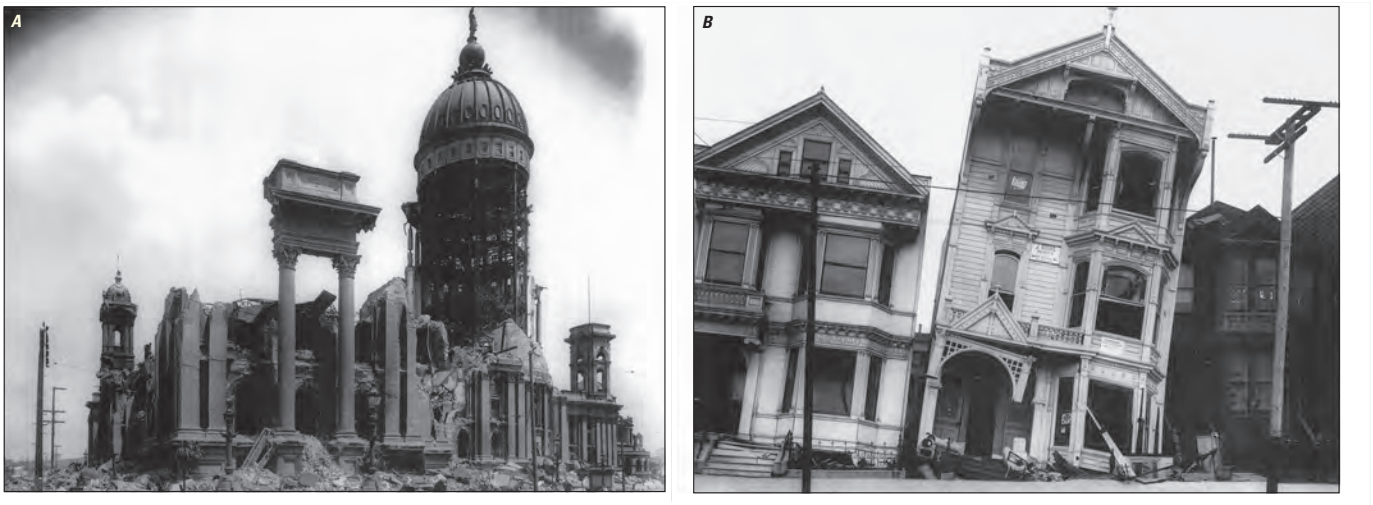

Figure 1. Photographs of damage in San Francisco, California, after the 1906 Great San Francisco earthquake and subsequent fire. The ground shaking from this magnitude-7.8 earthquake caused destruction throughout the San Francisco Bay region. *A*, The remains of San Francisco City Hall following the earthquake; *B*, houses in San Francisco damaged by the earthquake. (Images from National Information Service for Earthquake Engineering-Pacific Earthquake Engineering Research Center (NISEE-PEER), University of California, Berkeley, used with permission.)

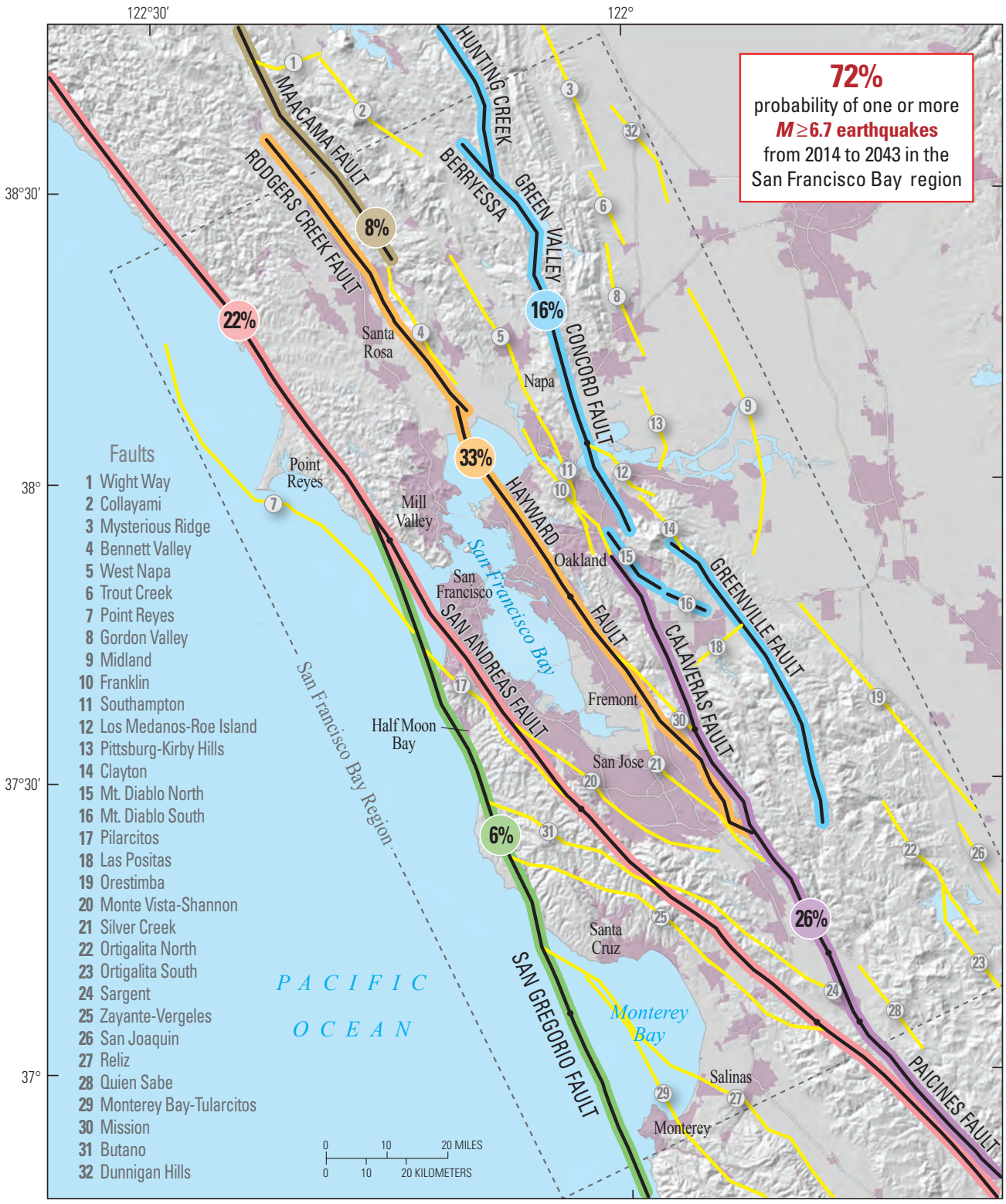

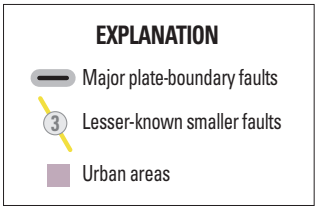

Figure 2. Map of known active geologic faults in the San Francisco Bay region, California, including the Hayward Fault. The 72 percent (%) probability of a magnitude (*M*) 6.7 or greater earthquake in the region includes well-known major plate-boundary faults, lesser-known faults, and unknown faults. The percentage shown within each colored circle is the probability that a *M*6.7 or greater earthquake will occur somewhere on that fault system by the year 2043. The probability that a *M*6.7 or greater earthquake will involve one of the lesser known faults is 13 percent. ≥, greater than or equal. (From Aagaard and others, 2016.)

a *M*6.8 earthquake in 1868 (fig. 3). Damage was limited in 1868 because the region was sparsely populated and barely developed.

The Hayward Fault now threatens more than 7 million people, approximately 2 million buildings, the San Francisco Bay region's and the Nation's economies, and dozens of major infrastructure lifelines including freeways and tunnels, pipelines, aqueducts, electric substations, electric-transmission and distribution lines, phone lines and fiber-optic routes, and rail lines. The surface trace of the Hayward Fault runs beneath the foundations of more than 300 homes, as well as under other structures, including the football stadium at the University of California, Berkeley, which has been extensively seismically retrofitted.

Although the Hayward Fault regularly produces smaller earthquakes, such as a *M*4.0 event on August 17, 2015, recent scientific investigations show that large earthquakes on the fault occur about once every 100 to 220 years (Lienkaemper and others, 2002, 2010). Therefore, it is of concern that the 1868 earthquake was 149 years ago because about one average "recurrence interval" has elapsed since the last large earthquake on the fault. The next large Hayward Fault earthquake could happen at any time, and such an earthquake is certain to occur in the future.

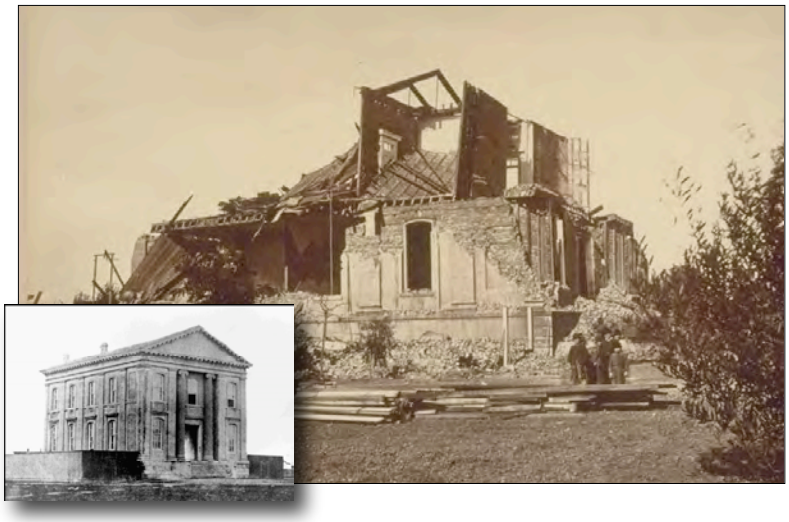

Figure 3. Photograph showing shaking damage from the 1868 magnitude-6.8 Hayward Fault earthquake, which caused collapse of the Alameda County Courthouse in San Leandro, California (photograph courtesy of the Bancroft Library, University of California, Berkeley). Inset shows the same building before the earthquake (photograph courtesy of courtesy of San Leandro Public Library).

The HayWired Scenario

What might the impacts and consequences be if another earthquake like the 1868 event were to happen today on the Hayward Fault? The HayWired scenario examines one such hypothetical earthquake—a *M*7.0 earthquake on April 18, 2018, at 4:18 p.m.[5] The HayWired scenario asks the following questions:

- What is a scientifically reasonable size earthquake that people can expect and prepare for along the Hayward Fault?
- What could happen as a result of the HayWired scenario earthquake and its cascading effects (or in other future damaging events in the San Francisco Bay region), and what can we do about it?
- What can San Francisco Bay region residents, communities, and businesses do to prepare for an event like that in the HayWired scenario?
- How can we learn more about the effects of a disaster like that modeled in the HayWired scenario and take action and support actions by others to prepare for such an event?

The HayWired Scenario is Not an Earthquake Prediction

The HayWired scenario is not an earthquake prediction. Scientists cannot predict the particular date and time of an earthquake. However, when (not if) the Hayward Fault next produces a large earthquake, it could happen in many different ways. The HayWired scenario is one of 39 scenario earthquakes with magnitudes ranging between magnitude (*M*) 6.6 and 7.2 that have been simulated on various segments of the Hayward Fault. An effectively infinite variety of earthquake magnitudes, locations, and other fault-rupture details are possible. Real outcomes of the next earthquake someday in the future will differ from what is presented here, but visualizing, analyzing, and planning for this particular scenario earthquake can help reduce damage and enable communities to more quickly recover when an actual earthquake occurs. The *M*7.0 scenario earthquake described here is not a worst case. Larger earthquakes could occur on the Hayward Fault and elsewhere in the San Francisco Bay region. For example, the northern part of the Hayward Fault last experienced a large rupture about 300 years ago, so an earthquake of even larger magnitude than the 1868 *M*6.8 Hayward earthquake is a distinct possibility. Recent studies have suggested that a future rupture of the Hayward Fault could generate an earthquake as large as *M*7.4, if the rupture were to link up with the Rodgers Creek Fault to the north. However, a *M*7.0 earthquake like the HayWired scenario mainshock occurs frequently enough, and its consequences are serious enough, to make it an earthquake worth planning for.

[5]The year 2018 corresponds with the sesquicentennial (150th anniversary) of the last large earthquake on the Hayward Fault. The date corresponds with the annual observation and activities surrounding the April 18 anniversary of the 1906 San Francisco earthquake on the nearby San Andreas Fault. The time of day is selected for easy recollection, because the time "4:18" resembles the date "4/18/2018."

In the HayWired scenario earthquake, the rupture of the Hayward Fault starts beneath southeast Oakland and, in less than a minute, travels along more than 83 kilometers (about 52 miles) of its length, both northward toward Richmond and San Pablo Bay and southward toward Fremont, at speeds as great as 11,000 kilometers per hour (about 7,000 miles per hour). As the fault break reaches the Earth's surface, it damages roads and buried pipelines and electrical conduits that cross the fault north of Hayward. In Berkeley, for example, the ground shifts by as much as 1 to 1.5 meters (about 3 to 5 feet) in a matter of seconds. As the USGS map of expected ground shaking (called a scenario ShakeMap) for the HayWired mainshock shows (fig. 4), the earthquake produces severe shaking and moderate to heavy damage

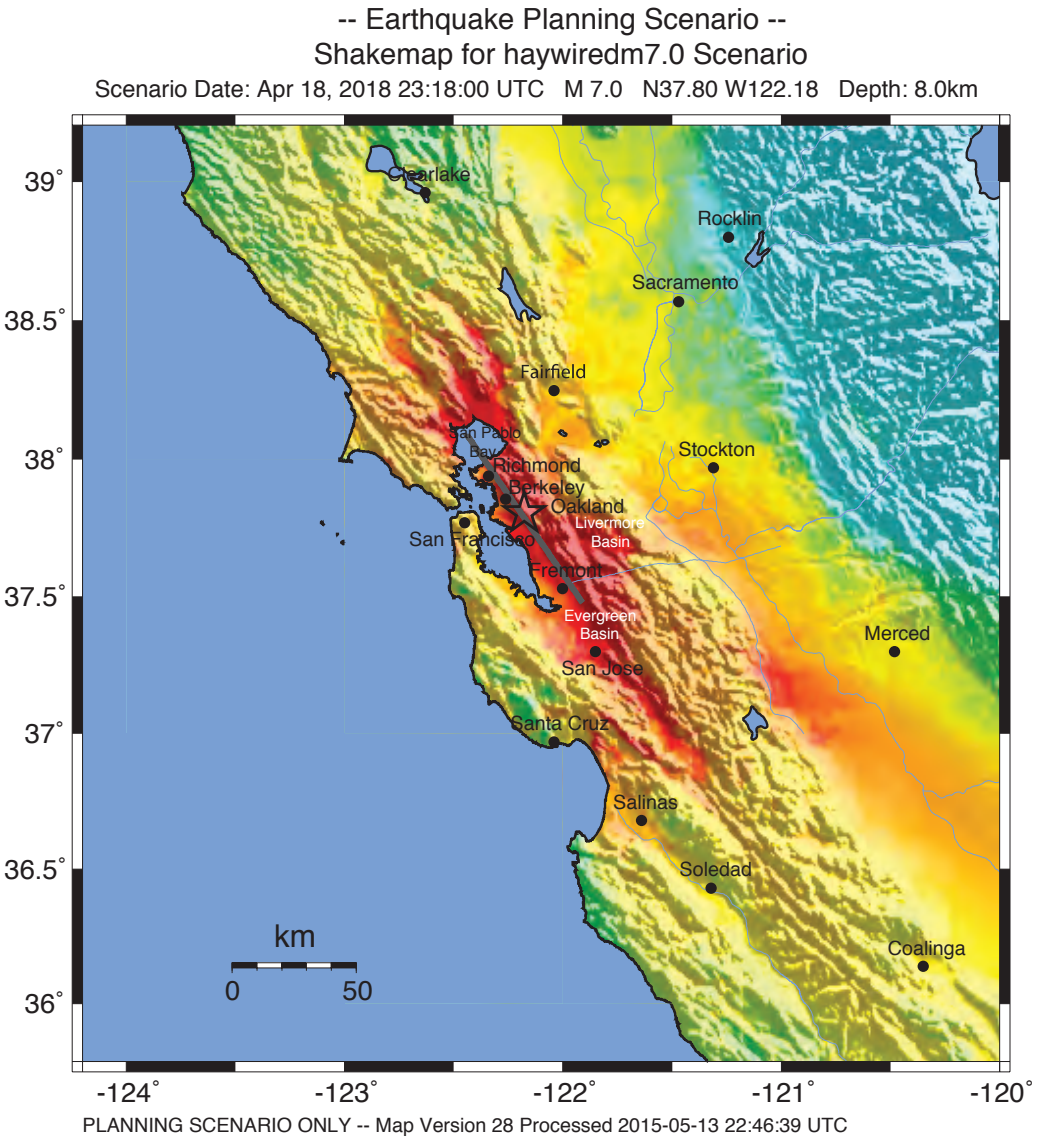

PERCEIVED SHAKING	Not felt	Weak	Light	Moderate	Strong	Very Strong	Severe	Violent	Extreme
POTENTIAL DAMAGE	none	none	none	Very light	Light	Moderate	Mod./Heavy	Heavy	Very Heavy
PEAK ACC.(%g)	<0.05	0.3	2.8	6.2	12	22	40	75	>139
PEAK VEL.(cm/s)	<0.02	0.1	1.4	4.7	9.6	20	41	86	>178
INSTRUMENTAL INTENSITY	I	II-III	IV	V	VI	VII	VIII	IX	X+

Figure 4. U.S. Geological Survey ShakeMap of the San Francisco Bay region, California, showing instrumental intensity (estimated Modified Mercalli Intensity) for the hypothetical magnitude-7.0 mainshock of the HayWired earthquake scenario on the Hayward Fault. The earthquake begins under the City of Oakland (star) and ruptures the Hayward Fault along more than 83 kilometers (about 52 miles) of its length in both directions. km, kilometer; peak acc., peak acceleration; peak vel., peak velocity; %g, amount of ground acceleration caused by the scenario mainshock, expressed in terms of the percentage of gravity's acceleration at the Earth's surface; cm/s, centimeter per second. (Modified from Aagaard, Boatwright, and others, this volume; modified from U.S. Geological Survey, 2014.)

in the east bay and Silicon Valley (roughly the part of the bay area at the southern end of San Francisco Bay) and widespread strong shaking throughout the region. San Francisco Bay region residents feel ground shaking that lasts 30 seconds or longer, and many people have difficulty walking and standing. Effects and destruction from the fault rupture and ground shaking are severe (fig. 5), but adding to this are a cascade of other hazards, including liquefaction, landslides, and fire following earthquake.

The hypothetical HayWired mainshock disrupts lifelines, supply chains, and the economy not only in the San Francisco Bay region but also disrupts the U.S. economy because of the economic importance of the region, particularly Silicon Valley (see Joint Ventures Silicon Valley, 2017). Dozens of significant aftershocks and fault afterslip (the Hayward Fault continues to creep in the weeks and months after the mainshock) will cause additional damage, requiring repeated repairs. Water supplies could be impaired for months, hindering household and

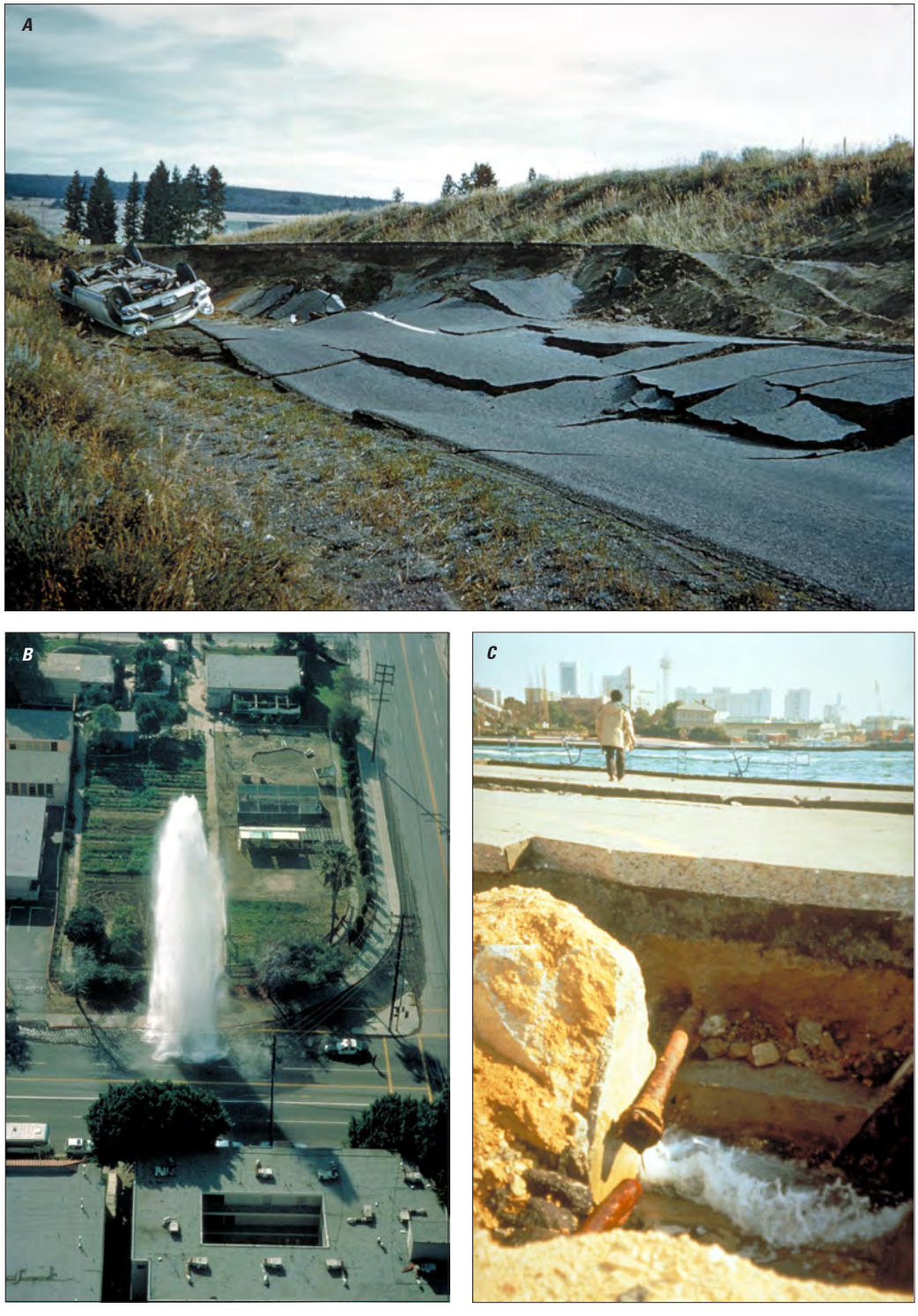

Figure 5. Photographs showing examples of types of damage to lifelines and infrastructure expected to occur along the Hayward Fault in the San Francisco Bay region, California, in an earthquake like the magnitude-7 mainshock modeled in the HayWired scenario. *A*, Damage to a road from fault offset; *B*, column of water gushing from a damaged pipeline; and *C*, large electrical conduit broken by fault offset. (Photographs from National Information Service for Earthquake Engineering-Pacific Earthquake Engineering Research Center (NISEE-PEER), University of California, Berkeley, used with permission.)

business recovery even in undamaged buildings. The effects on the region's and the Nation's economy will continue for years and will be costly and wide reaching. Because relatively few buildings are insured for earthquakes, owners will face challenges financing repairs. Occupants will have to find alternative housing or business space, and some people might be forced to move away from the region for at least some period of time and possibly not return.

Because our lives and economy are now fully intertwined with the Internet, the hypothetical disruption from the HayWired scenario is compounded. Our society takes for granted that information, goods, and services are available at a moment's notice through the Internet. A large earthquake on the Hayward Fault could be the first major U.S. earthquake for which much of our commerce ("e-commerce," including shipping and distribution management) and our daily interactions happen online.

What happens if Internet services are disrupted following a natural-hazard event? What will such a disaster mean to you, your family, your job, and your community? Scientists, engineers, and social scientists created the HayWired scenario to help you answer these questions and prioritize actions you can take now to protect lives, businesses, neighborhoods, and homes.

Preparing for the next large, damaging earthquake in the San Francisco Bay region is not an insurmountable task, and governments, critical infrastructure managers and providers, businesses, and residents have already taken enormous strides toward that goal. The 1989 *M*6.9 Loma Prieta earthquake served as a "wake-up call" for the bay region, inciting continued efforts to prepare for earthquakes, including a better understanding of earthquakes and their hazards, active risk reduction, and improvement of societal resilience. The HayWired scenario may be especially informative to young people in the San Francisco Bay region, many of whom were not yet born or have no memory of the Loma Prieta earthquake, as well as newcomers to the region. It is hoped that the HayWired scenario will energize new efforts and a next generation of proponents and champions acting along a line of purposeful, thoughtful, and responsible action, similar to earlier efforts, to help the bay region prepare for its next large earthquake.

Extraordinary Investment in Earthquake Resilience Already Accomplished

Earthquake scenarios and seismic-resilience efforts are not new to the San Francisco Bay region (see the appendix for background on previous initiatives and accomplishments). All told, the bay region has invested at least $25 billion (Association of Bay Area Governments, 2014a), and reportedly as much as $50 billion (KQED, 2014), in earthquake countermeasures since the 1989 magnitude-6.9 Loma Prieta earthquake, strengthening potential points of failure in buildings and infrastructure. Concurrently, local and regional organizations have started to confront many of the complex, interrelated societal issues that can limit resilience. An extraordinary amount has already been done in the San Francisco Bay region to reduce the earthquake risk to communities and critical facilities and lifelines and to increase societal resilience in response to natural hazards.

However, the HayWired earthquake scenario shows that much more needs to be done. Many reasonable mitigation options can take decades to complete, such as the costly replacement of brittle water-distribution pipelines. Time is of the essence if decision makers wish to complete these actions before the next large earthquake actually occurs in the bay region. Society has a strong interest in continuing to strengthen infrastructure to reduce damage and better sustain us during response and recovery from a natural disaster. It also has a strong interest in planning and preparedness activities, not only engineering approaches, to improve community resilience.

Motivation—Why Revisit a Hayward Fault Scenario Now?

The HayWired earthquake scenario is being done at a time when the economy of the San Francisco Bay region is healthy and thriving. Strong economic growth comes with strains on infrastructure, affordable housing shortages, and more pronounced income disparities. Although the strength of the bay region's economy is an asset in building more resilient infrastructure and communities, emerging issues increase the region's vulnerability to an earthquake, and these issues need attention.

It is time to update earthquake scenarios for the San Francisco Bay region to leverage new knowledge, capabilities, and developments. Some new key themes extend previous scenario analyses (see Objectives of the HayWired Scenario discussed below) to enhance collaborations with traditional audiences and to target new audiences to help increase the region's resilience in a natural disaster.

The HayWired scenario includes the following new or updated developments that were not included (or given as much attention) in previous disaster and earthquake scenarios or studies (see appendix):

- A comparison of the use of ground-motion-estimation methods.
- An estimate of landslide probability and liquefaction probability.
- Forecasting effects of fault afterslip and aftershocks.
- Public expectations for the performance of new buildings and potential benefits of enhancing building-code requirements for new buildings.
- New methods to estimate urban search-and-rescue needs in response to building collapse and stalled elevators.
- Expected complications of fire following earthquake and the interoperability of portable water-supply systems used for firefighting.

- Anticipation of environmental-health issues.
- A new method to estimate water-supply damage and service-restoration time in an earthquake sequence, and quantifying lifeline interdependencies.
- An estimation of communication and infrastructure damage and service restoration time.
- Potential benefits of earthquake early warning.
- Identification of potential long-term recovery challenges for the region's communities.
- Impacts to and resilience of the digital economy and strategies to bolster economic resilience.

Objectives of the HayWired Scenario

Objectives of the HayWired scenario are to (1) improve the communication and use of earthquake-hazard science in decision-making, (2) advance basic knowledge of earthquake risks and to inform actions to reduce earthquake risks, and (3) help build community capacity to respond to and recover from earthquakes. Each of these objectives is given in greater detail below:

1. Improve the communication of earthquake-hazard science for use in decision-making:
    A. Support the use of earthquake-hazard science in risk reduction with engineering, environmental science, and social sciences.
    B. Improve understanding among Earth scientists, engineers, and others of numerical simulation of earthquake ground motion for earthquake scenarios, as opposed to the use of empirical ground-motion-prediction equations.
    C. Improve understanding of the benefits of earthquake early warning.
    D. Educate about liquefaction and landslides.
    E. Educate about aftershocks and afterslip.
    F. Educate about operational earthquake forecasts.
2. Advance basic knowledge of earthquake risks and inform actions to reduce earthquake risks:
    A. Evaluate the societal impacts of the seismic-performance objectives in building codes. Evaluate public preferences for the seismic performance of new buildings. Identify an option for the public to provide input into the seismic performance of new buildings. Evaluate its costs and benefits. Educate community leaders and structural engineers about that new knowledge. Formulate an option for a community to enhance new buildings with a simple enhancement to the language of a building-code adoption ordinance.
    G. Develop a new method to estimate water-supply-network recovery considering lifeline interaction, resource limitations, aftershocks, and afterslip, without reliance on expert opinion, proprietary computer models, or "black-box" software (only inputs and outputs can be viewed, not underlying code). Educate and facilitate conversations about reducing damage and speeding recovery of water-supply systems.
    H. Educate and facilitate conversations about enhancing firefighting capabilities to resist fire following earthquake.
    I. Develop methods to estimate the number of people trapped in collapsed buildings and inside stalled elevators. Educate and facilitate conversations about reducing the number of people potentially trapped inside stalled elevators.
    J. Help anticipate environmental health issues.
    K. Engage stakeholders in discussions about the vulnerabilities and resilience of cyber infrastructure and the Internet economy.
3. Help build community capacity to respond to and recover from earthquakes:
    A. Facilitate conversations about lifeline-restoration interdependencies.
    B. Help inform and stimulate the development of predisaster plans and policy interventions in emergency management, hazard mitigation, and recovery management that can work toward keeping residents and businesses in their communities.
    C. Provide materials for emergency response, business continuity, and recovery exercises, as well as for many other uses.

HayWired Scenario Process Will Tackle Urgent Questions

From April 2017 through April 2018, the HayWired Coalition and the authors of the HayWired scenario plan to continue the process of working together on developing it. One goal is to improve the transfer of scientific information to those who need it and to expand the application of science and earthquake engineering to earthquake-risk reduction. We plan to advance the discussion of key earthquake issues in the San

Francisco Bay region, staging new conversations that update resilience strategies and boost ongoing decision-making and policy-making on seismic issues. We seek to reach audiences beyond emergency responders (who use scenarios extensively) to directly engage communities and businesses in earthquake response and recovery planning.

Using the HayWired scenario as a topic for focus during the coming year of workshops and meetings presents an opportunity to ask and address new, urgent questions about disaster resilience following an earthquake. In addition to the objectives listed in the preceding section, the following questions may also help to provoke thoughts for discussion in the upcoming year:

- Why might one want to use numerical simulation of earthquake ground motion rather than empirical ground-motion-prediction equations to better understand and prepare for earthquakes?
- How well do building codes intend new buildings to perform in a large metropolitan earthquake, and how well do those performance objectives align with the public's preferences?
- How would a simple increase in the design strength of new buildings reduce building impairment following an earthquake, and how much would such strength increases cost?
- How many people should fire departments anticipate having to rescue from collapsed buildings and stalled elevators?
- How can fire departments better prepare for fire following earthquake with portable water-supply systems, and how can fire departments that already have such systems coordinate their use?
- How do lifelines—water, power, communication, roads, and transit—interact during and following an earthquake, and how do they interact during damage restoration?
- How can a water utility estimate earthquake damage, restoration time, and the macroeconomic losses resulting from water-service interruption without relying on expert opinion, proprietary computer models, or black-box software?
- To what extent do shaking, liquefaction, landslide, fault slip, aftershocks, and afterslip contribute to water-system damage and hinder recovery?
- What can a water utility do to speed restoration and reduce its dependence on other lifelines?
- How many injuries can be avoided by combining earthquake early warning with "drop-cover-and-hold-on" actions taken by people to protect themselves when ground shaking starts?
- What will happen to an Internet-dependent society when a large earthquake occurs?
- How can resilience be further improved to ensure that supply chains for many basic needs such as food, water, fuel, and pharmaceuticals will not be disrupted?
- What are the environmental-health concerns following a large earthquake?
- How will earthquake early warning, fault afterslip, aftershocks, and fire following earthquake affect disaster management and recovery?
- What types of long-term outcomes could communities and neighborhoods face as a result of earthquake damage, impacts, and cascading effects, including the potential displacement of people and businesses?
- Long-term community recovery will be at risk; how will people collectively respond?

HayWired Scenario Builds on the Success of Past SAFRR Scenarios

The USGS Science Application for Risk Reduction project, as did its predecessor the Multi-Hazards Demonstration project, uses the latest Earth-science advances in novel ways to inform decisions on how to improve disaster resilience. SAFRR has created detailed, science- and natural-hazard-event-based scenarios of (1) a *M*7.8 San Andreas Fault earthquake in southern California (ShakeOut—Jones and others, 2008), (2) atmospheric-river storms rivaling those that caused California's Great Flood of 1862 (ARkStorm—Porter and others, 2010), (3) an earthquake the size of the 2011 Tohoku, Japan, earthquake (*M*9.0), and (4) a tsunami generated off the Alaska Peninsula that severely impacts the Ports of Los Angeles and Long Beach (SAFRR Tsunami—Ross and others, 2013) and now HayWired. Each of these scenarios was developed to provide science for decision-making and to engage potential users of the information throughout the scenario development process.

Each SAFRR scenario depicts a scientifically plausible natural-hazard source and its cascading effects, with impacts and consequences severe enough to demand attention but not so severe as to be unbelievable. The scenarios address interacting hazards and involve multiple science, engineering, and other disciplines and user communities. The scenarios explore previously unknown or less-studied vulnerabilities and cascading effects that only come into focus when one looks beyond impacts and stakeholders considered in isolation. They provide decision makers with clear explanations and information for mitigation and preparedness actions and have been used for national-to-local disaster-response exercises and planning.

As with previous SAFRR-led scenarios, the initiating event of the HayWired scenario is described (the mainshock fault rupture and strong ground motion) and then expanded to

cover secondary hazards, in particular liquefaction, landslides, aftershocks, and afterslip, which are described in this volume, USGS SIR 2017–5013–A–H (https://doi.org/10.3133/sir20175013v1). Physical damage to structures, critical facilities, and infrastructure, environmental health concerns, and social and economic consequences for policy consideration are planned to be described in two following volumes of SIR 2017–5013. This broad-based approach is intended to inform decisions about how to enhance earthquake resilience.

A combined approach is used that involves working as a team to describe not only the natural-hazard event and its cascading effects but also the impacts and consequences. The combined team includes the following:

- Physical scientists working to understand the natural hazard.
- Engineers working to understand the earthquake effects and solving problems of how to improve the performance and recovery of critical facilities and infrastructure.
- Biogeochemists shedding light on the human health aspects of building materials exposed during a disaster.
- Social scientists working to understand the consequences to communities—economic, health, and quality of life.

Through new and innovative methods of crafting disaster scenarios, developed in each case by a USGS SAFRR-led team, and beginning with ShakeOut, scenarios and exercises have been used as effective methods to engage the public and elected officials. One goal of the HayWired scenario is to expand efforts to coordinate with decision makers who can use the scenario. Another goal is to engage residents of the San Francisco Bay region, especially to update and refresh similar work (for example, Algermissen and others, 1972; Steinbrugge and others, 1987; and Earthquake Engineering Research Institute, 1996, among others). In terms of culture and community, the HayWired scenario builds on previous efforts in the bay region to form a new coalition to identify and address remaining and evolving vulnerabilities to earthquakes and other disasters and to further reduce risk.

The HayWired Coalition

SAFRR has partnered with a number of organizations to form a group named the HayWired Coalition to disseminate and make use of the HayWired scenario (see sidebar, HayWired Coalition Partners). The HayWired Coalition aims to identify the scenario's potential impacts on their constituents and to align the scenario with the concerns of their respective communities. The coalition began forming in mid-2016 to help with the process of receiving input and organizing the interactions of a broad range of stakeholders. The coalition has assisted the scenario-development team in helping to identify previously unrecognized vulnerabilities of communities, lifelines, infrastructure, and supply chains. In the development of previous disaster scenarios, much of this interaction took place organically after the scenario was finalized and published. Instead, for the HayWired scenario, a deliberate effort is underway to engage partners, help them identify mitigation actions, and begin to use the scenario to reduce risk even before full publication of SIR 2017–5013.

HayWired Coalition Partners

ARUP—Design and Engineering Consultants
Association of Bay Area Governments
Aurecon
Bay Area Center for Regional Disaster Resilience
Bay Area Rapid Transit Authority
Boston University
California Department of Public Health
California Department of Transportation
California Earthquake Authority
California Earthquake Clearinghouse
California Geological Survey
California Governor's Office of Business and Economic Development
California Governor's Office of Emergency Services
California Public Utilities Commission
California Resiliency Alliance
California Seismic Safety Commission
Carnegie Mellon University Silicon Valley
City of Berkeley
City of Oakland
City of San Francisco, Department of Emergency Management
City of Walnut Creek
Earthquake Country Alliance
Earthquake Engineering Research Institute
East Bay Municipal Utilities District
Federal Emergency Management Agency
Joint Venture Silicon Valley
Laurie Johnson Consulting
MMI Engineering
Pacific Earthquake Engineering Research Center
Pacific Gas and Electric
Palo Alto University
Red Cross
Rockefeller Foundation—100 Resilient Cities
San Jose Water Company
Southern California Earthquake Center
SPA Risk LLC
San Francisco Bay Area Planning and Urban Research Association
Strategic Economics
Structural Engineers Association of Northern California
University of California Berkeley Seismological Laboratory
University of Colorado Boulder
University of Southern California
U.S. Geological Survey

A Call to Action for the Coming Year

The release of SIR 2017–5013–A–H, detailing the hazards of the HayWired scenario earthquake, comes about 1 year before the hypothetical date of the HayWired mainshock of April 18, 2018. To better understand the potential impacts and consequences of the HayWired scenario, Earth scientists, engineers, and social scientists plan to use the upcoming year (April 2017 through April 2018) to share information and to work with State of California and San Francisco Bay region partners in the HayWired Coalition, representing agencies and experts in lifelines, engineering, local government, public-health, business, and emergency management to further enhance earthquake- and disaster-resilience planning, policy, and action across the region.

Through a collaborative and intensive series of workshops and user-engagement activities, scenario researchers and potential users of the information plan to build on the San Francisco Bay region's already strong foundation of earthquake preparedness, to further strengthen infrastructure, and to help communities become even more resilient. The HayWired scenario is expected to serve as an earthquake-planning resource for many years to come, to help heighten and sustain attention, to focus action on the San Francisco Bay region's remaining vulnerabilities, and to continue to reach out to communities and the public.

References Cited

Aagaard, B.T., Blair, J.L., Boatwright, J., Garcia, S.H., Harris, R.A., Michael, A.J., Schwartz, D.P., and DiLeo, J.S., 2016, Earthquake outlook for the San Francisco Bay region 2014–2043 (ver. 1.1, August 2016): U.S. Geological Survey Fact Sheet 2016–3020, 6 p., accessed April 10, 2017, at http://dx.doi.org/10.3133/fs20163020.

Algermissen, S.T., Rinehart, W.A., Dewey, J., Steinbrugge, K.V., Degenkolb, H.J., Cluff, L.S., McClure, F.E., Gordon, R.F., Scott, S., and Lagorio, H.J., 1972, A study of earthquake losses in the San Francisco Bay area: Washington, D.C., National Oceanic and Atmospheric Administration, Office of Emergency Preparedness, 220 p.

Association of Bay Area Governments, 2014a, LP25—Policy Actions, Loma Prieta 25 Symposium: Association of Bay Area Governments, accessed March 31, 2017, at http://resilience.abag.ca.gov/wp-content/documents/LP25/LP25_PolicyActions.pdf.

Association of Bay Area Governments, 2014b, Cascading failures—Earthquake threats to transportation and utilities: Association of Bay Area Governments, 47 p., accessed April 12, 2017, at http://resilience.abag.ca.gov/wp-content/documents/Cascading_Failures/InfrastructureReport_2014.pdf.

California Governor's Office of Emergency Services and Federal Emergency Management Agency, 2016, Bay Area earthquake plan: California Governor's Office of Emergency Services and Federal Emergency Management Agency, 46 p., accessed April 12, 2017, at http://www.caloes.ca.gov/PlanningPreparednessSite/Documents/BayAreaEQConops(Pub_Version)_2016.pdf.

California Seismic Safety Commission, 1991, Loma Prieta's call to action—Report on the Loma Prieta earthquake of 1989: California Seismic Safety Commission, 97 p., accessed April 12, 2017, at https://ia801402.us.archive.org/33/items/lomaprietascallt1991cali/lomaprietascallt1991cali.pdf.

City and County of San Francisco, 2016, Resilient San Francisco, stronger today, stronger tomorrow: City and County of San Francisco, 137 p., accessed April 12, 2017, at http://sfgov.org/orr/sites/default/files/documents/Resilient%20San%20Francisco_0.pdf.

Earthquake Engineering Research Institute, 1996, Scenario for a magnitude 7.0 earthquake on the Hayward Fault: Oakland, Calif., Earthquake Engineering Research Institute, 109 p.

Earthquake Engineering Research Institute, 2006, Managing risk in earthquake country—Estimated losses for a repeat of the 1906 San Francisco earthquake and the earthquake professionals' action agenda for northern California: Earthquake Engineering Research Institute, 24 p., accessed April 12, 2017, at http://www.1906eqconf.org/mediadocs/managingrisk.pdf.

Johnson, L.A., 2014, Lifelines interdependency study|report: City and County of San Francisco Lifelines Council, 47 p., accessed April 12, 2017, at http://sfgov.org/esip/sites/default/files/Documents/homepage/LifelineCouncil%20Interdependency%20Study_FINAL.pdf.

Joint Ventures Silicon Valley, 2017, Silicon Valley index: Joint Ventures Silicon Valley web page, accessed February 28, 2017, at http://www.siliconvalleyindicators.org/.

Jones, L.M., Bernknopf, R., Cox, D., Goltz, J., Hudnut, K., Mileti, D., Perry, S., Ponti, D., Porter, K., Reichle, M., Seligson, H., Shoaf, K., Treiman, J., and Wein, A., 2008, The ShakeOut Scenario: U.S. Geological Survey Open-File Report 2008–1150 and California Geological Survey Preliminary Report 25, 312 p. and appendixes, accessed April 12, 2017, at https://pubs.usgs.gov/of/2008/1150/.

Kircher, C.A., Seligson, H.A., Bouabid, J., and Morrow, G.C., 2006, When the big one strikes again—Estimated losses due to a repeat of the 1906 San Francisco earthquake: Earthquake Spectra, v. 22, no. S2, p. S297–S339, accessed April 12, 2017, at http://www.nehrpscenario.org/wp-content/uploads/2009/03/kircher_etal.pdf.

KQED, 2014, 25 years after the Loma Prieta earthquake, are we safer?: KQED Science web page, accessed April 11, 2017, at https://ww2.kqed.org/science/2014/10/13/25-years-after-the-loma-prieta-earthquake-are-we-safer/.

Lawson, A.C., chairman, 1908, The California earthquake of April 18, 1906—Report of the State Earthquake Investigation Commission: Washington, D.C., Carnegie Institution of Washington Publication 87, 2 vols.

Lienkaemper, J.J., Williams, P.L., and Guilderson, T.P., 2010, Evidence for a twelfth large earthquake on the southern Hayward Fault in the past 1900 years: Bulletin of the Seismological Society of America, v. 100, no. 5A, p. 2024–2034, doi: 10.1785/0120090129.

Lienkaemper, J.J., Dawson, T.E., Personius, S.F., Seitz, G.G., Reidy, L.M., and Schwartz, D.P., 2002, A record of large earthquakes on the southern Hayward Fault for the past 500 years: Bulletin of the Seismological Society of America, v. 92, no. 7, p. 2637–2658.

Maffei, Janiele, 2010, The coming Bay Area earthquake—2010 update of scenario for a magnitude 7.0 earthquake on the Hayward Fault: Earthquake Engineering Research Institute Northern California Chapter, 115 p., accessed April 12, 2017, at http://www.eerinc.org/wp-content/uploads/2009/06/Building_Earthquake_Resiliency_in_SF_Bay_Area_V17-2.pdf.

National Research Council, 1994, Practical lessons from the Loma Prieta earthquake: Washington, D.C., National Academy Press, 288 p. doi: 10.17226/2269.

Northridge 20 Symposium, 2014, Northridge 20 Symposium summary report—The 1994 Northridge earthquake—Impacts, outcomes, and next steps: Northridge 20 Symposium, January 16–17, 2014, Los Angeles, California, 30 p., accessed April 12, 2017, at http://www.northridge20.org/wp-content/uploads/2014/05/Northridge20_Summary_Report.pdf.

Porter, K., Wein, A., Alpers, C., Baez, A., Barnard, P., Carter, J., Corsi, A., Costner, J., Cox, D., Das, T., Dettinger, M., Done, J., Eadie, C., Eymann, M., Ferris, J., Gunturi, P., Hughes, M., Jarrett, R., Johnson, L., Dam Le-Griffin, H., Mitchell, D., Morman, S., Neiman, P., Olsen, A., Perry, S., Plumlee, G., Ralph, M., Reynolds, D., Rose, A., Schaefer, K., Serakos, J., Siembieda, W., Stock, J., Strong, D., Sue Wing, I., Tang, A., Thomas, P., Topping, K., and Wills, C.; Jones, L., chief scientist, Cox, D., project manager, 2011, Overview of the ARkStorm scenario: U.S. Geological Survey Open-File Report 2010–1312, 183 p. and appendixes, accessed April 10, 2017, at https://pubs.usgs.gov/of/2010/1312/.

Risk Management Solutions, Inc., 2008, 1868 Hayward earthquake—140-year retrospective: Risk Management Solutions, Inc., special report, revised 2013, 26 p., accessed April 12, 2017, at http://forms2.rms.com/rs/729-DJX-565/images/eq_1868_hayward_eq_retrospective.pdf.

Ross, S., and Jones, L., eds., 2013, The SAFRR (Science Application for Risk Reduction) tsunami scenario: U.S. Geological Survey Open-File Report 2013–1170 and California Geological Survey Preliminary Report 229, accessed April 11, 2017, at https://pubs.usgs.gov/of/2013/1170/.

San Francisco Bay Area Planning and Urban Research Association, 2010, After the disaster—Rebuilding our transportation infrastructure: San Francisco Bay Area Planning and Urban Research Association, 30 p., accessed April 12, 2017, at http://www.spur.org/publications/spur-report/2010-07-06/after-disaster.

Steinbrugge, K., Lagorio, H.J., Davis, J.F., Bennett, J.H., Borchardt, G., and Toppozada, T.R., 1987, Earthquake planning scenario for a magnitude 7.5 earthquake on the Hayward Fault in the San Francisco Bay area: California Department of Mines and Geology, Special Publication 78, 235 p.

U.S. Geological Survey, 2014, Earthquake planning scenario—ShakeMap for Haywired M7.05-scenario: U.S. Geological Survey web page, accessed April 11, 2017, at https://earthquake.usgs.gov/scenarios/eventpage/ushaywiredm7.05_se#shakemap?source=us&code=gllegacyhaywiredm7p05_se.

U.S. Geological Survey and cooperators, 1990, The next big earthquake in the Bay Area may come sooner than you think—Are you prepared?: U.S. Geological Survey, newspaper insert, 23 p., accessed April 18, 2017, at https://pubs.er.usgs.gov/publication/70186988.

Working Group on California Earthquake Probabilities, 1990, Probabilities of large earthquakes in the San Francisco Bay region, California: U.S. Geological Survey Circular 1053, 51 p., accessed April 11, 2017, at https://pubs.usgs.gov/circ/1990/1053/report.pdf.

Appendix. History of San Francisco Bay Region Earthquake Scenarios and Seismic-Resilience Efforts

Algermissen and others (1972) and Steinbrugge and others (1987) provided early and comprehensive analyses of a hypothetical Hayward Fault earthquake. They focused on lifelines in their planning scenario for a *M*7.5 earthquake on the fault. The *M*6.9 Loma Prieta earthquake of October 17, 1989, helped to generate a focus and a more regional perspective on seismic vulnerabilities in the San Francisco Bay region. Documents such as the California Seismic Safety Commission's (CSSC) 1991 report, "Loma Prieta's Call to Action" (California Seismic Safety Commission, 1991), and the National Research Council's (NRC) 1994 report, "Practical Lessons from the Loma Prieta Earthquake" (National Research Council, 1994), established a baseline for assessing the region's major seismic vulnerabilities and policy needs at the time, as well as a baseline for considering the region's progress on these issues over the past 26 years. However, as these reports aptly cautioned, the 1989 earthquake was not a rigorous test of the region's built environment, preparedness, or hazard mitigation.

The combination of the 1989 Loma Prieta earthquake and follow-on assessments also helped to create a more integrated, regional perspective on the earthquake vulnerability of the San Francisco Bay region and encouraged people to work together as a region on earthquake-hazard mitigation, response, and recovery planning. The newspaper insert, "The Next Big Earthquake in the Bay Area May Come Sooner Than You Think. Are You Prepared?" (U.S. Geological Survey and cooperators, 1990), first published in 1990 and updated and reissued in 1994, is one of the first widely disseminated public-education documents with a holistic view of the region's earthquake risk and needed preparedness actions (fig. 6). It gave greater public visibility to the Working Group on California Earthquake Probabilities' 1990 report, "Probabilities of Large Earthquakes in the San Francisco Bay Region, California" (Working Group on California Earthquake Probabilities, 1990), which showed that the region's high-risk geologic faults had a combined 67-percent likelihood of generating another *M*7 earthquake in the next 30 years. This was a substantial increase in risk over the group's 1988 estimation of a 50-percent likelihood of such an event.

It was also in the 1980s and 1990s that the Bay Area Regional Earthquake Preparedness Project (BAREPP) existed and

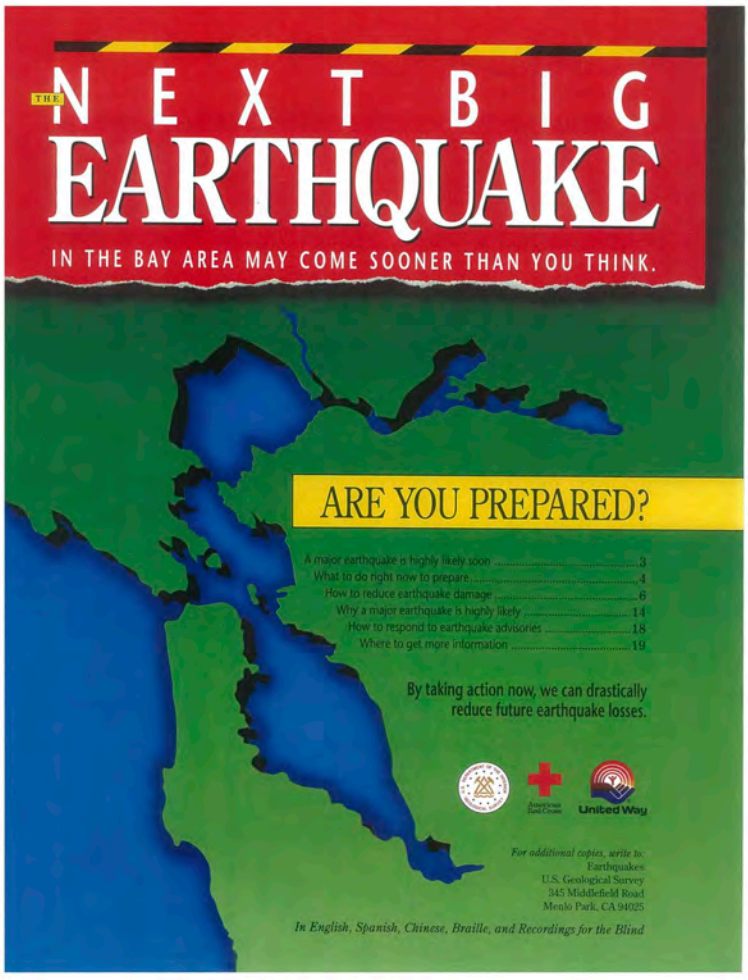

Figure 6. Image of the cover of "The Next Big Earthquake in the Bay Area May Come Sooner Than You Think—Are You Prepared?" (U.S. Geological Survey and cooperators, 1990). This 1990 newspaper insert, updated and reissued again in 1994, was widely distributed in newspapers in the San Francisco Bay region. Specifically designed for the general public, it is one of the first documents with a holistic view of the region's earthquake risk and needed preparedness actions.

helped to develop plans, model policies and ordinances for seismic safety, and build coalitions across local governments, lifeline providers, and in the housing and business sectors. Originally formed by the CSSC, BAREPP became part of the California Governor's Office of Emergency Services (Cal OES) and was co-housed with the Association of Bay Area Governments (ABAG) for a number of years before it closed in about 2000, and its staff were mostly absorbed into Cal OES.

At the 1995 Earthquake Engineering Research Institute (EERI) annual meeting, a multidisciplinary panel of speakers laid out the potential impacts and issues associated with a *M*7.2 earthquake on the northern end of the Hayward Fault with ground motions directed primarily southward along the fault system. Again, this was fundamental work to pull together a regional perspective on seismic vulnerabilities and policy needs with an emphasis on the heavily urbanized east bay corridor of San Francisco Bay. The scenario report was recapped and updated in a 2010 report by Janiele Maffei and the EERI Northern California Chapter, "The Coming Bay Area Earthquake—2010 Update of Scenario for a Magnitude 7.0 Earthquake on the Hayward Fault" (Maffei, 2010). It is one of the most recent assessments of mitigation activities across the region, as well as of the likely effects of a Hayward Fault earthquake. Advances made in mitigating the earthquake risk for critical infrastructure and facilities, improving emergency-response planning, and initial steps taken to address vulnerable commercial and residential building stock are compiled throughout the report. It was developed as part of regional activities surrounding the 140th anniversary of the 1868 Hayward Earthquake. It also draws on damage and loss estimates in a 2008 Risk Management Solutions (RMS) special report, "1868 Hayward Earthquake: 140-Year Retrospective" (Risk Management Solutions, Inc., 2008). Using its proprietary software, RMS estimated total economic losses of $174.3 billion from shaking and fire following earthquake damages to residential and commercial properties for a *M*7 earthquake on the Hayward Fault. Maffei (2010) concludes with:

> Ten years into the new century, we have not yet reached an acceptable level of seismic safety, and it is clearly necessary for earthquake professionals to continue their advocacy. But they must take their message beyond enclosed spaces out to the stakeholders in whatever arena they can be found. Every private property owner in the Bay Area must come to understand the losses each and all of us will face, and how those impacts will harm the quality of life we enjoy in this unique part of the world.

The economic recession in 2010 was considered to constrain the capacity to invest in earthquake mitigation.

Another major multidisciplinary scenario and regional seismic-safety-policy assessment occurred in 2006 for the 100th anniversary of the 1906 Great San Francisco earthquake on the San Andreas Fault. The EERI Northern California Chapter undertook an effort to integrate seismic-safety progress and needs in the San Francisco Bay region that are contained in the 2006 anniversary conference briefing packet, "Managing Risk in Earthquake Country—Estimated Losses for a Repeat of the 1906 San Francisco Earthquake and the Earthquake Professionals' Action Agenda for Northern California" (Earthquake Engineering Research Institute, 2006). Cal OES, the Federal Emergency Management Agency (FEMA) and other organizations also helped to fund the development of the scenario presented at the 2006 conference, and it was used as the basis for a Golden Guardian exercise led by Cal OES (see http://cdphready.org/cal-oes-annual-exercise-series-golden-guardian/). The scenario results are summarized in a 2006 paper by Kircher and others, "When the Big One Strikes Again—Estimated Losses due to a Repeat of the 1906 San Francisco Earthquake" (Kircher and others, 2006). A key feature of the modeling effort was the detailed update of the building stock for the 19-county northern California region. The loss estimation results focused primarily on casualties, building damage, and economic losses.

Other regional emergency-planning work in the San Francisco Bay region has tended to look at either a very large *M*7.9 San Andreas Fault earthquake or a *M*7.0 Hayward Fault earthquake, for which the 2006 and 2008 efforts, respectively, have served as key sources of information. Some additional noteworthy resources with a regional perspective on immediate earthquake impacts and needs in the San Francisco Bay region are:

- The San Francisco Bay Area Planning and Urban Research Association (SPUR) 2010 report, "After the Disaster: Rebuilding our Transportation Infrastructure" (San Francisco Bay Area Planning and Urban Research Association, 2010). This report looks at transportation system redundancy on a corridor-by-corridor basis and the effects of failures in each of these corridors, as well as regionwide.

- The Bay Area Urban Areas Security Initiative regional catastrophic earthquake plans (see http://www.bayareauasi.org/catastrophicplans/). Many of these plans were developed in about 2010–2011 and use a *M*7.9 San Andreas Fault earthquake scenario. The plans cover debris removal, donations management, interim housing, logistics, mass care and sheltering, mass fatality, mass transportation and evacuation, and volunteer management.

- The ABAG 2014 report, "Cascading Failures: Earthquake Threats to Transportation and Utilities" (Association of Bay Area Governments, 2014b). This report considers impacts to airports, transportation, fuel, electricity, and water, as well as system interdependencies considering *M*7.0 Hayward Fault, *M*7.9 San Andreas Fault, and *M*6.8 Concord Fault earthquake scenarios.

- The ABAG 2015 reports, "Stronger Housing, Safer Communities" (see http://resilience.abag.ca.gov/projects/stronger_housing_safer_communities_2015/). These reports evaluate the seismic and flood vulnerability of the region's communities and housing stock and provide strategies for local governments to mitigate those risks. For seismic vulnerability, it

looks at areas where strong ground shaking is expected from *M*7.8 (San Andreas Fault) and *M*6.9 (Hayward Fault) earthquakes. Data developed for community-vulnerability assessments will inform the communities-at-risk assessment in the HayWired scenario.

- The Cal OES-FEMA 2016 report, "Bay Area Earthquake Plan," (California Governor's Office of Emergency Services and Federal Emergency Management Agency, 2016). This is a catastrophic planning document that looks at both *M*7.0 Hayward Fault and *M*7.9 San Andreas Fault earthquake scenarios. The *M*7.0 Hayward Fault scenario has an epicenter in north Richmond and ruptures southward. There is a general-audience video for the plan at https://www.fema.gov/media-library/assets/videos/118139/.

The year 2014 marked the 25th and 20th anniversaries, respectively, of two significant California earthquakes—the 1989 *M*6.9 Loma Prieta and the 1994 *M*6.7 Northridge earthquakes. Commemorative symposiums were held both in Los Angeles in January and Oakland in October 2014. Both of these symposia acknowledged the tremendous seismic-resilience work that has been accomplished in California over the past decades (Association of Bay Area Governments, 2014a; Northridge 20 Symposium, 2014).

Resilience strategies (developed with funding from the Rockefeller Foundation—100 Resilient Cities initiative) in the cities of Berkeley (see http://www.ci.berkeley.ca.us/Resilience/), San Francisco (see http://sfgsa.org/resilient-sf/), and Oakland (see https://beta.oaklandca.gov/issues/resilient-oakland/) provide more city-specific information on previous seismic-risk assessments, past resilience investments, and future strategies and plans. Additional detailed seismic-risk assessments for San Francisco include:

- The SPUR Resilient City initiative that has a series of policy papers on needed improvements to San Francisco's lifelines, new buildings, and existing buildings, particularly housing, to ensure that residents can safely stay in the city following a major earthquake (see http://www.spur.org/featured-project/resilient-city).
- The Citizens Advisory Panel on Seismic Safety (CAPSS) studies assessed the seismic vulnerability of San Francisco's private building stock and looked at potential mitigation needs based on a series of scenarios. This was then turned into the 50-task, 30-year Earthquake Safety Improvement Program (ESIP). CAPSS and ESIP documents are available at http://sfgov.org/esip/program/.
- The San Francisco Lifelines Council's lifelines interdependency study (Johnson, L.A., 2014), which resulted in a 5-year collaborate work program for lifeline operators (see http://sfgov.org/esip/sites/default/files/Documents/homepage/LifelineCouncil%20Interdependency%20Study_FINAL.pdf).
- The City of San Francisco's resilience strategy (City and County of San Francisco, 2016), which provides an integrated approach to hazard planning (see http://sfgov.org/orr/resilient-san-francisco/).

The ABAG Loma Prieta (LP) 25 report (Association of Bay Area Governments, 2014a), identifies four key seismic-safety issues where significant policy gaps remain and encourages the San Francisco Bay region's more than 100 cities to work together on a regional legislative agenda:

- *Update building codes.*—Adopt building-code standards to improve the seismic performance of new and existing buildings and ensure that building codes meet community performance expectations.
- *Upgrade vulnerable apartments and condominiums.*—Enact statewide guidelines for the identification, evaluation, and retrofit of seismically unsafe apartment and condominium buildings.
- *Develop financial incentives.*—Establish regional financial-incentive programs for improving the seismic safety of apartments and condominium buildings.
- *Convene lifeline providers and cities.*—Establish a State lifelines council and convene regional lifeline councils in the San Francisco Bay region and in southern California.

The HayWired Earthquake Scenario—Earthquake Hazards
Edited by Shane T. Detweiler and Anne M. Wein
Scientific Investigations Report 2017–5013–A–H
[Also see https://doi.org/10.3133/sir20175013]

Chapter B

Overview of the HayWired Scenario Earthquake-Hazards Volume

By Ruth A. Harris

Introduction

The HayWired scenario is a hypothetical earthquake sequence that is being used to better understand hazards for the San Francisco Bay region during and after an earthquake of magnitude 7 on the Hayward Fault. The Working Group on California Earthquake Probabilities calculates that there is a 33-percent likelihood of a large (magnitude 6.7 or greater) earthquake occurring on the Hayward Fault in the next few decades (Aagaard and others, 2016). A large Hayward Fault earthquake will produce strong ground shaking, permanent displacement of the Earth's surface, landslides, liquefaction (soils becoming liquid-like during shaking), and subsequent earthquakes, known as aftershocks.

The most recent large earthquake on the Hayward Fault occurred on October 21, 1868, and it ruptured the southern part of the fault. The 1868 magnitude-6.8 earthquake occurred when the San Francisco Bay region had far fewer people, buildings, and infrastructure (roads, communication lines, and utilities) than it does today, yet the strong ground shaking from the earthquake still caused significant building damage and loss of life (fig. 1). Because the region is now densely populated and has many more homes and buildings and much more critical infrastructure than it did in 1868, the next large Hayward Fault earthquake is anticipated to affect thousands of structures and disrupt the lives of millions of people. To help provide the crucial scientific information that the San Francisco Bay region will need to prepare for the next large earthquake, The HayWired Earthquake Scenario—Earthquake Hazards volume describes the strong ground shaking modeled in the scenario and the hazardous movements of the Earth's surface that the shaking will activate.

Modeling the Mainshock

The HayWired scenario mainshock consists of a three-dimensional (3D) computer simulation of a hypothetical magnitude 7.0 earthquake that begins on April 18, 2018, at 4:18 p.m. on the Hayward Fault at 8 kilometers (about 5 miles) depth beneath Oakland (see Aagaard, Boatwright, and others, this volume). In less than a minute, the Hayward Fault ruptures along more than 83 kilometers (about 52 miles) of its length, both northward toward San Pablo Bay and southward toward Fremont. The scenario mainshock generates ground offset along both the northern and southern parts of the fault. The HayWired mainshock is larger than the 1868 Hayward earthquake and produces strong ground shaking over a larger part of the San Francisco Bay region.

Determining and understanding the impacts of expected future large earthquakes requires realistic estimates of the ground shaking. The 3D computer simulations of strong ground shaking caused by the HayWired mainshock are an improvement over those based solely on ground-motion prediction equations that do not include the details of how the geology of the San Francisco Bay region affects earthquakes (see Porter, this volume). Strong ground shaking in general is primarily affected by three factors—(1) earthquake magnitude, (2) proximity of a site (such as a building) to an earthquake, and (3) the geologic conditions under a site. Additional important parts of the simulations of the HayWired mainshock are the 3D structure of the Earth's crust below the bay region, particularly the basins, and the incorporation of a factor to account for the fact that the Hayward Fault slowly moves (creeps) between large earthquakes. In the HayWired ground-shaking simulations, more than 40 percent of the San Francisco Bay region experiences shaking stronger than Modified Mercalli Intensity VII, a level of shaking that typically causes slight to moderate damage to better built structures and considerable damage to poorly built structures (fig. 2).

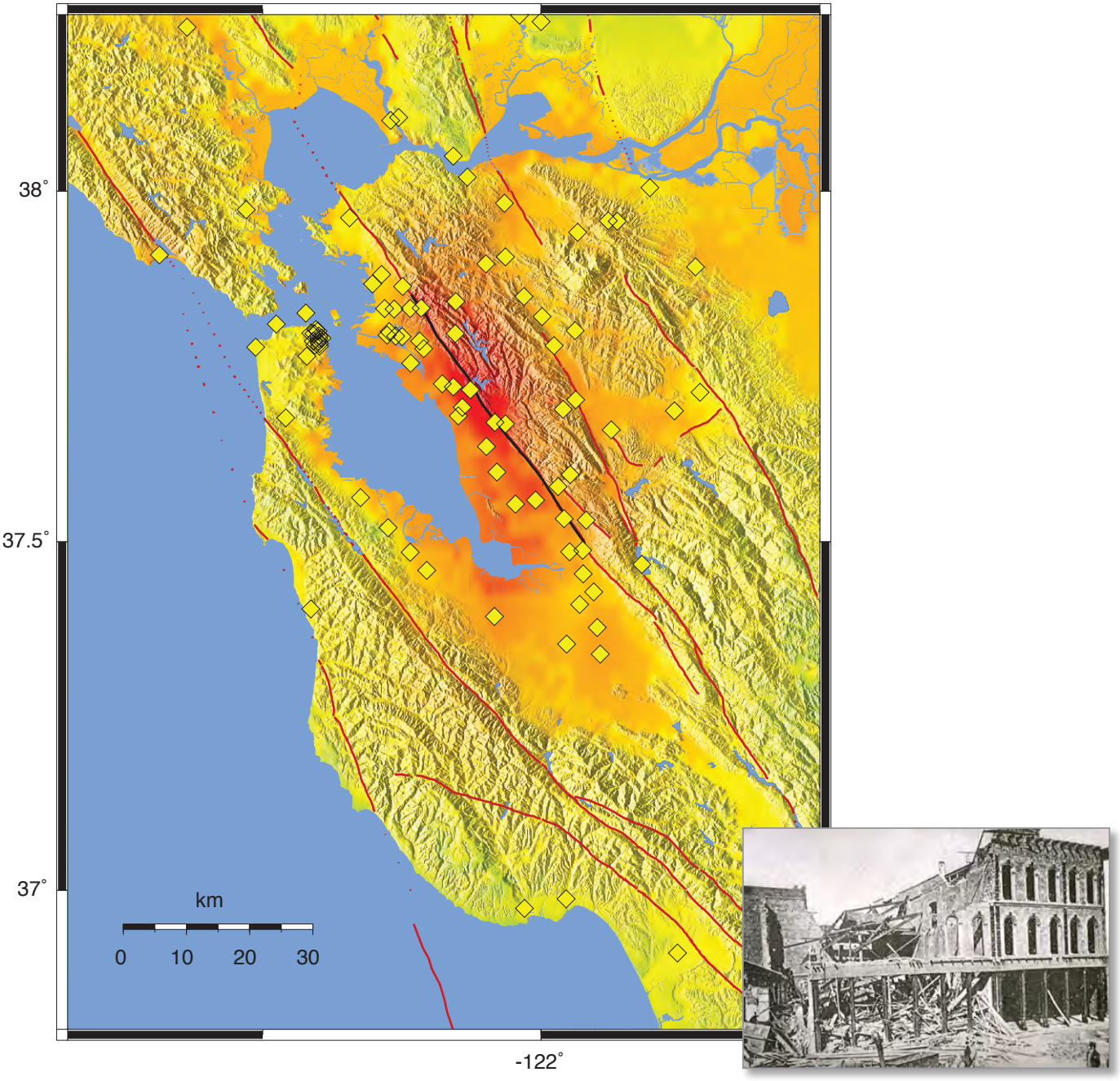

PERCEIVED SHAKING	Not felt	Weak	Light	Moderate	Strong	Very strong	Severe	Violent	Extreme
POTENTIAL DAMAGE	none	none	none	Very light	Light	Moderate	Moderate/Heavy	Heavy	Very Heavy
MMI	I	II-III	IV	V	VI	VII	VIII	IX	X+

Figure 1. U.S. Geological Survey ShakeMap of the San Francisco Bay region, California, showing the inferred intensity of ground shaking in the 1868 magnitude-6.8 Hayward earthquake (compare to fig. 2, which is for the larger, HayWired scenario mainshock) (figure modified from Boatwright and Bundock, 2008). Red lines are geologic faults; black line shows the part of the Hayward Fault that ruptured in 1868; diamonds show locations of 1868 damage reports used to infer the Modified Mercalli Intensity, MMI. The 1868 earthquake damaged or destroyed many buildings throughout the region and caused the deaths of about 30 people. The inset photograph shows one wrecked building in what is now San Francisco's Financial District (courtesy of the Karl V. Steinbrugge Collection, Earthquake Engineering Research Center, University of California, Berkeley). km, kilometer.

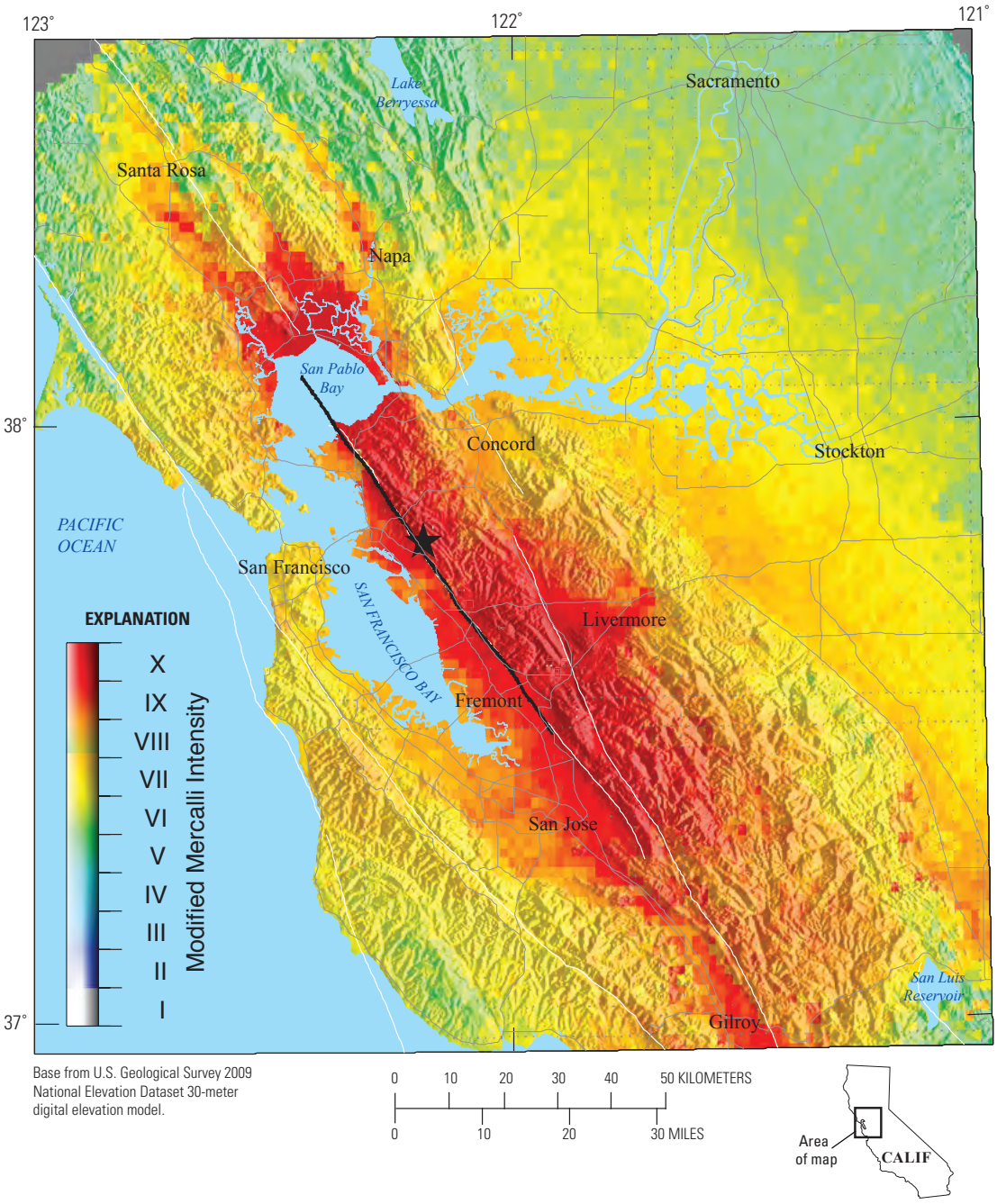

PERCEIVED SHAKING	Not felt	Weak	Light	Moderate	Strong	Very strong	Severe	Violent	Extreme
POTENTIAL DAMAGE	none	none	none	Very light	Light	Moderate	Mod./Heavy	Heavy	Very Heavy
PEAK ACC.(%g)	<0.05	0.3	2.8	6.2	12	22	40	75	>139
PEAK VEL.(cm/s)	<0.02	0.1	1.4	4.7	9.6	20	41	86	>178
INSTRUMENTAL INTENSITY	I	II-III	IV	V	VI	VII	VIII	IX	X+

Figure 2. Map of the San Francisco Bay region, California, showing simulated ground shaking caused by the hypothetical magnitude-7 mainshock of the HayWired earthquake scenario on the Hayward Fault. Ground shaking is colored to show how strong it is from a number of perspectives. These include the perceived shaking, the potential damage, the peak ground acceleration (peak acc.; relative to the percentage of the acceleration of gravity at the Earth surface, %g), the peak ground velocity (peak vel.; cm/s, centimeters per second), and the Instrumental Intensity (estimated Modified Mercalli Intensity). The Modified Mercalli Intensity describes how the earthquake is felt and its effects. The mainshock begins beneath the City of Oakland (star) and causes the Hayward Fault to rupture along 83 kilometers (about 52 miles; thick black line) of its length. Strong ground shaking occurs throughout the region. (Figure modified from Aagaard, Boatwright, and others, this volume.)

Fault Slip

The HayWired scenario mainshock causes slip (relative movement between opposite sides of a fault) along both the southern and northern parts of the Hayward Fault (see Aagaard, Schwartz, and others, this volume). The offset distance along the fault where the fault intersects the Earth's surface (called the fault trace) is of concern, because lifelines (for example, transportation infrastructure and buried utilities) and other structures that cross the fault need to be able to accommodate fault movement, both during and after a large earthquake. To examine fault-trace offset in the HayWired scenario, a variation of the HayWired scenario mainshock is used that assumes that sudden offset occurs along the Hayward Fault trace from San Pablo Bay to Fremont, with a maximum of more than 2 meters (m; about 7 feet) of offset in the San Pablo area. Longer duration slip on the fault, called afterslip, following the HayWired mainshock and its strong shaking is also calculated. Additional fault-trace offset, called afterslip, of as much as 0.5 to 1.5 m might occur along the Hayward Fault, with most of it occurring during the first months after the mainshock.

Liquefaction

A large earthquake on the Hayward Fault will cause liquefaction, especially in soft, water-saturated soils around the margins of San Francisco Bay (see Jones and others, this volume). Liquefaction is a type of earthquake-induced ground failure in which solid ground temporarily transforms into a softened or liquefied state during strong shaking. Liquefaction can cause severe damage to lifelines, as well as to structures and their foundations, as a result of settlement, spreading or lateral motions of the shallow soils, and damage to engineered structures such as embankments, levees, and dams.

For the HayWired scenario, the strong ground shaking during the hypothetical mainshock is used to estimate and map the likelihood of liquefaction in western Alameda and northern Santa Clara Counties (fig. 3). Information about how soils respond to strong ground shaking, data on the depth to the water table from the California Geological Survey, and geologic maps of the San Francisco Bay region showing deposits younger than 2.6 million years (Quaternary and younger) are used for the liquefaction estimates. In areas where insufficient soil-response information is available, the Federal Emergency Management Agency's (FEMA) HAZUS computer program is used to identify areas susceptible to liquefaction hazards.

For the HayWired scenario, the likelihood of liquefaction in western Alameda County is as much as 75 percent for some areas along major creeks and for areas of artificial fill near the margins of San Francisco Bay. The HayWired scenario also generates high liquefaction probabilities in the Quarry Lakes Regional Recreation Area in Fremont and at several places along Alameda Creek, Arroyo de la Laguna, and Arroyo Valle between Fremont and Livermore. The northern part of the western Alameda County shoreline, where most of the shoreline area is developed, such as the city shorelines of Alameda, Oakland, and Hayward, has a relatively high probability of liquefaction of 40–50 percent. In the Santa Clara Valley, liquefaction probability for the HayWired scenario reaches a high of about 50 percent, with 40–50 percent liquefaction probability around the southernmost part of San Francisco Bay and along the banks of the Guadalupe River and Coyote Creek.

Landslides

In the HayWired scenario, the hypothetical mainshock triggers landslides throughout the San Francisco Bay region (see McCrink and Perez, this volume). Calculations are made of the likely slope failures (landslides) generated by strong ground shaking in the 10-county region surrounding San Francisco Bay. Information is incorporated from geologic maps of the region, geologic-material strength parameters compiled by the California Geological Survey, and slope-gradient data at 10-m (about 33 feet) resolution calculated from the U.S. Geological Survey 2009 National Elevation Dataset. The analyses assume that slopes of hillsides are not water saturated.

The highest probabilities of landsliding in the HayWired scenario, greater than 32 percent, occur on steep to very steep slopes and on existing landslides (fig. 4). Lower probabilities of landsliding occur on moderate to gentle slopes in areas near the Hayward Fault that are subject to the strongest ground shaking and on steeper slopes with increasing distance from the fault that experience weaker ground shaking. For the HayWired scenario, the area of significant landsliding for loss-estimation purposes is where peak ground shaking during the magnitude-7 mainshock is expected to be greater than 20 centimeters per second (cm/s; about 8 inches per second). Most models that assess earthquake-triggering of landslides are primarily studies of landslide initiation and are not yet able to predict landslide runout, which is how far a landslide travels down a hillside.

Aftershocks

The magnitude-7 mainshock of the HayWired scenario is followed by aftershocks (Wein and others, this volume). Large earthquakes are sometimes viewed as standalone events; however, this is rarely, if ever, the case. Instead, large earthquakes are accompanied over the course of the subsequent minutes to years by additional nearby earthquakes (aftershocks), along with occasional, more distant "triggered" earthquakes. Aftershocks occur as a result of readjustments of the Earth's crust following an initial large earthquake.

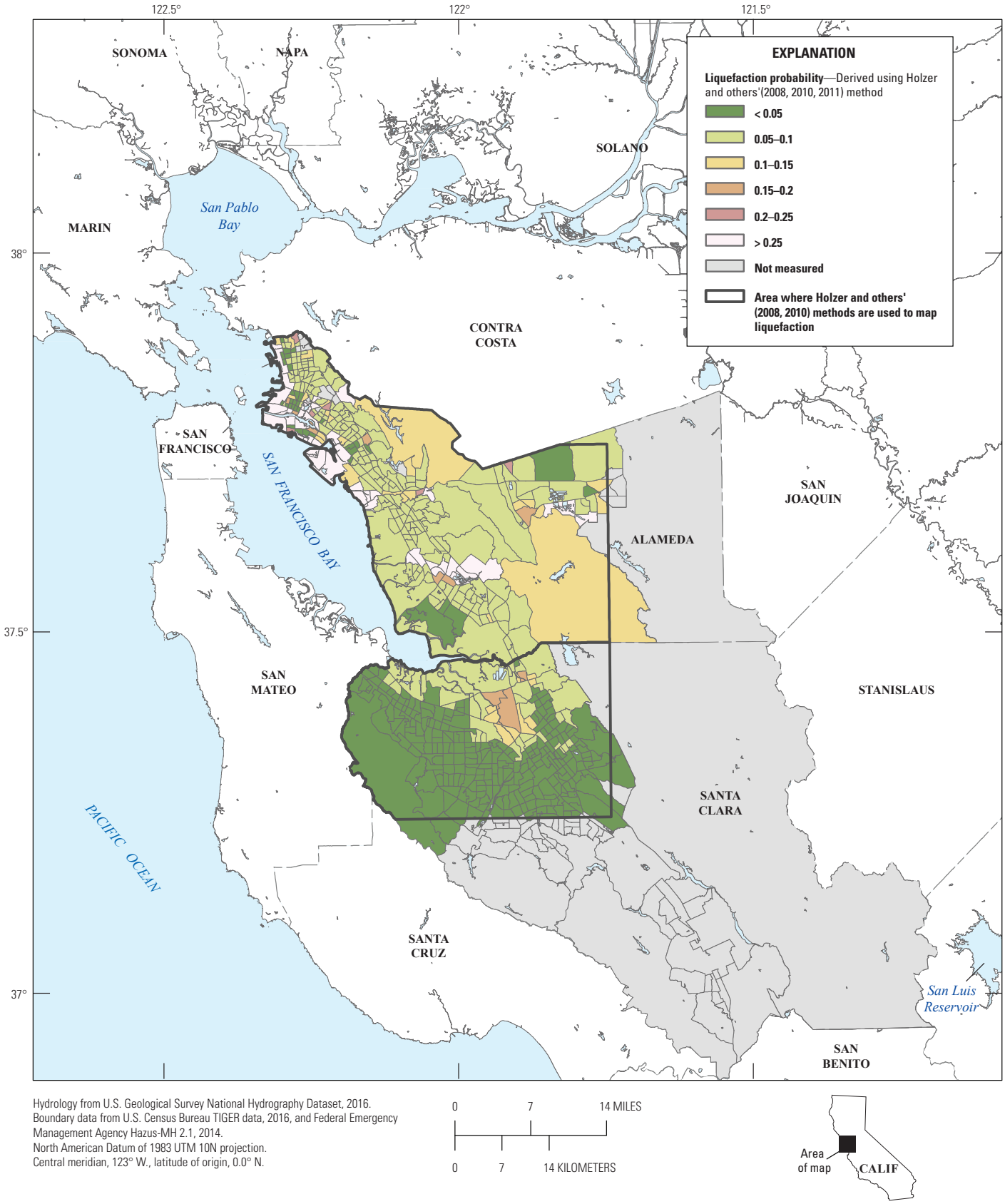

Figure 3. Map of the San Francisco Bay region, California, showing liquefaction (soils becoming liquid-like during shaking) probabilities for western Alameda and northern Santa Clara Counties as a result of strong ground shaking during the hypothetical magnitude-7 mainshock of the HayWired earthquake scenario on the Hayward Fault. <, less than; >, greater than. (From Jones and others, this volume.)

For the HayWired scenario, it is estimated that there is at least a 1-in-5 chance of a magnitude 6.4 or larger aftershock occurring in the months and years after the mainshock. Statistical methods based on decades of aftershock observations from around the world are used to simulate aftershock sequences during the first 2 years following the HayWired scenario mainshock. Although aftershocks generated by a Hayward Fault earthquake are expected to continue for much longer than 2 years, the 2-year aftershock timeline was chosen to match the recovery horizon of FEMA's San Francisco Bay Area Catastrophic Earthquake Plan.

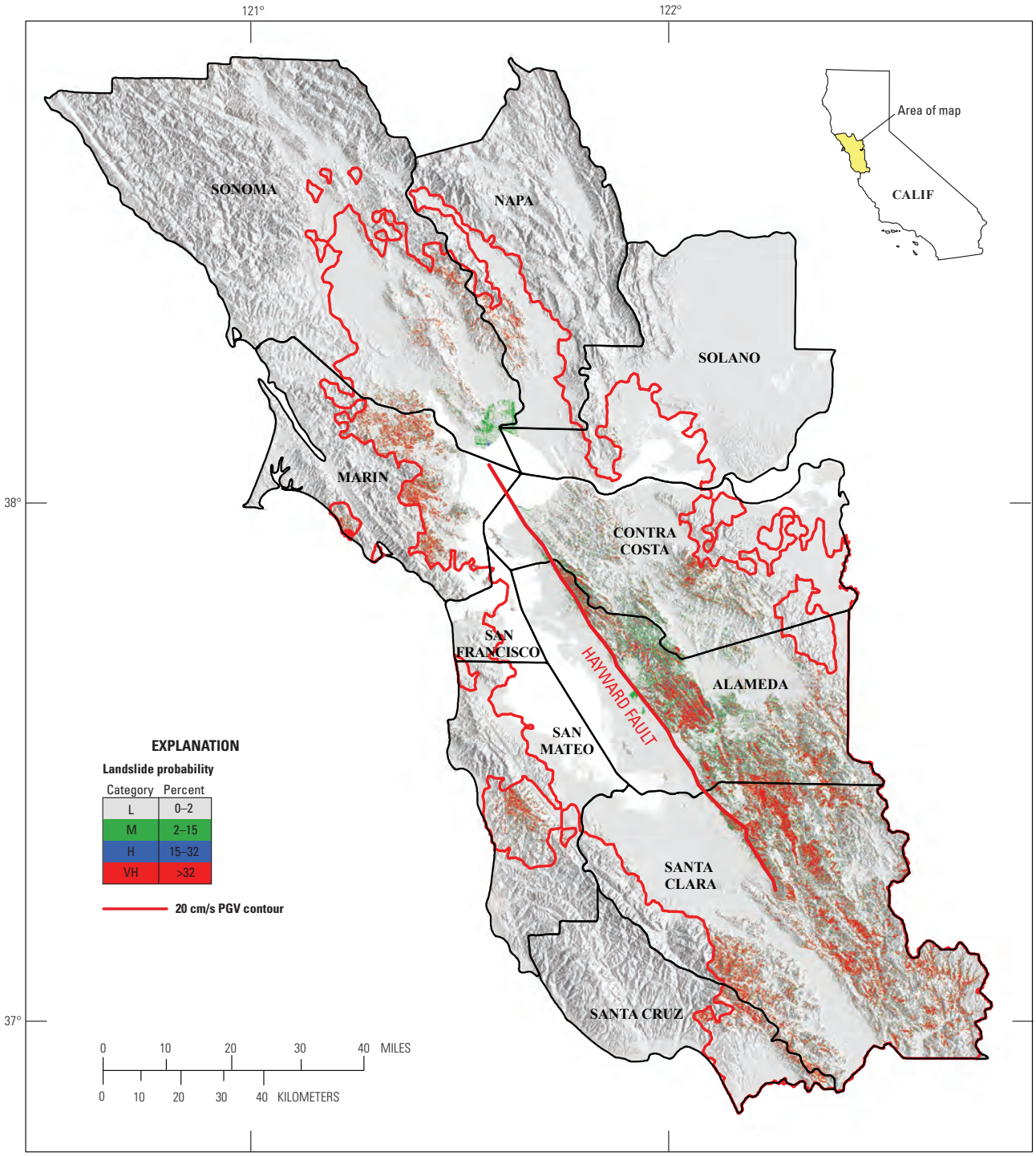

Base from U.S. Geological Survey 2009 National Elevation Dataset 10-meter digital elevation model showing land-surface elevations as shaded-relief. County boundaries from California Department of Forestry and Fire Protection, 2009.

Figure 4. Map of landslide probabilities for the 10-county San Francisco Bay region, California, resulting from shaking during the hypothetical magnitude-7 mainshock of the HayWired earthquake scenario on the Hayward Fault. The red contours outline areas where shaking (peak ground velocity, PGV) exceeds 20 centimeters per second (cm/s; about 8 inches per second). Landslide probability: L, low; M, medium; H, high; VH, very high. (Modified from McCrink and Perez, this volume.)

Aftershocks are modeled to occur after the HayWired scenario magnitude-7 mainshock. One particular feature of the HayWired aftershock estimation model is that it does not necessarily place the aftershocks on known geologic faults, instead they are placed based using statistical calculations alone. Because geologists think that large earthquakes do not randomly occur in space but instead occur on geologic faults, the largest HayWired scenario aftershocks, those greater than magnitude 6, are moved to nearby known faults (fig. 5).

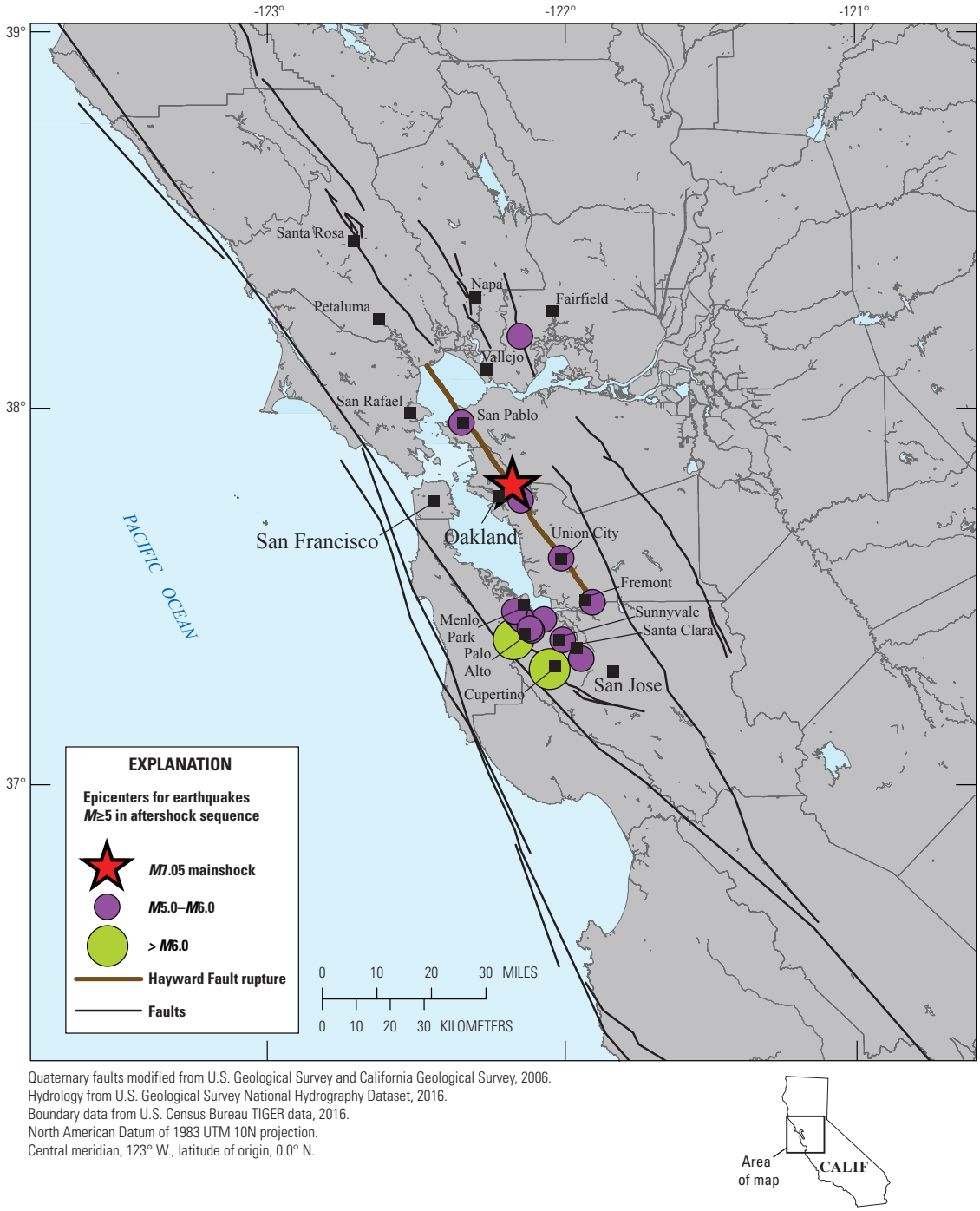

Figure 5. Map of the San Francisco Bay region, California, showing larger aftershocks of magnitude (*M*) 5 or greater following the hypothetical magnitude-7 mainshock of the HayWired earthquake scenario on the Hayward Fault. >, greater than. (From Wein and others, this volume.)

As expected based on assumptions of aftershock locations in general, most of the simulated HayWired aftershocks occur near the Hayward Fault. This is because the fault is the location of the HayWired scenario mainshock. However, the HayWired scenario does include some aftershock locations away from the Hayward Fault, including in the furthest reaches of the greater San Francisco Bay region. Many of the HayWired scenario aftershocks, especially the larger ones, would be potentially damaging and felt throughout the San Francisco Bay region.

Conclusion

This overview of The HayWired Earthquake Scenario—Earthquake Hazards volume summarizes the major findings by the authors of the individual chapters. Each set of authors has recommendations for future work. The recommendations range from follow-on studies of how creeping faults, such as the Hayward Fault, produce large earthquakes and subsequent fault offset to investigations of the response of soils to sudden ground shaking. For further, detailed information, see the individual chapters within this volume. As additional HayWired volumes are published, they will be made available at https://doi.org/10.3133/sir20175013.

References Cited

Aagaard, B.T., Blair, J.L., Boatwright, J., Garcia, S.H., Harris, R.A., Michael, A.J., Schwartz, D.P., and DiLeo, J.S., 2016, Earthquake outlook for the San Francisco Bay region 2014–2043 (ver. 1.1, August 2016): U.S. Geological Survey Fact Sheet 2016–3020, 6 p., accessed April 10, 2017, at http://dx.doi.org/10.3133/fs20163020.

Boatwright, John, and Bundock, Howard, 2008, Modified Mercalli Intensity Maps for the 1868 Hayward earthquake plotted in ShakeMap format: U.S. Geological Survey Open-File Report 2008–1121, accessed April 11, 2017, at https://pubs.usgs.gov/of/2008/1121/.

The HayWired Earthquake Scenario—Earthquake Hazards
Edited by Shane T. Detweiler and Anne M. Wein
Scientific Investigations Report 2017–5013–A–H
[Also see https://doi.org/10.3133/sir20175013]

Chapter C

HayWired Scenario Mainshock Ground Motions

By Brad T. Aagaard,[1] John L. Boatwright,[1] Jamie L. Jones,[1] Tim G. MacDonald,[1] Keith A. Porter,[2] and Anne M. Wein[1]

Abstract

The HayWired scenario examines a hypothetical earthquake (mainshock) with a moment magnitude (M_w) of 7.0 occurring on April 18, 2018, at 4:18 p.m. on the Hayward Fault in the east bay part of California's San Francisco Bay area. Determining and understanding the impacts of expected future large earthquakes requires realistic estimates of the ground shaking. The ground motions for the HayWired scenario mainshock come from a three-dimensional computer simulation of a magnitude 7.0 earthquake that incorporates (1) variability in fault slip over the complex geometry of the Hayward Fault, (2) the effects of starting the rupture at a specific point below the city of Oakland, and (3) propagation of the seismic waves through the complex geologic structure of the San Francisco Bay region. These effects give rise to a complex pattern of shaking. Some features are specific to the choice of parameters for this scenario, such as the starting location of the rupture and the distribution of slip over the fault surface. Others are more general as a result of known variations in the geologic structure that cause some areas to consistently have more intense shaking than others.

Introduction

The sudden slip of one side of a fault past the other releases strain energy by radiating seismic waves. When the waves reach the Earth's surface, we feel the passage of the seismic waves in the form of earthquake ground shaking. Strong shaking can throw people to the ground, cause ground failure (in the forms of cracks, liquefaction, landslides, and lateral spreading), and generates most of the earthquake damage to buildings, roads, pipelines and other structures. Thus, estimating the damage and other impacts of a large earthquake relies on accurate estimates of the ground motion.

Ground motions depend on three primary effects, as well as on additional smaller, but still significant, secondary effects. The first factor is **magnitude**—a bigger earthquake releases more strain energy, which means more energy is carried in the seismic waves. The earthquake magnitude depends on the length and depth of the fault that moves as well as the amount of slip. The second factor is **distance from the fault**. Because the radiated energy spreads over a greater volume as it propagates outward from the fault rupture, the amplitudes of the seismic waves decrease as they travel away from the fault. As a result, sites farther from the fault rupture tend to experience less intense shaking. The third factor is **soil conditions**—the characteristics of the soil or rock at a particular location affect the amplitude and duration of the shaking at that site. Softer soils, such as alluvial sediments that accumulate in basins and river valleys, generally cause stronger shaking than nearby rock, all other things being equal. The secondary factors include (1) **directivity**, in which ground motions are most focused in the direction of rupture propagation along the fault, (2) **radiation pattern**, variations in energy distribution that depend on the orientation of the rupturing fault and the direction of the slip, and (3) the **spatial variability in the amount of slip**, with stronger shaking surrounding parts of the fault where slip is greater.

To determine how structures respond to earthquake shaking, engineers quantify ground motion by several measures—peak horizontal ground acceleration (PGA), peak horizontal ground velocity (PGV), and, most commonly, 5-percent-damped spectral acceleration (SA) response at several periods of vibration, especially 0.3 second (s), 1.0 s, and 3.0 s. SA response can be thought of as the PGA measured at the roof of a building as a result of the ground shaking at its base. The period of vibration depends on the height of the building—approximately 0.3 s for a low-rise building, 1.0 s for a 12-story building, and 3.0 s for a 40-story building. In other words, a given ground motion having a SA of 0.5 the acceleration due to gravity (*g*) at a period of 1.0 s corresponds to measuring an acceleration of 0.5 *g* at the roof a 12-story building with the ground motion input at the building's base.

It is also common to express ground motion in the subjective terminology of the Modified Mercalli Intensity (MMI) scale. MMI is quantified based on damage and human response in an earthquake, but it can be estimated from the instrumental measurements of PGV and PGA. ShakeMaps, for example, depict MMI that are estimated from PGA and PGV and using ground-motion-to-intensity conversion equations (for example, Wald and others, 2005; Worden and others, 2012).

[1]U.S. Geological Survey.

[2]University of Colorado, Boulder.

HayWired Scenario Mainshock

The HayWired scenario examines a hypothetical earthquake (mainshock) with a moment magnitude (M_w) of 7.0 occurring on April 18, 2018, at 4:18 p.m. on the Hayward Fault in the east bay part of California's San Francisco Bay area. This scenario mainshock is a specific scenario (HS+HN G04 HypoO) from a suite of 39 scenario earthquakes for the Hayward Fault developed by Aagaard and others (2010a). The scenario parameters make use of the considerable geologic and geophysical data that have been collected over the past several decades. The scenario includes the three-dimensional (3D) geometry of the Hayward Fault based on mapping of its surface trace and location of microearthquakes at depth. The scenario earthquake rupture starts under the city of Oakland, with fault slip progressing north into San Pablo Bay and south to the city of Fremont (fig. 1). The slip varies over the fault with patches of high and low slip, consistent with observations from earthquakes on other faults. Additionally, the slip tapers in areas where other studies (for example, Funning and others, 2007) have imaged interseismic creep (slow, more or less continuous or episodic slip). Aagaard, Schwartz, and others (this volume) discusses the coseismic slip at the surface and an estimate of creep (afterslip) triggered by the mainshock rupture.

The 3D computer simulation solves the wave equation in a 250-kilometer (km)-long, 100-km-wide, and 40-km-deep region given the imposed slip on the fault. The U.S. Geological Survey (USGS) Bay Area Seismic Velocity Model 08.3.0 (Aagaard and others, 2010b) describes the properties in the 3D volume. The properties include the different geologic units and how the density and stiffness of those units vary from one another, as well as how they vary with depth. This complex geologic structure affects the seismic waves as they propagate. The amplitude of the motion increases in softer materials, and reflections and refractions occur as the waves encounter interfaces between different geologic units.

HayWired Scenario Mainshock Ground Motions

The ground motions from the simulation are characterized in terms of PGA, PGV, SA, and MMI in the form of a ShakeMap, which is available from the USGS ShakeMap website (U.S. Geological Survey, 2014). The simulation domain from Aagaard and others (2010a) does not span the entire 16-county region participating in the San Francisco Bay Area Earthquake Plan (California Governor's Office of Emergency Services, 2016), so ground-motion prediction equations (GMPEs) of Wald and others (2005) are used to extend the ShakeMap an additional 20 km to the north, 80 km to the south, 65 km to the west, and 45 km to the east (see appendix for details).

Figure 2 shows the Instrumental Intensity (an estimate of MMI) throughout the study region. Table 1 presents an abbreviated description of the effects of shaking for each level of intensity. More than 40 percent of the San Francisco Bay urban area experiences shaking stronger than MMI VII, which corresponds to slight to moderate damage in ordinary structures and considerable damage in poorly built or badly designed structures. The strongest shaking occurs near the fault rupture and decreases with distance. Additional features include (1) stronger shaking along the strike of the Hayward Fault both to the northwest and southeast away from the epicenter in Oakland as a result of rupture directivity, (2) amplification of motions in several sedimentary basins scattered about the San Francisco Bay region (especially the Livermore Basin, the Evergreen Basin east of San Jose, and the sedimentary basin underneath San Pablo Bay), and (3) variability in shaking at sites along the fault corresponding to the spatial variation in slip for this scenario (for example, the high intensities just north of the epicenter associated with a large slip patch at depth and lower intensities a little southeast of the epicenter in an area with lower than average slip at depth). Over the past 100,000 years, the region just east of the Hayward Fault has undergone substantially more deformation than the region just west of the fault. As a result, the material is less rigid and this leads to greater amplification east of the Hayward Fault compared to west of the Hayward Fault, despite having a much thinner sediment cover (Aagaard and others, 2010a).

We also expect local amplification of ground motions in the very thin, very soft bay mud and artificial fills around the margins of San Francisco Bay. The discretization of the simulation domain does not have sufficient resolution to capture these small-scale features that are less than a grid size. They are captured in an approximate way through site amplification factors (Graves and Pitarka, 2010) in postprocessing of the simulation ground motions using the same approach that is used in many ground-motion prediction equations. Furthermore, with a focus on capturing the variability in ground motion at the regional scale, the simulation output was captured on a 1/60-degree grid (spacing of approximately 2 km), so features smaller than 2 km in size are not resolved very well. Thus, the simulations capture site amplification associated with features larger than about 2 km in size but have poor resolution of amplification at smaller length scales.

Some details of the scenario rupture, such as the hypocenter and slip distribution, will likely be different in the next large Hayward Fault earthquake. To explore the associated uncertainty in ground shaking, Aagaard and others (2010a) considered variations in a variety of scenario parameters, such as hypocenter, slip distribution, rupture length, and magnitude, in their suite of 39 scenarios. Shorter rupture lengths resulting in smaller magnitude earthquakes reduce the amplitude of the ground motions. For example, in one of the M_w 6.8 scenarios, only 10 percent of the San Francisco Bay urban area is subjected to shaking as strong as MMI VII, compared to more than 40 percent for the HayWired scenario mainshock. Shifting the hypocenter away from the middle of the rupture toward either end increases the directivity and asymmetry in the shaking distribution, with larger motions in the direction the rupture propagates away from the hypocenter and smaller motions near the hypocenter (fig. 3). The distribution of slip also strongly affects the intensity of shaking along the length of the rupture. On the other hand, some ground-shaking patterns persist across the scenarios, most notably, the intense shaking and extended duration

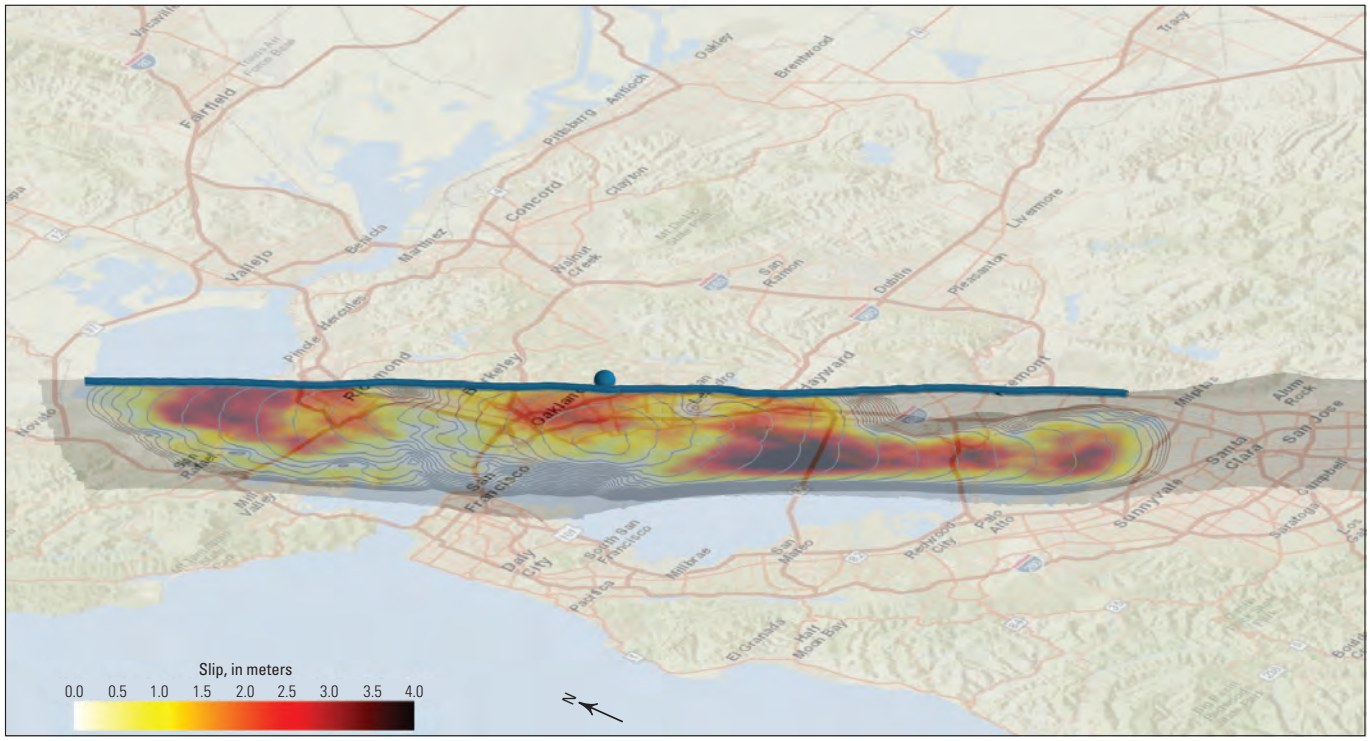

Base map © OpenStreetMap contributors, and the GIS User Community.

Figure 1. Map image of of the San Francisco Bay region, California, showing a three-dimensional perspective view of the slip distribution and rupture propagation on the Hayward Fault for the magnitude-7 mainshock of the HayWired earthquake scenario. The white-yellow-red-black colors show the distribution of slip on the Hayward Fault, and the gray contours show the leading edge of the fault slip propagation away from the hypocenter (rupture initiation point) at 1-second intervals. The thick blue line delineates the surface trace and the blue sphere identifies the epicenter.

Table 1. Effects of earthquake shaking intensity (reproduced from U.S. Geological Survey, 2015).

Intensity	Shaking	Description/Damage
I	Not felt	Not felt except by a very few under especially favorable conditions.
II	Weak	Felt only by a few persons at rest, especially on upper floors of buildings.
III	Weak	Felt quite noticeably by persons indoors, especially on upper floors of buildings. Many people do not recognize it as an earthquake. Standing motor cars may rock slightly. Vibrations similar to the passing of a truck. Duration estimated.
IV	Light	Felt indoors by many, outdoors by few during the day. At night, some awakened. Dishes, windows, doors disturbed; walls make cracking sound. Sensation like heavy truck striking building. Standing motor cars rocked noticeably.
V	Moderate	Felt by nearly everyone; many awakened. Some dishes, windows broken. Unstable objects overturned. Pendulum clocks may stop.
VI	Strong	Felt by all, many frightened. Some heavy furniture moved; a few instances of fallen plaster. Damage slight.
VII	Very strong	Damage negligible in buildings of good design and construction; slight to moderate in well-built ordinary structures; considerable damage in poorly built or badly designed structures; some chimneys broken.
VIII	Severe	Damage slight in specially designed structures; considerable damage in ordinary substantial buildings with partial collapse. Damage great in poorly built structures. Fall of chimneys, factory stacks, columns, monuments, walls. Heavy furniture overturned.
IX	Violent	Damage considerable in specially designed structures; well-designed frame structures thrown out of plumb. Damage great in substantial buildings, with partial collapse. Buildings shifted off foundations.
X	Extreme	Some well-built wooden structures destroyed; most masonry and frame structures destroyed with foundations. Rails bent.

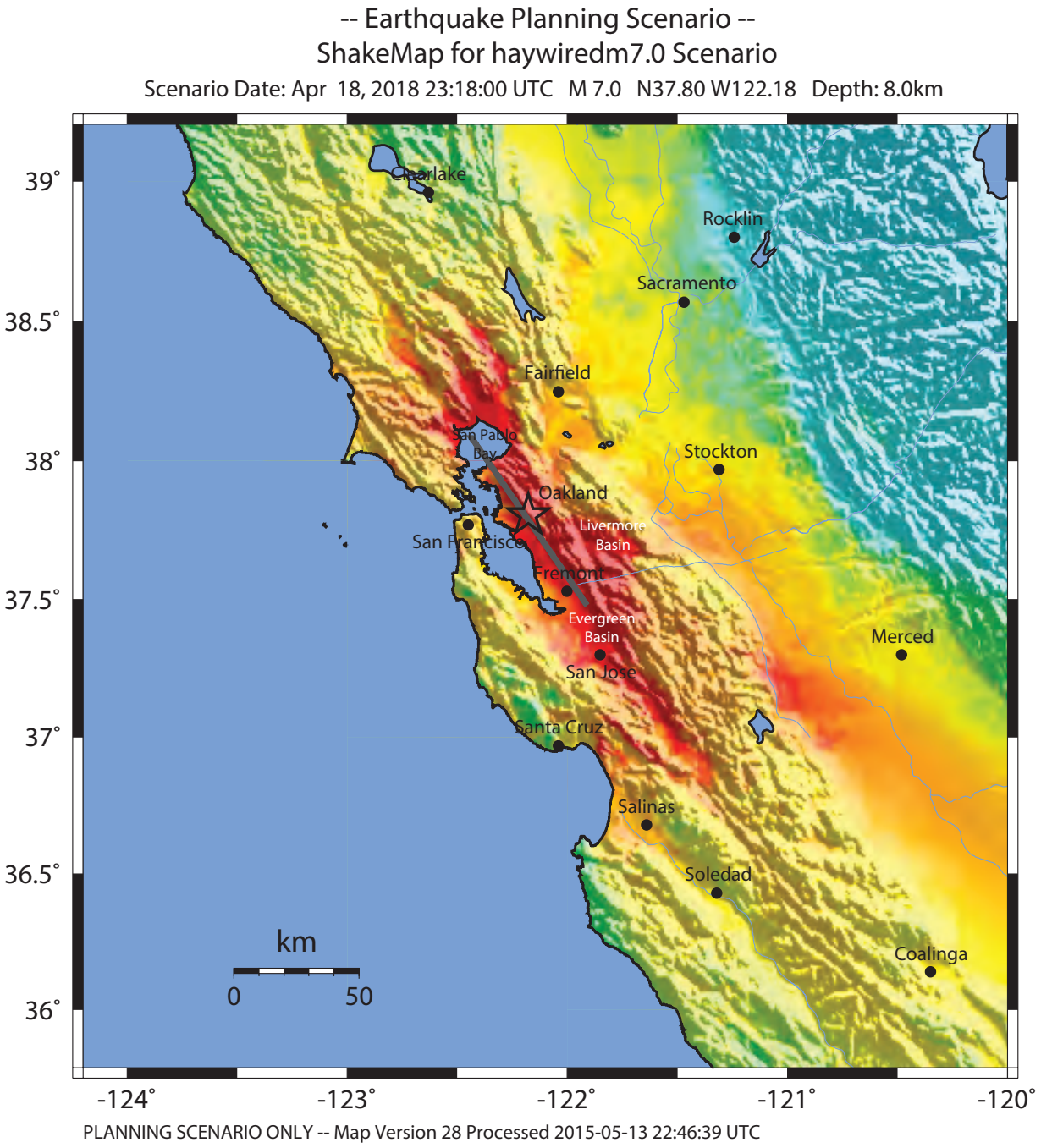

PERCEIVED SHAKING	Not felt	Weak	Light	Moderate	Strong	Very strong	Severe	Violent	Extreme
POTENTIAL DAMAGE	none	none	none	Very light	Light	Moderate	Mod./Heavy	Heavy	Very Heavy
PEAK ACC.(%g)	<0.05	0.3	2.8	6.2	12	22	40	75	>139
PEAK VEL.(cm/s)	<0.02	0.1	1.4	4.7	9.6	20	41	86	>178
INSTRUMENTAL INTENSITY	I	II-III	IV	V	V I	VII	VIII	IX	X+

Scale based on Worden and others, 2012.

Figure 2. ShakeMap of the San Francisco Bay region, California, showing instrumental intensity (estimated Modified Mercalli Intensity) for the magnitude-7 mainshock of the HayWired earthquake scenario. The earthquake ruptures the Hayward Fault in both directions from the hypocenter (star) under the City of Oakland. Shaking is amplified in the Livermore and Evergreen sedimentary basins. Figure modified (roadways removed) from U.S. Geological Survey (2014). See table 1 for explanation of intensity. km, kilometer; %g, percentage of acceleration due to gravity; cm/s, centimeter per second.

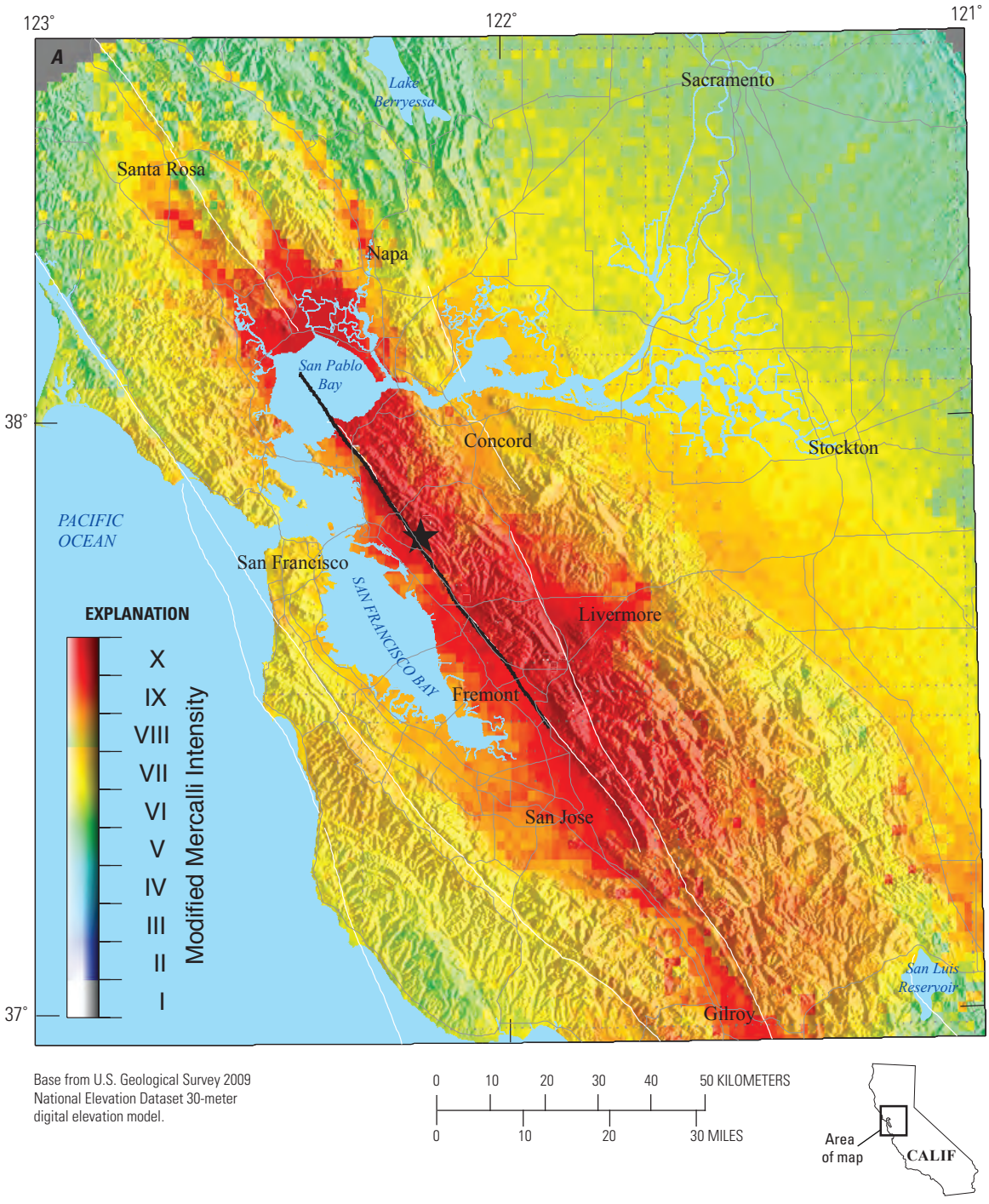

Figure 3. Maps of the San Francisco Bay region, California, showing instrumental intensity (estimated Modified Mercalli Intensity; see table 1) for the magnitude-7 mainshock of the HayWired earthquake scenario (*A*) and two alternative scenarios with different epicenters (indicated by the black stars) from Aagaard and others (2010b). The scenario in *B* has an epicenter in San Pablo Bay and directs more energy southeast along the fault, whereas the scenario in *C* with the Fremont epicenter directs more energy northwest along the Hayward Fault. The colors in *A* do not precisely match those in figure 2 due to slight differences in the rendering workflow. Hayward Fault rupture shown as black line.

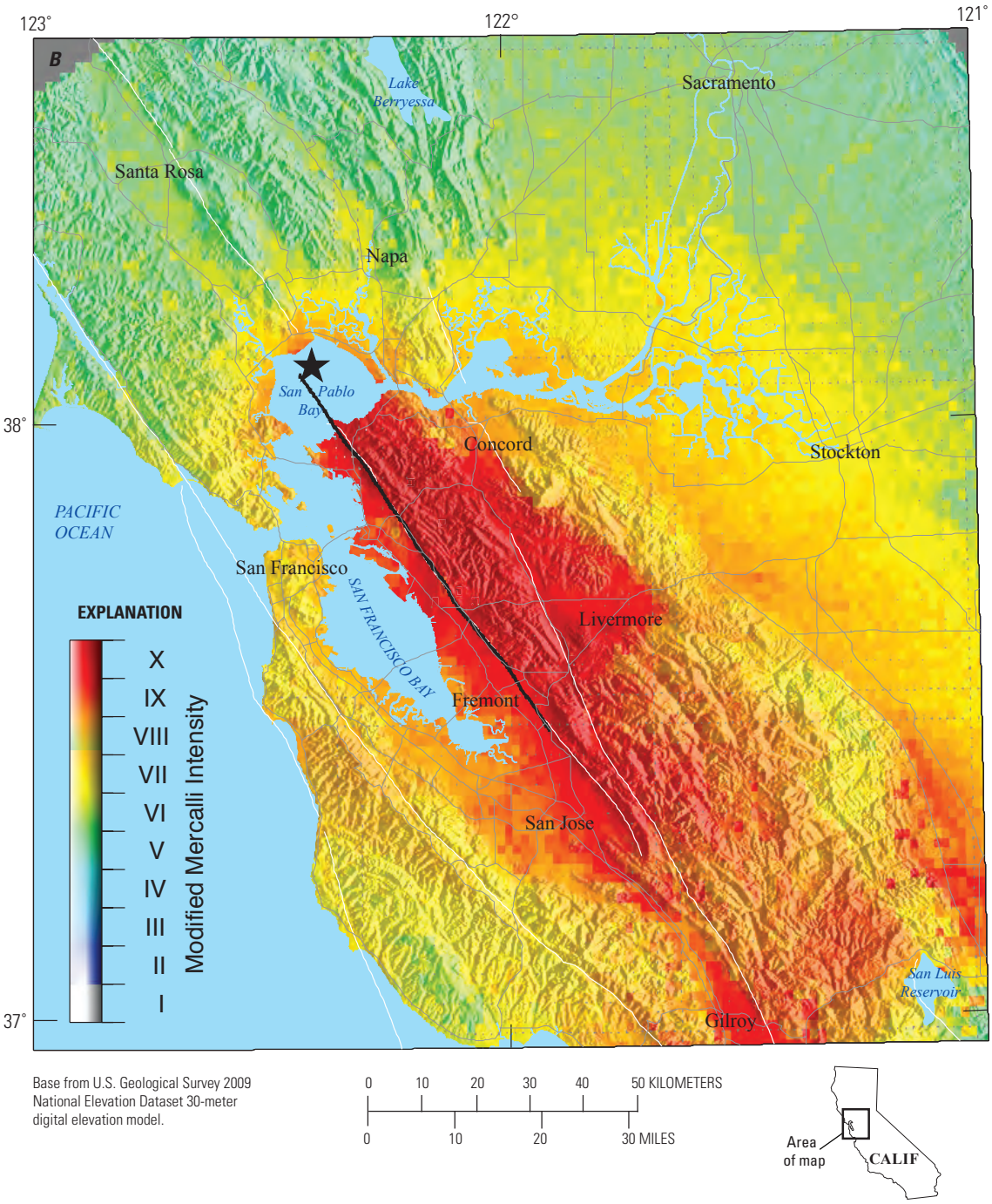

Figure 3.—Continued

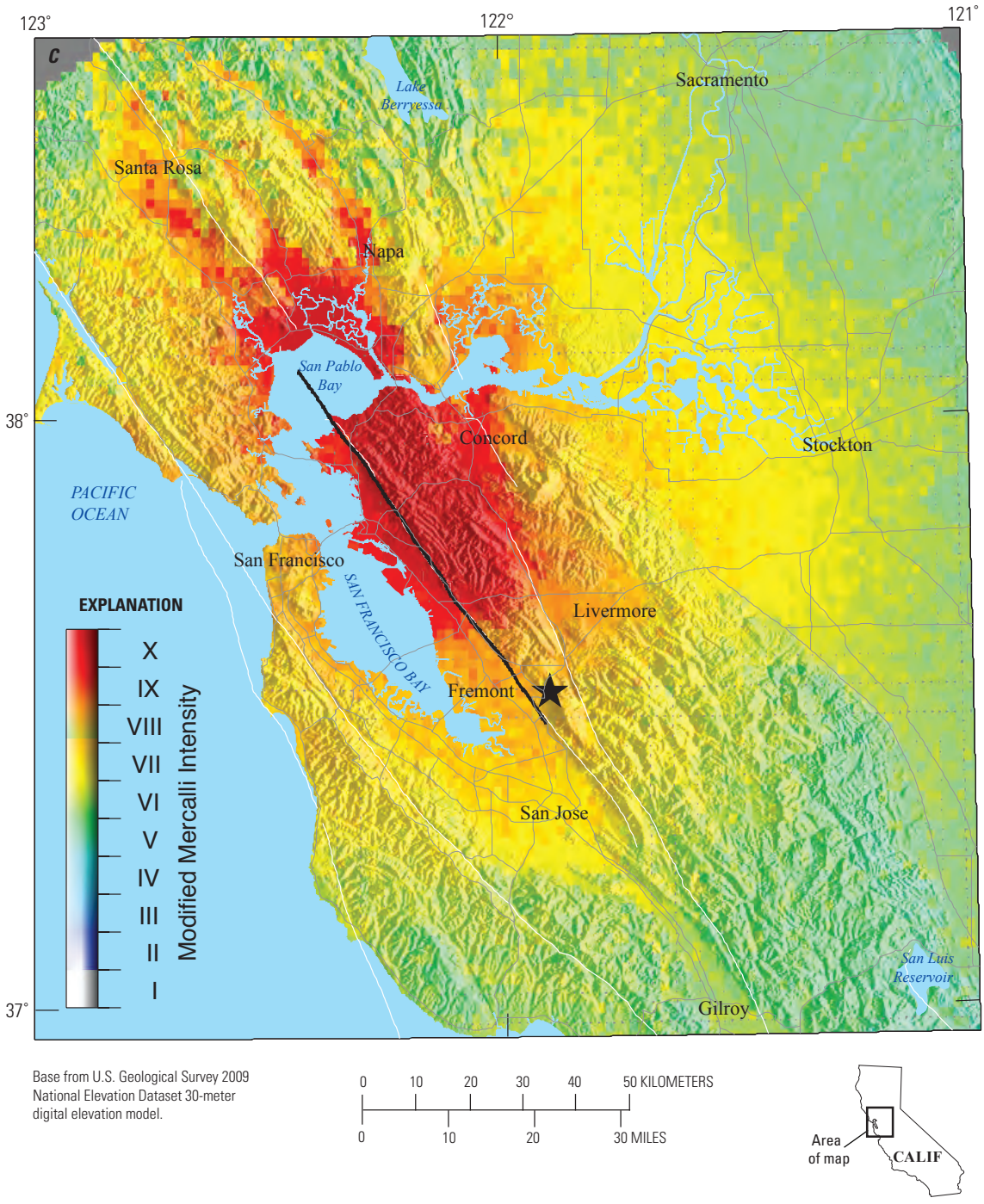

Figure 3.—Continued

of shaking in several sedimentary basins across the region, as mentioned earlier. See Aagaard and others (2010b) for a more detailed discussion of the potential variability in ground motions for large Hayward Fault earthquakes.

Knowledge Gaps and Modeling Limitations

To more fully understand the effects of future large earthquakes of the Hayward Fault, the following knowledge gaps and modeling limitations need to be addressed:

- We need additional scientific studies of the Hayward Fault to better understanding how observations of interseismic creep (slow, more or less continuous or episodic slip) can be used to improve forecasts of future large earthquakes and the resulting ground motions for the Hayward Fault.
- The HayWired scenario mainshock ground-motion simulation uses a coarse and generic representation of the soil properties based on the time-averaged shear-wave velocity to a depth of 30 meters (V_{S30}) mapping of Wills and others (2000). For example, very soft soil translates to a V_{S30} of 180 meters per second in this mapping. The ground-motion simulation methods may not accurately capture the nonlinear seismic response of very soft soils, and the nonlinear effects depend on many factors including the amplitude and frequency of the motion. As a result, it is difficult to predict whether the simulations underestimate or overestimate the amplitude of the ground motion in very soft soils. Site-specific investigations with detailed local geologic information need to be used to evaluate the seismic hazard in these regions.
- The realistic distribution of shaking for the HayWired scenario mainshock computed using a 3D computer simulation is fundamentally different from those based solely on median values from GMPEs. The GMPEs correspond to the median expected value of ground motion based on the collected history of observed earthquake ground motions. As a result, GMPEs include an average of the effects of the rupture propagation, variability in the spatial distribution of slip, and complex interactions with the local geology. These median-based distributions of shaking lack the spatial variability produced in real earthquakes and sophisticated scenarios, such as the HayWired mainshock, that are needed to accurately forecast damage (see Porter, this volume).
- A single scenario, such as HayWired, is not a basis for probabilistic design. Future studies may provide additional realizations of specific scenarios within a probabilistic framework to provide localized ground-motion models for design (for example, Graves and others, 2010).

Conclusion

The ground motions for the mainshock of the HayWired earthquake scenario are a product of a sophisticated 3D computer simulation that includes a realistic distribution of slip on the complex geometry of the Hayward Fault and propagation of the seismic waves through the 3D geologic structure surrounding the fault. The resulting ground motions exhibit significant variability across the San Francisco Bay region and highlight the ability to capture complex interactions between the propagating fault rupture and the 3D geologic structure, especially sedimentary basins. Detailed ground-motion simulations like the HayWired scenario mainshock play an important role by providing the essential information for assessing and mitigating the risk to buildings, bridges, pipelines, and other infrastructure associated with damaging earthquakes. They also provide crucial inputs for estimating ground failure (liquefaction, landslides, and lateral spreading) used in making decisions about land use and land remediation.

Acknowledgments

We thank the USGS National Earthquake Information Center for making the HayWired mainshock ShakeMap available in the ShakeMap Scenario Archive. Sarah Minson and Peggy Hellweg provided helpful feedback on an early version of the manuscript.

References Cited

Aagaard, B.T., Graves, R.W., Schwartz, D.P., Ponce, D.A., and Graymer, R.W., 2010a, Ground-motion modeling of Hayward Fault scenario earthquakes, part I—Construction of the suite of scenarios: Bulletin of the Seismological Society of America, v. 100, no. 6, p. 2927–2944.

Aagaard, B.T., Graves, R.W., Rodgers, A., Brocher, T.M., Simpson, R.W., Dreger, D., Petersson, N.A., Larsen, S.C., Ma, S., and Jachens, R.C., 2010b, ground-motion modeling of Hayward Fault scenario earthquakes, part II—Simulation of long-period and broadband ground motions: Bulletin of the Seismological Society of America, v. 100, no. 6, p. 2945–2977.

Boore, D.M., and Atkinson, G.M., 2008, Ground-motion prediction equations for the average horizontal component of PGA, PGV, and 5%-damped PSA at spectral periods between 0.01 s and 10.0 s: Earthquake Spectra, v. 24, no. 1, p. 99–138.

California Governor's Office of Emergency Services, 2016, Bay Area earthquake plan—July 2016: California Governor's Office of Emergency Services, accessed August 25, 2016, at http://www.caloes.ca.gov/for-individuals-families/catastrophic-planning.

Funning, G.J., Bürgmann, R., Ferretti, A., and Novali, F., 2007, Asperities on the Hayward fault resolved by PS-InSAR, GPS and boundary element modeling: Eos (Transactions of the American Geophysical Union), v. 88, no. 52, S23C-04.

Graves, R.W., and Pitarka, A. 2010, Broadband ground-motion simulation using a hybrid approach: Bulletin of the Seismological Society of America, v. 100, no. 5A, p. 2095–2123, doi: 10.1785/0120100057.

Graves, R., Jordan, T.H., Callaghan, S., Deelman, E., Field, E., Juve, G., Kesselman, C., Maechling, P., Mehta, G., Milner, K., Okaya, D., Small, P., and Vahi, K., 2010, CyberShake—A physics-based seismic hazard model for southern California: Pure Applied Geophysics, v. 168, no. 3–4, p. 367–381, doi: 10.1007/s00024-010-0161-6.

U.S. Geological Survey, 2014, Earthquake planning scenario—ShakeMap for Haywired M7.05-scenario: U.S. Geological Survey web page, accessed August 25, 2016, at https://earthquake.usgs.gov/scenarios/eventpage/ushaywiredm7.05_se#shakemap?source=us&code=gllegacyhaywiredm7p05_se.

U.S. Geological Survey, 2015, The Modified Mercalli Intensity scale: U.S. Geological Survey web page, accessed August 25, 2016, at https://earthquake.usgs.gov/learn/topics/mercalli.php.

Wald, D., Worden, B., Quitoriano, V., and Pankow, K., 2005, ShakeMap Manual: technical manual, users guide, and software guide: U.S. Geological Survey Techniques and Methods 12–A1, ver. 1.0, accessed August 25, 2016, at https://pubs.usgs.gov/tm/2005/12A01/.

Wills, C., Petersen, J.M., Bryant, W.A., Reichle, M., Saucedo, G.J.,Tan, S., Taylor, G., and Treiman, J., 2000, A site-conditions map for California based on geology and shear-wave velocity: Bulletin of the Seismological Society of America, v. 90, no. 6B, p. S187–S208, doi 10.1785/0120000503.

Worden, C.B., Gerstenberger, M.C., Rhoades, D.A., and Wald, D.J., 2012, Probabilistic relationships between ground-motion parameters and Modified Mercalli Intensity in California: Bulletin of the Seismological Society of America, v. 201, no. 1, p 204–221, doi: 10.1785/0120110156.

Appendix

This appendix provides details on extrapolating the simulated ground motions for the *M*7.0 mainshock of the HayWired earthquake scenario to a larger region. The ground-motion parameters are extrapolated for a grid of points (spaced at about 1.6-km intervals) outside of the simulation region using median expected ground motions according to the following procedure:

1. For a point outside the simulation model extent, a transect line is drawn between it and the earthquake epicenter (fig. A1); each point has a unique transect.
2. Along the transect a 20×20-km area is constructed on the border of the inside edge of the simulated model extent, such that the transect bisects that area (green square in fig. A1);
3. Within the 20×20-km area, the average difference between the simulated ground-motion value (for example, PGA, PGV, SA03) and the median motions estimated by the Boore and Atkinson (2008) ground-motion prediction equation is calculated;
4. The median ground motion value for the point outside the model extent is adjusted by the difference calculated in step 3 for the 20×20-km area.

This results in estimates of the ground motions outside the simulation domain having the expected decrease in amplitude with distance and local site effects captured in the ground-motion prediction equation while retaining consistency with the ground motions predicted by the simulation at its edges.

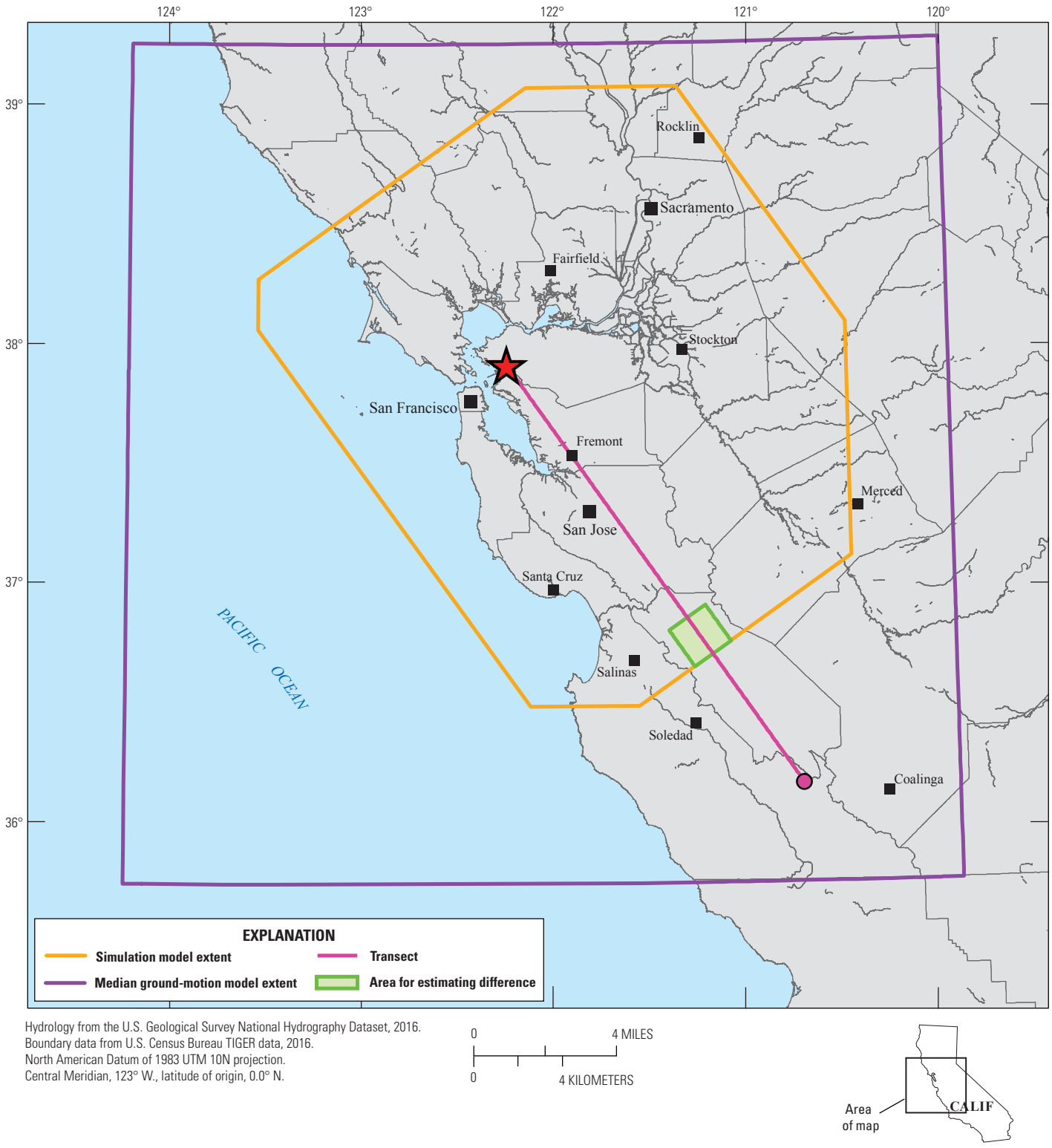

Figure A1. Map of the San Francisco Bay region, California, showing earthquake-simulation extent, median ground-motion extent, and one transect from the mainshock epicenter of the HayWired earthquake scenario to a point outside the simulation extent. The median ground-motion values for the point outside the simulation extent are adjusted by adding the average difference in ground-motion values in the square area to dovetail the median ground-motion data with the simulated data.

The HayWired Earthquake Scenario—Earthquake Hazards
Edited by Shane T. Detweiler and Anne Wein
Scientific Investigations Report 2017–5013–A–H
[Also see https://doi.org/10.3133/sir20175013]

Chapter D

HayWired Scenario Mainshock Coseismic and Postseismic Surface Fault Slip

By Brad T. Aagaard, David P. Schwartz, Anne M. Wein, Jamie L. Jones, and Kenneth W. Hudnut

Abstract

The HayWired scenario examines a hypothetical earthquake (mainshock) with a moment magnitude (M_w) of 7.0 occurring on April 18, 2018, at 4:18 p.m. on the Hayward Fault in the east bay part of California's San Francisco Bay area. Earthquake shaking produces damage, and so can fault slip at the ground surface. The HayWired scenario mainshock includes slip on the Hayward Fault during the earthquake rupture, as well as longer duration slip on the fault, called afterslip. When fault slip occurs suddenly during an earthquake rupture, or over a longer duration after the earthquake rupture, it can damage facilities and systems straddling the fault, such as buildings, pipelines, electrical transmission lines, roads, bridges, and tunnels. Because much of the length of the HayWired scenario mainshock fault rupture breaks through a highly developed area, we give special consideration to the amount, extent, and severity of the fault slip during dynamic earthquake rupture along the Hayward Fault, as well as to the amount and duration of subsequent fault afterslip.

Introduction

When a fault ruptures in a large shallow crustal earthquake, the two sides of the fault slip relative to each other, and this slip rupture commonly propagates to the surface during the earthquake. Surface slip is the measurement of the slip (relative displacement of formerly adjacent points on opposite sides of a fault) at the ground surface. Fault slip may occur suddenly during an earthquake (coseismic slip); continue to occur gradually in the days, weeks, months, and even years that follow an earthquake (postseismic slip or afterslip); or occur very slowly between earthquake events (interseismic fault creep). Afterslip (postseismic slip) is an accelerated form of fault creep. All three types of fault slip (coseismic slip, afterslip, and interseismic slip) are an engineering concern for manmade structures that cross the surface traces of active faults, although in most cases postseismic and interseismic slip are negligible.

The HayWired scenario examines a hypothetical earthquake (mainshock) with a moment magnitude (M_w) of 7.0 occurring on April 18, 2018, at 4:18 p.m. on the Hayward Fault in the east bay part of California's San Francisco Bay area. The Hayward Fault behaves differently from many other faults; it accommodates part of its long-term surface slip through interseismic fault creep. Many cultural features along the fault, such as roadways, curbs, utility pipelines, and buildings, have been deformed or offset by creep at the surface (McFarland and others, 2009). This is in contrast to a locked fault that lacks interseismic surface creep. On most locked faults the long-term geologic surface slip occurs almost entirely as coseismic slip. Because the Hayward Fault creeps, and accelerated surface creep on the Hayward Fault was observed in the town of Haywards (now called Hayward) following the 1868 magnitude (M) 6.8 earthquake (Lawson, 1908; Lienkaemper and others, 1991) and near Oakland following a 2007 M4.2 earthquake (Lienkaemper and others, 2012), we expect that afterslip will also occur following for the next large earthquake on the Hayward Fault. On faults with interseismic surface creep, it is not uncommon for afterslip to account for more than half the total fault offset; afterslip of this nature was observed from the 1976 M7.5 Guatemala (Bucknam and others, 1978), the 1987 M6.6 Superstition Hills, California (Sharp and others, 1989); the 2004 M6.0 Parkfield, California (Lienkaemper and others, 2006); the 2009 M6.3 L'Aquila, Italy (Wilkinson and others, 2010); and the 2014 M6.0 South Napa, California, (Lienkaemper and others, 2016; Hudnut and others, 2014) earthquakes.

Like aftershocks, the longer duration phenomenon of afterslip is associated with relaxation of the Earth's crust following the strong shaking and rapid release of energy in the earthquake mainshock. Afterslip is related to coseismic slip in much of the same way that aftershocks are related to the mainshock. For a large Hayward Fault earthquake, we expect that utilities and transportation infrastructure, as well as commercial buildings and homes, that straddle the fault will be damaged by coseismic slip and will continue to be seriously affected by afterslip, especially in areas where afterslip fills in deficits of coseismic slip (Aagaard and others, 2012). Afterslip interferes with efforts to make needed repairs in the hours and days following a large earthquake and

during longer-term reconstruction. For example, afterslip following the 2014 South Napa earthquake continued to twist roads, foundations, and curbs as much as a year after the mainshock (Hudnut and others, 2014; Lienkaemper and others, 2016). Water distribution lines were broken and remained threatened by afterslip; the City of Napa reported a complex pattern of ongoing breaks over a period that lasted several weeks after the earthquake (Buehrer, 2015). After the California Department of Transportation (Caltrans) initially patched the Highway 12 road surface across the coseismic surface rupture on the south section of the fault, they needed to repatch it within 5 days (Lienkaemper, written commun., 2016). The South Napa afterslip also occurred near homes; faulting ruptured directly through the foundations of about 100 homes in the Browns Valley section of the City of Napa. The homeowners faced the dual dilemma of replacing their slab foundation and possibly having to replace it again in the future. We expect similar situations along the Hayward Fault, with a larger earthquake resulting in a longer duration of afterslip and creating longer term effects on repair and recovery of cross-fault infrastructure than the 1-year effects of the rapid slip that occurred after the South Napa earthquake (Lienkaemper and others, 2016).

Mainshock Rupture and Coseismic Slip

The distribution of slip for the HayWired scenario mainshock rupture accounts for the various places along the Hayward Fault where interseismic fault creep has been observed. The creeping regions and their spatial distribution over the fault likely influence the partitioning of the long-term geologic slip into interseismic creep, coseismic slip, and afterslip. Consequently, estimating the slip along the Hayward Fault involves understanding how the creeping regions affect the coseismic-slip distribution and how much afterslip occurs at a site. Aagaard and others (2010) developed a simple model for estimating reduced coseismic slip in areas with interseismic creep imaged by Funning and others (2007). Because the interseismic creep rate in these areas is less than the long-term geologic slip rate for the Hayward Fault, the HayWired scenario mainshock (scenario HS+HN G04 HypoO in Aagaard and others, 2010) has some coseismic slip occurring in these areas with interseismic creep.

The HayWired scenario mainshock has fault rupture for a distance of 83 kilometers (km) from San Pablo Bay in the north extending south through the City of Fremont (fig. 1). In the scenario, coseismic slip exceeds 2 meters (m) in the San Pablo area, it decreases through Richmond and Berkeley with some sections of the rupture having less than 0.25 m of slip, and the amount of coseismic surface offset increases to more than 1 m from Berkeley to Oakland and again from just south of the epicenter to Hayward. At Hayward, the slip drops to less than 0.5 m, and there is no coseismic surface faulting along the southern 22 km of the fault rupture. Approximately 63 km of the rupture is on land. In contrast to the ShakeOut scenario on the southern San Andreas Fault (Jones and others, 2008), which ruptured through mostly rural

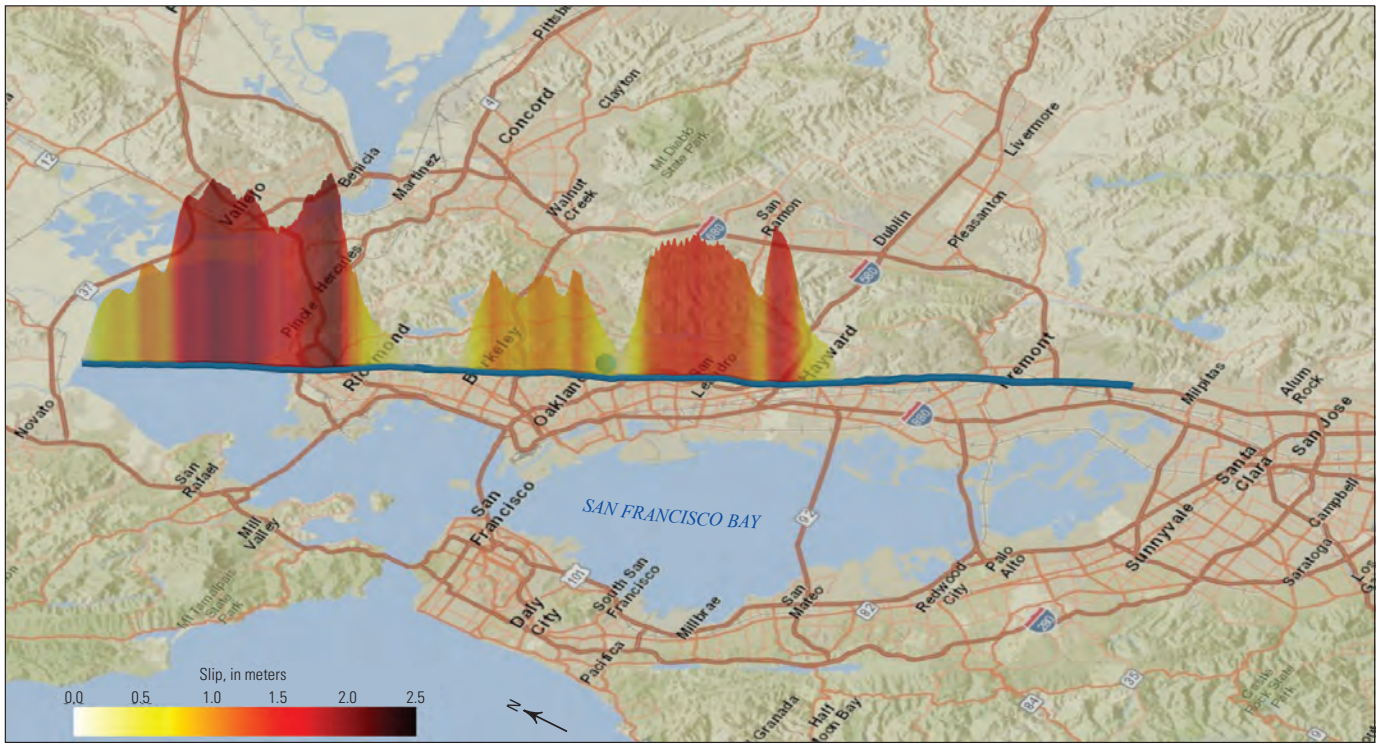

Base map © OpenStreetMap contributors, and the GIS User Community.

Figure 1. Map image of of the San Francisco Bay region, California, showing a three-dimensional perspective view of coseismic surface slip along the fault rupture for the magnitude-7 mainshock of the HayWired earthquake scenario. The colors and height show the amount of slip. The thick blue line denotes the length of the fault rupture (including subsurface slip) and the green sphere in Oakland identifies the scenario mainshock epicenter.

areas, the HayWired scenario mainshock ruptures through populated areas. Referring to the 2011 National Land Cover Database (Homer and others, 2015), approximately 43 percent of the land cover disturbed by the Hayward Fault rupture is classified as developed (table 1); nearly half of the surface rupture is passing through residential or commercial areas. The percentage of open water (table 1) reflects the extension of surface fault rupture into San Pablo Bay.

The slip distribution for the HayWired scenario mainshock is one possible realization for a large earthquake rupture on the Hayward Fault. The spatial distribution of slip could be significantly different in the next large Hayward Fault earthquake and likely varies from earthquake to earthquake. For example, such an event might have greater slip along the southern Hayward Fault compared to the northern Hayward Fault. This slip would be consistent with paleoseismic interpretations of past coseismic slip on the fault in the Fremont area (Lienkaemper and others, 1999; Lienkaemper and others, 2002; Lienkaemper and others, 2010). The initial distribution of coseismic surface slip plays an important role in determining the amount of afterslip that is likely to occur at any location along the fault.

Table 1. Land cover in the San Francisco Bay region, California, disturbed by coseismic slip along the Hayward Fault during the magnitude-7 mainshock of the HayWired earthquake scenario.

[%, percent]

Land-cover class	Percentage of land cover along mainshock fault rupture with measurable coseismic slip
Open water	25
Developed, open space	24
Developed, low density[1]	19
Developed, medium density[2]	22
Developed, high density[3]	2
Forest, scrub, grassland, wetlands	8

[1]Low-density developed often corresponds with single-family residential areas and is a mix of impervious surface and vegetation (20–49% impervious).

[2]Medium-density developed is commonly single-family residential with 50–79% impervious surface.

[3]High-density developed includes multifamily housing and commercial areas; 80–100% impervious surface is found in these areas.

Distributed or Off-Fault Deformation

In addition to estimating the amount of expected coseismic surface slip, another aspect of slip is the degree to which it is concentrated along the main fault trace (or in a narrow zone about it) or is partially distributed across a zone that could be many tens to hundreds of meters (or even kilometers) wide at various points along the rupture. This distributed deformation can occur as warping, within a few to a few tens of meters of the main fault trace, or as discrete fractures. Discrete fractures are usually located within several hundred meters of the main trace and have a smaller amount of slip. Some controls on the amount of deformation that may occur include: changes in fault geometry, the thickness of the sedimentary fill that the rupture propagates through, and the degree of smoothness (maturity) of the fault.

Distributed deformation has long been recognized. Lawson (1908) noted locations along the San Andreas Fault rupture in the 1906 San Francisco earthquake where fence lines across the fault were displaced by multiple fault traces across zones as much as 115 m wide. Petersen and others (2011) summarize distributed faulting from eight well-mapped strike-slip surface ruptures that include the 1968 Borrego Mountain (California), 1979 Imperial Valley (California), 1987 Superstition Hills (California), 1992 Landers (California), 1995 Kobe (Japan), 1999 Hector Mine (California), 1999 Izmit (Turkey), and 1999 Duzce (Turkey) earthquakes. They show that for these ruptures, distributed faulting occurs primarily within a couple of hundred meters to as far as 2 km from the main fault trace and that the potential for the occurrence of distributed-fault displacement decreases as a function of distance from the main trace.

Analysis of the 200-km surface rupture from the 2013 *M*7.7 Balochsitan, Pakistan, earthquake provides a recent example of the along-strike variation of off-fault deformation. Using pre- and post-event satellite optical images of the rupture, Gold and others (2015) measured on-fault (within 10 m), midfield (<350 m), and far-field (distances >350 m) deformation. Gold and others (2015) conclude that, on average, 28 percent of the surface slip occurred off-fault with significant along-strike variability, although nearly 100 percent of the total slip occurs within a few hundred meters of the main fault trace.

These noted examples are for large events on essentially locked faults. There are no mapped examples of a large rupture on a creeping fault, such as the Hayward Fault, for comparison. In the HayWired scenario mainshock, it is expected that surface rupture will occur primarily where the fault is currently creeping at the surface. This is expressed as a zone averaging from ~2 to 15 m in width along most of the fault. This does not preclude the occurrence of some off-fault coseismic displacement on previously identified parallel, subparallel, or branching fault traces that are not creeping (Radbruch, 1969; Lienkaemper, 1992) or on unmapped locked fault traces, as was the case for the 2004 *M*6.0 Parkfield earthquake with coseismic slip on the "Southwest Fracture Zone" and afterslip on the main trace (Rymer and others, 2006). Although the potential for distributed deformation has not been quantified for the Hayward Fault, and is not a component of the HayWired scenario, in planning construction of long baseline structures that must cross the fault (pipelines, tunnels), the potential width of the fault zone needs to be taken into account. The lifeline exposure to coseismic slip along the Hayward Fault is summarized in table 2 (Jamie L. Jones, U.S. Geological Survey, written commun., 2016).

Table 2. Lifeline exposure to coseismic slip in the San Francisco Bay region, California, for the magnitude-7 mainshock of the HayWired earthquake scenario (Jamie L. Jones, U.S. Geological Survey, written commun., 2016).

Lifeline	Number of fault rupture crossings	Number with surface offsets	Range of offset, in meters
Roadways, highway	37	27	0.3–2.0
Roadways, secondary	127	80	0.0–2.1
Roadways, surface streets	424	270	0.0–2.1
Railways	8	4	0.9–1.6
Water supply conveyance systems	13	3	0.0–0.9
Oil/gas pipelines	25	15	0.7–2.1
Electric transmission lines	37	8	0.1–1.7
Fiber-optic telecommunications	241	132	0.0–2.0

Afterslip

As explained in the introduction, coseismic slip would account for only some of the slip associated with this large scenario earthquake. In particular, afterslip is expected along the creeping regions of the Hayward Fault, which extend over the entire length of the rupture.

Aagaard and others (2012) used Monte-Carlo methods to develop probabilistic estimates of coseismic slip and afterslip at four sites along the Hayward Fault for earthquake rupture lengths ranging from 35 to 90 km. Here we show results from that study for one site (alinement array site HTEM near the southern edge of a large, deep creeping region beneath Berkeley, California) for 90-km-long earthquake ruptures with magnitudes of approximately 7.1, to illustrate the progression in time, of the amount of afterslip and the associated uncertainty. The 500,000 realizations in the Monte Carlo analysis were constructed using nearly identical techniques as those used to construct the HayWired scenario mainshock rupture.

Empirical studies of historical afterslip data have firmly established that afterslip accumulates as a logarithmic progression in time (Smith and Wyss, 1968; Boatwright and others, 1989; Savage and Langbein, 2008). Therefore, the afterslip occurs most rapidly immediately after the earthquake and slows down (or decays) over time. Aagaard and others (2012) explicitly include both the coseismic slip and afterslip in the total slip estimates by modifying the power-law expression for afterslip from Boatwright and others (1989) to match the coseismic-slip value at 1 second (s) and end at the total slip value (coseismic+afterslip). This leads to a temporal evolution for the total slip given by:

$$D(t) = A + B\frac{1}{\left(1+T/t\right)^{C}}, \tag{1}$$

$$A = \frac{1}{1-a}\left(D_{\text{total}} - aD_{\text{coseismic}}\right), \tag{2}$$

$$B = \frac{-a}{1-a}\left(D_{\text{total}} - D_{\text{coseismic}}\right), \tag{3}$$

$$a = \left(1+\frac{T}{1\text{s}}\right)^{C}, \tag{4}$$

where the accumulated surface slip, D, grows from the coseismic slip, $D_{\text{coseismic}}$, at a decreasing rate and approaches a final value, D_{total} asymptotically, and t is time. The time constant, T, tends to be poorly determined, but in most cases it is about 1 year or more. The power-law exponent, C, tends to vary with the earthquake magnitude; for consistency with increasing coseismic slip with earthquake magnitude ($6.0 \le M_w \le 7.5$) and theoretical formulations for afterslip and empirical results, $C = 0.881 - 0.111 M_w$.

Figure 2 shows the temporal evolution of the afterslip across three time scales (24 hours, 4 weeks, and 12 months), starting from the coseismic-slip value. The thick solid orange lines display the median trajectory, and the thick dashed orange lines display the trajectory for the median plus one standard deviation from the Monte Carlo analysis. The power-law temporal evolution results in a rapid onset that decays with time. For example, 10 percent of the afterslip occurs in the first minute, 25 percent in the first hour, 35 percent in the first 6 hours, 40 percent in the first 24 hours, 70 percent in the first 30 days, and 85 percent in the first 6 months. The median trajectory grows from a coseismic slip of 0.1 m to a total slip value of 1.1 m. The median plus one standard deviation trajectory grows from a coseismic slip of 1.1 m to a total slip value of 2.4 m. The median trajectory has a very small amount of coseismic surface slip, so much of the damage due to slip on the fault would not happen immediately but would occur in the hours, days, and weeks following the earthquake as a result of afterslip. At one standard deviation above the median, the coseismic slip and afterslip are comparable, so damage would likely occur at the time of the earthquake as well as in the hours, days, and weeks following the earthquake.

Figure 2 also illustrates the wide range of behavior associated with the uncertainty in the model parameters and expected spatial variation of coseismic slip. It does not show the uncertainty for the form of the mathematical model itself. The blue (lowest thin dashed curve) delineates a progression that is about one half of the median trajectory, consistent with a coseismic-slip value of one half of the median coseismic slip and total slip of one half of the median total slip. In other realizations, the coseismic-slip and total-slip values may not be proportional to the median values. For example, the green (highest thin dashed curve) illustrates a trajectory with a coseismic slip near the median plus one standard deviation but with a total slip only about half of a standard deviation above the median value. The red (middle thin dashed curve) shows another example with coseismic slip slightly above

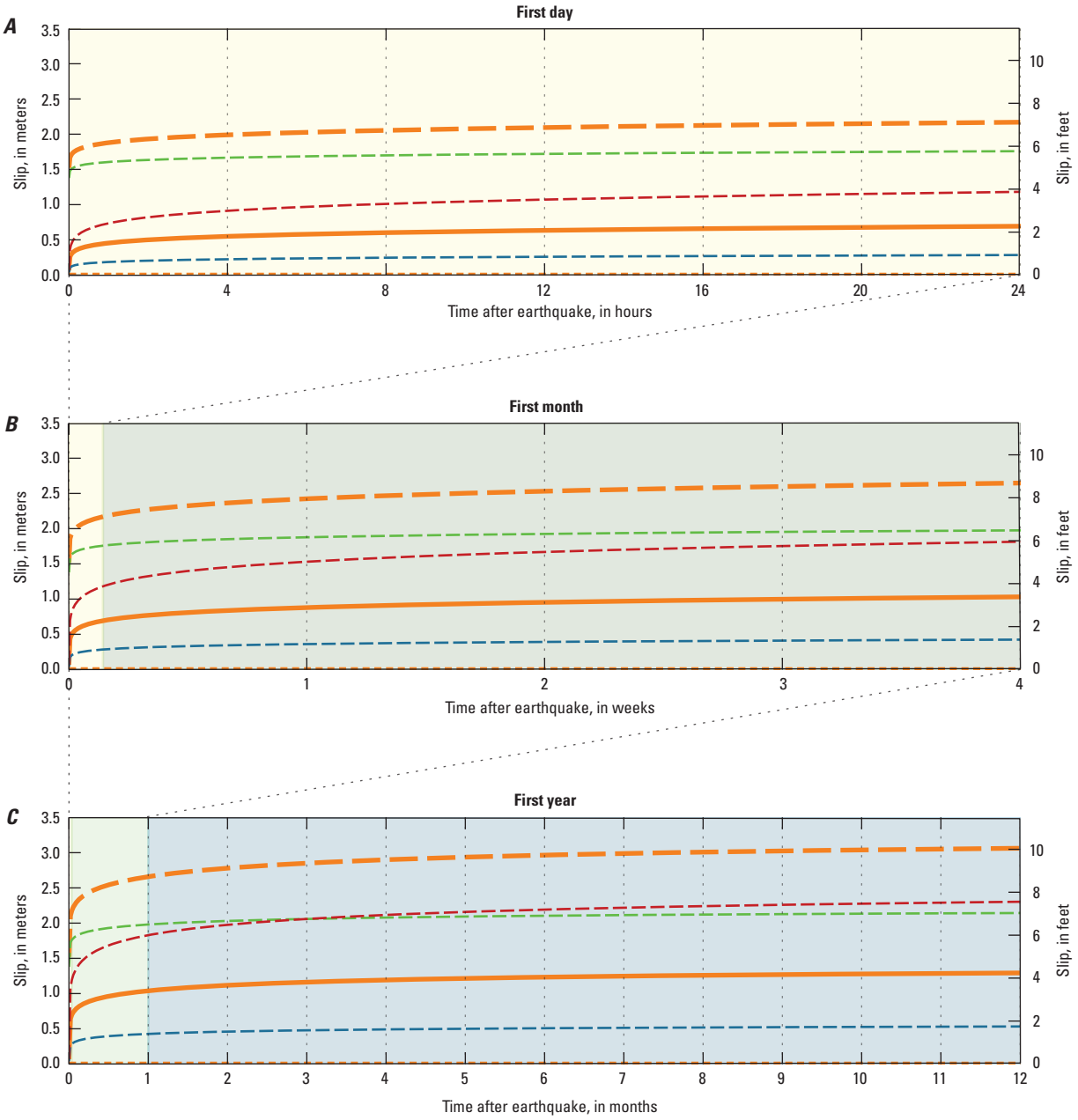

Figure 2. Graphs showing accumulation of fault afterslip on time scales of hours (*A*), weeks (*B*), and months (*C*) after an earthquake. The thick solid orange line shows the median trajectory and the thick dashed orange line shows the median plus one standard deviation trajectory. The thin red, blue, and green dashed lines show three realizations illustrating the variability in behavior associated with the uncertainty in the coseismic slip and afterslip. The yellow background shows the time span of the first day, the green background shading shows the time span from 1 day to 1 month, and the blue background shows the time span from 1 month to 1 year.

the median value, but a larger relative total slip. Other realizations exhibit similar behavior with values above or below the median.

The afterslip behavior can also vary significantly from location to location along the length of the rupture. For example, in the 1987 *M*6.6 Superstition Hills earthquake, the local variation in the proportion of coseismic slip to total slip ranged from about 2 to 18 percent (Harsh, 1982), and we expect similar variability for comparable magnitude earthquakes on the Hayward Fault. The amount of coseismic surface slip will affect the amount of total slip (coseismic slip plus afterslip) along the fault. Where coseismic slip is large, as in the San Pablo area at the north end of the scenario rupture (fig. 1), the amount of afterslip will likely be small. In contrast, locations where the amount of coseismic slip is small will likely experience larger amounts of afterslip. Small or negligible values of coseismic slip, as modeled for the Hayward-Fremont section of the fault in the scenario (fig. 1), could lead to overly optimistic estimates of the effect of a large earthquake on utility, transportation, and building infrastructure immediately following such an earthquake, because the infrastructure could be significantly affected by up to 0.5–1.5 m (median plus one standard deviation) of afterslip in the hours following the earthquake. Due to the large uncertainty in the coseismic and afterslip estimates, real-time geodetic and rapid postearthquake response measurements of coseismic and early afterslip are crucial for accurate forecasts of the total slip that will develop. Therefore, following a large Hayward Fault earthquake, observations made along the fault of the amount of coseismic slip and rate of afterslip will provide a clearer forecast of the total slip expected to develop. These efforts would likely need to be much more extensive than those of Hudnut and others (2014) following the 2016 *M*6.0 South Napa earthquake, in order to accurately forecast afterslip along the length of a much longer Hayward Fault rupture.

Knowledge Gaps, Modeling Limitations, and Communication Needs

To better prepare for the effects of coseismic slip and afterslip from future large earthquakes of the Hayward Fault, the following knowledge gaps, modeling limitations, and communications issues need to be addressed:

- The details of the physical relations among interseismic fault creep, coseismic fault slip, and afterslip are not well known. To reduce the uncertainty in forecasting coseismic slip and afterslip for large earthquakes on the Hayward Fault and on other faults with interseismic creep, additional research is necessary to better understand the physics involved in fault creep and sudden slip in earthquake ruptures.
- Given the current state of knowledge of fault afterslip, near real-time measurements of coseismic fault slip and the progression of afterslip following a large Hayward Fault earthquake will be crucial for developing accurate and precise estimates of the amount and ultimate duration of afterslip.
- Operational procedures, similar to those used for forecasting aftershock behavior, need to be developed for forecasting afterslip. These forecasts will provide important scientific guidance to building owners, utility and infrastructure operators, and municipalities as they repair damage, rebuild, and recover from a large earthquake.
- Afterslip of 0.5–1.5 m on the Hayward Fault following a large earthquake will complicate repairs of structures straddling, and infrastructure crossing, the fault. This hazard needs to be communicated to the associated stakeholders so that they can incorporate these complications into their earthquake mitigation and response plans.
- There is potential for the occurrence of distributed faulting many tens to hundreds of meters from the main creeping fault trace during a large Hayward Fault rupture. This has importance in planning long baseline structures such as pipelines and transportation infrastructure that cross or are astride the fault.

Conclusion

In the HayWired scenario some slip occurs coseismically at the surface as the Hayward Fault ruptures in the large mainshock earthquake, but it is expected to be only part of the total surface slip associated with the earthquake (Aagaard and others, 2012). The remaining surface slip occurs postseismically, that is after the shaking has stopped, which is a seismic fault movement called afterslip. This afterslip is expected to make a substantial contribution to the total slip and may be responsible for up to 0.5–1.5 m of additional slip along the fault. In this particular HayWired scenario, the coseismic slip peaks at 2.1 m, and it will have immediate impacts at some locations. However, utilities, transportation infrastructure, and structures straddling the Hayward Fault where little coseismic slip occurred will likely be affected by significant afterslip following a large Hayward earthquake.

Acknowledgments

We thank Ben Brooks and Jessica Murray (U.S. Geological Survey) for their constructive reviews, which helped improve the manuscript.

References Cited

Aagaard, B.T., Graves, R.W., Schwartz, D.P., Ponce, D.A., and Graymer, R.W., 2010, Ground-motion modeling of Hayward Fault scenario earthquakes, part I—Construction of the suite of scenarios: Bulletin of the Seismological Society of America, v. 100, no. 6, p. 2927–2944, doi: 10.1785/0120090324.

Aagaard, B.T., Lienkaemper, J.J., and Schwartz, D.P., 2012, Probabilistic estimates of surface coseismic slip and afterslip for Hayward Fault earthquakes: Bulletin of the Seismological Society of America, v.102, no. 3, p. 961–979, doi: 10.1785/0120110200.

Boatwright, J., Budding, K.E., and Sharp, R.V., 1989, Inverting measurements of surface slip on the Superstition Hills Fault: Bulletin of the Seismological Society of America, v. 79, no. 2, p. 411–423.

Bucknam, R.C., Plafker, G., and Sharp, R.V., 1978, Fault movement (afterslip) following the Guatemala earthquake of February 4, 1976: Geology, v. 6, no. 3, p. 170–173.

Buehrer, J., 2015, Hey Napa—Your afterslip is showing: Journal—American Water Works Association, v. 107, no. 9, p. 68–75, doi: 10.5942/jawwa.2015.107.0111.

Funning, G.J., Bürgmann, R., Ferretti, A., and Novali, F., 2007, Asperities on the Hayward Fault resolved by PS-InSAR, GPS and boundary element modeling: Eos (Transactions of the American Geophysical Union), v. 88, no. 52, S23C–04.

Gold, R.D., Reitman, N.G., Briggs, R.W., Barnhart, W.D., Hayes, G.P., and Wilson, E., 2015, On- and off-fault deformation associated with the September 2013 M_w7.7 Balochistan earthquake—Implications for geologic slip rate measurements: Tectonophysics, v. 660, p. 65–78, doi: 10.1016/j.tecto.2015.08.019.

Harsh, P.W., 1982, Distribution of afterslip along the Imperial Fault, in the Imperial Valley, California, earthquake of October 15, 1979: U.S. Geological Survey Professional Paper 1254, p. 193–204. [Also available at https://pubs.usgs.gov/pp/1254/report.pdf.]

Homer, C.G., Dewitz, J.A., Yang, L., Jin, S., Danielson, P., Xian, G., Coulston, J., Herold, N.D., Wickham, J.D., and Megown, K., 2015, Completion of the 2011 National Land Cover Database for the conterminous United States-Representing a decade of land cover change information. Photogrammetric Engineering and Remote Sensing, v. 81, no. 5, p. 345–354, , accessed April 16, 2016, at https://www.mrlc.gov/nlcd2011.php.

Hudnut, K.W., Brocher, T.M., Prentice, C.S., Boatwright, J., Brooks, B.A., Aagaard, B.T., Blair, J.L., Fletcher, J.B., Erdem, J.E., Wicks, C.W., Murray, J.R., Pollitz, F.F., Langbein, J., Svarc, J., Schwartz, D.P., Ponti, D.J., Hecker, S., DeLong, S., Rosa, C., Jones, B., Lamb, R., Rosinski, A., McCrink, T.P., Dawson, T.E., Seitz, G., Rubin, R.S., Glennie, C., Hauser, D., Ericksen, T., Mardock, D., Hoirup, D.F., and Bray, J.D., 2014, Key recovery factors for the August 24, 2014, South Napa earthquake: U.S. Geological Survey Open-File Report 2014–1249, 51 p., accessed August 31, 2016, at https://doi.org/10.3133/ofr20141249.

Jones, L.M., Bernknopf, R., Cox, D., Goltz, J., Hudnut, K., Mileti, D., Perry, S., Ponti, D., Porter, K., Reichle, M., Seligson, H., Shoaf, K., Treiman, J., and Wein, A.M., 2008, The ShakeOut Scenario: U.S. Geological Survey Open-File Report 2008-1150 and California Geological Survey Preliminary Report 25, 312p., accessed August 31, 2016, at https://pubs.usgs.gov/of/2008/1150/.

Lawson, A.C., 1908, The earthquake of 1868, *in* Lawson, A.C., ed., The California earthquake of April 18, 1906—Report of the State Earthquake Investigation Commission (volume I): Washington, D.C., Carnegie Institution, p. 434-448.

Lienkaemper, J. J., Borchardt, G., and Lisowski, M., 1991, Historic creep rate and potential for seismic slip along the Hayward Fault, California: Journal of Geophysical Research v. 96, no. B11, p. 18261–18283.

Lienkaemper, J.J., 1992, Map of recently active traces of the Hayward Fault, Alameda and Contra Costa counties, California: U.S. Geological Survey, Miscellaneous Field Studies Map MF-2196, scale 1:24,000. [Also available at https://pubs.usgs.gov/mf/1992/2196/.]

Lienkaemper, J.J., Baker, B., and McFarland, F.S., 2006, Surface slip associated with the 2004 Parkfield, California, earthquake measured on alinement arrays: Bulletin of the Seismological Society of America, v. 96, no. 48, p. S239–S249, doi: 10.1785/0120050806.

Lienkaemper, J.J., Dawson, T.E., Personius, S.F., Seitz, G.G., Reidy, L.M., and Schwartz, D.P., 2002, A record of large earthquakes on the southern Hayward fault for the past 500 years: Bulletin of the Seismological Society of America, v. 92, no. 7, p. 2637–2658.

Lienkaemper, J.J., DeLong, S.B., Domrose, C.J., and Rosa, C.M., 2016, Afterslip behavior following the 2014 *M*6.0 South Napa earthquake with implications for afterslip forecasting on other seismogenic faults: Seismological Research Letters, v. 87, no. 3, doi: 10.1785/0220150262.

Lienkaemper, J.J., McFarland, F.S., Simpson, R.W., Bilham, R.G., Ponce, D.A., Boatwright, J.J., and Caskey, S.J., 2012, Long-term creep rates on the Hayward Fault: Evidence for controls on the size and frequency of large earthquakes: Bulletin of the Seismological Society of America v. 102, no. 1, p. 31–41.

Lienkaemper, J.J., Schwartz, D.P., Kelson, K.I., Lettis, W.R., Simpson, G.D., Southon, J.R., Wanket, J.A., Williams, P.L., 1999, Timing of paleoearthquakes on the northern Hayward Fault—Preliminary evidence in El Cerrito, California: U.S. Geological Survey Open-File Report 99–318, 33 p. [Also available at https://pubs.usgs.gov/of/1999/0318/.]

Lienkaemper, J.J., Williams, P.L., and Guilderson, T.P., 2010, Evidence for a 12th large earthquake on the southern Hayward fault in the past 1900 years: Bulletin of the Seismological Society of America, v. 100, no. 5A, p. 2024–2034.

McFarland, F.S., Lienkaemper, J. J., and Caskey, S.J., 2009, revised 2015,, Data from theodolite measurements of creep rates on San Francisco Bay Region faults, California, 1979–2014: U.S. Geological Survey Open-File Report 2009–1119, v. 1, no. 6, 21 p. and data files, accessed August 31, 2016, at https://pubs.usgs.gov/of/2009/1119/.

Petersen, M.D., Dawson, T.E., Rui, C., Cao, T., Wills, C.J., Schwartz, D.P., and Frankel, A.D., 2011, Fault displacement hazard for strike-slip faults: Bulletin of the Seismological Society of America, v. 101, no.2, p. 805–825, doi: 10.1785/0120100035.

Radbruch, D.H., 1969, Areal and engineering geology of the Oakland East Quadrangle, California: U.S. Geological Survey Quadrangle Map GQ-769, scale 1:24,000. [Also available at https://pubs.er.usgs.gov/publication/gq769.]

Rymer, M.J., Tinsley, J.C., Treiman, J.A., Arrowsmith, J.R., Clahan, K.B., Rosinski, A.M., Bryant, W.A., Snyder, H.A., Fuis, G.S., Toké, N.A., and Bawden, G.W., 2006, Surface fault slip associated with the 2004 Parkfield, California, earthquake: Bulletin of the Seismological Society of America, v. 96, no. 4B, p. S11–S27.

Savage, J.C., and Langbein, J., 2008, Postearthquake relaxation after the 2004 *M*6 Parkfield, California, earthquake and rate-and-state friction: Journal of Geophysical Research: Solid Earth, v. 113, no. B10, p. 407, doi: 10.1029/2008JB005723.

Sharp, R.V., Budding, K.E., Boatwright, J., Ader, M.J., Bonilla, M.G., Clark, M.M., Fumal, T.E., Harms, K.K., Lienkaemper, J.J., Morton, D.M., O'Neill, B.J., Ostergren, C.L., Ponti, D.J., Rymer, M.J., Saxton, J.L., and Sims, J.,1989, Surface faulting along the Superstition Hills fault zone and nearby faults associated with the earthquakes of 24 November 1987: Bulletin of the Seismological Society of America, v. 79, no. 2, p. 252–281.

Smith, S.W., and Wyss, M., 1968, Displacement on the San Andreas fault subsequent to the 1966 Parkfield earthquake: Bulletin of the Seismological Society of America, v. 58, no. 6, p. 1955–1973.

Wilkinson, M., McCaffrey, K.J.W., Roberts, G., Cowie, P.A., Phillips, R.J., Michetti, A.M., Vittori, E., Guerrieri, L., Blumetti, A.M., Bubeck, A., Yates, A., and Sileo, G., 2010, Partitioned postseismic deformation associated with the 2009 M_w 6.3 L'Aquila earthquake surface rupture measured using a terrestrial laser scanner, Geophysical Research Letters, v. 37, no. 10, doi: 10.1029/2010GL043099.

The HayWired Earthquake Scenario—Earthquake Hazards
Edited by Shane T. Detweiler and Anne M. Wein
Scientific Investigations Report 2017–5013–A–H
[Also see https://doi.org/10.3133/sir20175013]

Chapter E

HayWired Scenario Mainshock—Liquefaction Probability Mapping

By Jamie L. Jones, Keith L. Knudsen, and Anne M. Wein

Abstract

The HayWired scenario examines a hypothetical earthquake (mainshock) with a moment magnitude of 7.0 occurring on April 18, 2018, at 4:18 p.m. on the Hayward Fault in the east bay part of California's San Francisco Bay area. For the HayWired scenario mainshock, we provide maps of earthquake-induced liquefaction probability (the likelihood of surface manifestations of liquefaction) using liquefaction probability estimates from the Federal Emergency Management Agency's loss estimation tool Hazus-MH 2.1. We also produce more detailed liquefaction probability maps of northern Santa Clara County and western Alameda County by using the approach of Holzer, Noce, and Bennett (U.S. Geological Survey), who used the liquefaction potential index parameter as an index for liquefaction hazard in their mapping of a smaller part of northern Santa Clara County and western Alameda County. We apply their methods and extend their mapping as far from the area over which they collected subsurface (cone penetration test) data as may be practicable. The more detailed analysis of liquefaction probability, where available, is used to update liquefaction probabilities from Hazus in these areas. To assess liquefaction hazards in the remainder of the area impacted by the HayWired scenario earthquake (that is, not western Alameda County and northern Santa Clara County), we rely on the approach used in Hazus, which makes use of liquefaction susceptibility mapping.

Results of our liquefaction probability mapping of northern Santa Clara County and western Alameda County, and the Hazus mapping, show that areas of artificial fill along the San Francisco Bay margin and youthful alluvial deposits along the larger streams feeding into the bay have the highest likelihood of producing liquefaction-related ground-surface damage. The range and variability of the mapped ground motions (peak ground accelerations) in the HayWired mainshock contribute to a more variable depiction of liquefaction hazard, and in some cases a higher probability of liquefaction, than has been shown previously.

Introduction

The HayWired scenario examines a hypothetical earthquake (mainshock) with a moment magnitude (M_w) of 7.0 occurring on April 18, 2018, at 4:18 p.m. on the Hayward Fault in the east bay part of California's San Francisco Bay area. The purpose of this earthquake-induced liquefaction assessment is to characterize liquefaction hazards and map their probability for the HayWired scenario mainshock. Liquefaction is a form of earthquake-induced ground failure in which formerly solid ground transforms temporarily to a softened or liquefied state. Liquefaction occurs where strong ground motions produce a rise in pore-water pressure that in turn causes granular material to briefly lose strength and liquefy (Youd, 1973). The occurrence of liquefaction is restricted to certain geologic and hydrologic settings that experience relatively high levels of ground shaking. Areas susceptible to liquefaction are underlain by water-saturated, cohesionless, granular sediment. These conditions are typically found in areas of geologically youthful (Knudsen and others, 2009; Knudsen and Bott, 2011), sandy and silty deposits near water bodies, including artificial fill placed around the margin of San Francisco Bay (for example, Witter and others, 2006). Liquefaction probability estimates can be developed to describe two ways of thinking about the hazard—(1) the likelihood of a specific location experiencing liquefaction (for example, at the location of a cone penetration test, CPT, sounding) and (2) the percent of the ground surface area likely to experience liquefaction (for example, Holzer and others, 2008, 2010, 2011).

Several types of liquefaction-induced ground failure can occur in larger earthquakes, including lateral spread, ground oscillation, flow failure, and loss of bearing strength. Each of these liquefaction-induced ground-failure phenomena affect the built environment differently. Lateral spreading occurs on gentle slopes when subsurface liquefaction allows upper strata and surface soils to displace downslope or toward a steep slope or free face (for example, a stream bank). Pipelines, roads, utilities, bridge piers, and structures with shallow foundations can be severely damaged by lateral spread (Rausch, 1997; Cubrinovski and others, 2014). Flow failure generally occurs on steeper slopes when liquefied

material flows downslope at high velocity (Rausch, 1997; Youd, 1973). Flow failures, due to their high speed and potential for the liquefied material to flow and spread out over the landscape, have the potential to cause the greatest amount of damage to buildings and other infrastructure but are relatively rare. Ground oscillation is similar to lateral spread but occurs in areas where the slope is too gentle to permit permanent lateral movement (Holzer and Youd, 2007). Ground oscillations may affect structures and utilities buried underground. Finally, loss of bearing strength results from soils losing their ability to support structures when deeper soils lose shear strength and weaken due to liquefaction. Infrastructure resting either on top of or within soils losing bearing strength can settle unevenly and be damaged (Tinsley and Ponti, 2008). Buoyant objects, such as partially empty fuel or water tanks and sewers, can "float" to the surface through the more dense liquefied material.

An example of liquefaction catastrophically impacting a community occurred in Christchurch, New Zealand, during the 2010 to 2012 earthquake sequence, and most extensively after the February 22, 2011, M_w 6.2 earthquake. This earthquake sequence caused properties and streets to be buried in thick layers of sand, silt, and water ejected from the subsurface, as well as by sewage from sewer lines broken by the ground deformation (McSaveney, 2014; van Ballegooy and others, 2014; Green and others, 2014). House foundations cracked and buckled, wrecking many homes. Despite the damage to homes, there were few serious injuries that resulted from liquefaction. Several thousand homes have been demolished and some sections of Christchurch will never be reoccupied as the result of the damage and permanent loss of elevation due to ground settlement (Scott and Carville, 2016; Tonkin and Taylor, Ltd., 2013).

Liquefaction occurred in the San Francisco Bay area as a result of several early historical earthquakes, including the 1868 Hayward and the 1906 San Francisco earthquakes; liquefaction also was one cause of damage in the 1989 Loma Prieta earthquake (Youd and Hoose, 1978; Tinsley and others, 1998). The most extensive and damaging liquefaction in the bay area has occurred in areas of poorly engineered artificial fill in San Francisco in 1906 and along the east bay shoreline in 1989. In the 1906 earthquake, liquefaction-related ground deformation in San Francisco damaged water pipelines and this disruption to the water supply contributed significantly to the extent of the fire following the earthquake. A digital compilation of past occurrences of liquefaction in the nine-county bay area is presented in Knudsen and others (2000); these data have been used to review results of the analyses in this assessment. We have filtered the historical occurrences shown in our figures and attempted to include only those occurrences where the historical accounts allowed for confident location of the occurrences by Knudsen and others (2000).

Data

To compute liquefaction probabilities using the Holzer and others (2008, 2010, 2011) methodology, several types of data are needed—geologic maps, scenario estimates of peak ground acceleration (PGA), and depth to groundwater. Detailed 1:24,000-scale Quaternary geologic mapping of the area is available from Witter and others (2006) (fig. 1). Shaking information is from the Aagaard, Boatwright, and others (this volume) scenario shaking map being used in the HayWired scenario. Depth to groundwater is available from the California Geological Survey (CGS) Seismic Hazard Zonation Program (Tim McCrink, CGS, written commun., 2014).

Holzer and others (2008, 2010) grouped geologic map units from Witter and others (2006) into just a few categories based on comparable liquefaction susceptibilities. For example, the geologic map units most susceptible to liquefaction based on Holzer and others' (2008, 2010) CPT and liquefaction potential index (LPI) analyses include latest Holocene alluvial-fan levee deposits (Qhly) in Santa Clara Valley and artificial fill (af) in the greater Oakland area. These geologic units, due to the similarities in their liquefaction probability curves, are grouped into one category, which we refer to as group 1 (see table 1). A second group of geologic map units with similarities in their liquefaction probability curves showing lower liquefaction potential, which we refer to as group 2, was broken out by Holzer and others (2008, 2010) and treated separately in the liquefaction probability analysis. Holzer and others (2008, 2010) did not compute liquefaction potential for a number of geologic map units, including Holocene San Francisco Bay mud (Qhbm) and early Quaternary and older (>1.4 million years ago or mega-annum, Ma) deposits and bedrock (br); these geologic units with no computed liquefaction potential are referred to as "not assessed" in this analysis.

Figure 2 shows the shaking (PGA) distribution for the HayWired scenario study area along with the boundaries for the areas where liquefaction probability was modeled using the methods of Holzer and others (2008, 2010). The shaking depiction is from the work of Aagaard, Boatwright, and others (this volume); it is based on three-dimensional physical modeling. In such modeling, accounting for site conditions, like the likely amplifications of longer period motions by soft soils around the margin of San Francisco Bay, is not easily accomplished. It is possible that the shaking model used underpredicts shaking in these areas. Because liquefaction is most likely to occur around the margins of the bay and near larger active creeks (Witter and others, 2006) where there are softer soils, we may be underpredicting the extent of liquefaction by using this shaking model. Note that most of the area of intense shaking is contained within the area where Holzer and others' (2008, 2010) liquefaction probability modeling is applied. To estimate liquefaction probabilities for tracts in areas outside the black line, we use the Federal Emergency Management Agency's (FEMA) loss estimation tool Hazus-MH 2.1 (Federal Emergency Management Agency, 2012; Hope Seligson, Seligson Consulting, written commun., 2016) and the liquefaction susceptibility mapping of Witter and others (2006) and Knudsen and others (2000).

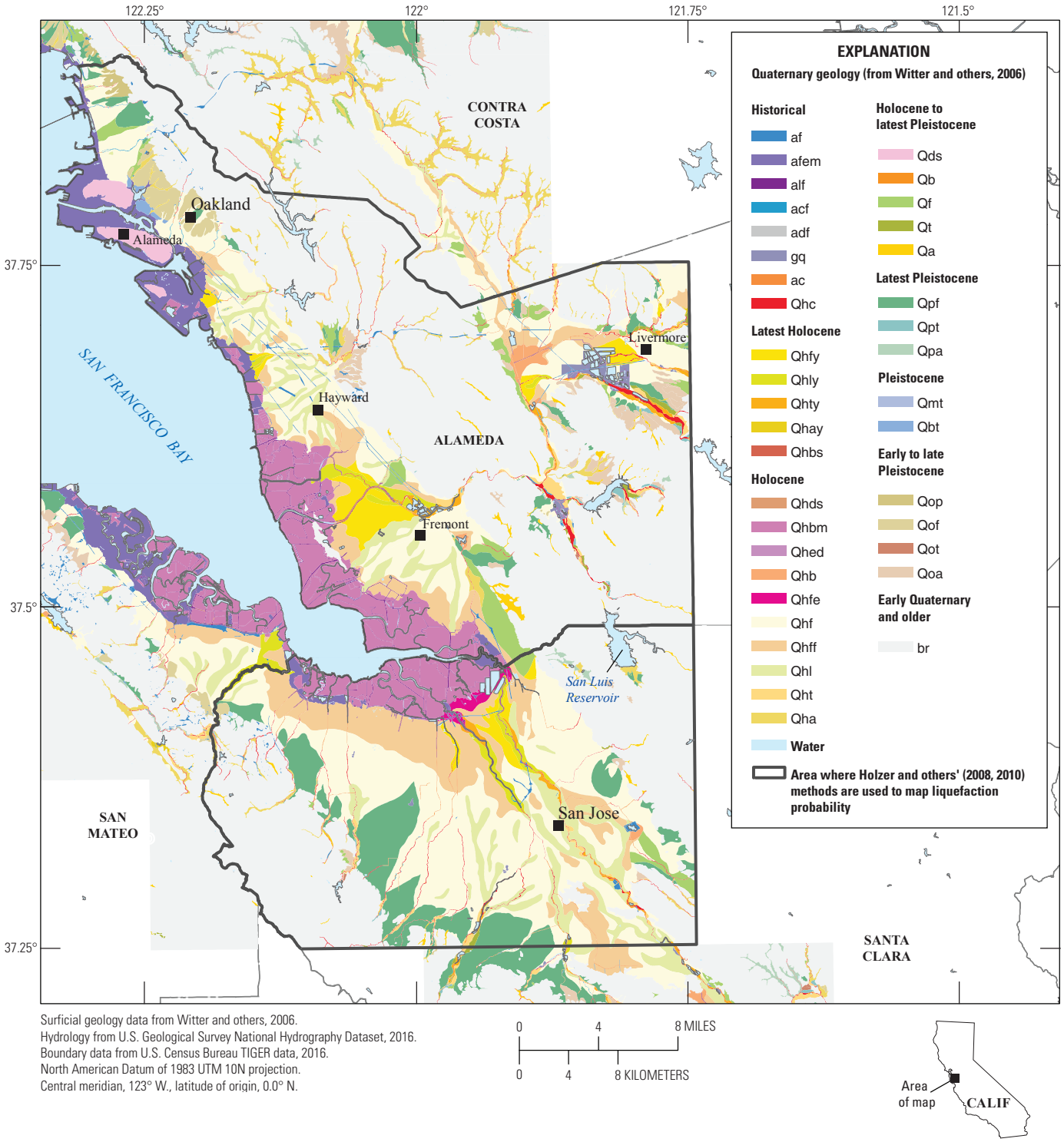

Figure 1. Map of the southeastern San Francisco Bay area, California, showing Quaternary geologic mapping (from Witter and others, 2006) used to estimate liquefaction probabilities in the HayWired earthquake scenario using Holzer and others' (2008, 2010, 2011) methodology. Liquefaction probabilities for the remainder of the area affected by shaking in this scenario were calculated using the Hazus-MH 2.1 loss estimation tool (Federal Emergency Management Agency, 2012) and existing liquefaction-susceptibility mapping. Black line shows areas in which Holzer and others' (2008, 2010, 2011) methodology is applied. See table 1 for map unit descriptions.

Table 1. San Francisco Bay area, California, Quaternary geologic map units (from Witter and others, 2006) and assigned liquefaction probability group for the HayWired earthquake scenario.

[Ma, mega-annum or millions of years ago]

Geologic unit name	Geologic map unit abbreviation	Holzer and others (2008, 2010, 2011) liquefaction group	Liquefaction group[1]
Artificial fill	af	Group 1	Group 1 and group 2[2]
Artificial fill over estuarine mud	afem	Not assessed	Group 1
Artificial fill, levee	alf	Not assessed	Group 2
Artificial fill, channel	acf	Not assessed	Group 2
Artificial fill, dams	adf	Not assessed	Group 2
Gravel quarries and percolation ponds	gq	Not assessed	Not assessed
Artificial stream channel	ac	Not assessed	Group 2
Modern stream-channel deposits	Qhc	Not assessed	Group 1
Latest Holocene alluvial-fan deposits	Qhfy	Group 2	Group 2
Latest Holocene alluvial-fan levee deposits	Qhly	Group 1	Group 1
Latest Holocene stream-terrace deposits	Qhty	Group 1	Group 1
Latest Holocene alluvial deposits, undifferentiated	Qhay	Not assessed	Group 1
Latest Holocene beach sand	Qhbs	Not assessed	Group 1
Holocene dune sand	Qhds	Not assessed	Group 2
Holocene San Francisco Bay mud	Qhbm	Not assessed	Group 2
Holocene estuarine delta deposits	Qhed	Not assessed	Not assessed
Holocene basin deposits	Qhb	Not assessed	Group 2
Holocene fine grained alluvial-fan/estuarine complex deposits	Qhfe	Not assessed	Group 2
Holocene alluvial-fan deposits	Qhf	Group 2	Group 2
Holocene alluvial-fan deposits, fine-grained facies	Qhff	Group 2	Group 2
Holocene alluvial fan levee deposits	Qhl	Group 2	Group 2
Holocene stream terrace deposits	Qht	Not assessed	Group 2
Holocene alluvium, undifferentiated	Qha	Not assessed	Group 2
Late Pleistocene to Holocene dune sand	Qds	Not assessed	Group 2
Late Pleistocene to Holocene basin deposits	Qb	Not assessed	Not assessed
Late Pleistocene to Holocene alluvial-fan deposits	Qf	Not assessed	Group 2
Late Pleistocene to Holocene stream-terrace deposits	Qt	Not assessed	Group 2
Late Pleistocene to Holocene alluvium, undifferentiated	Qa	Not assessed	Group 2
Late Pleistocene alluvial-fan deposits	Qpf	Not assessed	Group 2
Late Pleistocene stream-terrace deposits	Qpt	Not assessed	Group 2
Late Pleistocene alluvium, undifferentiated	Qpa	Not assessed	Group 2
Pleistocene marine-terrace deposits	Qmt	Not assessed	Not assessed
Pleistocene bay-terrace deposits	Qbt	Not assessed	Not assessed
Early to late Pleistocene pediment deposits	Qop	Not assessed	Not assessed
Early to middle Pleistocene alluvial-fan deposits	Qof	Not assessed	Not assessed
Early to middle Pleistocene stream-terrace deposits	Qot	Not assessed	Not assessed
Early to middle Pleistocene undifferentiated alluvial deposits	Qoa	Not assessed	Not assessed
Early Quaternary and older (>1.4 Ma) deposits and bedrock	br	Not assessed	Not assessed

[1]Two liquefaction curves/groups are available for use in assessing liquefaction probability for this area (from Holzer and others, 2008, 2010, 2011); see tables 2 and 3, as well as Methods section. "Not assessed" means that we judged the liquefaction hazard for these units to be very low to negligible, and the probability of liquefaction was not calculated for polygons with these map unit designations.

[2]Assignment of liquefaction grouping to artificial fill depends on the nature of geologic map unit thought to underlie the fill.

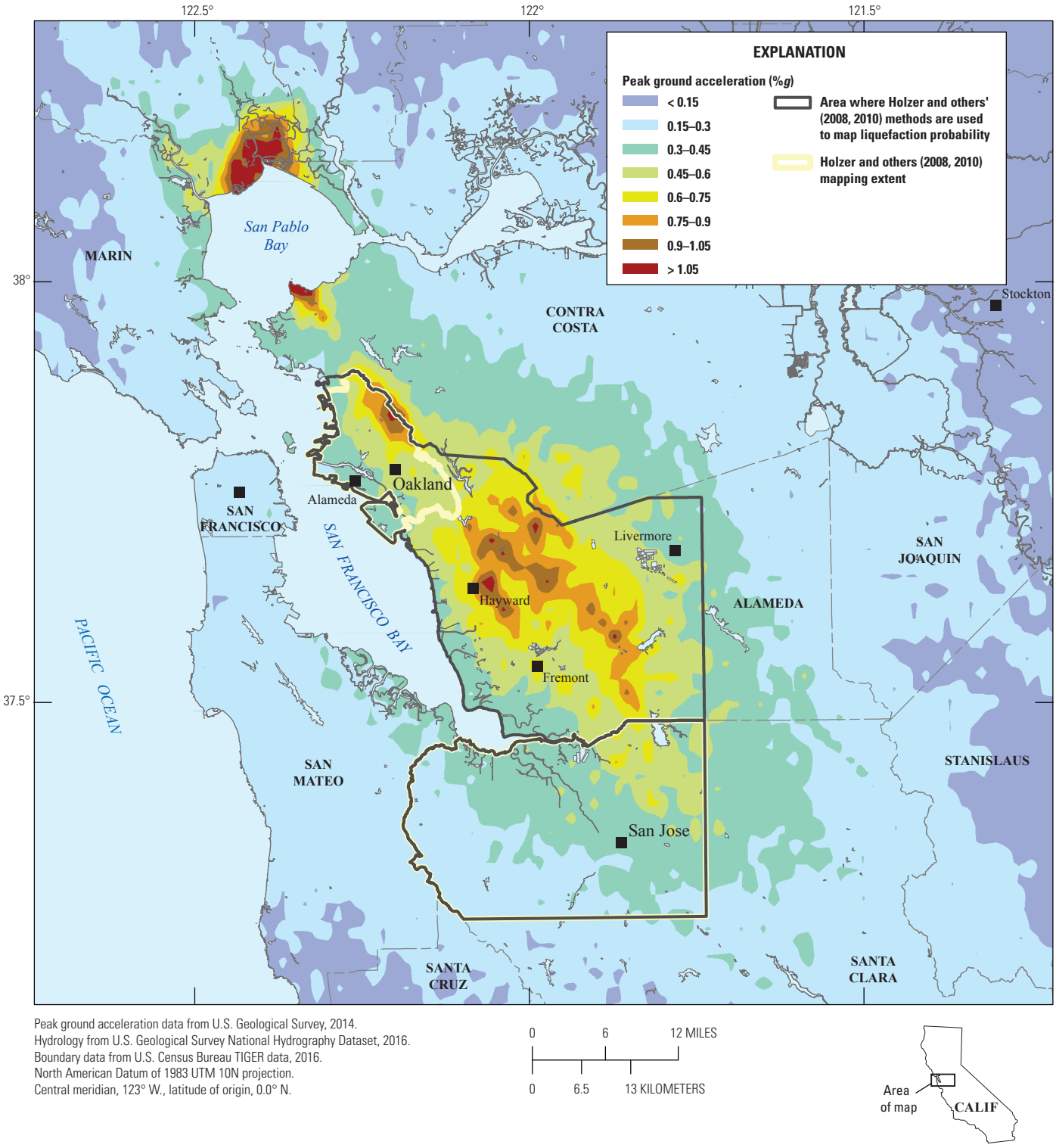

Figure 2. Map of the San Francisco Bay region, California, showing peak ground acceleration (PGA) used for characterizing liquefaction hazard in the HayWired earthquake scenario (from Aagaard, Boatwright, and others, this volume). Areas outlined in black are the areas where the Holzer and others' (2008, 2010) methods are used to estimate liquefaction probability. <, less than; >, greater than; %*g*, percentage of acceleration due to gravity.

Depth to Groundwater

Contours of 3 meters (m) depth to groundwater in Santa Clara Valley and western Alameda County were provided by the California Geological Survey (CGS) (Tim McCrink, CGS, written commun., 2014). The depth to groundwater for the areas of interest is shown on figure 3. For Santa Clara Valley, the 3-m water-table depth line divides the region of interest into two areas we treated differently following the approach of Holzer and others (2008, 2010, 2011). Areas on the San Francisco Bay side of the line are generally considered to have water-table depths less than 3 m, and areas on the inland side are believed to have water-table depths greater than 3 m. Parts of the 3-m groundwater contour have been omitted from this analysis because they were either not complete contours (they could not be closed off to definitively say whether the groundwater level was above or below 3 m) or they were not included in Holzer and others' (2008, 2010) work.

Methods

In this liquefaction assessment, which will be used in Hazus (Federal Emergency Management Agency, 2012) loss estimation and other earthquake consequences modeling in the HayWired scenario project, we supplement the Hazus liquefaction probability mapping being done by Hope Seligson (Seligson Consulting, written commun., 2016) by expanding the probabilistic liquefaction hazard mapping of Holzer and others (2008, 2010) to cover broader areas.

A probabilistic assessment of liquefaction potential includes evaluation of both the susceptibility of surficial deposits to liquefaction and the probability that earthquake ground motions will exceed a specified threshold level, or "liquefaction opportunity." A liquefaction susceptibility map reflects the distribution of surficial deposits with different physical properties and variations in hydrologic conditions (for example, Witter and others, 2006; Knudsen and others, 2000). A liquefaction potential map is the product of a liquefaction susceptibility map and a liquefaction opportunity map depicting ground motions. In this project, we use the HayWired ground motions described by Aagaard, Boatwright, and others (this volume) and geologic mapping by Witter and others (2006) in a relatively new approach to liquefaction probability mapping developed by Holzer and others (2008, 2010) to provide liquefaction probability maps for the HayWired scenario.

Holzer and others (2008, 2010) map liquefaction probabilities in western Alameda County and northern Santa Clara County for magnitude 6.7 and 7.0 earthquakes on the Hayward Fault. They collected CPT data in both of these areas in sufficient density to characterize the liquefaction susceptibility of many of the more extensive and likely more hazardous Quaternary geologic map units. They computed distributions of the LPI from CPT data for surficial geologic map units. Geologic map units are then grouped together if their LPI distributions are similar. These distributions are then used to develop liquefaction probability curves for each of the groupings and to develop probabilistic liquefaction hazard maps for different earthquake scenarios. We follow their procedure, except we use the simulated ground motions for the HayWired scenario mainshock (Aagaard, Boatwright, and others, this volume). We have also expanded the area to map liquefaction probabilities in areas outside of the areas characterized by Holzer and others (2008, 2010).

The liquefaction probability curves of Holzer and others (2008, 2010, 2011) are based on the following functional form:

$$P_H = \frac{A}{1 + \left(\frac{PGA / MSF}{B}\right)^C} \quad (1)$$

where PGA is the peak ground acceleration, MSF is the liquefaction magnitude scaling factor, and A, B, and C are liquefaction probability constants empirically derived by Holzer and others (2008, 2010, 2011) based on probabilities inferred from LPI distributions. Holzer and others (2008, 2010, 2011) adopted the definition of MSF described by Youd and others (2001) where:

$$MSF = 10^{2.24} / M^{2.56} \quad (2)$$

and M is the earthquake moment magnitude, which is M_w 7.05 for the HayWired scenario (magnitude reported to two decimal places based on original data from Aagaard and others, 2010). For the HayWired scenario, MSF equals 1.17.

Toprak and Holzer (2003) showed that areas in Monterey County with calculated LPI values of more than 5 showed surface manifestation of liquefaction 58 percent of the time during recent earthquakes, agreeing with earlier research that an LPI of 5 or greater is a good indicator of liquefaction occurrence (Iwasaki and others, 1982). In this case, following the approach of Holzer and others (2008, 2010, 2011), liquefaction probability at a location is the likelihood that an area will have an LPI greater than 5. For further discussion of their methodology, see Holzer and others (2011).

According to Holzer and others (2008, 2010), their liquefaction probability estimates describe both how likely liquefaction is to occur at a random point in a geologic map unit polygon, as well as the percent of ground surface area in that geologic map unit polygon likely to be affected by liquefaction.

Tables 2 and 3 show the liquefaction probability constants A, B, and C from Holzer and others (2011) used to calculate liquefaction probability in equation 1 for Santa Clara Valley (table 2) and the greater Oakland area (table 3). Holzer and others (2011) developed unique constants for geological units in each of the two areas they studied. We used the geologic map unit groupings of Holzer and others (2008, 2010, 2011), and added geologic map units that weren't included in their analysis to the groups, based on our understanding of the nature of the liquefaction susceptibility of each of these units, as well as their similarity in age and depositional environment to map units in groups 1 and 2

Figure 3. Map of the southeastern San Francisco Bay area, California, showing 3-meter (m) contour from historical high groundwater data for northern Santa Clara and western Alameda Counties (from Tim McCrink, California Geological Survey, written commun., 2014). We use a standard groundwater depth of 1.5 m throughout western Alameda County for calculating liquefaction probability in the HayWired earthquake scenario, which is consistent with the approach of Holzer and others (2010, 2011). For areas in Santa Clara County shown with depths to historical high groundwater of less than 3 m, to be consistent with Holzer and others (2008, 2010, 2011), we use the constants for 1.5-m depth shown in table 2 for calculating liquefaction probability. For Santa Clara County areas with depth to groundwater greater than 3 m, to be consistent with Holzer and others (2008, 2010, 2011), we use the constants associated with the 5-m depth to groundwater shown in table 2. Parts of the 3-m groundwater contour have been omitted from this analysis because they were either not complete contours (they could not be closed off) or they were not included in Holzer and others' (2008, 2010) work.

(see table 1 and fig. 4). In the map database of Witter and others (2006), artificial fill polygons are tagged with the geologic map unit likely to underlie the manmade artificial fill. Polygons mapped as artificial fill by Witter and others (2006) were assigned to group 1 or 2 based primarily on which geologic map unit the artificial fill bodies rest. If the artificial fill was placed over Holocene San Francisco Bay mud, then that area is assigned to group 1, the more susceptible deposits, because a significant fraction of all liquefaction occurrences in past bay area earthquakes have occurred in this setting.

The need for two unique sets of constants in the two different areas suggests that the liquefaction potential of Quaternary geologic map units used by Witter and others (2006) (fig. 1, table 1) may vary from region to region within the bay area. Holzer and others (2008, 2010) did not collect CPT data in areas outside of the greater Oakland area and Santa Clara Valley—without CPT data available to develop the liquefaction probability constants, expanding the analysis outside of Alameda and Santa Clara Counties is not appropriate.

For areas outside the extent of Holzer and others' (2008, 2010) mapping, we use liquefaction probabilities estimated by Hope Seligson (Seligson Consulting, written commun., 2016), who applies the Hazus (Federal Emergency Management Agency, 2012) methodology. When using FEMA's nationally applicable geographic information systems (GIS)-based Hazus software, one can start with a geologic map, produce a liquefaction susceptibility map based on recommendations by Youd and Perkins (1978), and then Hazus uses that map, along with scenario or probabilistic ground motions, to estimate liquefaction probability and permanent ground deformations. However, when suitable liquefaction susceptibility mapping is available, it is best to start with that, and Hope Seligson (Seligson Consulting, written commun., 2016) has used the Knudsen and others (2000) liquefaction susceptibility maps for the bay area. Because the extent of liquefaction in future earthquakes is not expected to cover 100 percent of even the most hazardous areas, Hazus uses a factor referred to as "the proportion of map unit susceptible to liquefaction" (that is, the likelihood of susceptible conditions existing at any given location within the unit) to limit the areal extent of liquefaction. Hazus allows a maximum of 25 percent of an area to liquefy when the area has been assigned very high liquefaction susceptibility and assigns lower "proportions" to less susceptible areas. The liquefaction probability is then estimated by the following equation:

$$P[L_{SC}] = \frac{P[L_{SC} \mid PGA = a]}{K_M \times K_W} \times P_{ml} \qquad (3)$$

where $P[L_{SC} \mid PGA=a]$ is the conditional liquefaction probability for the liquefaction susceptibility category given a specific PGA (calculated within Hazus based on empirical procedures and statistical modeling by Liao and others, 1988), K_M is the moment magnitude correction factor (this corrects from a baseline magnitude of 7.5; for the HayWired scenario mainshock this is 1.09), K_W is the groundwater correction factor (this corrects from a baseline depth of 5 feet), and P_{ml} is the proportion of the geologic map unit assumed susceptible to liquefaction, described above. Hazus identifies the centroid of each census tract and calculates the values for each parameter in equation 3 at the centroid. Hazus makes use of these liquefaction probabilities and then calculates expected permanent ground deformation. These ground-deformation values are then used in the Hazus loss calculations.

Holzer and others (2008, 2010) identified map units Qhly in Santa Clara Valley and af in the greater Oakland area as having a high likelihood of experiencing liquefaction; we grouped these into one set of similar map units, which we refer to as group 1. Holzer and others (2008, 2010) grouped Qhf, Qhff, and Qhl into another group of similar map units, which we refer to as group 2. Group 1 is more susceptible to liquefaction than is group 2. See table 1 for assignments to the different liquefaction hazard groupings for the Quaternary geologic map units identified by Witter and others (2006) in our study area. For northern Santa Clara Valley, Holzer and others (2008, 2010) developed curves for two water-table depths. The main difference between our approach and that used by Holzer and others (2008, 2010) is that we use the HayWired ground motions (Aagaard, Boatwright, and others, this volume), whereas Holzer and others (2008, 2010) estimated ground motions using the Next Generation Attenuation of Ground Motions (NGA) project ground-motion prediction equation (GMPE) developed by Boore and Atkinson (2008) for two southern Hayward Fault earthquake scenarios. An additional difference between our approach and Holzer and others' (2008, 2010) approach is that the HayWired scenario ground motions used data for V_{S30}, the time-averaged shear-wave velocity (V_S) to a depth of 30 m, from Wills and others (2000) to account for site conditions (Aagaard, Boatwright, and others, this volume), whereas the Holzer and others (2008, 2010) analysis used V_{S30} generated using site-specific CPT soundings. Both the Holzer and others' (2008, 2010) and Aagaard, Boatwright, and others' (this volume) PGA data were corrected to account for local site conditions based on the site correction in Boore and Atkinson (2008).

Our analysis was conducted using GIS applications and a grid composed of approximately 50-m cells to represent the area. Liquefaction probabilities were calculated by first assigning each grid cell a Quaternary geologic map unit based on the Witter and others (2006) mapping (fig. 1), a groundwater depth (Santa Clara Valley only), and the associated liquefaction probability constants from table 2 for Santa Clara Valley or table 3 for western Alameda County. PGA values are also assigned to each cell. Equation 1 is then used to calculate the liquefaction probability for each grid cell. Data are available in Jones and Knudsen (2017).

For further discussion of the methods used to map liquefaction probabilities, and the associated uncertainties, please refer to Holzer and others (2008, 2010, 2011).

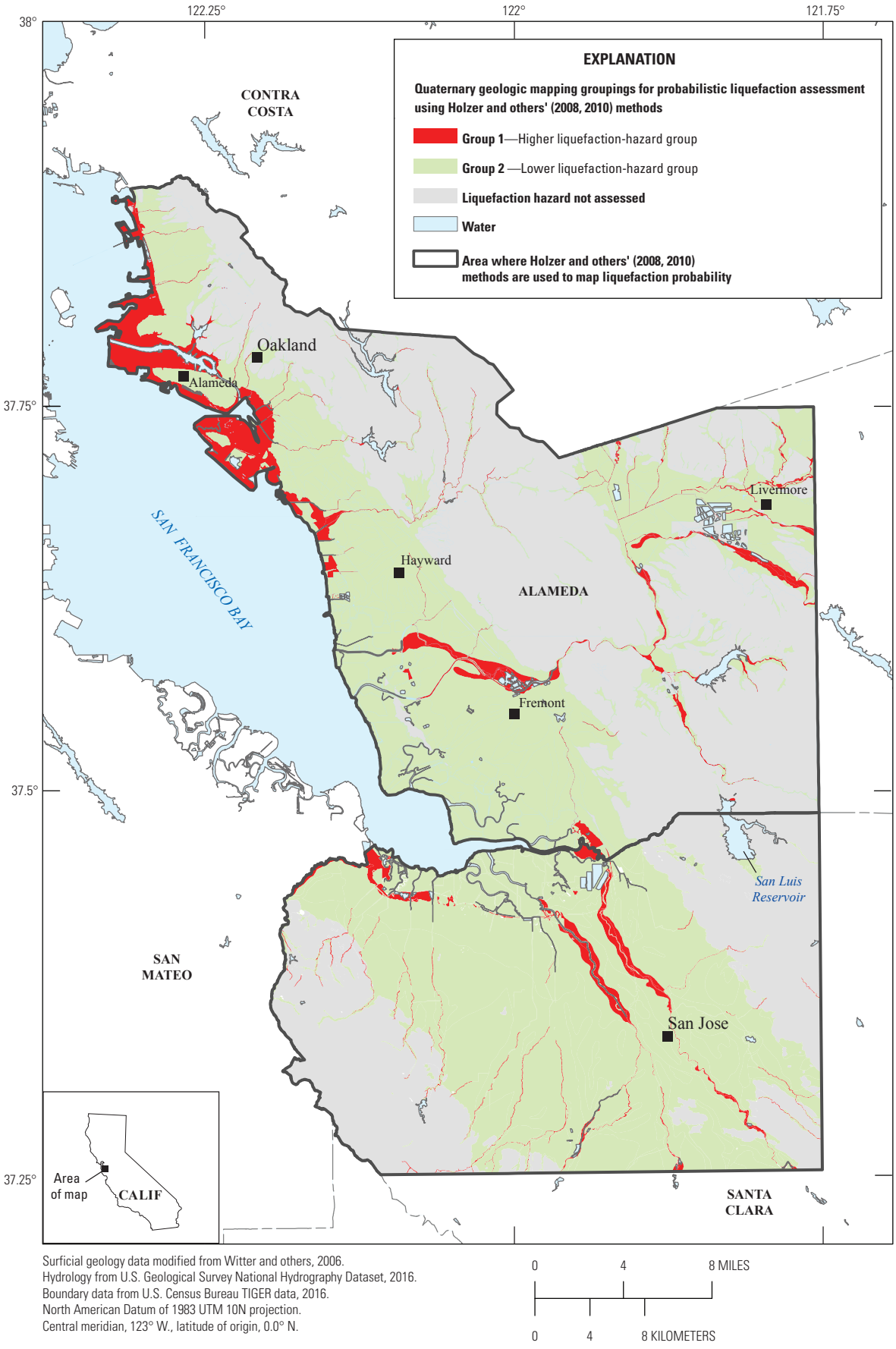

Figure 4. Map of the southeastern San Francisco Bay area, California, showing grouping of Quaternary geologic map units in liquefaction-hazard groups 1 (higher hazard) and 2 (lower hazard) for the HayWired earthquake scenario (see table 1) using the methods of Holzer and others (2008, 2010).

Table 2. Santa Clara Valley, California, liquefaction probability constants for equation 1 (summarized from Holzer and others, 2011) for the HayWired earthquake scenario.

Area	Water table depth, in meters	Group 1, map units Qhly, Qhty			Group 2, map units Qhf/Qhfy, Qhff, Qhl		
		A	B	C	A	B	C
Santa Clara Valley	1.5	0.6503	0.2981	–3.7789	1.8336	1.2479	–2.5577
	5.0	0.5886	0.4586	–3.5751	0.2268	0.6571	–3.4305

Table 3. Greater Oakland, California, area liquefaction probability constants for equation 1 (summarized from Holzer and others, 2011) for the HayWired earthquake scenario.

Area	Water table depth, in meters	Group 1, map units af			Group 2, map units Qhf, Qhff, Qhl		
		A	B	C	A	B	C
Oakland	1.5	0.7826	0.2315	–4.6645	0.0645	0.3366	–6.2881

Results

In the western Alameda County study area (fig. 5), calculated probabilities of liquefaction are as much as 75 percent for some areas along major creeks and for areas of artificial fill near the San Francisco Bay margin. According to Holzer and others (2008, 2010), the probability estimates describe both how likely liquefaction is to occur at the point where the calculation is conducted (at the location of the CPT sounding), as well as the percentage of ground surface area in that geologic map unit polygon likely to be affected by liquefaction (assuming sufficient CPT sampling for the geologic map unit). High liquefaction probabilities are mapped in the Quarry Lakes Regional Recreation Area in Fremont and at several places along Alameda Creek, Arroyo de la Laguna, and Arroyo Valle between Fremont and Livermore (fig. 5). Much of the northern part of the western Alameda County shoreline also has a relatively high probability of liquefaction (40–50 percent) where the majority of the shoreline area is developed (for example, shorelines of the cities of Alameda, Oakland, and Hayward). Comparison of the locations of past occurrences of liquefaction shown in figure 5 with the liquefaction probability mapping shows that, in general, sites of liquefaction in past earthquakes lie in areas mapped as having a high probability of liquefaction.

In the Santa Clara Valley (fig. 6), liquefaction probability reaches a high of about 50 percent. Those areas that are mapped with 40–50 percent liquefaction probability are along the southernmost part of San Francisco Bay and along the banks of Guadalupe River and Coyote Creek. These areas are generally occupied by commercial development (for example, office buildings) rather than residential development. The majority of developed land in Santa Clara Valley lies in areas with lower liquefaction probability (5–10 percent). Sites of liquefaction occurrences in past earthquakes in Santa Clara Valley are mostly located in or near areas mapped with higher probabilities of liquefaction (fig. 6).

The two liquefaction probability modeling approaches yield slightly different probability estimates for census tracts. Hazus probabilities (fig. 7) are calculated using existing liquefaction susceptibility maps (Knudsen and others, 2000; Witter and others, 2006) and water-table depths (as used in Holzer and others, 2008, 2010, 2011) at the centroid of the census tract. Probabilities for the Holzer and others' (2008, 2010, 2011) method shown in figure 8 are averages of the liquefaction probabilities in developed areas of the census tract. The average for each census tract is calculated by (1) selecting the 50-m grid cells classified as developed (low-, medium-, or high-intensity) in the 2011 National Land Cover Database (Homer and others, 2015) with nonzero liquefaction probabilities and (2) summing the probabilities and dividing by the count of the selected grid cells. Figure 9 compares liquefaction probabilities by census tract derived using the Holzer and others (2008, 2010, 2011) approach with liquefaction probabilities calculated using Hazus. Hazus estimates larger probabilities of liquefaction in most census tracts (figs. 8, 9). Liquefaction probabilities derived using Holzer and others' (2008, 2010, 2011) approach are larger than 60 percent and exceed Hazus liquefaction probabilities for those census tracts. Where the liquefaction probabilities in Hazus are capped at 25 percent (for example, in areas of artificial fill around the margins of San Francisco Bay), the liquefaction probabilities derived using the Holzer and others' (2008, 2010, 2011) methods are mostly in the range of 40–60 percent.

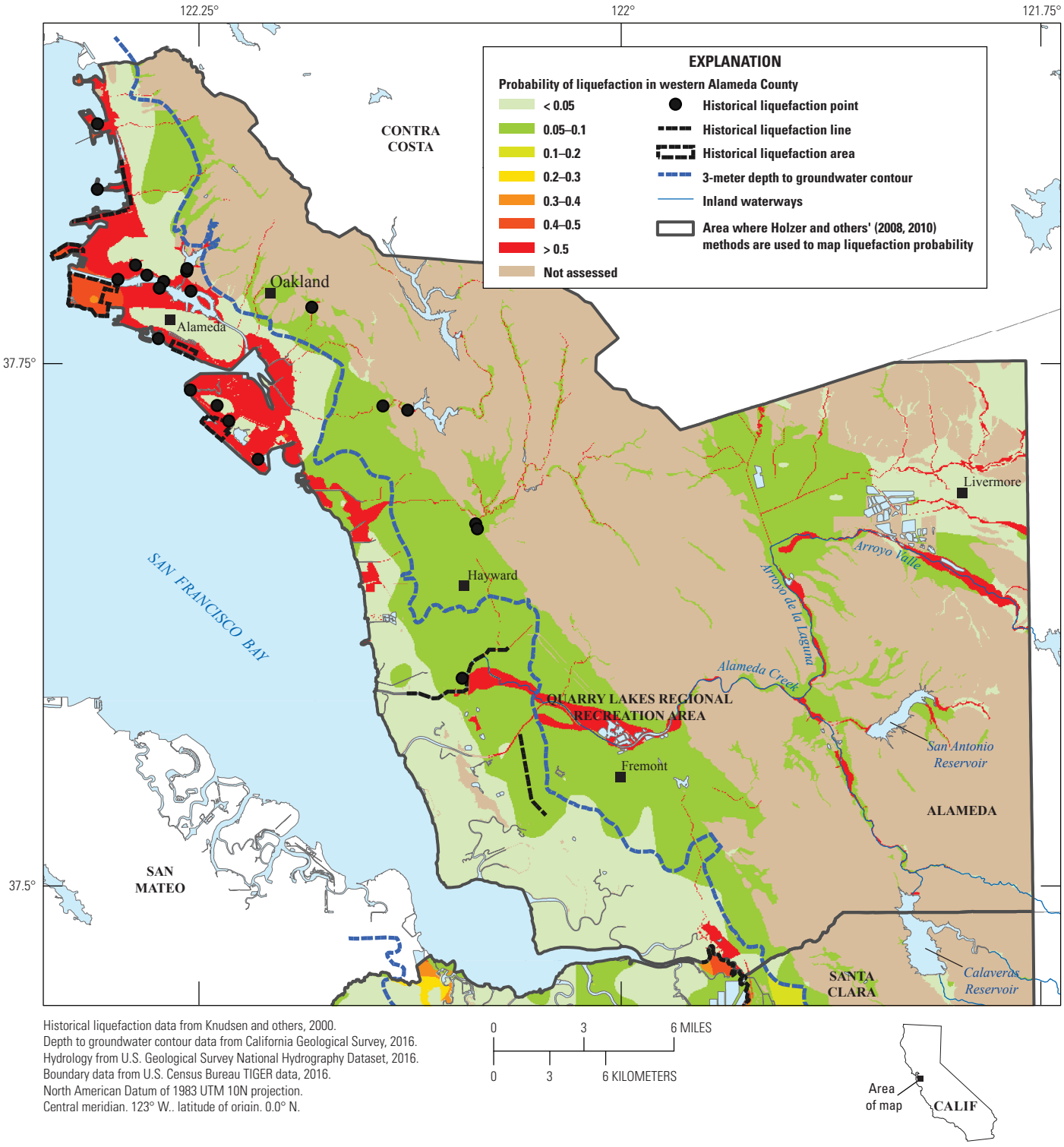

Figure 5. Map of the southeastern San Francisco Bay area, California, showing probability of liquefaction in the HayWired earthquake scenario for western Alameda County. Historical liquefaction occurrences are from the compilation by Knudsen and others (2000). We have chosen to show lateral spread, ground settlement, or sand boil points for which Knudsen and others (2000) assigned a moderate to high degree of location certainty ("S" events, defined as having indefinite or approximate locations by Knudsen and others, 2000, were excluded due to higher uncertainty in positional accuracy). Note the good correlation between past occurrences of liquefaction and the mapping of higher liquefaction probabilities. <, less than; >, greater than.

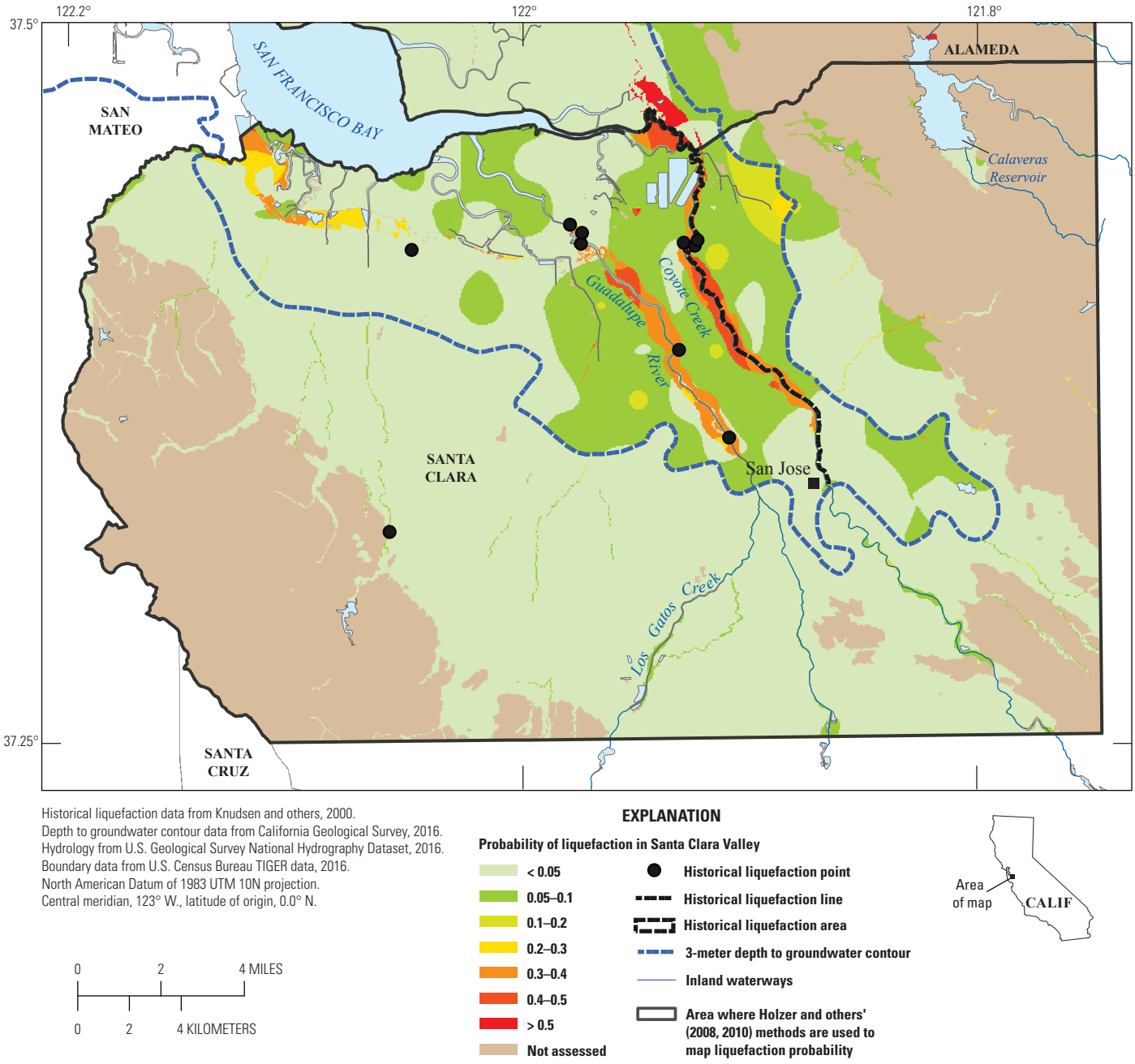

Figure 6. Map of the southeastern San Francisco Bay area, California, showing probability of liquefaction in the HayWired earthquake scenario for the Santa Clara Valley. Historical liquefaction occurrences are from the compilation by Knudsen and others (2000). We have chosen to show lateral spread, ground settlement, or sand boil points for which Knudsen and others (2000) assigned a moderate to high degree of location ("S" events, defined as having indefinite or approximate locations by Knudsen and others, 2000, were excluded due to higher uncertainty in positional accuracy). Note the good correlation between past occurrences of liquefaction and the mapping of higher liquefaction probabilities. <, less than; >, greater than.

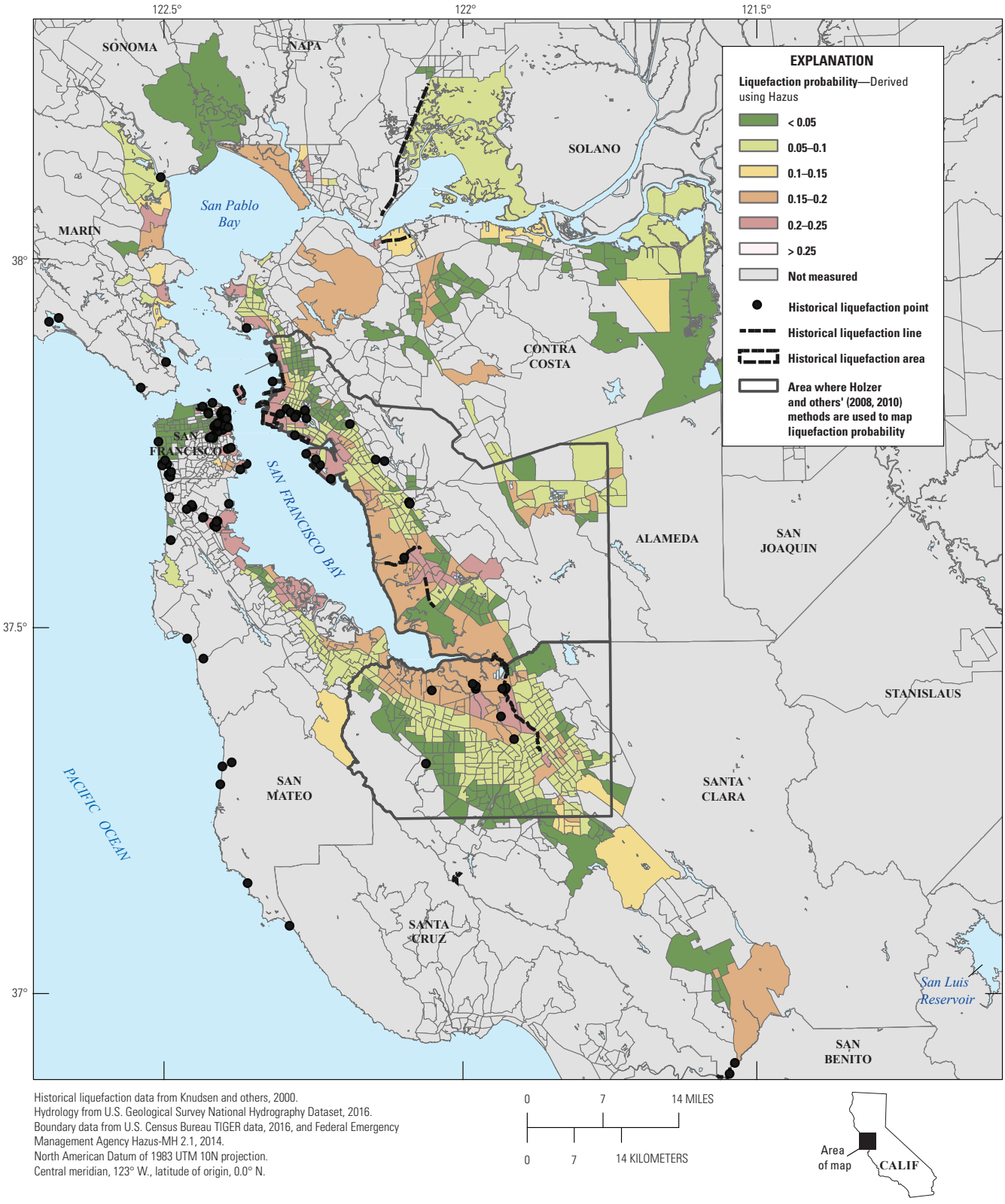

Figure 7. Map of the San Francisco Bay region, California, showing tract-level liquefaction probabilities for the HayWired earthquake scenario as estimated using Hazus-MH 2.1 (Federal Emergency Management Agency, 2012). Tract-level probabilities are estimated by Hazus at the tract centroid using liquefaction susceptibility, peak ground acceleration, magnitude, depth to groundwater, and the geologic map unit's liquefaction susceptibility proportion. Historical liquefaction occurrences are from the compilation by Knudsen and others (2000). We have chosen to show lateral spread, ground settlement, or sand boil points for which Knudsen and others (2000) assigned a moderate to high degree of location. <, less than; >, greater than.

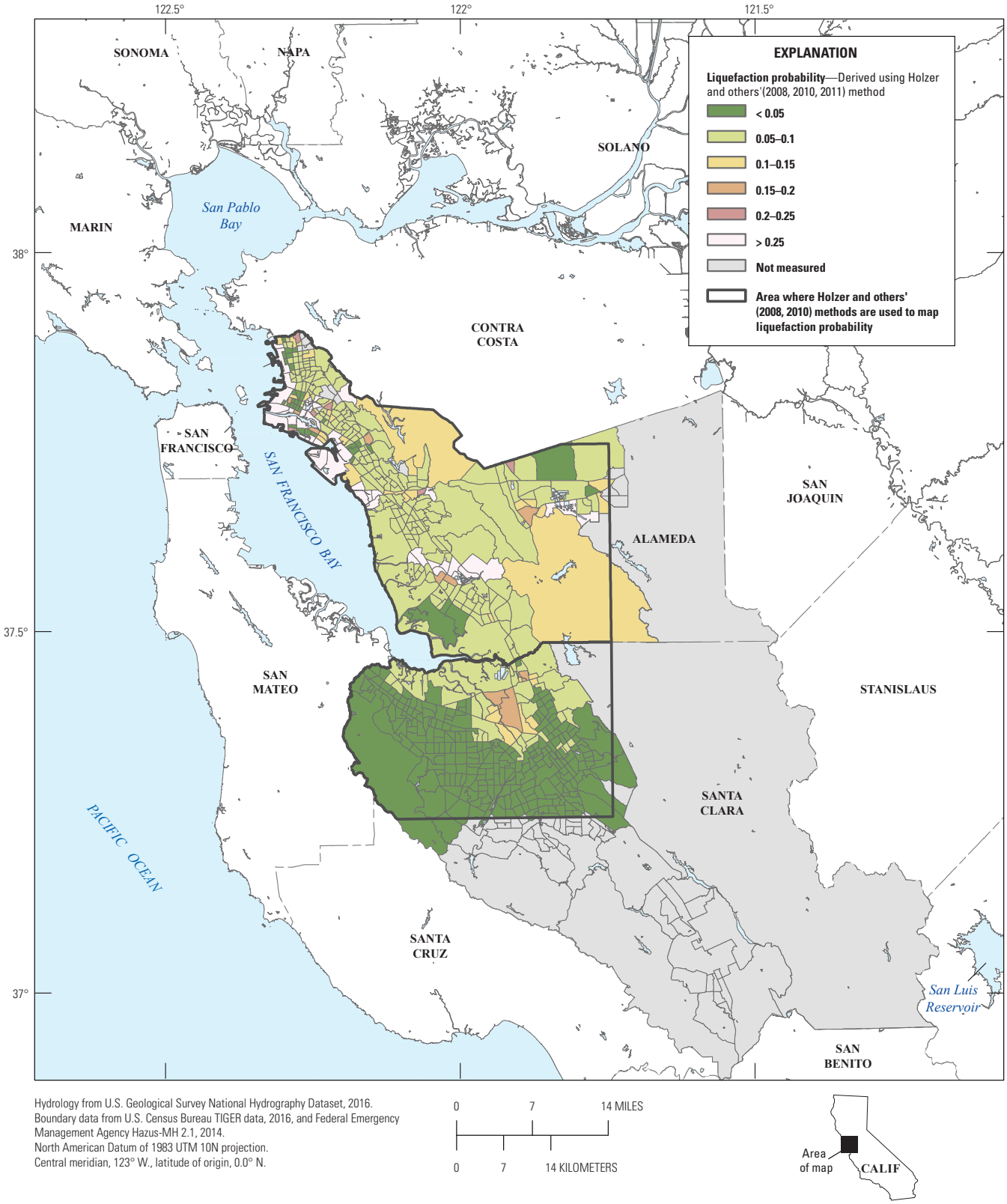

Figure 8. Map of the San Francisco Bay region, California, showing tract-level liquefaction probabilities in the HayWired earthquake scenario for Alameda and Santa Clara Counties, as estimated based on Holzer and others (2008, 2010, 2011). Tract-level probabilities are estimated by taking the sum of all non-zero 50-meter-resolution grid-cell-based probabilities in 2011 National Land Cover Database (Homer and others, 2015) developed (low-, medium-, or high-intensity) areas in a tract and dividing by the count of summed grid cells in the tract. <, less than; >, greater than.

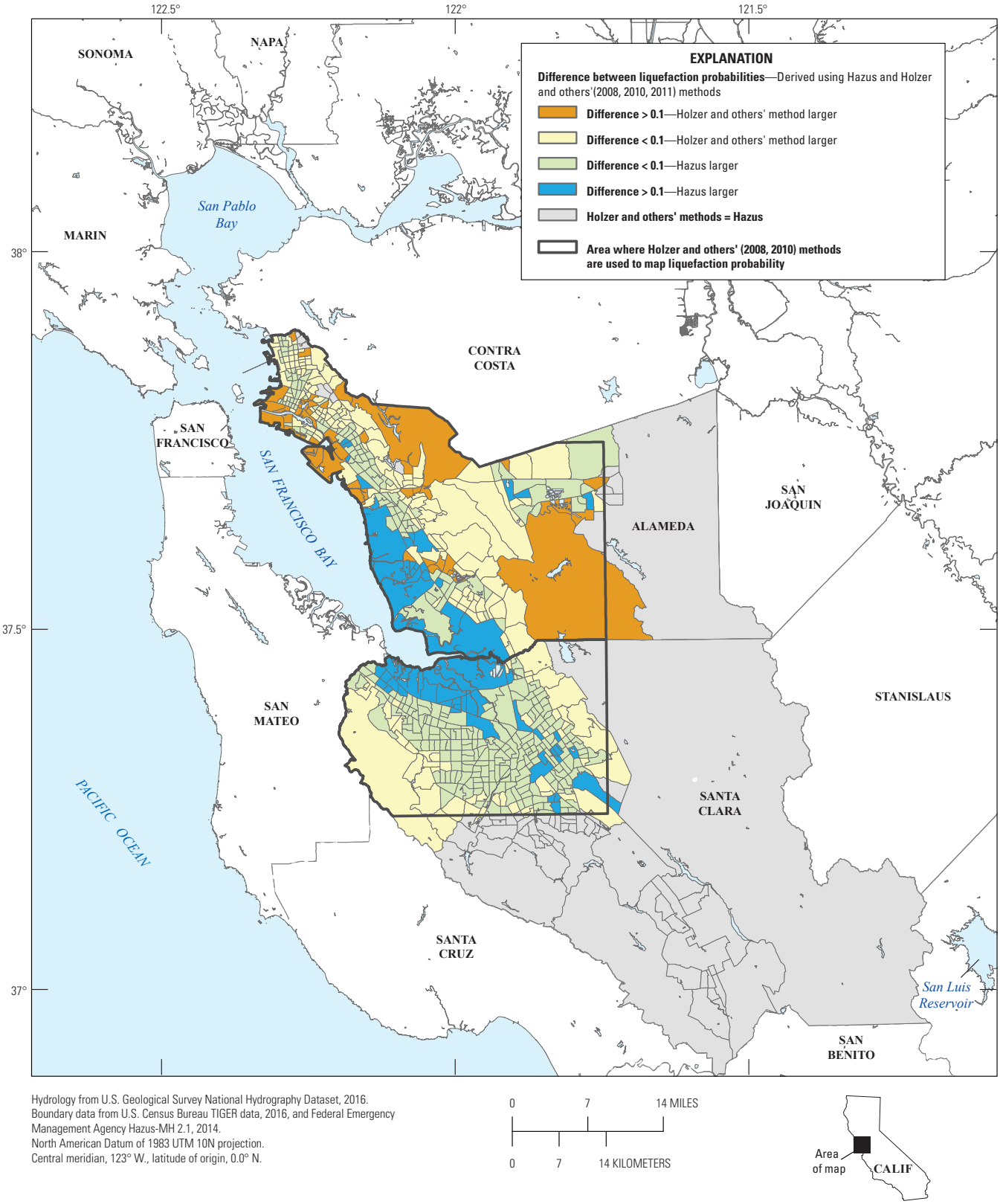

Figure 9. Map of the San Francisco Bay region, California, showing the difference between Hazus-MH 2.1 (Federal Emergency Management Agency, 2012) derived liquefaction probability values and liquefaction probability derived using the methods of Holzer and others (2008, 2010, 2011) for Alameda and Santa Clara Counties in the HayWired earthquake scenario. Probabilities are represented at the census-tract level; Hazus uses census tract centroid data, whereas values derived using the Holzer and others' (2008, 2010, 2011) methods are averages (the sum of all non-zero 50 meter-resolution grid-cell-based liquefaction probabilities in 2011 National Land Cover Database (Homer and others, 2015) developed (low-, medium-, or high-intensity) areas in a tract divided by the count of summed grid cells in the tract). <, less than; >, greater than; =, equal to.

Knowledge Gaps and Modeling Limitations

Holzer and others (2008, 2010) did not collect sufficient CPT data to characterize all Quaternary geologic map units in their study area. Thus, Holzer and others (2008, 2010) simplified the Quaternary geologic mapping from Witter and others (2006) by grouping map units into one of three groups with high, lower, and negligible potential for liquefaction; we did the same. To fully explore the range in liquefaction probability and provide more detailed mapping, a much greater number of CPT soundings would need to be collected for each geologic map unit mapped in the area of interest.

In earlier work, Toprak and Holzer (2003) concluded that, in general, areas with CPT soundings with calculated LPI values of 5 or greater are assumed to experience surface manifestations of liquefaction. Holzer and others' (2008, 2010) subsequent liquefaction-probability mapping is based on this conclusion, and the calculated "probabilities of liquefaction" are actually probabilities of calculated LPI being greater than 5. Further, Holzer and others (2008, 2010) are able to both calculate a probability of liquefaction at a point on the land surface where their CPT data are collected and use that same probability to represent an extent of the area likely to liquefy, based on the assumption that they have adequately sampled the extent and variability of the map unit polygons with their CPT soundings. This assumption may or may not be valid for all of the Quaternary geologic map units.

Holocene San Francisco Bay mud (Qhbm) around the southern margin of San Francisco Bay was not evaluated by Holzer and others (2008, 2010) because it was mostly inaccessible to their CPT truck. This area is sparsely developed, but there may be implications for the lifeline infrastructure located in areas mapped as Qhbm. Infrastructure found on Holocene San Francisco Bay mud deposits around the southern margin of the bay includes substations, electric-power-generation plants, transmission lines, railways, and pipelines. We assigned Qhbm to group 2, the moderate liquefaction-hazard group.

Existing regional geologic mapping has been conducted and compiled at a 1:24,000 scale. Site-specific conditions may be different than those portrayed, particularly in areas of sandy artificial fill, where mitigation of soil to preclude liquefaction and (or) related damage to structures may have been conducted. The mapping by Witter and others (2006) and Knudsen and others (2000) is based on the most recent 7.5-minute topographic maps, and land-surface topography has been altered in many places since publication of the most recent version of the topographic maps. Where large-scale grading/earth movement for development has occurred, the Quaternary geologic maps may not capture the finer resolution nature of geologic materials.

In Holzer and others (2008, 2010), the calculation of liquefaction probabilities includes use of historical high-groundwater data from CGS, as well as depths to groundwater collected at the time of CPT soundings. The methodology used by Holzer and others (2008, 2010), and this study, does not account for seasonal fluctuations in depth to groundwater nor for differences between the historical high groundwater and the depth to groundwater at the time of a future earthquake. Drought conditions in California will increase the depth to groundwater in some parts of the San Francisco Bay area. At the time of this report, California had been experiencing drought conditions for several years, and groundwater levels can start to show measurable changes (increasing depth to groundwater) after at least one year of drought (U.S. Geological Survey, 2015). As the depth to groundwater increases, liquefaction potential decreases. However, around the bay margins, where most of the high liquefaction probability deposits have been identified, the depth to groundwater is typically controlled by water levels in the bay. Furthermore, sea-level rise may have increased the liquefaction hazard in some Bay margin areas, like the City of San Francisco (Thomas Holzer, U.S. Geological Survey, written commun., 2015).

In assessing liquefaction hazards, earthquake magnitude is generally used as a surrogate for earthquake duration (for example, Youd and others, 2001). The Holzer and others (2008, 2010, 2011) methodology uses earthquake magnitude to calculate the liquefaction factor of safety, which is the basis for estimating liquefaction potential. Earthquake duration has a direct impact on the occurrence, extent and intensity of liquefaction surface manifestations, with longer durations increasing the damage from liquefaction. Earthquake durations longer or shorter than the average for a given magnitude may lead to underpredictions or overpredictions of liquefaction probability, respectively.

The calculation of liquefaction probability is highly dependent on the ground motions used. For the HayWired scenario mainshock, the PGA estimates we use were simulated by Aagaard, Boatwright, and others (this volume) using a three-dimensional physics-based model. The limitations of that model in areas with soft soil, such as around the margins of San Francisco Bay, are described by Aagaard, Boatwright, and others (this volume). Also, because our analysis makes use of a relatively fine 50-m grid, and the PGA values are provided by Aagaard, Boatwright, and others (this volume) as a much coarser grid, we interpolated between the provided PGA values. Use of shaking maps generated by other Hayward Fault earthquake scenarios would likely result in a different depiction of liquefaction hazard; for example, shaking in San Francisco might be greater for other scenario earthquakes.

Improved hazard-mapping approaches by geologic and geotechnical communities would help to better assess liquefaction hazards. For example, relatively detailed topographic information is increasingly available for many areas, and the identification of scarps and gentle slopes could be used, along with better methods of predicting liquefaction-related ground-surface displacement. Finer-resolution input data and improved models for predicting liquefaction-related ground-surface displacement would be useful to a wide range of interested parties.

Conclusion

The liquefaction-probability mapping based on the methods of Holzer and others (2008, 2010, 2011) for western Alameda County and Santa Clara Valley provides insight into the liquefaction hazard for a large earthquake on the Hayward

Fault. For the M_w 7.0 HayWired scenario mainshock, a high likelihood of liquefaction is calculated for several areas, and thus liquefaction may be a major source of significant damage. Impacts from liquefaction-induced ground failure are expected to occur in residential areas, commercial areas, and especially around the San Francisco Bay margin, where much of the region's extensive network of lifelines are located. Liquefaction is expected to be less extensive in the northern Santa Clara Valley than in western Alameda County and the areas affected are expected to be mostly commercial. Note that our liquefaction probability estimates do not account for site-specific engineering solutions that have been implemented to reduce either the extent and severity of liquefaction or the resulting damage to existing structures.

Liquefaction probabilities for western Alameda County and the Santa Clara Valley differ (in some cases are higher) from Holzer and others' (2008, 2010) results, because we use the Aagaard, Boatwright, and others (this volume) HayWired shaking depiction, which takes advantage of earthquake simulations. Therefore, there are higher (and lower) shaking levels than the estimates used in the Holzer and others' (2008, 2010) studies where PGA was derived from the NGA ground-motion prediction equation by Boore and Atkinson (2008).

The liquefaction-probability mapping using the Holzer and others' (2008, 2010) methodology is being used in other analyses of the HayWired scenario project, including in calculating loss estimates using Hazus (Hope Seligson, Seligson Consulting, written commun., 2016). However, for other areas shaken by the scenario earthquake (including in San Francisco, where liquefaction has occurred in the past), we only have liquefaction-probability estimates based on the Hazus approach. Results of our analyses are being incorporated into analyses of infrastructure/lifeline exposure, damages, and potential service disruptions.

Acknowledgments

Thomas Holzer and Thomas Noce (U.S. Geological Survey, USGS) were consulted on application of their methods to the HayWired scenario mainshock and expanded geographical area. Thomas Holzer contributed to the knowledge gaps analyses. Reviewers Thomas Holzer and Eric Thompson (USGS) provided thoughtful reviews of the material. Amandine Dhellemmes (USGS) ran the preliminary analysis, explained differences in results from using the HayWired scenario compared to previously-used scenarios, and helped to identify geologic units that were not accounted for in the extended region.

References Cited

Aagaard, B.T., Graves, R.W., Schwartz, D.P., Ponce, D.A., and Graymer, R.W., 2010, Ground-motion modeling of Hayward Fault scenario earthquakes, Part I—Construction of the suite of scenarios: Bulletin of the Seismological Society of America, v. 100, no. 6, p. 2927–2944, accessed December 23, 2016, at http://dx.doi.org/10.1785/0120090324.

Boore, D.M., and Atkinson, G.M., 2008, Ground-motion prediction equations for the average horizontal component of PGA, PGV, and 5%-damped PSA at spectral periods between 0.01s and 10.0s: Earthquake Spectra, v. 24, no. 1, p. 99–138, accessed December 15, 2016, at http://dx.doi.org/10.1193/1.2830434.

Cubrinovski, M., Taylor, M., Robinson, K., Winkley, A., Hughes, M., Haskell, J., and Bradley, B., 2014, Key factors in the liquefaction-induced damage to buildings and infrastructure in Christchurch—Preliminary findings: 2014 New Zealand Society for Earthquake Engineering, Auckland, New Zealand, March 21–23, 2014, accessed December 15, 2016, at http://db.nzsee.org.nz/2014/Orals.htm.

Federal Emergency Management Agency, 2012, Hazus multi-hazard loss estimation methodology, earthquake model, Hazus®-MH 2.1 technical manual: Federal Emergency Management Agency, Mitigation Division, accessed December 15, 2016, at http://www.fema.gov/media-library-data/20130726-1820-25045-6286/hzmh2_1_eq_tm.pdf.

Green, R.A., Cubrinovski, M., Cox, B., Wood, C., Wotherspoon, L., Bradley, B., and Maurer, B., 2014, Select liquefaction case histories from the 2010–2011 Canterbury earthquake sequence: Earthquake Spectra, v. 30, no. 1, p. 131–153, accessed December 15, 2016, at http://dx.doi.org/10.1193/030713EQS066M.

Holzer, T.L., and Youd, T.L., 2007, Liquefaction, ground oscillation, and soil deformation at the Wildlife Array, California: Seismological Society of America Bulletin, v. 97, no. 3, p. 961–976.

Holzer, T.L., Noce, T.E., and Bennett, M.J., 2008, Liquefaction hazard maps for three earthquake scenarios for the communities of San Jose, Campbell, Cupertino, Los Altos, Los Gatos, Milpitas, Mountain View, Palo Alto, Santa Clara, Saratoga, and Sunnyvale, northern Santa Clara County, California: U.S. Geological Survey Open-File Report 2008–1270, 29 p., 3 plates, and database, https://pubs.usgs.gov/of/2008/1270/.

Holzer, T.L., Noce, T.E., and Bennett, M.J., 2010, Predicted liquefaction in the greater Oakland area and northern Santa Clara Valley during a repeat of the 1868 Hayward Fault (*M*6.7–7.0) earthquake: Proceedings of the Third Conference on Earthquake Hazards in the Eastern San Francisco Bay Area October 22–24, 2008.

Holzer, T.L., Noce, T.E., and Bennett, M.J., 2011, Liquefaction probability curves for surficial geologic deposits: Environmental and Engineering Geoscience, v. XVII, no. 1, p. 1–21.

Homer, C.G., Dewitz, J.A., Yang, L., Jin, S., Danielson, P., Xian, G., Coulston, J., Herold, N.D., Wickham, J.D., and Megown, K., 2015, Completion of the 2011 National Land Cover Database for the conterminous United States—Representing a decade of land cover change information: Photogrammetric Engineering and Remote Sensing, v. 81, no. 5, p. 345–354, accessed December 15, 2016, at http://www.asprs.org/a/publications/pers/2015journals/PERS_May_2015/HTML/files/assets/basic-html/index.html#345/z#noFlash.

Iwasaki, T., Tokida, K., Tatsuoka, F., Watanabe, S., Yasuda, S., and Sato, H., 1982, Microzonation for soil liquefaction potential using simplified methods: Proceedings of the 3rd International Earthquake Microzonation Conference, Seattle, p. 1319–1330.

Jones, J.L., and Knudsen, K.L., 2017, Liquefaction potential as a result of HayWired earthquake scenario mainshock (April 18, 2018) shaking in Alameda and Santa Clara Counties, San Francisco Bay area, California: U.S. Geological Survey data release, accessed April 18, 2017, at https://doi.org/10.5066/F74X5610.

Knudsen, K.L., and Bott, J.D.J., 2011, Geologic and geomorphic evaluation of liquefaction case histories for rapid hazard mapping [abs]: Seismological Research Letters, v. 82, p. 334.

Knudsen, K.L., Bott, J.D.J., Woods, M.O., and McGuire, T.L., 2009, Development of a liquefaction hazard screening tool for Caltrans bridge sites: Technical Conference on Lifeline Engineering, Lifeline Earthquake Engineering in a Multihazard Environment, p. 573–584.

Knudsen, K.L., Sowers, J.M., Witter, R.C., Wentworth, C.M., and Helley, E.J., 2000, Preliminary maps of Quaternary deposits and liquefaction susceptibility, nine-county San Francisco Bay region, California—a digital database: U.S. Geological Survey Open-File Report 00–444, 21 p. and database, https://pubs.usgs.gov/of/2000/of00-444/.

Liao, S.S., Veneziano, D., and Whitman, R.V., 1988, Regression models for evaluating liquefaction probability: Journal of Geotechnical Engineering, v. 114, no. 4, p. 389–411.

McSaveney, E., 2014, 13.—Historic earthquakes: Te Ara—The Encyclopedia of New Zealand, accessed December 15, 2016, at http://www.teara.govt.nz/en/historic-earthquakes/page-13.

Rausch, A.L., 1997, EPOLLS: An empirical method for predicting surface displacements due to liquefaction-induced lateral spreading in earthquakes: Blacksburg, Virginia Polytechnic Institute and State University, Ph.D. dissertation, 333 p., 80 figs.

Scott, M., and Carville, O., 2016, Christchurch earthquake—Eerie images of city's red-zone, five years on: New Zealand Herald, Feb. 17, 2016, accessed December 20, 2016, at http://www.nzherald.co.nz/nz/news/article.cfm?c_id=1&objectid=11591021.

Tinsley, J.C., III, and Ponti, D., 2008, ShakeOut scenario appendix C—Characteristics of earthquake-induced permanent ground deformation and examples from past earthquakes: U.S. Geological Survey Open-File Report 2008–1150, appendix C, 35 p., https://pubs.usgs.gov/of/2008/1150/.

Tinsley, J.C., III, Egan, J.A., Kayern, R.E., Bennett, M.J., Kropp, A., and Holzer, T.L., 1998, Appendix—Maps and descriptions of liquefaction and associated effects, *in* Holzer, T.L., ed., The Loma Prieta, California, Earthquake of October 17, 1989—Liquefaction: U.S. Geological Survey Professional Paper 1551–B.

Tonkin and Taylor, Ltd., 2013, Liquefaction vulnerability study: Tonkin and Taylor, Ltd., report 52020.0200/v1.0, February 2013, prepared for Earthquake Commission [New Zealand], 52 p. and 14 appendixes, accessed December 15, 2016, at http://www.eqc.govt.nz/sites/public_files/documents/liquefaction-vulnerability-study-final.pdf.

Toprak, S., and Holzer, T.L., 2003, Liquefaction potential index—Field assessment: Journal of Geotechnical and Geoenvironmental Engineering, v. 129, no. 4, p. 315–322.

U.S. Geological Survey, 2015, Drought Impacts: U.S. Geological Survey California Water Science Center website, accessed December 15, 2016, at http://ca.water.usgs.gov/data/drought/drought-impact.html.

van Ballegooy, S., Malan, P., Lacrosse, V., Jacka, M.E., Cubrinovski, M., Bray, J.D., O'Rourke, T.D., Crawford, S.A., and Cowan, H., 2014, Assessment of liquefaction-induced land damage for residential Christchurch: Earthquake Spectra, v. 30, no. 1, p. 31–55.

Wills, C J., Petersen, M., Bryant, W.A., Reichle, M., Saucedo, G.J., Tan, S., Taylor, G., and Treiman, J., 2000, A site-conditions map for California based on geology and shear-wave velocity: Bulletin of the Seismological Society of America, v. 90, no. 6B, p. S187–S208, doi: 10.1785/0120000503.

Witter, R.C., Knudsen, K.L., Sowers, J.M., Wentworth, C.M., Koehler, R.D., and Randolph, C.E., 2006, Maps of Quaternary deposits and liquefaction susceptibility in the central San Francisco Bay region, California, part 3—Description of mapping and liquefaction interpretation: U.S. Geological Survey Open-File Report 2006–1037, ver. 1.1., https://pubs.usgs.gov/of/2006/1037/.

Youd, T.L., 1973, Liquefaction, flow and associated ground failure: U.S. Geological Survey Circular 688, 12 p., https://pubs.er.usgs.gov/publication/cir688.

Youd, T.L., and Hoose, S.N., 1978, Historical ground failures in Northern California triggered by earthquakes: U.S. Geological Survey Professional Paper 993, 177 p., https://pubs.usgs.gov/pp/1978/pp0993.

Youd, T.L., Idriss, I.M., Andrus, R.D., Arango, I., Castro, G., Christian, J.T., Dobry, R., Finn, W.D.L., Harder, L.F., Jr., Hynes, M.E., Ishihara, K., Koester, J.P., Liao, S.S.C., Marcuson, W.F., III, Martin, G.R., Mitchell, J.K., Moriwaki, Y., Power, M.S., Robertson, P.K., Seed, R.B., and Stokoe, K.H., II, 2001, Liquefaction resistance of soils: Summary report from the 1996 NCEER and 1998 NCEER/NSF workshops on evaluation of liquefaction resistance of soils: Journal of Geotechnical and Geoenvironmental Engineering, v. 127, no. 10, p. 817–833.

Youd, T.L., and Perkins, D.M., 1978, Mapping liquefaction-induced ground failure potential: Journal of the Geotechnical Engineering Division, v. 104, no. GT4, p. 443–446.

The HayWired Earthquake Scenario—Earthquake Hazards
Edited by Shane T. Detweiler and Anne M. Wein
Scientific Investigations Report 2017–5013–A–H
[Also see https://doi.org/10.3133/sir20175013]

Chapter F

HayWired Scenario Mainshock—Earthquake-Induced Landslide Hazards

By Timothy P. McCrink[1] and Florante G. Perez[1]

Abstract

The HayWired scenario examines a hypothetical earthquake (mainshock) with a moment magnitude (M_w) of 7.0 occurring on April 18, 2018, at 4:18 p.m. on the Hayward Fault in the east bay part of California's San Francisco Bay area. The probability of widespread slope failures (landslides) triggered by the scenario earthquake has been estimated for a 10-county area surrounding San Francisco Bay. The four primary datasets essential to this estimation are a regional-scale geologic map of the area, geologic-strength parameters compiled as a part of the California Geological Survey Seismic Hazard Mapping Program, earthquake-shaking data from the U.S. Geological Survey (USGS) ShakeMap developed for this scenario, and 10-meter digital elevation data from the USGS 2009 National Elevation Dataset (NED). A map of earthquake-triggered landslide susceptibility was prepared in terms of yield acceleration, which incorporates geologic-material strength and slope gradient. A simplified Newmark rigid sliding-block slope-stability model was used to estimate cumulative downslope displacement of hillslopes for the scenario ground shaking, and probability of landslide failure as a function of predicted Newmark displacement was calculated. Known limitations to the methodology used and areas for improvement are discussed. In a later section of this report, calculated landslide displacements and probabilities are used to identify vulnerable highways and utility infrastructure and to estimate economic loss to structures in developed areas of the San Francisco Bay region.

Introduction

The HayWired scenario examines a hypothetical earthquake (mainshock) with a moment magnitude (M_w) of 7.0 occurring on April 18, 2018, at 4:18 p.m. on the Hayward Fault in the east bay part of California's San Francisco Bay area. One component of the scenario is to examine infrastructural impacts in the San Francisco Bay area from the earthquake. Slope failures (landslides) triggered by such a seismic event can be expected to cause extensive damage affecting major transportation corridors, communications networks, and lifeline infrastructure, as well as numerous structures in densely populated hilly areas of the San Francisco Bay region. This study estimates the probability of earthquake-triggered slope failure in a 10-county area surrounding San Francisco Bay (fig. 1) to assist in the estimation of damages and losses for this scenario mainshock event.

A number of methods to predict the occurrence of earthquake-triggered landslides have been developed over the past 15 years (for example, Jibson and others, 2000; Jibson, 2007; Bray and Travasarou, 2007; Saygili and Rathje, 2008; Rathje and Saygili, 2008; Rathje and Antonakos, 2011). Generally, these methods require estimates of one or more ground-shaking parameters, slope gradient, and geologic-material strength. More recently, and similar to this project, attempts have been made to develop near-real-time assessments of the likelihood of earthquake-triggered slope failures as a part of the U.S. Geological Survey (USGS) Prompt Assessment of Global Earthquakes for Response (PAGER) system using ground-motion estimates as input (Godt and others, 2009; Nowicki and others, 2014). A major goal of this study was the development of a procedure that would lead to the development of a statewide earthquake-triggered landslide-susceptibility map of California using the methodologies listed above along with maps and data being compiled at the California Geological Survey (CGS). If available, such a map could be used to rapidly identify areas of concentrated earthquake-induced slope failures given only ShakeMap ground-motion input. This product would be valuable to Earth scientists and emergency responders following a large urban earthquake in California.

The methodology used to estimate landslide hazards for the HayWired scenario uses the Jibson (2007) Newmark rigid sliding-block displacement analysis regression equation, which has been adopted by the CGS Seismic Hazard Mapping Program. The Seismic Hazard Mapping Program, initiated after the M_w 6.9 1989 Loma Prieta earthquake, produces regulatory "zones of required investigation." The purpose of the zone maps for earthquake-triggered landslides created by CGS is to identify areas with a high potential for slope failure during

[1]California Geological Survey.

Figure 1. Generalized map of the San Francisco Bay region, California, showing the 10-county HayWired earthquake scenario study region.

earthquake shaking so that local governmental agencies can require site-specific geologic and geotechnical investigations to assess the presence of, and if necessary, require mitigations for seismic slope-instability hazards. Soon after the Loma Prieta earthquake, CGS conducted a pilot study in the southern Santa Cruz Mountains, where a methodology developed by the USGS (Wieczorek and others, 1985) in San Mateo County was applied to slope failures triggered by the 1989 earthquake (McCrink and Real, 1996; McCrink, 2001). The purpose of the CGS study was to not only evaluate the ability of the USGS model to identify the Loma Prieta slope failures but also to find ways to improve it. The USGS approach in San Mateo County used conservative estimates of best-available geologic-material strength for broad groups of rock types, upper and lower bound earthquake strong-motion records, and saturated and unsaturated slope conditions in a Newmark rigid sliding-block analysis. When applied directly to the Loma Prieta earthquake slope failures, the CGS pilot study found that roughly 50 percent of the triggered slope failures were included in the higher levels of hazard potential, and the other 50 percent fell in the lowest level of hazard potential. The advisory committee established to provide input to CGS on zone-map preparation had recommended that regulatory zone maps should strive to include 80 to 90 percent of the hazard, and the pilot study went on to find improvements to the USGS methodology.

Although the basic Newmark sliding-block model was retained, the CGS pilot study applied several data improvements to the methodology—a new 10-meter (m) digital elevation model (DEM) was used to prepare a slope-gradient map, a detailed digital map of existing landslides was prepared, and a map identifying areas underlain by adverse bedding conditions was prepared. In addition, a considerable number of geotechnical laboratory strength tests were compiled for most of the geologic formations that experienced earthquake-triggered slope failures in the Loma Prieta earthquake. Statistical analyses of these laboratory tests were performed and used to categorize geologic formations into geologic material strength groups. A number of stability analyses were run using a representative strong-motion recording from the earthquake with varying strength parameters, thickness of the failure mass, and slope-saturation conditions. An optimal parameter set for preparing zone maps was selected by comparing the percentage of mapped ground failures captured by each parameter set with the percentage of the map area that would need to be included in a hazard zone. For the purpose of preparing regulatory zones, a conservative parameter set was selected, where strength parameter cohesion is set to zero. However, for this study, we selected a set of parameters that was termed "optimum" in the CGS pilot study (fig. 2). The parameter set selected for the HayWired scenario uses mean values of effective internal angle of friction (ϕ') and median values of effective cohesion in pounds per square foot (c'), a landslide thickness of 50 feet, and unsaturated slope conditions. It was called optimum in the pilot study, because it performed the best in capturing the slope failures triggered by the scenario earthquake (78 percent), while simultaneously minimizing the amount of area considered hazardous (40 percent).

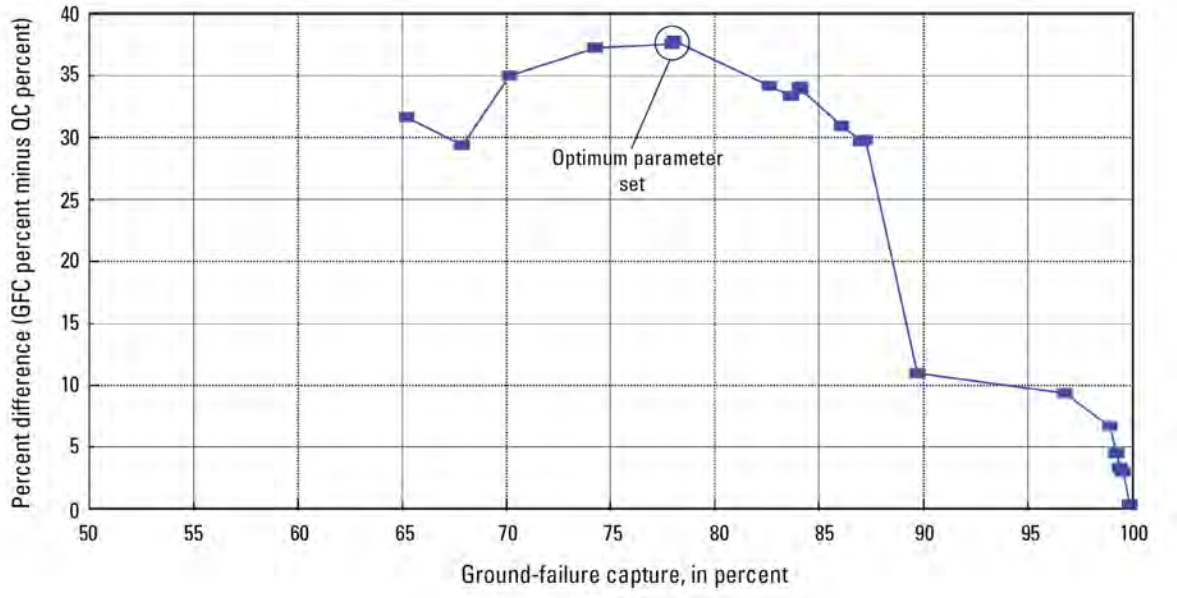

Figure 2. Graph of the parameter-set efficiency from a California Geological Survey pilot study in the Santa Cruz Mountains, California, using ground failures from the moment magnitude (M_w) 6.9 1989 Loma Prieta earthquake (modified from McCrink, 2001). The point labeled "optimum parameter set" reflects the parameter set used in this study—mean effective internal angle of friction (ϕ'), median values of effective cohesion (c'), unsaturated slopes, and landslide thickness of 50 feet. GFC, ground-failure capture; QC, quadrangle area covered.

The challenge in conducting the present study was applying a procedure developed for 1:24,000-scale mapping, where scale-appropriate details could be incorporated, to the whole San Francisco Bay region at a much smaller map scale. Certain details that improve zone-mapping results, such as identifying areas with adverse bedding conditions, could not be included at the smaller scale required in this project. More significantly, rock strength values correlated with detailed geologic mapping at 1:24,000 scale had to be applied to more generalized mapping covering the entire study region. The primary effect of significant reductions in map scale is the aggregation of many similar-age rock units into a few map units. These generalizations undoubtedly decrease the accuracy of the maps by some unknown amount, but the overall approach in this study, using locally derived geologic-material strengths and higher resolution digital-terrain data, is expected to perform better than earlier regional hazard-mapping methods (for example, Wieczorek and others, 1985) or the methodologies for global application at much coarser resolution under development for Prompt Assessment of Global Earthquakes for Response (PAGER) (Godt and others, 2009; Nowicki and others, 2014).

Methodology and Data

Estimation of cumulative permanent slope displacements requires three general data types. A geologic-material-strength map and slope-gradient data are required to calculate yield acceleration (a_y), the key earthquake-landslide susceptibility parameter (described below), and ground shaking parameters from the HayWired scenario ShakeMap are combined with a_y to estimate displacements. The following sections describe sources of these data and processing performed to prepare them for analyses.

Geologic-Material-Strength Map

The determination of appropriate dynamic geologic-material strengths to use over a large map area is simultaneously the most important and the most difficult task. Material-strength properties can have wide ranges of values within mapped geologic formations depending on interformational stratigraphy, along-strike facies changes, and variations in structural-deformation history. In addition, it has been shown that even the best laboratory testing procedures performed on small diameter samples of failed-slope materials can do a poor job of providing reliable strength values (Leighton and Associates and William Cotton and Associates, 1991). CGS landslide zone-mapping procedures address some of the uncertainty associated with characterizing material strength within geologic map units by limiting statistical analyses of laboratory shear tests to a 7.5-minute quadrangle area (~180 square kilometers, km^2). Limiting the analyses to this relatively smaller area is intended to partially account for spatial variability within geologic formations due to stratigraphic, facies, and deformation variability. Other strategies employed in zone-map preparation include grouping geologic units with similar strength characteristics, mapping preexisting landslides and treating them separately from the geologic unit in which they occur, and identifying potential adverse bedding conditions and treating those areas as distinct geologic units. For the HayWired scenario mainshock, because of the large area considered, most of these strategies could not be employed.

Characterization of geologic-material strength in the study region requires two components: laboratory shear-strength testing of the various geologic units and a scale-appropriate geologic map so the strength parameters can be applied spatially. Strength data were available for the 29 7.5-minute quadrangles where CGS seismic-hazard-zone (SHZ) maps have been prepared (fig. 3). More than 2,000 laboratory shear tests, primarily direct shear and a lesser number of triaxial shear tests, were available to characterize the geologic units in the zoned quadrangles, and these data were extrapolated to the rest of the study region, an area approximately five times larger (~150 quadrangles) as described below. The geologic mapping available for seismic-hazard zoning was from a variety of 1:24,000-scale sources (see appendix 1 for a list of seismic-hazard zoning reports) and had differing geologic nomenclature in many cases.

Because uniform 1:24,000-scale geologic mapping does not yet exist for the entire HayWired scenario study region, we used an unpublished, statewide, generalized geologic-compilation map (C. Gutierrez, CGS, 2014, written commun.), from which the 10-county study region was extracted. The geologic data sources for the extracted San Francisco Bay region map include bedrock geology from Graymer and others (2006), and Quaternary geology from Knudsen and others (2000) and Witter and others (2006). This unpublished compilation of bay region geology was an intermediate product in the preparation of the site-conditions map of California (Wills and others, 2015), which may be the map of choice to use as the primary input for a future statewide a_y map. The Wills and others (2015) site-conditions map is intended to show potential seismic amplification due to near-surface soils, so it provides added detail to Quaternary geologic map units compared to the CGS SHZ maps, and generalizes and combines bedrock units where shear-wave velocity is expected to be similar. The unpublished generalized geologic-compilation map includes data on existing landslides where available, as well as data for artificial fill and colluvium. The existing landslide data was considered important for the HayWired scenario. The generalized geologic-compilation map is composed of 66 unique geologic map units. In contrast, the 1:24,000-scale maps in the 29 7.5-minute quadrangle study region for which shear-strength data exist contain 240 geologic units.

The approach taken to correlate the SHZ maps and generalized geologic-compilation map was to evaluate the geologic-map explanations and background literature of the maps to determine which geologic units stratigraphically and lithologically belong together within the 10-county study region. Table 1 shows the 66 geologic map units from the generalized geologic-compilation map correlated with the 240 geologic map units found in CGS SHZ maps that cover the HayWired study region (map unit symbols only). Some units, such as Kgr (Cretaceous granitic rocks), are directly correlated between maps,

whereas others, such as map unit Tms (Sedimentary rocks—Miocene) on the generalized geologic-compilation map, represents as many as 36 distinct geologic units on the SHZ maps. Five map units, TKs, TKss, Tss, Tst, and Tv, that cover a considerable area on the compilation map do not have equivalents on the SHZ geologic maps because either they are map units that occur outside the SHZ map area or represent units within the SHZ map area for which no strength data are available.

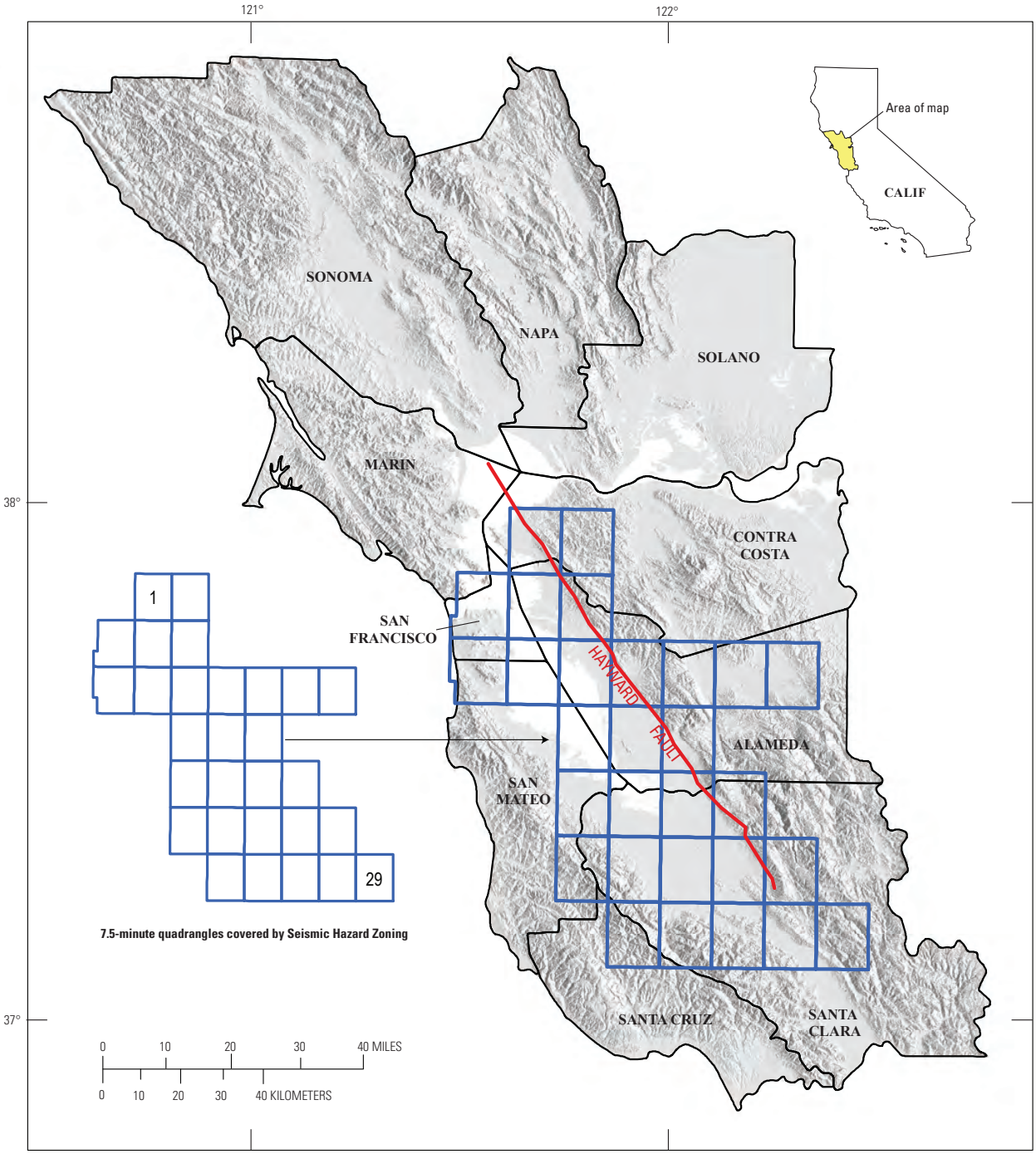

Base from U.S. Geological Survey 2009 National Elevation Dataset 10-meter digital elevation model showing land-surface elevations as shaded-relief. County boundaries from California Department of Forestry and Fire Protection, 2009.

Figure 3. Map of the San Francisco Bay region, California, showing the 10-county HayWired earthquake scenario study region with an inset of the 29 7.5-minute quadrangles covered by California Geological Survey seismic hazard zone maps.

Table 1. The 66 geologic map units from the unpublished California Geological Survey (CGS) generalized geologic-compilation map (GGCM) for the San Francisco Bay region (C. Gutierrez, CGS, 2014, written commun.) correlated with the 240 geologic map units found in CGS seismic-hazard maps that cover the 29 7.5-minute quadrangles in the HayWired study region (map unit symbols only; see appendix 2 for map unit descriptions).

GGCM	CGS seismic-hazard maps that cover the 29 7.5-minute quadrangles in the HayWired study region																	
Quaternary sediments																		
af	ac	af	afbm	alf	PP	pp	Qaf	Qaf/tf	Qafs	Qhbr								
Qal-deep	Qal-deep																	
Qal-thin	Qal-thin																	
Qb	Qhbs	Qs																
Qha	gq	Qal	Qha	Qhaf	Qhay	Qhb	Qhf	Qhf1	Qhf2	Qhff	Qhfp	Qht	Qht1	Qht2	Qhl	Qhl1	Qhl2	
Qal	Qa	Qf	Ql	Qt														
Qhy	Qhasc	Qhc	Qhfy	Qhsc	Qhty	Qhly												
Qhym	Qhbm	Qhfe																
Qls	Qls																	
Qoa	Qc	Qcl	Qot1	Qot2														
Qpa	Qoa	Qoa1	Qoa2	Qof	Qop	Qot	Qpa	Qpaf	Qpaf1	Qpaf2	Qpf	Qpoaf	Qu	Qpt				
Qs	Qd	Qds	Qob															
Qsl	Qsr																	
Qt	Qbt	Qmt																
Sedimentary rocks																		
Kfs	fb1	fh	fms	Kfn	Kfs	Kfsh	Kfss	KJfa										
Ks	Kau	Kc	Kcg	Kcm	Kcs	Kcu	Kcus	Kcusm	Kcv	Kd	Kkh	Ko	Kp	Kr	Ksc	Ksh	Kshu	Kslt
	Kslto	Kss	Ksu	Ksuh	Ksus	KsVII	Ku	Kuc	KuII	Kull	Kus							
KJf	fsp	gi	KJg	KJsu														
KJfs	fss	KJf	KJfs															
KJs	Kbc	Kbs	KJk	Kjk	KJkc	KJkv	KJms	spFR	spFr									
QTs	QTgt	QTi	QTl	Qtl	QTm	QTp	QTsc	QTsc?	QTsl	QTu								
Tepas	Tgsm	Tshs																
Tes	Tb	Tbm	Tbmw	Tbs	Tcm	Tcm?	Tcml	Tcs	Tdi	Tes	Tls	Tmru	Tshc	Tsrm	Tstw	Ttls	Ttss	Tu
	Tvb?	Tw	Tws															
TKfs	TKfs																	
TKs																		
TKss																		
Tmoes	Tlsl																	
Tmos	Tbms	Tla		Tsl	Tsm	Tsms	Tts	Ttv										
Tms	Tbd	Tbe	Tbg	Tbh	Tbi	Tbl	Tbr	Tbu	Tc	Tcc	Tccs	TccsI	Th	Tld	Tlo	Tm	Tms	Tmsu
	Tn	To	Tor	Tord	Tr	Tro	Ts	Tsa	Tso	Tss	Tssc	Tsso	Tst	Tt	Tte	Tul	Tus	Tush
Toes	dbm	Tsr																
Tos	Tz																	
Tpas	Ta	Tpsu	Tvh	Tvhl	Tvhu													
Tpms	Tcgl	Tcglt	Tmll	Tmlu	Tol?	Tp	Tptm	Tsg										

Table 1.—Continued

GGCM	CGS seismic-hazard maps that cover the 29 7.5-minute quadrangles in the HayWired study region										
Tps	Tps										
Tsh	Tsh										
Tss											
Tst											
Volcanic rocks											
Qv	Qv										
QTv	QTv										
Tmov	Tmb	Tv	Tvq								
Tmv	Tbp	Torv	Tpm	Tuss	Tusv	Tvo					
Tov	Tov										
Tpmv	Tgvt	Tgvtt	Tub								
Tpv	Tba	br									
Tv											
fcv	fcv										
Tkfv	Tkfv										
Kfv	fpv	md	v								
KJfv	fg	fmv	fu	KJu							
KJfvc	KJfvc										
KJfvs	KJfvs										
KJv	KJv										
Jfv	Jfv										
Jv	db	Jb	Jbk	Jdb	Jpb	Jsv	Jt				
Intrusive rocks											
Jhg	Jhg										
Ji	gb	Jgb	Jic	Jog	Joi	Jou	Jov				
Kgr	Kgr										
Metamorphic rocks											
fcm	fcm										
fsr	am	bi	bl	bs	cg	ch	fpl	fs	fsr	fws	gs
Jsp	Jfg	Jfgs	Jos	Jsp	Jspm	Jssp	KJfsp	KJfy	sc	scm	sp
Kfc	Kfc										
Kfm	Kfm										
KJfc	fc	fmc	Kfgwy	KJc	KJfch	KJflg	KJs	KJsk			
KJfm	fl	fm	fmm	fy1	fy2	fys	KJfe	KJfm	KJfmw	Kjm	KJm
MzPzm	MzPzm										
Mzv	Mzv										
Serp	no data/no equivalent										

Half of the units in the generalized geologic-compilation map had corresponding SHZ geologic map units with geologic material strength data. For these units, ϕ', c', and moist unit weight (γ) data were compiled and the appropriate average (mean or median) values were derived for each. The other half of the units that had no geologic-material strength data were grouped with those that had data, based on whether or not they had correlative units within the SHZ geologic maps. If the units in the generalized geologic-compilation map had correlative SHZ units but the SHZ units had no data, we referred back to the seismic hazard zoning reports for the San Francisco Bay region (appendix 1) to see how these units were grouped. Then, based on the geologic-material strength values assigned for zone map production, that unit was assigned to a generalized geologic-compilation map unit with similar strength characteristics. The remaining units that did not have equivalent units from the SHZ geologic maps were assigned the strengths of other units on the basis of age, lithology and geologic judgement. The generalized geologic-compilation map became a map of geologic-materials strength by assigning the recompiled laboratory strength values (ϕ', c', γ) to the map database. Table 2 provides a list of the units in the generalized geologic-compilation map with ϕ' and c' values that were used in the analyses. Appendix 2 (available as a .csv or .xlsx file) contains a detailed listing of all SHZ geologic map units, shows which 7.5-minute quadrangles contain strength

Table 2. The 66 geologic map units from the unpublished California Geological Survey (CGS) generalized geologic-compilation map for the San Francisco Bay region (C. Gutierrez, CGS, 2014, written commun.) with material-strength values used in the landslide analyses for the HayWired earthquake scenario.

[Strength values in blue indicate that laboratory data were not available and values were assigned based on age, lithology, and geologic judgement. The bedrock geologic-data source for the generalized geologic-compilation map (Graymer and others, 2006) does not distinguish between Great Valley sequence and Great Valley complex rocks as do other geologic maps in the San Francisco Bay region, and we have adopted their terminology that uses only Great Valley complex. phi', mean values of effective internal angle of friction; c', median values of effective cohesion; lb/ft^2, pound per square foot]

Map symbol	Generalized geologic-compilation map units	Mean phi', in degrees	Median c', in lb/ft^2
	Quaternary sediments		
af	Artificial fill	25	450
Qal-deep	Quaternary alluvium - deep	25	500
Qal-thin	Quaternary alluvium - thin	25	500
Qb	Quaternary beach deposits	27	500
Qha	Alluvium (Holocene)	23	500
Qal	Quaternary alluvium	25	250
Qhy	Alluvium (late Holocene)	25	550
Qhym	Mud deposits (late Holocene)	19	250
Qls	Quaternary landslide deposits	13	650
Qoa	Alluvium (early Pleistocene)	36	300
Qpa	Alluvium (Pleistocene)	26	550
Qs	Beach and dune sand (Quaternary)	33	100
Qsl	Hillslope deposits (Quaternary)	30	575
Qt	Marine terrace deposits (Pleistocene)	21	400
	Sedimentary rocks		
Kfs	Franciscan Complex sedimentary rocks (Cretaceous)	33	800
Ks	Great Valley complex sedimentary rocks (Cretaceous)	31	485
KJf	Franciscan Complex sedimentary rocks (Early Cretaceous and (or) Late Jurassic)	36	580
KJfs	Franciscan Complex sedimentary rocks (Early Cretaceous and (or) Late Jurassic)	36	950
KJs	Great Valley complex sedimentary rocks (Early Cretaceous and (or) Late Jurassic)	28	740
QTs	Sediments (early Pleistocene and (or) Pliocene)	26	800
Tepas	Sedimentary rocks (Eocene and (or) Paleocene)	26	200
Tes	Sedimentary rocks (Eocene)	29	646
TKfs	Franciscan Complex sedimentary rocks (Eocene, Paleocene, and (or) Late Cretaceous)	31	650
TKs	Sedimentary rocks (Paleocene and (or) Late Cretaceous)	31	650
TKss	Sedimentary rocks (Paleocene and (or) Late Cretaceous)	31	650
Tmoes	Sedimentary rocks (Miocene, Oligocene, and (or) Eocene)	31	650

Table 2.—Continued

Map symbol	Generalized geologic-compilation map units	Mean phi′, in degrees	Median c', in lb/ft^2
Tmos	Sedimentary rocks (Miocene and Oligocene)	34	200
Tms	Sedimentary rocks (Miocene)	31	850
Toes	Sedimentary rocks (Oligocene and (or) Eocene)	28	800
Tos	Sedimentary rocks (Oligocene)	29	620
Tpas	Sedimentary rocks (Paleocene)	31	260
Tpms	Sedimentary rocks (Pliocene and early Miocene)	31	740
Tps	Sedimentary rocks (Pliocene)	31	700
Tsh	Merced sedimentary rocks (Miocene)	29	620
Tss	Sedimentary rocks (Miocene)	29	620
Tst	Sedimentary rocks (Miocene)	29	620
	Volcanic rocks		
Qv	Volcanic rocks (Pleistocene)	27	650
QTv	Volcanic rocks (early Pleistocene and (or) Pliocene)	27	650
Tmov	Volcanic rocks (Miocene and (or) Oligocene)	32	400
Tmv	Volcanic rocks (Miocene)	26	700
Tov	Volcanic rocks (Oligocene)	32	760
Tpmv	Volcanic rocks (Pliocene and early Miocene)	27	725
Tpv	Volcanic rocks (Pliocene)	27	725
Tv	Volcanic rocks (Miocene)	33	400
fcv	Franciscan Complex volcanic rocks (Eocene and (or) Paleocene)	33	700
Tkfv	Franciscan Complex volcanic rocks (Paleocene, and (or) Late Cretaceous)	31	740
Kfv	Franciscan Complex volcanic rocks (Cretaceous)	31	550
KJfv	Franciscan Complex volcanic rocks (Early Cretaceous and (or) Late Jurassic)	31	375
KJfvc	Franciscan Complex volcanic rocks and chert (Early Cretaceous and (or) Jurassic)	33	760
KJfvs	Franciscan Complex volcanic and sedimentary rocks (Early Cretaceous and (or) Jurassic)	31	700
KJv	Franciscan Complex or Great Valley complex volcanic rocks (Early Cretaceous and (or) Jurassic)	30	760
Jfv	Franciscan Complex volcanic rocks (Jurassic)	30	700
Jv	Great Valley complex volcanic rocks (Jurassic)	30	700
	Intrusive rocks		
Jhg	Salinian complex plutonic rocks (Jurassic)	32	760
Ji	Great Valley complex plutonic rocks (Jurassic)	32	350
Kgr	Salinian complex plutonic (granite) rocks (Cretaceous)	32	760
	Metamorphic rocks		
fcm	Franciscan Complex metamorphic rocks (Eocene and (or) Paleocene	28	500
fsr	Franciscan Complex mélange (Eocene, Paleocene, and (or) Late Cretaceous)	30	575
Jsp	Great Valley complex serpentinite (Jurassic)	29	750
Kfc	Metamorphic rocks (Cretaceous and (or) Jurassic)	33	760
Kfm	Franciscan Complex metamorphic rocks (Cretaceous)	28	700
KJfc	Franciscan Complex chert (Early Cretaceous and (or) Late Jurassic)	33	740
KJfm	Franciscan Complex metamorphic rocks (Early Cretaceous and (or) Late Jurassic)	28	500
MzPzm	Salinian complex metamorphic rocks (Mesozoic and (or) Paleozoic)	30	600
Mzv	Metamorphic rocks (Mesozoic)	30	600
Serp	Franciscan Complex serpentinite (Jurassic)	26	550

data, how they were correlated with the compilation map units, and provides the average strength values that were used.

Slope Gradient

Slope gradient was derived from the 2009 National Elevation Dataset (NED) produced and distributed by the USGS (2009) with a cell size of 1/3 arc-second (approximately 10 meters, m). The elevation of the 10-county study region ranges from −10 to 1,372 m. The original NED, which is in geographic coordinates (latitude and longitude), was projected to Universal Transverse Mercator, North American Datum of 1983 (NAD83). A slope-gradient map was made from the projected DEM, using the average maximum technique (also known as neighborhood-slope algorithm), where the maximum rate of change for each cell is calculated over the distance between the cell and its eight neighbors to identify the steepest downhill descent (Burrough and McDonnell, 1998). The resulting slope-gradient map is shown in figure 4.

Earthquake Shaking

Raster versions of the HayWired scenario mainshock shaking data used in this study were derived from the USGS ShakeMap (U.S. Geological Survey, 2014). These data represent one of the ground-motion simulations from a suite of earthquake scenarios that Aagaard and others (2010) developed for the Hayward-Rodgers Creek Fault system. The simulation is based on a three-dimensional (3D) ground-motion model that captures the variability in the earthquake-source parameters consistent with geophysical and seismic observations, as well as the uncertainty in how creep may affect the distribution of coseismic slip on the Hayward Fault. The model also identifies the important features in the ground motions, such as effects from the 3D geologic structure and fault-rupture directivity, and characterizes the distribution of shaking and its sensitivity to variations in the earthquake source (Aagaard and others, 2010). These data, originally with a 1-minute (approximately 1.6 kilometer, km) resolution, were converted from geographic coordinates, World Geodetic Survey 1984 (WGS84) datum, into Universal Transverse Mercator, NAD83, and resampled to a 10-m-pixel resolution to have the same resolution as the other raster data. The simulated ground motion for the M_w 7.05 HayWired earthquake scenario has a maximum peak ground acceleration (PGA) of 2.16 *g* (the acceleration due to gravity) (fig. 5) centered on the northern end of the Hayward Fault.

Peak ground velocity (PGV) was used to provide a practical limit to where earthquake-triggered landslides are considered significant. HayWired scenario PGV raster data were converted into contour line features representing 10, 20, and 40 centimeters per second (cm/s) PGV (fig. 6), and, as explained below, slope-failure probabilities were only considered in areas where PGV was greater than 20 cm/s.

Earthquake-Landslide Susceptibility

The susceptibility to earthquake-induced landsliding is defined by the yield acceleration (also referred to as critical acceleration). Yield acceleration (a_y) is defined as the earthquake inertial force required to initiate slope movement, that is, when the factor of safety equals 1.0. Newmark (1965) defined yield acceleration as:

$$a_y = (FS - 1) g \sin\alpha, \quad (1)$$

where *FS* is the Factor of Safety, *g* is the acceleration due to gravity, and α is the angle from the horizontal that the sliding mass initially moves. Physically what Newmark's equation means is that every time earthquake ground motion beneath a slope exceeds the a_y for that slope, the upper part of the slope, the "sliding block," detaches and slides downslope. For the duration of an entire earthquake, the sliding block will accumulate displacement from all the occurrences of ground motion that exceed a_y. For natural slopes, the total displacement from the earthquake shaking can be related to an overall hazard index for an area (Jibson and others, 2000).

We assume the landslide failure surface is relatively shallow and can be approximated by an infinite slope model, where the failure surface is parallel to the ground surface. We also assume that the earth materials are unsaturated at the time they are subject to the earthquake shaking. With these assumptions, the *FS* is determined by:

$$FS = c'\gamma h \sin\alpha + \cot\alpha \tan\phi', \quad (2)$$

where *c'* is effective cohesion, γ is the unit weight of the slide mass material and *h* is its thickness, α is the slope gradient of the ground surface, and ϕ' is the effective friction angle. Slide mass *h* was set to 50 feet and the geologic-materials map data (ϕ', *c'*, γ) were combined with the slope-gradient map to calculate *FS* and a_y.

Calculation of Newmark Displacements

Calculation of Newmark displacement (Newmark, 1965), representing earthquake-induced landslide-hazard potential, uses a regression equation developed by Jibson (2007). The particular regression selected for this study uses yield acceleration ratio (a_y/PGA) and earthquake magnitude (*M*) to estimate Newmark displacement (D_N):

$$\log D_N = -2.71 + \log[(1 - a_y / PGA)^{2.335} (a_y / PGA)^{-1.478}] + 0.424 M. \quad (3)$$

Although Jibson (2007) developed equations based on several ground motion parameters, this equation was chosen primarily because the ground-motion input parameter *PGA* is readily available from the USGS ShakeMap for the HayWired scenario (U.S. Geological Survey, 2014).

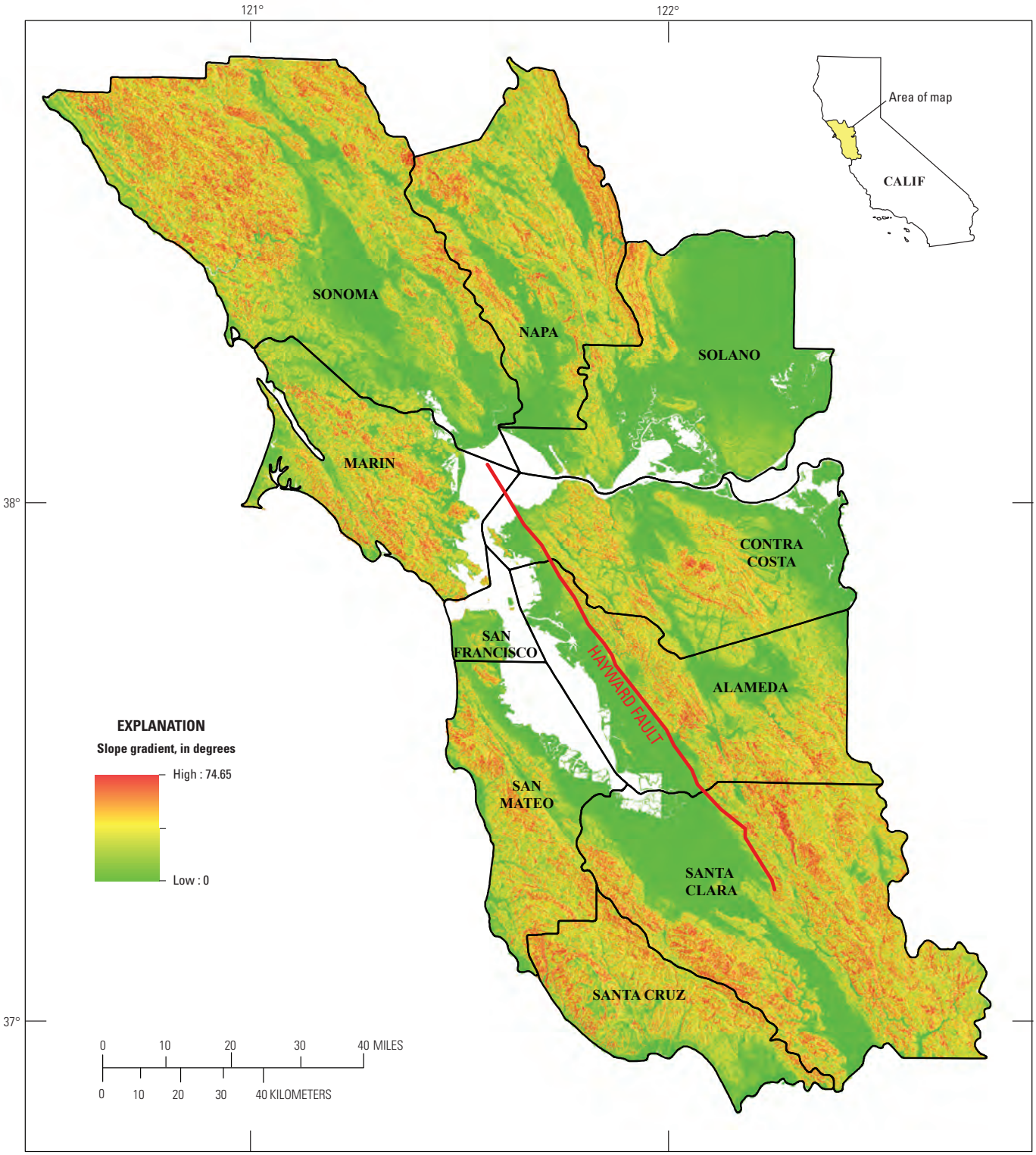

Slope gradient from U.S. Geological Survey 2009 National Elevation Dataset 10-meter digital elevation model. County boundaries from California Department of Forestry and Fire Protection, 2009.

Figure 4. Map showing slope-gradient for the 10-county San Francisco Bay region, California, studied in the HayWired scenario.

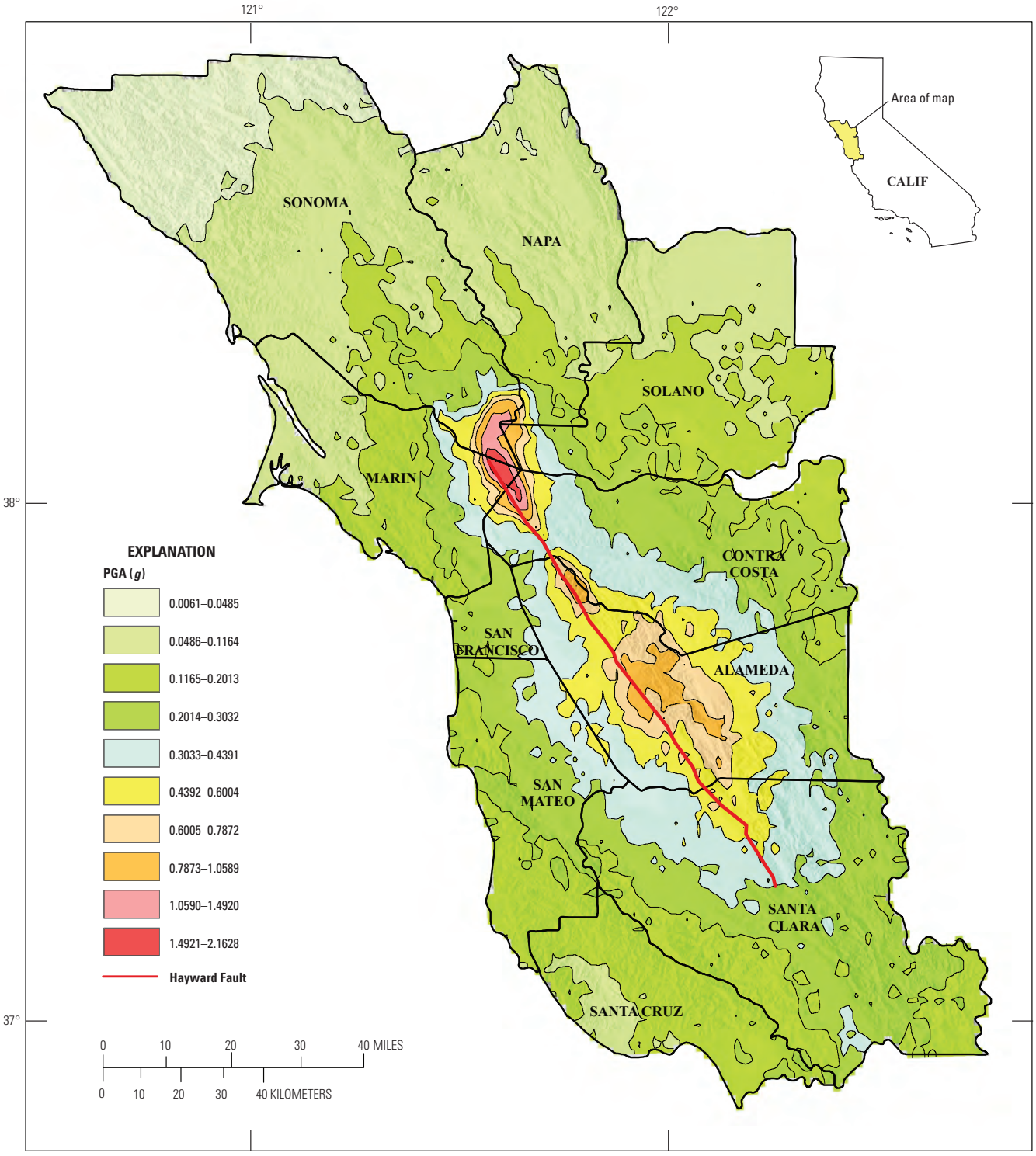

Base from U.S. Geological Survey 2009 National Elevation Dataset 10-meter digital elevation model showing land-surface elevations as shaded-relief. County boundaries from California Department of Forestry and Fire Protection, 2009.

Figure 5. Map of the San Francisco Bay region, California, showing peak ground acceleration (PGA) from the HayWired scenario ShakeMap (U.S. Geological Survey, 2014). *g*, acceleration due to gravity.

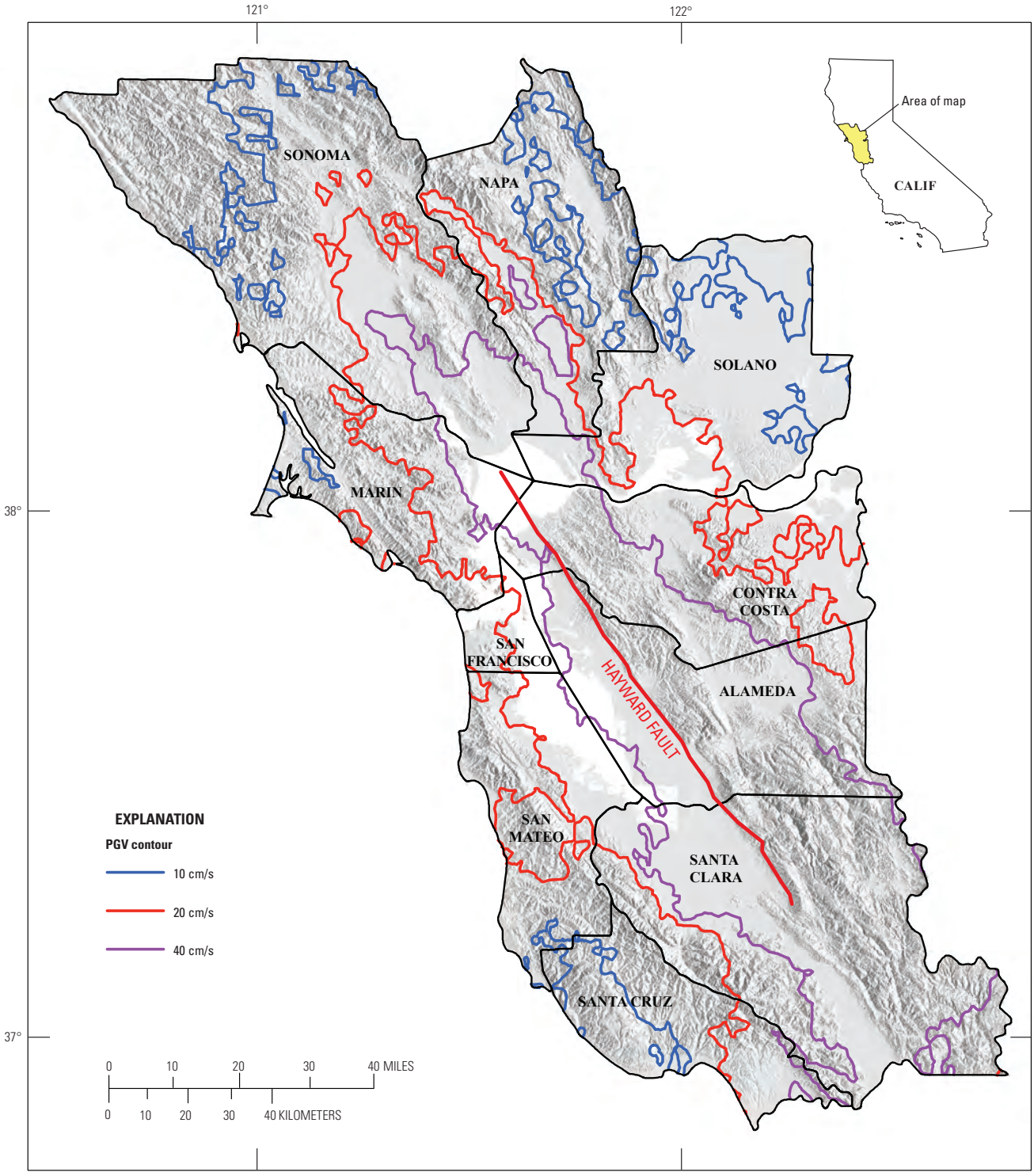

Base from U.S. Geological Survey 2009 National Elevation Dataset 10-meter digital elevation model showing land-surface elevations as shaded-relief. County boundaries from California Department of Forestry and Fire Protection, 2009.

Figure 6. Map of the San Francisco Bay region, California, showing peak ground velocity (PGV) contours from the HayWired scenario ShakeMap (U.S. Geological Survey, 2014). cm/s, centimeters per second.

These calculations were implemented within the geographic information system (GIS) and carried out for each 10-m grid cell throughout the study region. Moderate (15 to 30 centimeters, cm) to large (>100 cm) displacements are predicted in the upland areas of Marin, Contra Costa, Alameda, Santa Clara, and Santa Cruz Counties, where ground motions are predicted to be high (fig. 7). However, large displacements are also predicted in the northern reaches of Sonoma and Napa Counties where ground motions are expected to be considerably lower. Limiting the area where landslide occurrence and related damage are significant is necessary to address model limitations, primarily created by our inability to adequately define dynamic-strength values. A review of the landslides triggered by three recent California earthquakes found that for the 2003 M_w 6.6 San Simeon earthquake, 96 percent of the mapped landslides (L. Rosenberg, San Luis Obispo County Geologist, written commun., 2004), not including liquefaction-related features, occurred in areas where ShakeMap (http://earthquake.usgs.gov/earthquakes/shakemap/) indicates PGV shaking intensities greater than 20 cm/s. For the M_w 6.7 1994 Northridge earthquake, we found that 91 percent of the landslides mapped by Harp and Jibson (1995, 1996) occurred in that same range of PGV. In the case of the M_w 6.9 1989 Loma Prieta earthquake, 100 percent of the earthquake-triggered landslides mapped by Keefer and Manson (1998) in the epicentral area were in areas with greater than 20 cm/s PGV as indicated by ShakeMap, although there were a few notable landslides as far north as Stinson Beach where shaking was much lower. On the basis of these observations, we believe that the 20 cm/s PGV contour provides a reasonable limit to where damage from earthquake-triggered landsliding should be considered significant.

Calculation of Slope-Failure Probabilities

Slope failure probability (P_f) is based on predicted Newmark displacement (D_N) and is calculated using the relationship of Jibson and others (2000):

$$P_f = 0.335[1 - \exp(-0.048 D_N^{1.565})] \quad (4)$$

Like the calculation of D_N, P_f was calculated at a 10-m resolution throughout the study region and then trimmed back to the 20 cm/s PGV contour. The values produced by this relation represent the proportion of area expected to fail for a given D_N. It should be recognized that this equation was derived from examination of landslides triggered by the 1994 Northridge earthquake and has not been shown to be valid in other areas. However, to our knowledge there are no other equations available. Figure 8 shows the slope failure probability map for the study region, categorized to match the hazard-potential categories related to D_N and trimmed to the 20 cm/s PGV contour.

Failure probabilities of 2 to 15 percent, corresponding to displacements of 1–5 cm, are most prevalent in southernmost Sonoma County and the western parts of Contra Costa and Alameda Counties along the trace of the Hayward Fault. A scattered pattern of these displacements is also evident on gentle hills in the central to eastern areas of Contra Costa and Alameda Counties east of the fault. P_f in the range of 15 to 32 percent (D_N 5 to 15 cm) cover only the moderately steep hills of Contra Costa, Alameda, and Santa Clara Counties east of the fault. P_f greater than 32 percent (D_N>15 cm) are extensively mapped on steep to very steep slopes of Sonoma, Napa, Marin, Contra Costa, Alameda, San Mateo, Santa Clara, and Santa Cruz Counties.

Areas for Hazard-Model Improvement

One of the goals of our study was to evaluate the feasibility of preparing a statewide earthquake-induced landslide susceptibility map. On the basis of this study, we believe there are several issues to resolve before that goal can be achieved. The selection of representative geologic-material strength parameters is a key source of uncertainty in preparing landslide-hazard maps, including those prepared in this study. One drawback to using laboratory derived strength values is that they provide estimates of static strength within relatively intact materials. Earthquake loading of natural slopes can be expected to exploit discontinuities and other weak parts of weathered materials that are difficult to locate, sample, and test in typical geotechnical investigations. This is compounded by the difficulty in accounting for spatial variability within mapped geologic formations—there are just not enough test measurements to do so effectively. There are two notable implications of using the laboratory derived strength data in a regional hazard assessment such as this. First, to maximize the capture of the hazard identified by slope failures in the Loma Prieta earthquake, the modeled landslide thickness needs to be greater than originally used in the regression model for Newmark displacement. One way to view this is that the landslide mass must be thicker, and the driving forces greater, because the static strength data are too high relative to the actual dynamic strength. Second, as a consequence of the thicker slide mass in the model, the failure probabilities are high out into areas that are anticipated to have relatively low shaking intensities, and therefore a threshold, here a 20 cm/s PGV cutoff was used to limit where landslide losses should be considered significant. Recently, Saade and others (2016) demonstrated the value of replacing the rigid sliding-block model and infinite-slope failure with a model incorporating a limit equilibrium analysis and circular slip failure. They performed a parametric study to identify the relations among a_y, slope angle, and shear strength and showed a significant improvement in regional seismic-landslide-hazard assessment for an area damaged by the Northridge earthquake. This new methodology is currently being evaluated by CGS as a means to improve mapping of landslide-hazard zones in California and, if successful, might be useful for developing a statewide earthquake-landslide susceptibility map.

There also are geologic field observational methods that may improve our ability to address model limitations. Detailed geologic-material characterization in the San Francisco Bay region was done by Ellen and Wentworth (1995) in which they compiled detailed descriptions of unit composition,

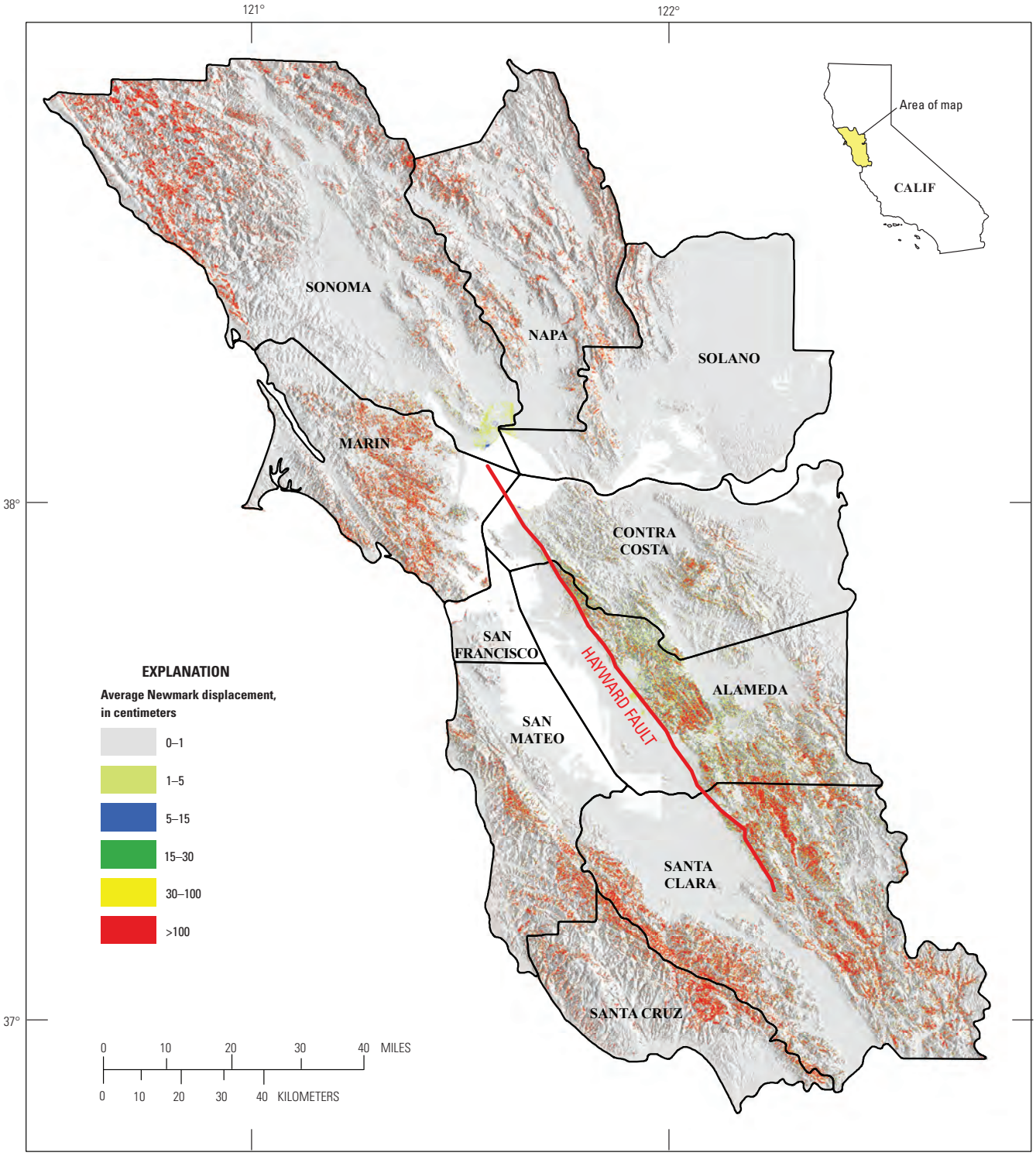

Base from U.S. Geological Survey 2009 National Elevation Dataset 10-meter digital elevation model showing land-surface elevations as shaded-relief. County boundaries from California Department of Forestry and Fire Protection, 2009.

Figure 7. Map of the San Francisco Bay region, California, showing landslide-hazard potential in terms of Newmark displacement (Newmark, 1965), which is a function of yield acceleration ratio and earthquake magnitude for the HayWired earthquake scenario. >, greater than.

bedding and fracture characteristics, topographic expression, weathering, and other properties relevant to seismic slope stability. In addition, the geologic strength index (GSI) developed by Hoek and Brown (1980; see also Marinos and others, 2005) has successfully been used for engineering projects in a variety of rock types and terrains and was used by Saade and others (2016) for regional mapping. CGS is currently evaluating GSI in the San Francisco Bay region to assess its applicability in assigning strength values where laboratory data do not exist. An obvious limitation to these observational techniques is the time and cost involved in visiting numerous sites to collect observations. However, it might be possible to use modern digital-terrain data along with Ellen and Wentworth's (1995) "hillside materials units" and relate these parameters to GSI to automate the process. Alternatively, remote-sensing technologies such as NASA's new hyperspectral thermal emission spectrometer (HyTES) may provide insight on the spatial distribution of geologic material strength properties (http://hytes.jpl.nasa.gov/).

Existing landslides were treated as distinct geologic units in our study, with strength properties that approximate a residual strength on an existing landslide slip surface. There are several limiting aspects to incorporation of existing landslides in this manner. First, landslide inventories are not uniformly available throughout the study region and thus are inconsistently handled. A prime example of this is Contra Costa County where CGS is currently preparing detailed inventory maps for seismic-hazard zoning. Because this work is still in progress and was largely unavailable for HayWired, relatively lower displacements and failure probabilities (fig. 8) are found in this county when compared to Alameda County, despite its close proximity to the Hayward Fault. This effect can also be seen in central Marin County where detailed inventories are available—larger areas of higher D_N were observed (figs. 7 and 8) despite having lower modeled ground motions than western Contra Costa County.

A second limitation lies in the treatment of all existing landslides as having the same strength parameters and a uniform thickness. Landslides formed in different rock materials have different strengths, but this simplification in the model is necessary in the absence of laboratory tests or other methods to determine landslide slip surface residual strengths. Applying a uniform slide thickness to existing landslides is, like in other areas, a simplification used to make the model work. The approach is not realistic, particularly for deep-seated, large landslides whose natural periods can be very different from that of the earthquake shaking to which they are subject in the near field, and are distinctly different from the shallow landslides that are best modeled by the Newmark method. All landslide inventories produced by CGS in the past 20 years capture an observational judgement on ranges of landslide thickness. We suggest that this information combined with a hybrid displacement model that considers both rigid and flexible sliding behaviors developed by Rathje and Antonakos (2011) may offer a path forward for addressing the hazards associated with existing landslides.

Another limitation to earthquake-landslide hazard maps is that not all seismic loading is accounted for in either probabilistic seismic-hazard analysis (PSHA) maps or in ShakeMap. Topographic amplification is a phenomenon shown through theoretical studies and postearthquake field observations (for example, Boore, 1972; Çelebi, 1987; Geli and others, 1988; Assimaki and others, 2005) to have significant effects at the tops of bluffs and ridges. Topographic effects can act in combination with site-response amplification caused by low velocity layers, such as deeply weathered rock underlying ridges (Bard and Tucker, 1985; Assimaki and Jeong, 2013). Incorporating amplified shaking, preferentially in ShakeMap, would remove some uncertainty from earthquake-landslide hazard models. Maufroy and others (2015) have introduced a method to estimate topographic amplification based on surface curvature, which is easily calculated from a DEM. This model needs to be evaluated in areas where damaging topographic effects have been documented (Çelebi, 1987; McCrink and others, 2010; Hough and others, 2010; Assimaki and Jeong, 2013) to test its validity.

Beyond the modeling for earthquake-triggered landslides, there are two issues that relate to the application of our results into loss modeling that warrant mention. First is the fact that landslide models estimate locations that are susceptible to slope-failure initiation and do not indicate any type of landslide runout, especially for shallow disrupted landslides that can travel large distances. Thus, vulnerability of various infrastructure elements and use of economic-loss models may have difficulty identifying a significant part of landslide damages. There currently are no methods to reliably estimate landslide runout, and cartographic/GIS techniques should be evaluated. Second, the landslide models used in this study produce displacement and failure probability maps at a 10-m resolution, whereas the Hazus loss-modeling software uses U.S. Census tracts as its minimum mapping unit. Aggregating the landslide-hazard data into the much coarser census tracts requires considerable knowledge and judgement, and creates some ambiguity in the resulting loss estimates.

Summary

In this analysis, we used a regional-scale geologic-compilation map, geologic-strength parameters collected as part of the CGS Seismic Hazard Mapping Program, earthquake shaking parameters from ShakeMap generated for the HayWired scenario mainshock, and digital terrain data from NED to produce earthquake-triggered landslide susceptibility (a_y), hazard potential (D_N), and probability of failure (P_f) maps for a 10-county region around San Francisco Bay. The a_y map (not shown) was prepared using Newmark's (1965) equation after applying some simplifying assumptions. The D_N map (fig. 7) was prepared using a regression equation developed by Jibson (2007) that uses, in addition to a_y, *PGA* and earthquake magnitude as ground shaking input. P_f was determined from an algorithm developed by Jibson and others (2000) that uses D_N as the sole input. The P_f map (fig. 8) was

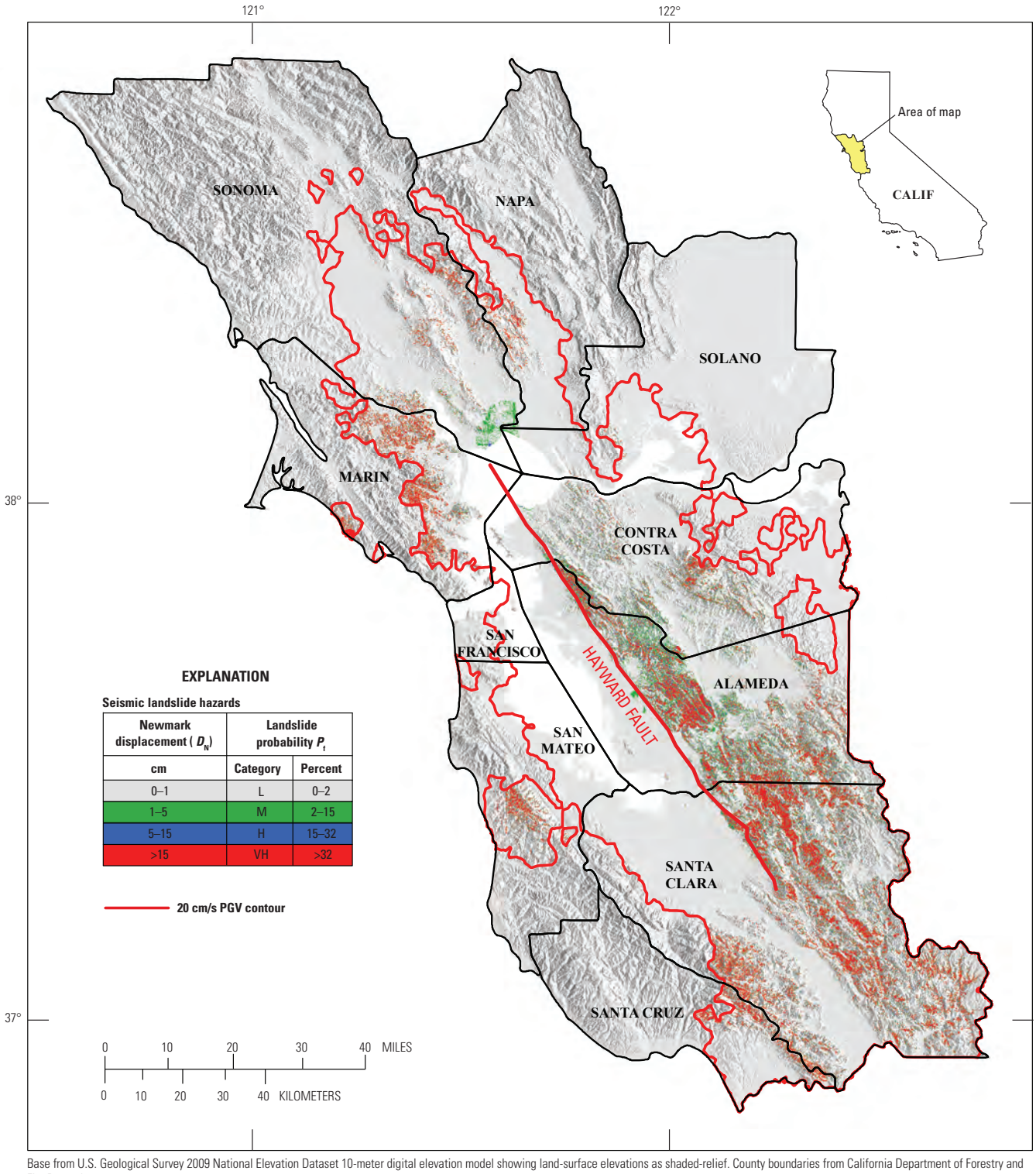

Base from U.S. Geological Survey 2009 National Elevation Dataset 10-meter digital elevation model showing land-surface elevations as shaded-relief. County boundaries from California Department of Forestry and Fire Protection, 2009.

Figure 8. Map of seismic-landslide hazards for the San Francisco Bay region, California, for the HayWired earthquake scenario, showing Newmark displacement (D_N, Newmark, 1965) and landslide probability (P_f) as a function of Newmark displacement trimmed to areas where peak ground velocity (PGV) exceeds 20 centimeters per second (cm/s). Categories of displacement and failure probability have been made to match only for display purposes. L, low; M, medium; H, high; VH, very high; cm, centimeter.

trimmed to the 20 cm/s PGV contour in an attempt to put a practical limit to the area likely to experience significant landsliding in the HayWired scenario earthquake.

Acknowledgments

The authors thank their colleagues at CGS— Carlos Gutierrez, Dave Branum, Mike Silva, Teri McGuire, Rick Wilson, Mark Wiegers, Rui Chen, and Badie Rowshandel for their assistance in the collation and interpretation of the hazard data. Thanks are also due to the USGS for providing the modeled earthquake shaking data. Jamie Jones (USGS) prepared the landslide input for Hazus that was run by Hope Seligson (Seligson Consulting). This report benefited from thoughtful reviews by Mike Silva, Chris Wills, and Kate Allstadt. Special thanks to Dale Cox and Anne Wein (USGS) for their conscientious management of the HayWired project and to Steve Hickman, Shane Detweiler, Andy Michael, and Ken Hudnut (all USGS), as well as the rest of the HayWired technical review panel, for their thorough evaluation of this study. The authors also would like to acknowledge the conscientious work of James Hendley and Claire Landowski, USGS technical editors, as well as the work of Cory Hurd, USGS graphics/layout specialist.

References Cited

Aagaard B.T., Graves, R.W., Rodgers, A., Brocher, T.M., Simpson, R.W., Dreger, D., Petersson, N.A., Larsen, S.C., Ma, S., and Jachens, R.C., 2010, Ground-motion modeling of Hayward Fault scenario earthquakes, part II—Simulation of long-period and broadband ground motions: Bulletin of the Seismological Society of America, v. 100, no. 6, p. 2945–2977.

Assimaki, D., Gazetas, G., and Kausel, E., 2005, Effects of local soil conditions on the topographic aggravation of seismic motion—Parametric investigation and recorded field evidence from the 1999 Athens earthquake: Bulletin of the Seismological Society of America, v. 95, p. 1059–1089.

Assimaki, D., and Jeong, S., 2013, Ground-motion observations at Hotel Montana during the *M* 7.0 2010 Haiti earthquake—Topography or soil amplification?: Bulletin of the Seismological Society of America, v. 103, no. 5, p. 2577–2590.

Bard, P-Y., and Tucker, B.E., 1985, Underground and ridge site effects—A comparison of observation and theory: Bulletin of the Seismological Society of America, v. 75, p. 905–922.

Boore, D.M., 1972. A note on the effect of simple topography on seismic SH waves: Bulletin of the Seismological Society of America, v. 62, p. 275–284.

Bray, J.D., and Travasarou, T., 2007, Simplified procedure for estimating earthquake-induced deviatoric slope displacements: Journal of Geotechnical and Geoenvironmental Engineering, v. 133, p. 381–392.

Burrough, P.A., and McDonnell, R.A., 1998, Principles of Geographic Information Systems: New York, Oxford University Press, 190 p.

Çelebi, Mehmet, 1987, Topographical and geological amplifications determined from strong-motion and aftershock records of the 3 March 1985 Chile earthquake: Bulletin of the Seismological Society of America, v. 77, p. 1147–1167.

Ellen, S.D., and Wentworth, C.M., 1995, Hillside materials and slopes of the San Francisco Bay region, California: U.S. Geological Survey Professional Paper 1357, 215 p., 7 plates.

Geli, L., Bard, P.-Y., and Jullien, B., 1988, The effect of topography on earthquake ground motion—A review and new results: Bulletin of the Seismological Society of America, v. 78, p. 42–63.

Godt, J.W., Sener, B., Verdin, K.L., Wald, D.J., Earle, P.S., Harp, E.L., and Jibson, R.W., 2009, Rapid assessment of earthquake-induced landsliding: Proceedings of the First World Landslides Forum, Tokyo, Japan, p. 219–222.

Graymer, R.W., Moring, B.C., Saucedo, G.J., Wentworth, C.M., Brabb, E.E., and Knudsen, K.L., 2006, Geologic map of the San Francisco Bay region: U.S. Geological Survey Scientific Investigations Map 2918. [Also available at https://pubs.usgs.gov/sim/2006/2918/.]

Harp, E.L., and Jibson, R.W., 1995, Inventory of landslides triggered by the 1994 Northridge, California, earthquake: U.S. Geological Survey Open-File Report 95–213, 17 p. [Also available at https://pubs.usgs.gov/of/1995/ofr-95-0213/.]

Harp, E.L., and Jibson, R.W., 1996, Landslides triggered by the 1994 Northridge, California, earthquake: Bulletin of the Seismological Society of America, v. 86B, p. S319–S332.

Hoek, E., and Brown E.T., 1980, Empirical strength criterion for rock masses: Journal of the Geotechnical Engineering Division, American Society of Civil Engineers, v. 106, no. GT9, p. 1013–1035.

Hough, S.E., Altidor, J.R., Anglade, D., Given, D., Janvier, M.G., Maharrey, J.Z., Meremonte, M., Mildor, B.S., Prepetit, C., and Yong, A., 2010, Localized damage caused by topographic amplification during the 2010 *M* 7.0 Haiti earthquake: Nature Geoscience, v. 3, p. 778–782.

Jibson, R.W., Harp, E.L., and Michael, J.A., 2000, A method for producing digital probabilistic seismic landslide hazard maps: Engineering Geology 58, p. 271–289.

Jibson, R.W., 2007, Regression models for estimating coseismic landslide displacement: Engineering Geology 91, p. 209–218.

Keefer, D.K., and Manson, M.W., 1998, Regional distribution and characteristics of landslides generated by the earthquake, *in* Keefer, ed., The Loma Prieta, California, Earthquake of October 17, 1989—Landslides: U.S. Geological Survey Professional Paper 1551-C, p. C7-C32. [Also available at https://pubs.usgs.gov/pp/pp1551/.]

Knudsen, K.L., Sowers, J.M., Witter, R.C., Wentworth, C.M., and Helley, E.J., 2000, Preliminary maps of Quaternary deposits and liquefaction susceptibility, nine-county San Francisco Bay region, California—A digital database, U.S. Geological Survey Open-File Report 00–444, accessed December, 22, 2016, at https://pubs.usgs.gov/of/2000/of00-444/.

Leighton and Associates and William Cotton and Associates, 1991, Investigation of landsliding triggered by the Loma Prieta earthquake and evaluation of analysis methods: Final technical report, U.S. Geological Survey grant award no. 14-08-0001-G1860, 29 p., 3 appendixes.

Marinos V., Marinos P., and Hoek, E., 2005, The geological strength index—Applications and limitations: Bulletin of Engineering Geology and the Environment, v. 64, p. 55–65.

Maufroy, E., Cruz-Atienza, V.M., Cotton, F., and Gaffet, S., 2015, Frequency-scaled curvature as a proxy for topographic site-effect amplification and ground-motion variability: Bulletin of the Seismological Society of America, v. 105, no. 1, p. 354–367.

McCrink, T.P., 2001, Mapping earthquake-induced landslide hazards in Santa Cruz County *in* Ferriz, H., and Anderson, R., eds., Engineering geology practice in northern California: California Geological Survey Bulletin 210/ Association of Engineering Geologists Special Publication 12, p.77–94.

McCrink, T.P., and Real, C.R., 1996, Evaluation of the Newmark method for mapping earthquake-induced land-slide hazards in the Laurel 7-1/2 minute quadrangle, Santa Cruz County, California: U.S. Geological Survey, Reston, Virginia, California Division of Mines and Geology final technical report for U.S. Geological Survey contract 143-93-G-2334, 31 p.

McCrink, T.P., Wills, C.J., Real, C.R., and Manson, M.W., 2010, Effects of topographic position and geology on shaking damage to residential wood-framed structures during the 2003 San Simeon earthquake, western San Luis Obispo County, California: Earthquake Spectra, v. 26, no. 3, p. 779–802.

Newmark, N.M., 1965, Effects of earthquakes on dams and embankments: Geotechnique, v. 15, no. 2, p. 139–160.

Nowicki, M.A., Wald, D.J., Hamburger, M.W., Hearne, M. and Thompson, E.M., 2014, Development of a globally applicable model for near real-time prediction of seismically induced landslides: Engineering Geology 173, p. 54–65.

Rathje, E.M., and Antonakos, G., 2011, A unified model for predicting earthquake-induced sliding displacements of rigid and flexible slopes: Engineering Geology 122, p. 51–60.

Rathje, E.M., and Saygili, G. 2008, Probabilistic seismic hazard analysis for the sliding displacement of slopes: scalar and vector approaches: Journal of Geotechnical and Geoenvironmental Engineering, v. 134, p. 804–814.

Saade, A., Abou-Jaoude, G., and Wartman, J., 2016, Regional-scale co-seismic landslide assessment using limit equilibrium analysis: Engineering Geology 204, p. 53–64.

Saygili, G., and Rathje, E.M., 2008, Empirical predictive models for earthquake-induced sliding displacements of slopes: Journal of Geotechnical and Geoenvironmental Engineering, v. 134, p. 790–803.

U.S. Geological Survey, 2009, National elevation dataset—Digital raster elevation: U.S. Geological Survey dataset, accessed December 8, 2011, at https://viewer.nationalmap.gov/basic/.

U.S. Geological Survey, 2014, Earthquake planning scenario—ShakeMap for Haywired M7.05-scenario: U.S. Geological Survey Earthquake Hazards Program website, accessed August 26, 2014, at https://earthquake.usgs.gov/scenarios/eventpage/ushaywiredm7.05_se#shakemap?source=us&code=gllegacyhaywiredm7p05_se.

Wieczorek, G.F., Wilson, R.C., and Harp, E.L., 1985, Map showing slope stability during earthquakes in San Mateo County, California, U.S. Geological Survey Miscellaneous Investigations Map I–1257E, scale 1:62,500.

Wills, C.J., Gutierrez, C.I., Perez, F.G., and Branum, D., 2015, A next-generation Vs30 map for California based on geology and topography: Bulletin of the Seismological Society of America, v. 105, no. 6, p. 3083–3091.

Witter, R.C., Knudsen, K.L., Sowers, J.M., Wentworth, C.M., Koehler, R.D., and Randolph, C.E., 2006, Maps of Quaternary deposits and liquefaction susceptibility in the central San Francisco Bay region, California: U.S. Geological Survey Open-File Report 2006–1037, ver. 1.1, accessed December 22, 2016, at https://pubs.usgs.gov/of/2006/1037/.

Appendix 1. Seismic Hazard Zoning (SHZ) Reports in the San Francisco Bay Region

[Chronological order]

Wilson, R.I., Wiegers, M.O., and McCrink, T.P., 2000, Evaluation report for earthquake-induced landslide hazard in the City and County of San Francisco, California: California Geological Survey Seismic Hazard Zone Report 043, section 2, p. 19–37.

Wiegers, M.O., Aue, K., and McCrink, T.P., 2000, Evaluation report for earthquake-induced landslide hazard in the San Jose East 7.5-Minute Quadrangle, Santa Clara County, California: California Geological Survey Seismic Hazard Zone Report 044, section 2, p. 25–44.

Wiegers, M.O., Aue, K., and McCrink, T.P., 2001, Evaluation report for earthquake-induced landslide hazard in the Calaveras Reservoir 7.5-Minute Quadrangle, Santa Clara County, California: California Geological Survey Seismic Hazard Zone Report 048, section 2, p. 23–43.

Wiegers, M.O., Aue, K., and McCrink, T.P., 2001, Evaluation report for earthquake-induced landslide hazard in the Milpitas 7.5-Minute Quadrangle, Santa Clara and Alameda Counties, California: California Geological Survey Seismic Hazard Zone Report 051, section 2, p. 27–44.

Slater, C.F., and Aue, K., 2002, Evaluation report for earthquake-induced landslide hazard in the San Jose West 7.5-Minute Quadrangle, Santa. Clara County, California: California Geological Survey Seismic Hazard Zone Report 058, section 2, p. 25–40.

Slater, C.F., Wiegers, M.O., and McCrink, T.P., 2002, Evaluation report for earthquake-induced landslide hazard in the Cupertino 7.5-Minute Quadrangle, Santa Clara County, California: California Geological Survey Seismic Hazard Zone Report 068, section 2, p. 23–42.

Wiegers, M.O., and Clahan, K.B., 2002, Evaluation report for earthquake-induced landslide hazard in the Los Gatos 7.5-Minute Quadrangle, Santa Clara County, California: California Geological Survey Seismic Hazard Zone Report 069, section 2, p. 25–47.

McCrink, T.P., and Wiegers, M.O., 2003, Evaluation report for earthquake-induced landslide hazard in the Richmond 7.5-Minute Quadrangle, Alameda County, California: California Geological Survey Seismic Hazard Zone Report 070, section 2, p. 23–45.

McCrink, T.P., Bott, J.D.J., Wiegers, M.O., Wilson, R.I., McMillan, J.R., and Haydon, W.D., 2003, Evaluation report for earthquake-induced landslide hazard in the San Leandro 7.5-Minute Quadrangle, Alameda County, California: California Geological Survey Seismic Hazard Zone Report 078, section 2, p. 25–44.

Wilson, R.I., Wiegers, M.O., McCrink, T.P., Haydon, W.D., and McMillan, J.R., 2003, Evaluation report for earthquake-induced landslide hazard in the Oakland East 7.5-Minute Quadrangle, Alameda County, California: California Geological Survey Seismic Hazard Zone Report 080, section 2, p. 25–47.

McCrink, T.P., Wilson, R.I., Haydon, W.D., McMillan, J.R., and Wiegers, M.O., 2003, Evaluation report for earthquake-induced landslide hazard in the Oakland West 7.5-Minute Quadrangle, Alameda County, California: California Geological Survey Seismic Hazard Zone Report 081, section 2, p. 25–44.

McCrink, T.P., Wiegers, M.O., Wilson, R.I., Haydon, W.D., and McMillan, J.R., 2003, Evaluation report for earthquake-induced landslide hazard in the Briones Valley 7.5-Minute Quadrangle, Alameda County, California: California Geological Survey Seismic Hazard Zone Report 084, section 2, p. 5–22.

Wiegers, M.O., and Bott, J.D.J., 2003, Evaluation report for earthquake-induced landslide hazard in the Newark 7.5-Minute Quadrangle, Alameda County, California: California Geological Survey Seismic Hazard Zone Report 090, section 2, p. 25–43.

Wiegers, M.O., Rosinski, A.M., and Bott, J.D.J., 2003, Evaluation report for earthquake-induced landslide hazard in the Hayward 7.5-Minute Quadrangle, Alameda County, California: California Geological Survey Seismic Hazard Zone Report 091, section 2, p. 25–46.

Slater, C.F., and Wiegers, M.O., 2003, Evaluation report for earthquake-induced landslide hazard in the Santa Teresa Hills 7.5-Minute Quadrangle, Santa Clara County, California: California Geological Survey Seismic Hazard Zone Report 097, section 2, p. 29–47.

Slater, C.F., and Wiegers, M.O., 2004, Evaluation report for earthquake-induced landslide hazard in the Morgan Hill 7.5-Minute Quadrangle, Santa Clara County, California: California Geological Survey Seismic Hazard Zone Report 096, section 2, p. 29–48.

Wiegers, M.O., 2004, Evaluation report for earthquake-induced landslide hazard in the Niles Quad 7.5-Minute Quadrangle, Alameda County, California: California Geological Survey Seismic Hazard Zone Report 098, section 2, p. 29–50.

Wiegers, M.O., and Bott, J.D.J., 2005, Evaluation report for earthquake-induced landslide hazard in the Castle Rock Ridge 7.5-Minute Quadrangle, Santa Clara County, California: California Geological Survey Seismic Hazard Zone Report 108, section 2, p. 19–39.

Slater, C.F., and Wiegers, M.O., 2006, Evaluation report for earthquake-induced landslide hazard in the Mountain View 7.5-Minute Quadrangle, San Mateo, Santa Clara and Alameda Counties, California: California Geological Survey Seismic Hazard Zone Report 060, section 2, p. 25–38.

Wilson, R.I., Thornburg, J., and Rosinski, A.M., 2006, Evaluation report for earthquake-induced landslide hazard in the Palo Alto 7.5-Minute Quadrangle, San Mateo and Santa Clara Counties, California: California Geological Survey Seismic Hazard Zone Report 111, section 2, p. 23–45.

Slater, C.F., Wiegers, M.O., Bott, J.D.J., and McCrink, T.P., 2006, Evaluation report for earthquake-induced landslide hazard in the Mt. Sizer 7.5-Minute Quadrangle, Santa Clara County, California: California Geological Survey Seismic Hazard Zone Report 118, section 2, p. 21–38.

Wilson, R.I., and Rosinski, A.M., 2008, Evaluation report for earthquake-induced landslide hazard in the Mindego Hill 7.5-Minute Quadrangle, Santa Clara and San Mateo Counties, California: California Geological Survey Seismic Hazard Zone Report 109, section 2, p. 21–43.

Wiegers, M.O., and Perez, F.G., 2008, Evaluation report for earthquake-induced landslide hazard in the Dublin 7.5-Minute Quadrangle, Alameda County, California: California Geological Survey Seismic Hazard Zone Report 112, section 2, p. 23–42.

Perez, F.G., 2008, Evaluation report for earthquake-induced landslide hazard in the Livermore 7.5-Minute Quadrangle, Alameda County, California: California Geological Survey Seismic Hazard Zone Report 114, section 2, p. 23–40.

Perez, F.G., and Haydon, W.D., 2009, Evaluation report for earthquake-induced landslide hazard in the Altamont 7.5-Minute Quadrangle, Alameda County, California: California Geological Survey Seismic Hazard Zone Report 119, section 2, p. 23–43.

Silva, M.A., Haydon, W.D., and McCrink, T.P., 2012, Evaluation report for earthquake-induced landslide hazard in the Lick Observatory 7.5-Minute Quadrangle, Santa Clara County, California: California Geological Survey Seismic Hazard Zone Report 110, section 2, p. 17–34.

Appendix 2. Geologic Map Unit Names/Descriptions for California Geological Survey Seismic-Hazard-Zone (SHZ) Maps for the San Francisco Bay Region and Their Correlation to the Generalized Geologic-Compilation Map

Appendix 2 is available online only as comma separated value (.csv) files and a .xlsx file at https://doi.org/10.3133/sir20175013v1. The appendix is a detailed listing of the 240 geologic map units shown on the California Geological Survey (CGS) seismic-hazard-zone maps for the San Francisco Bay region that cover the 29 7.5-minute quadrangles in the 10-county study region for the HayWired earthquake scenario. The appendix shows how the 240 units were correlated with the 66 geologic map units from the unpublished CGS generalized geologic-compilation map for the San Francisco Bay region (C. Gutierrez, CGS, 2014, written commun.), derived from bedrock geology from Graymer and others (2006) and Quaternary units from Knudsen and others (2000) and Witter and others (2006). The appendix also shows which of the map quadrangles contain strength data and provides the average strength values that were used in the landslide analyses for the HayWired earthquake scenario.

The HayWired Earthquake Scenario—Earthquake Hazards
Edited by Shane T. Detweiler and Anne M. Wein
Scientific Investigations Report 2017–5013–A–H
[Also see https://doi.org/10.3133/sir20175013]

Chapter G

HayWired Scenario Aftershock Sequence

By Anne M. Wein,[1] Karen R. Felzer,[1] Jamie L. Jones,[1] and Keith A. Porter[2]

Abstract

The HayWired scenario examines a hypothetical earthquake (mainshock) with a moment magnitude (M_w) of 7.0 occurring on April 18, 2018, at 4:18 p.m. on the Hayward Fault in the east bay part of California's San Francisco Bay area. Earthquakes are rarely isolated events. Instead, earthquakes usually occur in clusters within an area and over days, months, or even years. In the HayWired scenario, the mainshock is followed by a series of aftershocks that occur over the course of 2 years. The aftershock sequence includes 175 M_w 4 or larger earthquakes that occur in the vicinity of the mainshock fault rupture, as well as in the south end and northeast of the San Francisco Bay area. The largest scenario aftershock, an M_w 6.4 earthquake, is located in Cupertino. We estimate that the occurrence of an M_w 6.4 or larger aftershock following an M_w 7.0 mainshock has at least a 1 in 5 chance of occurring.

Scientists cannot currently predict earthquakes, but the occurrence of large earthquakes increases the chance that more earthquakes (their aftershocks) will occur. Aftershock forecasts provide an estimate of the frequency and probability of earthquakes for magnitude ranges during periods within confidence intervals. For example, an aftershock forecast after the HayWired mainshock states that "within the next week, the chance of an earthquake of magnitude 5 or greater is 99 percent, and it is most likely that 1 to 9 such earthquakes may occur." To illustrate, scenario forecasts are provided at points in time throughout the HayWired aftershock sequence—approximately 20 minutes, 1 day, 2 days, 1 week, and 40 days after the mainshock.

This HayWired aftershock scenario applies existing methods to simulate and forecast aftershock sequences for the purpose of improving the communication of aftershock forecasts by (1) informing stakeholders about aftershock sequences and forecasts; (2) allowing time for potential users to provide feedback on aftershock forecasts and consider their use in mitigation, preparedness, response, and recovery decisions; and (3) providing a working example for estimating cumulative damages and exercising disaster management during an earthquake sequence.

[1]U.S. Geological Survey.

[2]University of Colorado Boulder.

Introduction

Earthquakes are rarely isolated events. Instead, they usually cluster in time and space. Most commonly, the largest earthquake of the cluster, called the mainshock, is followed by a sequence of smaller earthquakes called aftershocks. Aftershocks generally occur near the mainshock and result from stresses that are redistributed in the Earth's crust following the mainshock. The majority of aftershocks occur within tens of miles corresponding to one or two rupture lengths of the mainshock, but if the mainshock is very large, the aftershocks could occur thousands of miles away. Aftershocks can continue over a period of weeks, months, years, or even decades, depending on the geologic setting in which they occur. In general, the larger the mainshock, the more numerous the aftershocks and the longer it will take to return to the background rate of earthquakes. (The background rate of earthquakes is the rate at which they were occurring immediately before the mainshock, assuming there was no other large earthquake in the area in the few years before the mainshock.)

In northern California, well-studied aftershock sequences include those that followed the 1989 moment magnitude (M_w) 6.9 Loma Prieta and 2014 M_w 6.0 South Napa earthquakes. The largest aftershocks for each sequence were an M_w 5.2 earthquake a few minutes after the Loma Prieta mainshock (Dietz and Ellsworth, 1990) and an M_w 3.9 earthquake 2 days after the South Napa mainshock (Brocher and others, 2015). Thousands of aftershocks, including 20 aftershocks of magnitude (M) 4 or greater, were recorded in the 1989 Loma Prieta aftershock zone that spanned 25 miles (between Los Gatos to the north and Watsonville to the south). In the San Francisco Bay area, Meltzner and Wald (2003) retrospectively estimated that following the April 18, 1906, M_w 7.8 San Francisco earthquake, the largest aftershock within 20 months had a magnitude of ~6.7 and occurred ~100 kilometers (km) west of Eureka on April 23, 1906. They deduced that the largest aftershocks occurred at the ends of the 1906 rupture or away from the rupture entirely; very few significant aftershocks occurred along the mainshock rupture itself. This aftershock pattern following the 1906 San Francisco M_w 7.8 mainshock has been explained to be the result of the stress shadow (reduction

in the Earth's stress available to produce earthquakes) (Simpson and Reasenberg, 1994; Harris and Simpson, 1998). Further back in time, the 1868 M_w 7 earthquake on the Hayward Fault reportedly had strong aftershocks into the next month (Stover and Coffman, 1993; Toppozada and Real, 1981) but was preceded by a seismically active period with 12 earthquakes of M>5.5 from 1855 to 1866 within 60 km of the Hayward Fault and was followed by 13 relatively quiet years (Toppozada and others, 2002).

Scientists cannot currently predict the exact location, magnitude, or occurrence time of any earthquake, and do not expect to be able to do so in the foreseeable future. However, using statistical relations, they can estimate the probability of earthquakes of specific magnitudes during specific periods. The U.S. Geological Survey (USGS) reports aftershock forecasts after sizeable earthquakes (for example, Reasenberg and Jones, 1989). These forecasts change over time because of the expected decay in the aftershock frequency over time. The forecasts also change after a large aftershock triggers more aftershocks. Furthermore, forecasts are updated because aftershock data allow the forecaster to improve and better tailor the forecast to the specific earthquake sequence and particular geologic setting.

Aftershock locations can be unexpected, and their magnitudes can be large enough to cause or aggravate damage and complicate emergency response and recovery. Therefore, emergency managers, community leaders, and others who respond to and recover from earthquakes can benefit from understanding aftershocks and earthquake forecast capabilities to better inform plans and procedures.

For example, a study of the communication of aftershock forecasts during the recent Canterbury, New Zealand, earthquake sequence of 2010–2012 (for example, Becker and others, 2015; Wein and others, 2016) reveals the following potential benefits:

5. Reassurance to the public and insurers when recorded earthquake frequencies are within the bounds of uncertainty of the scientific forecast;

6. Motivation for the public and community leaders to maintain preparedness, further develop emergency plans, and establish relationships with emergency managers;

7. Guidance for government, insurers, and businesses about the timing of restoration and recovery decisions that may be affected by aftershocks; and

8. Information for development of safer building standards and land-use policies.

The HayWired scenario is a hypothetical earthquake sequence that can be used to better inform potential users of aftershock forecast information. The HayWired scenario mainshock is a M_w 7.0 earthquake on the Hayward Fault with a hypocenter in Oakland, California, in the San Francisco Bay area (fig. 1; U.S. Geological Survey, 2014). The scenario planning assumes that the scenario Hayward Fault mainshock occurs at 4:18 p.m. Pacific Daylight Time (PDT) on April 18, 2018. The simulated ground shaking caused by the scenario Hayward Fault mainshock was produced by Aagaard and others (2010a, 2010b) and Aagaard, Boatwright, and others (this volume). We reiterate that scientists cannot predict the exact location, timing, or magnitude of future earthquakes, so our hypothetical scenario is just for educational purposes.

This chapter describes characteristics of earthquake sequences and refers to the method used to simulate 2 years of aftershocks for the HayWired scenario mainshock. The description of the selected earthquake-sequence scenario includes a time series of aftershock magnitudes; maps of the aftershock locations; and details for the times, locations, and depths of the larger aftershocks. This is followed by a series of scenario aftershock forecasts that could be transmitted soon after the HayWired scenario mainshock and updated forecasts that could be transmitted 24 hours, 48 hours, 7 days, and 40 days later. The likelihood of the largest simulated aftershock of magnitude (M) 6.4 occurring after a M7.0 mainshock in any earthquake sequence is calculated. The limitations of the statistical aftershock simulation and forecast methods are identified before suggesting potential uses of the analysis.

Characteristics of Earthquake Sequences—Magnitudes, Frequencies, Location, and Decay

Methods to simulate aftershock sequences and forecast earthquakes are based on the following empirical relations:

1. The occurrence rates of aftershocks. The frequency of aftershocks decays with time after the mainshock. This relation is called the Omori-Utsu law (table 1; Omori, 1894; Utsu, 1961).

2. The relation between the magnitude of the mainshock and the number of aftershocks. Utsu-scaling estimates that on average for each unit increase in mainshock magnitude approximately 10 times as many aftershocks are produced (table 2; Utsu, 1971, p. 420–427).

3. The distribution of the number of aftershocks across magnitude. The Gutenberg-Richter law holds that, on average, there are 10 times more aftershocks with magnitude M X than aftershocks with one unit greater magnitude, M (X+1); for example, 10 times as many M5 aftershocks than M6 aftershocks (table 3; Gutenberg and Richter, 1944).

4. The relation between spatial density of aftershocks and distance from the mainshock. Fewer aftershocks occur farther from the mainshock than occur closer to the mainshock. The Felzer and Brodsky (2006) hypothesis states that the decay of aftershocks between 0.2–50 km is well approximated by a basic inverse-power law (for every unit increase in distance, there is an exponential decrease in the number of aftershocks) (table 4).

These four statistical relations are described in tables 1–4.

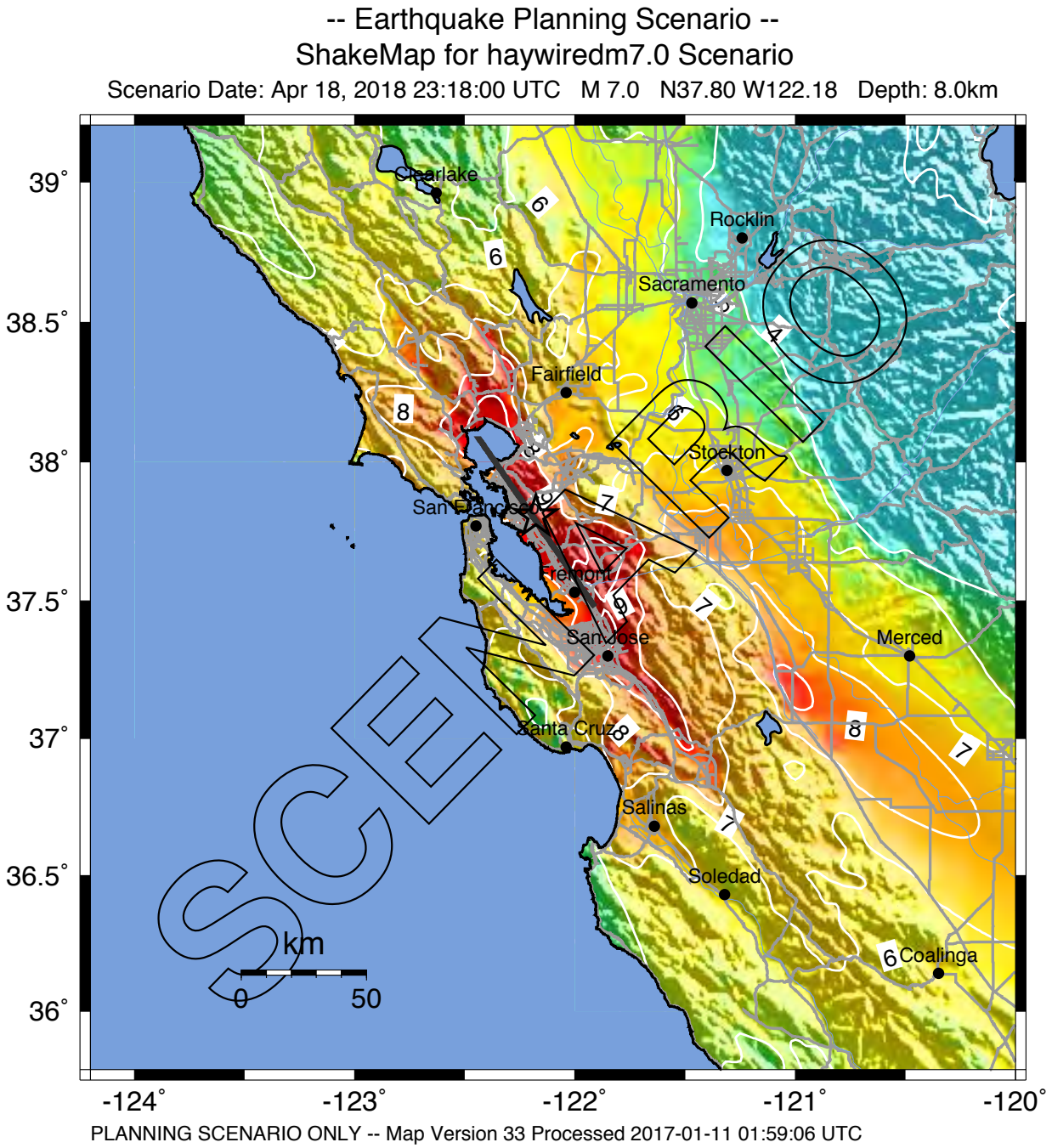

PERCEIVED SHAKING	Not felt	Weak	Light	Moderate	Strong	Very strong	Severe	Violent	Extreme
POTENTIAL DAMAGE	none	none	none	Very light	Light	Moderate	Mod./Heavy	Heavy	Very Heavy
PEAK ACC.(%g)	<0.05	0.3	2.8	6.2	12	22	40	75	>139
PEAK VEL.(cm/s)	*<0.02*	*0.1*	*1.4*	*4.7*	*9.6*	*20*	*41*	*86*	*>178*
INSTRUMENTAL INTENSITY	I	II-III	IV	V	VI	VII	VIII	IX	X+

Scale based on Worden and others, 2012.

Figure 1. ShakeMap of the San Francisco Bay region, California, showing instrumental intensity of the HayWired earthquake scenario magnitude-7 mainshock (modified from U.S. Geological Survey, 2014). km, kilometer; %g, percentage of acceleration due to gravity; cm/s, centimeter per second.

Table 1. Numeric illustration of the Omori-Utsu law (Omori, 1894; Utsu, 1961) regarding the rate of aftershock decay over time.

When	Observed number[1]	Expected number[2]
1st day (day 0.5–1.5)	420	733
10th day	44	70
100th day	4	7.1
1,000th day	0	0.71
10,000th day	Unknown until 2021	0.071

[1]Observed numbers of aftershocks for each day are the 1994 magnitude-6.7 Northridge earthquake aftershocks (magnitude 2 or larger, within 30 kilometers) (Northern California Earthquake Data Center, 2014).

[2]Expected numbers come from Reasenberg and Jones (1989) using the parameters from Michael (2012): a=–1.85, b=1, p=1, c=0.05 days.

Table 2. Numeric illustration of Utsu scaling (Utsu, 1971) regarding the number of aftershocks relative to the size of a mainshock.

[*M,* magnitude]

Magnitude of mainshock	Expected number of aftershocks *M*3 or larger in the first week[1]
5	6.7
6	67
7	670
8	6,700

[1]Expected numbers come from Reasenberg and Jones (1989) using the parameters from Michael (2012): a=–1.85, b=1, p=1, c=0.05 days.

Table 3. Numeric illustration of the Gutenberg-Richter law (Gutenberg and Richter, 1944) regarding the size of aftershocks relative to the size of a mainshock.

Minimum magnitude	Observed number in the first week[1]	Expected number in the first week[2]
3	310	340
4	42	34
5	6	3.4
6	0	0.34
7	0	0.034

[1]Observed numbers of aftershocks for each day are the 1994 magnitude-6.7 Northridge earthquake aftershocks (magnitude 3 or larger, within 30 kilometers) (Northern California Earthquake Data Center, 2014).

[2]Expected numbers come from Reasenberg and Jones (1989) using the parameters from Michael (2012): a=–1.85, b=1, p=1, c=0.05 days.

Table 4. Numeric illustration of the Felzer and Brodsky hypothesis (Felzer and Brodsky, 2006) regarding the distance of aftershocks relative to the location of a mainshock.

[km, kilometer; km^2, square kilometer]

Distance from mainshock epicenter (km)	Observed number of aftershocks	Area within distance range (km^2)	Number of aftershocks per km^2
0 to 10	689	314	2.2
10 to 20	1,649	942	1.7
20 to 30	340	1,571	0.22
30 to 40	30	2,199	0.014
40 to 50	15	2,827	0.0053

[1]Observed numbers of aftershocks for each day are the 1994 magnitude-6.7 Northridge earthquake aftershocks (magnitude 2 or larger, within 50 kilometers) (Northern California Earthquake Data Center, 2014).

Aftershock Simulations

Aftershock sequences for the HayWired scenario are simulated based on these aforementioned statistical relations and could therefore unfold in an infinite variety of ways after any given earthquake. We generated 13 hypothetical aftershock sequences that could follow the HayWired M_w 7.0 mainshock rupture. Each sequence depicts one possible outcome during the 2 years following the scenario mainshock. The 2-year period was chosen to match the recovery horizon of the Federal Emergency Management Agency's (FEMA) San Francisco Bay Area Catastrophic Earthquake Plan, under development at the same time as the HayWired scenario. The method used to generate earthquake sequences is the same as was used to simulate the 1-week aftershock sequence for the ShakeOut scenario in southern California (Felzer, 2008).

The statistical model that we used to generate an aftershock sequence (a time series of earthquake magnitudes) is known as the epidemic-type aftershock sequence (ETAS) model (Ogata, 1988). The version of the ETAS model used for the ShakeOut and HayWired scenarios also distributes the aftershocks in space (Felzer and others, 2002). Therefore, the model generates aftershocks stochastically using established empirical relations for aftershock magnitude, time, and location distributions (described above). The model also simulates secondary aftershocks—aftershocks caused by other aftershocks—which is an important process found in real aftershock sequences (Felzer and others, 2003). Because the ETAS model uses statistics for determining earthquake locations, without regard to existing geologic structures, expert opinion is used to move earthquakes on to known nearby faults. In particular, aftershocks with magnitudes greater than 6 are relocated to the closest faults capable of producing earthquakes of that size. This shift displaces these larger events away from their own aftershocks, so statistical relation 4 (see above) may not hold for the modeled secondary aftershock sequences.

The map series in figure 2 shows 13 statistical aftershock sequence simulations for the HayWired scenario mainshock, specifically including the aftershocks greater than *M*5. As expected, the earthquake sequences primarily produce aftershocks near the Hayward Fault (for example, HayWiredCatalog5). Some

Figure 2. Maps of the San Francisco Bay region, California, showing different sets (catalogs) of earthquake aftershock sequences generated by the epidemic-type aftershock sequence (ETAS) model for the HayWired earthquake scenario mainshock. Aftershocks of magnitude (*M*) 5 or greater are shown in each map as purple dots.

sequences are more active than others; the number of aftershocks greater than *M*4 ranges from 149 (HayWiredCatalog1) to 678 (HayWiredCatalog5), and the number of aftershocks greater than *M*5 ranges from 11 (HayWiredCatalog7) to 66 (HayWiredCatalog5). The largest aftershock magnitude in a sequence ranges from *M*5.8 (HayWiredCatalog7) to *M*7.3 (HayWiredCatalog9). The spatial distribution of the simulated aftershock sequences are also variable; some include triggered earthquakes farther to the north on the Rodgers Creek Fault (for example, HayWiredCatalog11), and other sequences include triggered activity east of the Hayward Fault (for example, HayWiredCatalog9 and HayWiredCatalog11) or in the south end of the San Francisco Bay area (for example, HayWiredCatalog13).

The selected HayWired scenario aftershock sequence (HayWiredCatalog13) produces 175 *M*4 or larger earthquakes and a largest aftershock of *M*6.4. This sequence has a diversity of features, and it includes aftershocks near Palo Alto, Cupertino, and San Jose, California, at the south end of the San Francisco Bay area, along with a significant aftershock northeast of the San Francisco Bay area, affecting the Sacramento-San Joaquin Delta and its system of potentially fragile flood-control levees. The two largest aftershocks are relocated to the closest known faults capable of producing *M*6 earthquakes. One thing this sequence lacks is having as many aftershocks along the Hayward Fault as many of the other sequences. Although the diversity of locations illustrates the importance of preparing for aftershocks throughout the region, we should not forget the possibility of more activity along the primary fault

Description of the HayWired Aftershock Sequence

The HayWired scenario aftershock sequence is a cluster of earthquakes in time and space. The *M*≥2.5 scenario aftershock temporal distribution during the first 2 years after the HayWired scenario mainshock is shown in figures 3 and 4. The statistical relations of decay in earthquake frequency over time and fewer earthquakes of larger magnitudes are evident in the figures. The figures also show the larger aftershocks triggering aftershocks of their own within the periods indicated by different colored dots.

The map in figure 5 shows the locations of all aftershocks of *M*≥2.5 in the HayWired aftershock sequence (data for

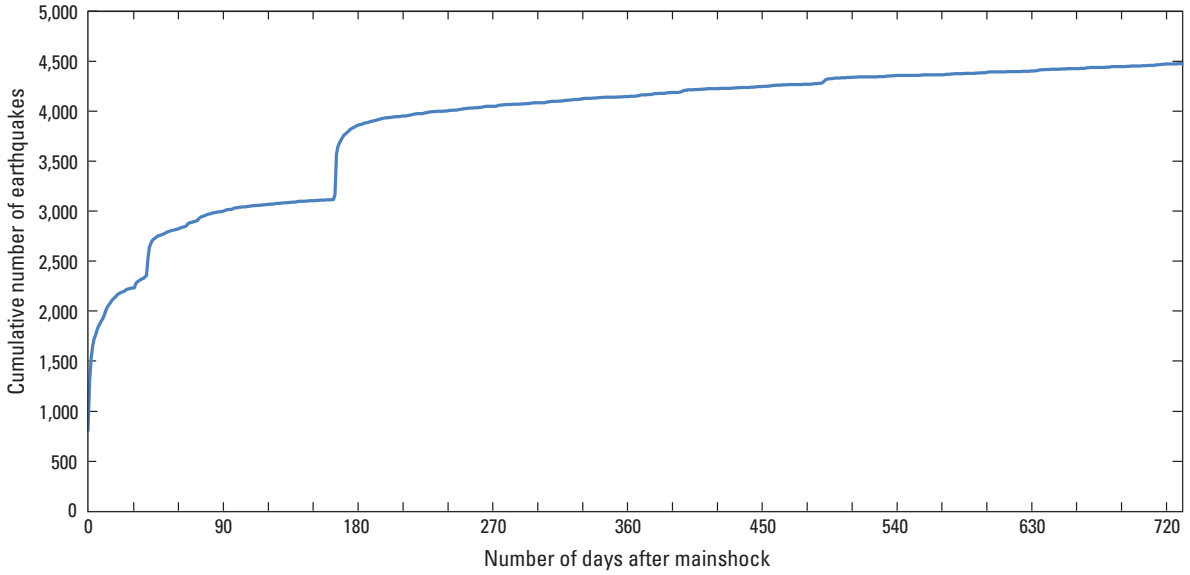

Figure 3. Graph showing the 2-year time series for cumulative number of HayWired earthquake scenario aftershocks of magnitude 2.5 or greater.

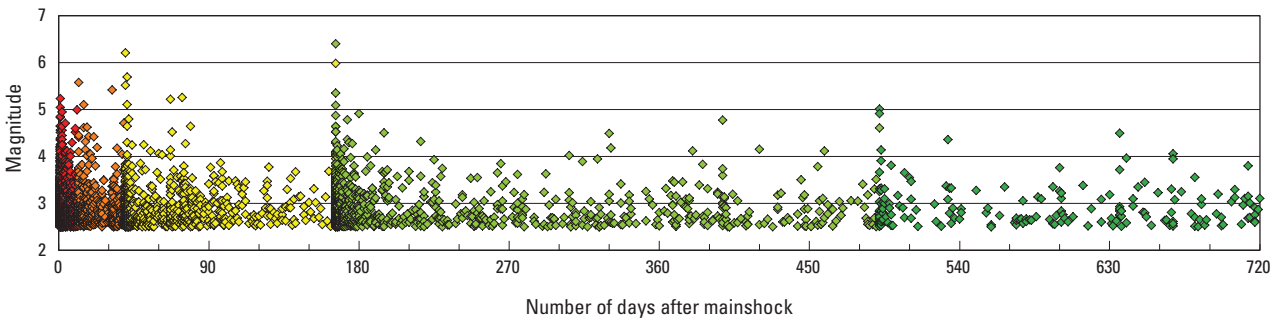

Figure 4. Graph showing the 2-year time series for HayWired earthquake scenario aftershocks of magnitude 2.5 or greater. The colored (red, orange, yellow, and green) dots mark periods in the sequence when a larger aftershock triggers more aftershocks. Color-coded time periods of the sequence are shown in figure 6.

point locations are available in Jones and Felzer, 2017). This sequence is one realization of the aftershock sequence simulation, and expert opinion found it reasonable. Note the density of activity in the Green Valley Fault Zone near Vallejo, near the Monte Vista-Shannon Fault Zone in the Palo Alto-Sunnyvale area, as well as along the Hayward Fault. A map view of the HayWired scenario mainshock and aftershock sequence, with color-coded time periods as in figure 4, is shown in figure 6.

The larger aftershocks (M>5) are located on the map in figure 7. The HayWired scenario earthquake sequence includes 2 aftershocks of M6 in Santa Clara County and 14 aftershocks of M5 near the Hayward Fault, near Vallejo, and in Santa Clara County. (The two M6 earthquakes are visibly shifted southwest

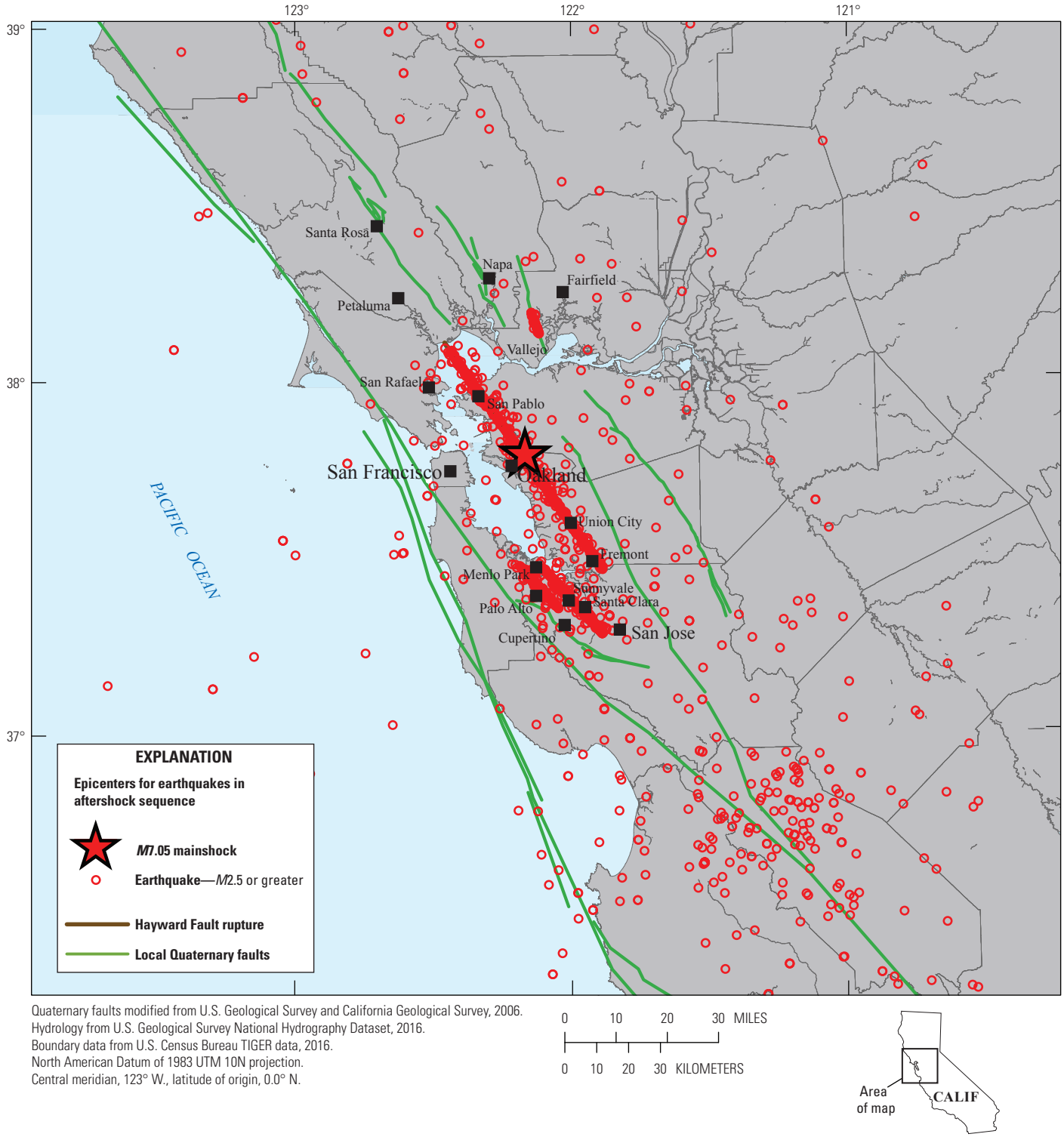

Figure 5. Map of the San Francisco Bay region, California, showing 2 years of HayWired earthquake scenario aftershocks of magnitude (M) 2.5 or greater (note that the Hayward Fault is mostly obscured by earthquake symbols).

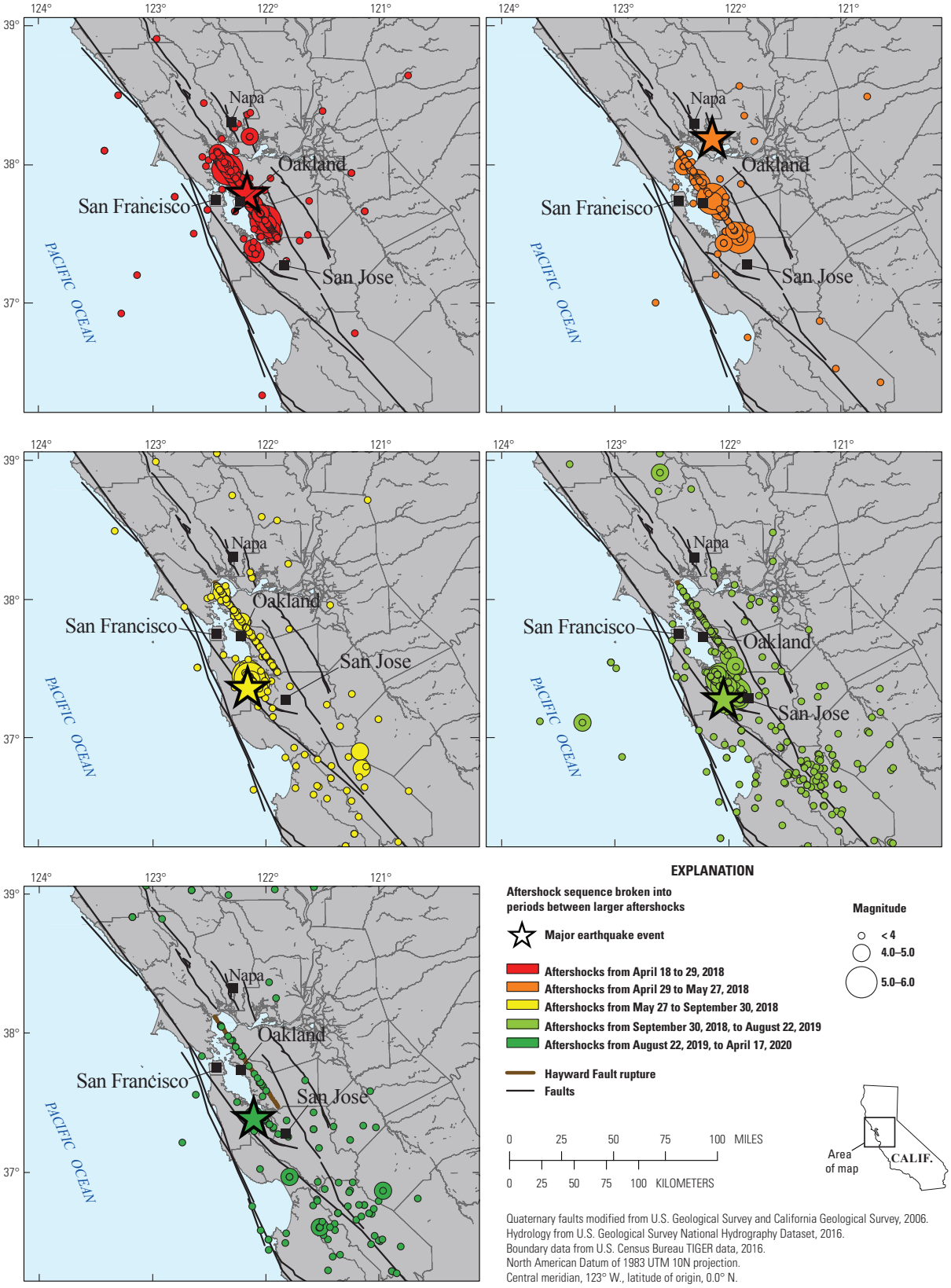

Figure 6. Maps of the San Francisco Bay region, California, showing the HayWired earthquake scenario aftershock sequence within periods between larger aftershocks that retrigger the sequence (see fig. 4). <, less than.

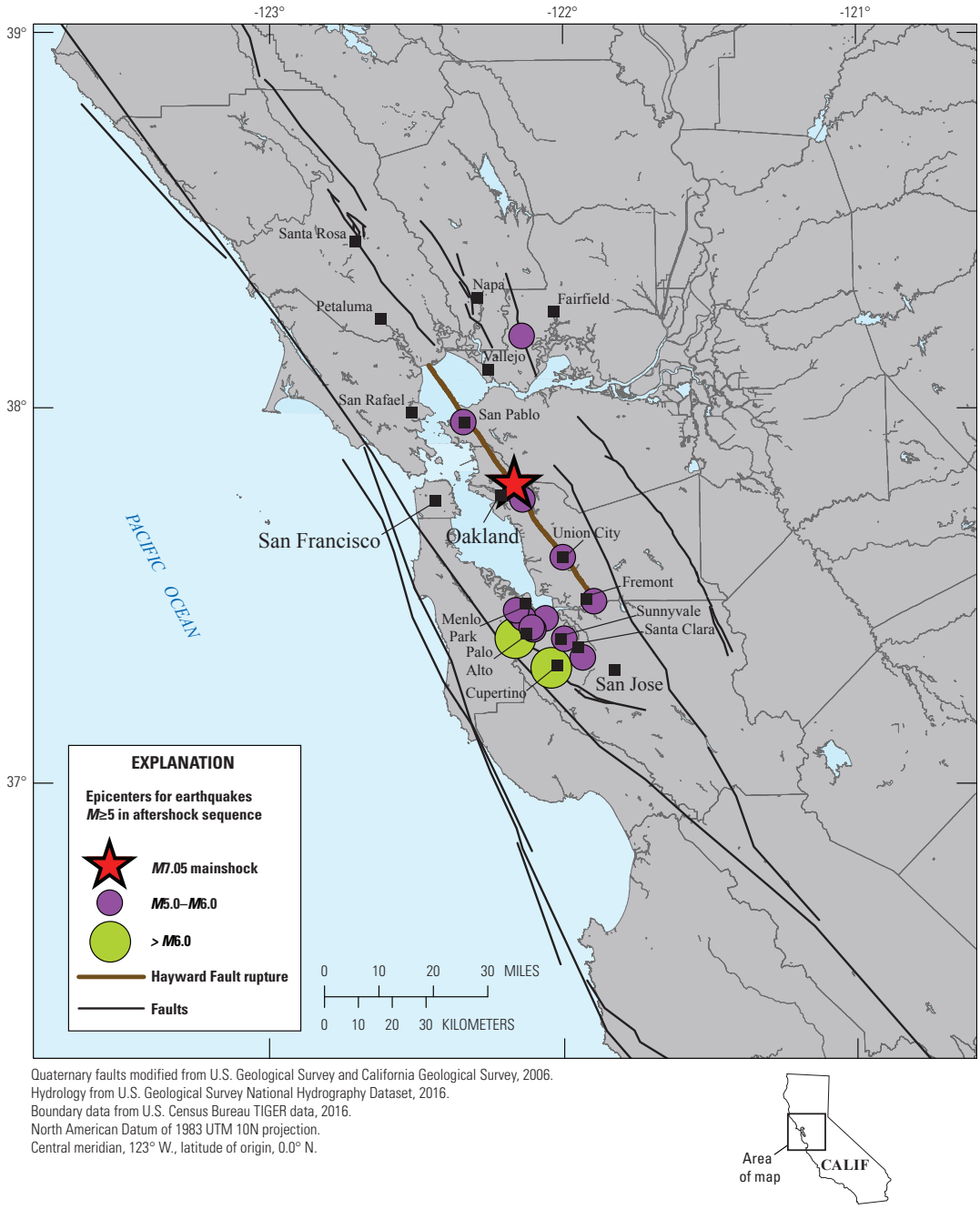

Figure 7. Map of the San Francisco Bay region, California, showing larger aftershocks of magnitude (*M*) 5 or greater in the HayWired earthquake scenario. >, greater than.

relative to their *M*5 aftershocks to place them on known faults. In a natural earthquake sequence, the *M*5 and *M*6 aftershocks would not be spatially separated, and most *M*5 events would be clustered around the *M*6 events on the known faults.) Attributes of the 14 aftershocks with $M \geq 5$ are listed in table 5. The aftershock depths are constrained within the 5th and 95th percentiles of the observed and expected depths of earthquakes in the San Francisco Bay area. For example, the 1989 M_w 6.9 Loma Prieta earthquake nucleated at a depth of 18 km, which is among the deepest recorded earthquakes in the San Francisco Bay area (for example, Hill and others, 1990). The two scenario aftershocks in table 5 with depths of 2.65 km are considered very shallow for moderately sized earthquakes, although on some young faults shallow nucleation may theoretically occur.

ShakeMaps for each of the $M \geq 5$ aftershocks can be accessed at http://escweb.wr.usgs.gov/share/shake2/haywired/archive/scenario.html (U.S. Geological Survey, 2015). They are labeled consistently with the table of aftershock attributes in terms of abbreviated city and magnitude. For example, Uc523 is the *M*5.23 earthquake with a hypocenter in Union City.

Table 5. Time, location, depth, and magnitude of aftershocks in the San Francisco Bay region, California, of magnitude 5 or greater in the HayWired earthquake scenario.

[Day is relative to the day the HayWired mainshock event occurred, with April 18, 2018, counted as day 1. All locations are in California. Latitude is in degrees north; longitude is in degrees west. Depth is how far below the Earth's surface the aftershock hypocenter is located. PDT, Pacific Daylight Time; km, kilometers]

Date	Day	Time (PDT)	Latitude	Longitude	Location	Depth (km)	Magnitude
April 18, 2018	1	4:49 p.m.	37.6008	122.0172	Union City	2.65	5.23
April 19, 2018	2	4:16 a.m.	37.9630	122.3473	San Pablo	2.65	5.04
April 29, 2018	12	11:13 p.m.	38.1916	122.1483	Fairfield	11.05	5.58
May 2, 2018	15	8:44 p.m.	37.4829	121.9146	Fremont	7.15	5.10
May 20, 2018	33	8:37 a.m.	37.7561	122.1508	Oakland	8.45	5.42
May 28, 2018	41	4:47 a.m.	37.3867	122.1780	Palo Alto	18.97	6.21
May 28, 2018	41	8:11 a.m.	37.4528	122.1671	Menlo Park	7.26	5.52
May 28, 2018	41	6:22 p.m.	37.4604	122.1753	Atherton	7.91	5.11
May 28, 2018	41	11:53 p.m.	37.4099	122.1184	Palo Alto	8.36	5.69
June 23, 2018	67	8:27 p.m.	37.4391	122.1511	Palo Alto	2.85	5.22
July 1, 2018	75	11:19 a.m.	37.4435	122.1561	Palo Alto	8.69	5.26
September 30, 2018	166	8:16 p.m.	37.4386	122.0770	Mountain View	11.29	5.98
October 1, 2018	167	12:33 a.m.	37.3068	122.0592	Cupertino	15.45	6.40
October 1, 2018	167	2:24 a.m.	37.3835	122.0153	Sunnyvale	18.89	5.35
October 1, 2018	167	6:10 a.m.	37.3334	121.9541	Santa Clara	7.00	5.09
August 22, 2019	492	10:45 p.m.	37.4145	122.1235	Palo Alto	11.98	5.01

Scenario Aftershock Forecasts

The first 40 days of the HayWired scenario aftershock sequence represent average seismicity rates for California aftershocks; the sequence is closely aligned with the expected numbers of aftershocks forecasted. We provide scenario aftershock forecasts for time windows after the HayWired scenario mainshock. In the HayWired scenario, these time-sensitive forecasts would be released soon after the scenario mainshock and updated over the days and weeks afterwards. The frequency of providing these aftershock forecasts would be reset if a larger aftershock occurs. In the HayWired scenario, another immediate forecast is released when a *M*6 aftershock occurs, so as to update the forecast information.

Scenario Aftershock Forecast 1—Soon After the Mainshock

The next page shows a sample advisory message that would be publicly issued shortly after the occurrence of the HayWired scenario mainshock at 4:18 p.m. on April 18, 2018. The forecast is based on the rapidly estimated scenario mainshock magnitude of 7, a value that would be confirmed as M_w 7.0. The information used to create this scenario aftershock forecast is shown in table 6. (Note that the following abbreviations are used in the advisory messages on the following pages: PDT, Pacific Daylight Time; %, percent. Because these messages are intended for the media and the public, distances in the messages are provided in miles—1 mile=1.61 km.)

Magnitude analysis would be performed on the Oakland earthquake, indicating that the most precise magnitude value is M_w 7.0. Within 24 hours after the mainshock, the Northern California Seismic Network would have recorded 32 aftershocks larger than *M*4, 2 aftershocks larger than *M*5, and no aftershocks larger than *M*6. This is close to the initial forecast (see table 6), so the scientists would continue to use generic mean California aftershock rates to forecast the expected number of aftershocks in this sequence.

HayWired Scenario Earthquake Aftershock Forecast

Aftershock advisory from the United States Geological Survey (USGS)

- An earthquake of magnitude 7 occurred at 4:18 p.m. PDT on April 18, 2018, near Oakland, California. More earthquakes than usual will continue to occur in the mainshock area.
- Be ready for more earthquakes: Find the California Governor's Office of Emergency Services (Cal OES) event page at http://www.caloes.ca.gov/. See Earthquake Country Alliance (ECA, http://www.earthquakecountry.org/sevensteps/) for advice on earthquake preparedness. See the Centers for Disease Control and Prevention (CDC, https://emergency.cdc.gov/coping/index.asp) for advice on coping with a disaster.
- During the next week, there are likely to be 437 to 508 aftershocks large enough to be felt, and there is a 99% chance of one or more aftershocks large enough to potentially cause damage.

What to Expect

It is normal for an earthquake of this size to cause an increase in the number of earthquakes (called aftershocks) in the area. The number of aftershocks will drop off over time, but a large aftershock can increase the numbers of earthquakes again, temporarily.

The aftershocks will occur mostly in the area affected by the magnitude-7 Oakland earthquake, within approximately 35 miles of Oakland, with some as far as 75 miles away.

When there are more earthquakes, the chance of a large earthquake is greater and the chance of damage is greater. The USGS advises everyone to remain aware of the possibility of aftershocks, especially when in or around vulnerable structures (such as unreinforced masonry buildings) and landslide areas.

No one can predict the exact time or place of any earthquake, including aftershocks. The USGS can forecast how many earthquakes to expect or the chance of having an earthquake within a given time period.

Current USGS Aftershock Forecast

The USGS estimates the chance of more aftershocks within the next week until April 25, 2018, 4:18 p.m. PDT as follows:

- The chance of an earthquake large enough to feel (magnitude 3 or greater) is greater than 99%, and it is most likely that 437 to 508 such earthquakes may occur. This chance is 1,500 times greater than it was before the magnitude-7 Oakland earthquake occurred.
- The chance of an earthquake of magnitude 5 or greater is 99%, and it is most likely that 1 to 9 such earthquakes may occur.
- The chance of an earthquake of magnitude 6 or greater is 2 in 5 (39%), and it is most likely that 0 to 2 such earthquakes may occur.
- The chance of an earthquake of magnitude 7 or greater is 1 in 20 (5%), such an earthquake is possible but with a low probability.
- The chance of any damaging earthquake is 1,500 times greater than it was before the magnitude-7 Oakland earthquake occurred.

The chance of earthquakes large enough to be felt or to cause damage remains elevated for the next month and the next year. The table provides forecasts for other time periods.

The USGS calculates this earthquake forecast using a statistical analysis based on past earthquakes and the aftershocks recorded for this sequence. The forecast changes as time passes due to the decay in the frequency of aftershocks, larger aftershocks that may trigger further earthquakes, and changes in forecast modeling based on the earthquake data collected.

This advisory was issued: April 18, 2018, at 4:18 p.m.
This advisory will be updated on or before: April 19, 2018, at 4:18 p.m.

SCENARIO----SCENARIO----SCENARIO----SCENARIO----SCENARIO
THIS IS NOT A REAL EARTHQUAKE OR REAL AFTERSHOCK FORECAST

Table 6. Aftershock forecast immediately after the HayWired earthquake scenario mainshock (moment magnitude 7, April 18, 2018, at 4:18 p.m.) for the next day, week, month, and year.

[The number of aftershocks is the expected or average value. The numbers in parentheses are lower- and upper-bound values associated with 5-percent and 95-percent probability of not being exceeded. The aftershock probability is the probability of at least one aftershock at the given magnitudes at the time of the forecast. *M*, magnitude; %, percent; ≥, greater than or equal]

Forecast period	Expected number of aftershocks		Aftershock probability		Increase in the seismicity rate relative to the rate before the mainshock
	M≥4	*M*≥5	*M*≥6	*M*≥7	
Next 24 hours	33 (24–43)	3 (1–6)	30%	3%	10,000
Next week	50 (39–62)	5 (1–9)	39%	5%	1,500
Next month	57 (45–70)	5 (2–10)	43%	6%	430
Next year	71 (57–85)	7 (3–13)	47%	6%	45

Scenario Aftershock Forecast 2—24 Hours After the Mainshock

The next page shows a sample advisory message that would be publicly issued 24 hours after the occurrence of the HayWired scenario mainshock, that is, at about 4:18 p.m. on April 19, 2018. The scenario forecast is based on the slightly revised M_w 7.0 for the mainshock. The information used to create this scenario aftershock forecast is shown in table 7.

In the scenario, within the past 24 hours, seven aftershocks larger than or equal to *M*4 and no aftershocks larger than *M*5 would be recorded. This is consistent with the forecast advisory issued 24 hours after the Oakland earthquake (see table 7).

Table 7. Aftershock forecast 24 hours after the HayWired earthquake scenario mainshock (moment magnitude 7, April 18, 2018, at 4:18 p.m.) for the next day, week, month, and year.

[The number of aftershocks is the expected or average value. The numbers in parentheses are lower- and upper-bound values associated with 5-percent and 95-percent probability of not being exceeded. The aftershock probability is the probability of at least one aftershock at the given magnitudes at the time of the forecast. *M*, magnitude; %, percent; ≥, greater than or equal]

Forecast period	Expected number of aftershocks		Aftershock probability		Increase in the seismicity rate relative to the rate before the mainshock
	M≥4	*M*≥5	*M*≥6	*M*≥7	
Next 24 hours	7 (2–11)	1 (0–2)	7%	0.7%	2,500
Next week	19 (14–32)	2 (1–4)	19%	2%	1,000
Next month	33 (20–87)	3 (0–10)	30%	3%	400
Next year	52 (43–157)	6 (4–16)	34%	3%	50

HayWired Scenario Earthquake Aftershock Forecast—24-Hour Update

Aftershock advisory from the United States Geological Survey (USGS)

- An earthquake of magnitude 7 occurred at 4:18 p.m. PDT on April 18, 2018, near Oakland, California. More earthquakes than usual will continue to occur in the mainshock area.
- Be ready for more earthquakes: Find the California Governor's Office of Emergency Services (Cal OES) event page at http://www.caloes.ca.gov/. See Earthquake Country Alliance (ECA, http://www.earthquakecountry.org/sevensteps/) for advice on earthquake preparedness. See the Centers for Disease Control and Prevention (CDC, https://emergency.cdc.gov/coping/index.asp) for advice on coping with a disaster.
- During the next week, there are likely to be 140 to 320 aftershocks large enough to be felt, and there is a 95% chance of one or more aftershocks large enough to potentially cause damage.

What to Expect

It is normal for a magnitude-7 earthquake to cause an increase in the number of earthquakes (called aftershocks) in the area. The number of aftershocks will drop off over time, but a large aftershock can increase the numbers of earthquakes again, temporarily.

The aftershocks will occur mostly in the area affected by the magnitude-7 Oakland earthquake, within approximately 35 miles of Oakland, with some as far as 75 miles away.

When there are more earthquakes, the chance of a large earthquake is greater and the chance of damage is greater. The USGS advises everyone to remain aware of the possibility of aftershocks, especially when in or around vulnerable structures (such as unreinforced masonry buildings) and landslide areas.

No one can predict the exact time or place of any earthquake, including aftershocks. The USGS can forecast how many earthquakes to expect or the chance of having an earthquake within a given time period.

Current USGS Aftershock Forecast

The USGS estimates the chance of more aftershocks within the next week until April 26, 2018, 4:18 p.m. PDT as follows:

- The chance of an earthquake large enough to feel (magnitude 3 or greater) is greater than 99%, and it is most likely that 140 to 320 such earthquakes may occur. This chance is about 1,000 times greater than it was before the magnitude-7 Oakland earthquake occurred.
- The chance of an earthquake of magnitude 5 or greater is 95%, and it is most likely that 1 to 4 such earthquakes may occur.
- The chance of an earthquake of magnitude 6 or greater is 1 in 5 (19%).
- The chance of an earthquake of magnitude 7 or greater is 1 in 50 (2%); such an earthquake is possible but with a low probability.
- The chance of any damaging earthquake is about 1,000 times greater than it was before the magnitude-7 Oakland earthquake occurred.

The chance of earthquakes large enough to be felt or to cause damage remains elevated for the next month and the next year. The table provides forecasts for other time periods.

The USGS calculates this earthquake forecast using a statistical analysis based on past earthquakes and the aftershocks recorded for this sequence. The forecast changes as time passes due to the decay in the frequency of aftershocks, larger aftershocks that may trigger further earthquakes, and changes in forecast modeling based on the earthquake data collected.

This advisory was issued: April 19, 2018, at 4:18 p.m.
This advisory will be updated on or before: April 20, 2018, at 4:18 p.m.

SCENARIO----SCENARIO----SCENARIO----SCENARIO----SCENARIO
THIS IS NOT A REAL EARTHQUAKE OR REAL AFTERSHOCK FORECAST

Scenario Aftershock Forecast 3—48 Hours After the Mainshock

The next page shows a sample advisory message that will be publicly issued by the USGS 48 hours after the occurrence of the HayWired scenario mainshock, that is, at about 4:18 p.m. on April 20, 2018. The information used to create this scenario aftershock forecast is shown in table 8.

Table 8. Aftershock forecast 48 hours after the HayWired earthquake scenario mainshock (moment magnitude 7, April 18, 2018, at 4:18 p.m.) for the next day, week, month, and year.

[The number of aftershocks is the expected or average value. The numbers in parentheses are lower- and upper-bound values associated with 5-percent and 95-percent probability of not being exceeded. The aftershock probability is the probability of at least one aftershock at the given magnitudes at the time of the forecast. *M*, magnitude; %, percent; ≥, greater than or equal]

Forecast period	Expected number of aftershocks		Aftershock probability		Increase in the seismicity rate relative to the rate before the mainshock
	M≥4	*M*≥5	*M*≥6	*M*≥7	
Next week	12 (8–29)	1 (1–4)	10%	1%	600
Next month	18 (11–42)	2 (0–6)	16%	1.6%	200
Next year	42 (35–120)	4–5 (3–13)	30%	3%	40

HayWired Scenario Earthquake Aftershock Forecast—48 Hour Update

Aftershock advisory from the United States Geological Survey (USGS)

- An earthquake of magnitude 7 occurred at 4:18 p.m. PDT on April 18, 2018, near Oakland, California. More earthquakes than usual will continue to occur in the mainshock area.
- Be ready for more earthquakes: Find the California Governor's Office of Emergency Services (Cal OES) event page at http://www.caloes.ca.gov/. See Earthquake Country Alliance (ECA, http://www.earthquakecountry.org/sevensteps/) for advice on earthquake preparedness. See the Centers for Disease Control and Prevention (CDC, https://emergency.cdc.gov/coping/index.asp) for advice on coping with a disaster.
- During the next week, there are likely to be 80 to 290 aftershocks large enough to be felt, and there is a 64% chance of one or more aftershocks large enough to potentially cause damage.

What to Expect

It is normal for a magnitude-7 earthquake to cause an increase in the number of earthquakes (called aftershocks) in the area. The number of aftershocks will drop off over time, but a large aftershock can increase the numbers of earthquakes again, temporarily.

The aftershocks will occur mostly in the area affected by the magnitude-7 Oakland earthquake, within approximately 35 miles of Oakland, with some as far as 75 miles away.

When there are more earthquakes, the chance of a large earthquake is greater and the chance of damage is greater. The USGS advises everyone to remain aware of the possibility of aftershocks, especially when in or around vulnerable structures (such as unreinforced masonry buildings) and landslide areas.

No one can predict the exact time or place of any earthquake, including aftershocks. The USGS can forecast how many earthquakes to expect or the chance of having an earthquake within a given time period.

Current USGS Aftershock Forecast

The USGS estimates the chance of more aftershocks within the next week until April 27, 2018, 4:18 p.m. PDT as follows:

- The chance of an earthquake large enough to feel (magnitude 3 or greater) is greater than 99%, and it is most likely that 80 to 290 such earthquakes may occur. This chance is 600 times greater than it was before the magnitude-7 Oakland earthquake occurred.
- The chance of an earthquake of magnitude 5 or greater is 64%, and it is most likely that 1 to 3 such earthquakes may occur.
- The chance of an earthquake of magnitude 6 or greater is 1 in 10 (10%).
- The chance of an earthquake of magnitude 7 or greater is 1 in 100 (1%); such an earthquake is possible but with a low probability.
- The chance of any damaging earthquake is 600 times greater than it was before the magnitude-7 Oakland earthquake occurred.

The chance of earthquakes large enough to be felt or to cause damage remains elevated for the next month and the next year. The table provides forecasts for other time periods.

The USGS calculates this earthquake forecast using a statistical analysis based on past earthquakes and the aftershocks recorded for this sequence. The forecast changes as time passes due to the decay in the frequency of aftershocks, larger aftershocks that may trigger further earthquakes, and changes in forecast modeling based on the earthquake data collected.

This advisory was issued: April 20, 2018, at 4:18 p.m.
This advisory will be updated on or before: April 25, 2018, at 4:18 p.m.

SCENARIO----SCENARIO----SCENARIO----SCENARIO----SCENARIO
THIS IS NOT A REAL EARTHQUAKE OR REAL AFTERSHOCK FORECAST

Scenario Aftershock Forecast 4—7 Days After the Mainshock

Within the week after the Oakland earthquake, 47 aftershocks larger than or equal to *M*4 and no aftershocks larger than *M*5 would be recorded. This is consistent with the initial forecast advisory issued (see table 6).

The next page shows a sample advisory message that the USGS would publically issue 1 week after the occurrence of the HayWired scenario mainshock, that is, at about 4:20 p.m. on April 25, 2018. The information used to create this scenario aftershock forecast is shown in table 9.

Table 9. Aftershock forecast 7 days after the HayWired earthquake scenario mainshock (moment magnitude 7, April 18, 2018, at 4:18 p.m.) for the next day, week, month, and year.

[The number of aftershocks is the expected or average value. The numbers in parentheses are lower- and upper-bound values associated with 5-percent and 95-percent probability of not being exceeded. The aftershock probability is the probability of at least one aftershock at the given magnitudes at the time of the forecast. *M*, magnitude; %, percent; ≥, greater than or equal]

Forecast period	Expected number of aftershocks		Aftershock probability		Increase in the seismicity rate relative to the rate before the mainshock
	M≥4	*M*≥5	*M*≥6	*M*≥7	
Next week	4 (0–15)	0 (0–3)	4%	0.4%	210
Next month	10 (8–18)	1 (1–3)	10%	1%	120
Next year	31 (26–127)	3 (2–13)	20%	2%	30

HayWired Scenario Earthquake Aftershock Forecast—7-Day Update

Aftershock advisory from the United States Geological Survey (USGS)

- An earthquake of magnitude 7 occurred at 4:18 p.m. PDT on April 18, 2018, near Oakland, California. More earthquakes than usual will continue to occur in the mainshock area.
- Be ready for more earthquakes: Find the California Governor's Office of Emergency Services (Cal OES) event page at http://www.caloes.ca.gov/. See Earthquake Country Alliance (ECA, http://www.earthquakecountry.org/sevensteps/) for advice on earthquake preparedness. See the Centers for Disease Control and Prevention (CDC, https://emergency.cdc.gov/coping/index.asp) for advice on coping with a disaster.
- During the next week, there are likely to be as many as 150 aftershocks large enough to be felt, and there is a 40% chance of one or more aftershocks large enough to potentially cause damage.

What to Expect

It is normal for a magnitude-7 earthquake to cause an increase in the number of earthquakes (called aftershocks) in the area. The number of aftershocks will drop off over time, but a large aftershock can increase the numbers of earthquakes again, temporarily.

The aftershocks will occur mostly in the area affected by the magnitude-7 Oakland earthquake, within approximately 35 miles of Oakland, with some as far as 75 miles away.

When there are more earthquakes, the chance of a large earthquake is greater and the chance of damage is greater. The USGS advises everyone to remain aware of the possibility of aftershocks, especially when in or around vulnerable structures (such as unreinforced masonry buildings) and landslide areas.

No one can predict the exact time or place of any earthquake, including aftershocks. The USGS can forecast how many earthquakes to expect or the chance of having an earthquake within a given time period.

Current USGS Aftershock Forecast

The USGS estimates the chance of more aftershocks within the next week until April 27, 2018, 4:18 p.m. PDT as follows:

- The chance of an earthquake large enough to feel (magnitude 3 or greater) is 98%, and it is most likely that as many as 150 such earthquakes may occur. This chance is 210 times greater than it was before the magnitude-7 Oakland earthquake occurred.
- The chance of an earthquake of magnitude 5 or greater is 40%, and it is most likely that 0 to 3 such earthquakes may occur.
- The chance of an earthquake of magnitude 6 or greater is 1 in 25 (4%), and it is most likely that 0 to 1 such earthquakes may occur.
- The chance of an earthquake of magnitude 7 or greater is 1 in 250 (0.4%); such an earthquake is possible but with a low probability.
- The chance of any damaging earthquake is 210 times greater than it was before the magnitude-7 Oakland earthquake occurred.

The chance of earthquakes large enough to be felt or to cause damage remains elevated for the next month and the next year. The table provides forecasts for other time periods.

The USGS calculates this earthquake forecast using a statistical analysis based on past earthquakes and the aftershocks recorded for this sequence. The forecast changes as time passes due to the decay in the frequency of aftershocks, larger aftershocks that may trigger further earthquakes, and changes in forecast modeling based on the earthquake data collected.

This advisory was issued: April 25, 2018, at 4:18 p.m.
This advisory will be updated on or before: May 2, 2018, at 4:18 p.m.

SCENARIO----SCENARIO----SCENARIO----SCENARIO----SCENARIO
THIS IS NOT A REAL EARTHQUAKE OR REAL AFTERSHOCK FORECAST

Scenario Aftershock Forecast 5—40 Days After the Mainshock

Forty days after the Haywired scenario mainshock, the expected number of aftershocks larger than *M*4 within the next week is one with a range of zero to two, and the seismicity over the next week is 30 times greater than what it would have been without the mainshock. There is a 0.8 percent (1 in 125) chance of an *M*6 or larger earthquake within the next week. In the scenario, a *M*6.2 earthquake occurs in Palo Alto and triggers more aftershocks. The next page shows a sample a special aftershock advisory message following the *M*6.2 aftershock. Supporting information is summarized in table 10.

The HayWired scenario aftershock sequence continues as described above. The aftershock forecast would again be reset after the largest aftershock, a *M*6.4 earthquake in Cupertino, and an immediate forecast would be released. The HayWired scenario earthquake sequence does not contain the largest or most aftershocks of the simulated sequences. There are many more possible sequences, but we can estimate the likelihood that an aftershock sequence has a largest aftershock of *M*6.4.

Table 10. Aftershock forecast 40 days after the HayWired earthquake scenario mainshock (moment magnitude 7, April 18, 2018, at 4:18 p.m.) for the next day, week, month, and year.

[The number of aftershocks is the expected or average value. The numbers in parentheses are lower- and upper-bound values associated with 5 percent and 95 percent probability of not being exceeded. The aftershock probability is the probability of at least one aftershock at the given magnitudes at the time of the forecast. *M*, magnitude; %, percent; ≥, greater than or equal]

Forecast period	Expected number of aftershocks		Aftershock probability		Increase in the seismicity rate relative to the rate before the mainshock
	M≥4	*M*≥5	*M*≥6	*M*≥7	
Next 24 hours	6 (4–9)	0–1 (0–2)	6%	0.06%	1,350
Next week	8 (7–18)	1 (0–2)	9%	0.9%	265
Next month	10 (8–30)	1 (0–4)	10%	1%	70
Next year	19 (17–40)	2 (1–5)	10%	1%	12.5

HayWired Scenario Earthquake—Special Aftershock Advisory due to Magnitude-6.2 Aftershock Scenario

Aftershock advisory from the United States Geological Survey (USGS)

- An earthquake of magnitude 6.2 occurred at 4:57 p.m. PDT on May 28, 2018, near Palo Alto, California. The earthquake is a large aftershock following the magnitude-7 Oakland earthquake that occurred at 4:18 p.m. PDT on April 18, 2018. More earthquakes than usual will continue to occur in the mainshock and the Palo Alto areas.
- Be ready for more earthquakes: Find the California Governor's Office of Emergency Services (Cal OES) event page at http://www.caloes.ca.gov/). See Earthquake Country Alliance (ECA, http://www.earthquakecountry.org/sevensteps/) for advice on earthquake preparedness. See the Centers for Disease Control and Prevention (CDC, https://emergency.cdc.gov/coping/index.asp) for advice on coping with a disaster.
- During the next week, there are likely to be 68 to 98 aftershocks large enough to be felt, and there is a 3 in 5 (56%) chance of one or more aftershocks large enough to potentially cause damage.

What to Expect

It is normal for a magnitude-7 earthquake of this size to cause an increase in the number of earthquakes (called aftershocks) in the area. The number of aftershocks will drop off over time, but a large aftershock can increase the numbers of earthquakes again, temporarily.

The aftershocks will occur mostly in the area affected by the magnitude-6.2 Palo Alto earthquake, within approximately 25 miles of Palo Alto, California, in addition to the area affected by the magnitude-7 Oakland earthquake, within approximately 35 miles of Oakland, California with some as far as 75 miles away.

When there are more earthquakes, the chance of a large earthquake is greater and the chance of damage is greater. The USGS advises everyone to remain aware of the possibility of aftershocks, especially when in or around vulnerable structures (such as unreinforced masonry buildings) and landslide areas.

No one can predict the exact time or place of any earthquake, including aftershocks. The USGS can forecast how many earthquakes to expect or the chance of having an earthquake within a given time period.

Current USGS Aftershock Forecast

The USGS estimates the chance of more aftershocks within the next week until June 4, 2018, 4:57 p.m. PDT as follows.

- The chance of an earthquake large enough to feel (magnitude 3 or greater) is greater than 99%, and it is most likely that 68 to 98 such earthquakes may occur. This chance is 265 times greater than it was before the magnitude-7 Oakland earthquake occurred.
- The chance of an earthquake of magnitude 5 or greater is 3 in 5 (56%), and it is most likely that 0 to 3 such earthquakes may occur.
- The chance of an earthquake of magnitude 6 or greater is 9 in 100 (9%).
- The chance of an earthquake of magnitude 7 or greater is 9 in 1,000 (1%); such an earthquake is possible but with a low probability.
- The chance of any damaging earthquake is 265 times greater than it was before the magnitude-7 Oakland earthquake occurred.

The chance of earthquakes large enough to be felt or to cause damage remains elevated for the next month and the next year. The table provides forecasts for other time periods.

The USGS calculates this earthquake forecast using a statistical analysis based on past earthquakes and the aftershocks recorded for this sequence. The forecast changes as time passes due to the decay in the frequency of aftershocks, larger aftershocks that may trigger further earthquakes, and changes in forecast modeling based on the earthquake data collected.

This advisory was issued: May 28, 2018, at 4:57 p.m.
This advisory will be updated on or before: June 4, 2018, at 4:57 p.m.

SCENARIO----SCENARIO----SCENARIO----SCENARIO----SCENARIO
THIS IS NOT A REAL EARTHQUAKE OR REAL AFTERSHOCK FORECAST

Probability of Largest Aftershock

The likelihood of an aftershock sequence having a largest aftershock of *M*6.4 or larger for an *M*7.0 mainshock can be estimated from Lombardi's (2002) statistical study of the difference (D_1) between the magnitude of the mainshock (M=7.0) and the largest aftershock (M_1=6.4)—that is, $D_1=M-M_1$. Lombardi reports that D_1 has been observed not to be exponential and in one dataset was observed to be adequately fit by a normal distribution. Using probability theory, Lombardi shows how the expected value of D_1 can be anywhere from 0.5 to 1.2, and how D_1 approaches the exponential distribution in theory only under conditions that do not seem to apply to the HayWired earthquake sequence. Lombardi examines an earthquake catalog compiled by the Southern California Earthquake Center (SCEC) of earthquake clusters between 1990 and 2001. For a subset of the data with mainshock magnitude greater than or equal to 4.0 and including aftershocks of magnitude at least 2.0, Lombardi finds an expected value of D_1, denoted here by m, of 1.2, as Richter (1958) had previously pointed out from work by Båth (1965), with a standard deviation of s=0.65. Here, D_1=7.0–6.4=0.6, which is within the $m\pm 1s$ bounds (that is, 0.6 is within 1.2±0.65 or 0.55 to 1.85). If we assume m=1.2 as Båth suggested, s=0.65 as in the SCEC subset with $M_0\geq 4.0$, and normally distributed D_1, we can estimate the probability that the largest aftershock would be at least *M*6.4 (that is, that D_1 would be at most 0.65) as in the selected HayWired aftershock simulation (see equation 1):

$$\begin{aligned} P_{normal} &= \Phi\left(\frac{D_1-\mu}{\sigma}\right) \\ &= \Phi\left(\frac{0.6-1.2}{0.65}\right) \\ &= 0.18 \end{aligned} \quad (1)$$

In equation 1, Φ denotes the cumulative standard normal cumulative distribution function. Equation 1 produces a probability P_{normal}=18 percent, that is, one can estimate that 1 in 5 earthquakes of *M*7.0 would produce an aftershock larger than the largest one hypothesized here. If instead we assume D_1 is exponentially distributed with expected value 1.2, we can estimate the nonexceedance probability P_{exp} as shown in equation 2:

$$\begin{aligned} P_{exp} &= 1-\exp\left(\frac{-D_1}{\mu}\right) \\ &= 1-\exp\left(\frac{-0.6}{1.2}\right) \\ &= 0.39 \end{aligned} \quad (2)$$

Equation 2 produces a probability P_{exp}=0.39, that is, 2 in 5 earthquakes of *M*7.0 would produce an aftershock larger than the largest one hypothesized here. In either case, the HayWired scenario aftershock sequence does not seem to be an extreme example or anywhere near a worst case.

Limitations of Aftershock Sequence Simulation and Forecasting

Simulations and forecasts of aftershock sequences are based on spatial and temporal earthquake sequence statistics. The results are affected by the simulation parameters (for example, average aftershock rates). Previous earthquake sequences and a comparison of the number of aftershocks for *M*5.5 or larger earthquakes in California suggests that average aftershock rates may be lower in northern California than in southern California, although rates can vary widely in both regions (Llenos and Michael, 2015). Rates at which aftershocks occur can even vary quite widely for closely colocated mainshocks. More scientific investigation is required to explain this substantial variability. Further research and modeling may improve both our ability to make more accurate forecasts immediately after a large earthquake has occurred and our ability to make forecasts when early data for an earthquake sequence are unreliable.

More sophisticated aftershock modeling is needed to mesh aftershock forecasting with traditional fault and stress-renewal-based seismic-hazard models. The Uniform California Earthquake Rupture Forecast, version 3 (UCERF3) epidemic-type aftershock sequence (ETAS) is developing this capability (Field and others, 2013). For instance, the working group is attempting to include spatiotemporal earthquake clustering by merging a point process ETAS model (Ogata, 1988) into the finite-fault based framework. The ultimate aim is to deploy UCERF3 as part of an operational earthquake forecast, although doing so will require additional work with respect to real-time network interoperability.

The forecasts provided here convey the type of information that is available in an earthquake forecast, but the message template used above is under development. Specifically, communication of aftershock forecasts with multiple intended audiences uses (1) communication guidelines from social and behavioral science, (2) studies of implemented aftershock forecast communications, and (3) message testing.

Conclusion

Although it is not possible to predict the location, magnitude, and timing of earthquakes, scientists can forecast frequency and probability of aftershock magnitudes within confidence intervals for time windows. Statistical relations can be used to simulate earthquake sequences over time and space as an approach to describing elevated levels of earthquake risk. The devastating outcomes of recent earthquake sequences in New Zealand and Italy have demonstrated the need for scientific and transparent information about earthquake risk (Jordan and others, 2014). The HayWired scenario earthquake sequence offers an opportunity to investigate the possible uses of earthquake forecasts and consequences of aftershocks before a large earthquake occurs. A description

of one simulated aftershock sequence and sample aftershock forecasts are provided to expose stakeholders and decision makers to information that will be produced and communicated. This allows future recipients of earthquake forecasts the time for understanding the information and its limitations; considering its use in mitigation, preparedness, response, and recovery decisions; and providing feedback on how to improve communication products and processes. Finally, the aftershock scenario timeline and ShakeMaps can be used to investigate the implications of a series of damaging earthquakes and to hold exercises that practice resetting response and recovery throughout the duration of an earthquake sequence.

Acknowledgments

USGS Earthquake Science Center (ESC) scientists Jeanne Hardebeck, Ruth Harris, Morgan Page, Andrew Michael, Jack Boatwright, and Shane Detweiler provided crucial input on various aspects of the HayWired scenario aftershock sequence and earthquake forecast statistics. We are indebted to Ruth Harris and Morgan Page for their constructive review of the manuscript. Tim MacDonald (USGS Earthquake Science Center IT Specialist) generated the aftershock ShakeMaps. This construction of the aftershock sequence was funded by the following USGS components: Land Change Science, Science Application for Risk Reduction (SAFRR), and ESC.

References Cited

Aagaard, B.T., Graves, R.W., Schwartz, D.P., Ponce, D.A., and Graymer, R.W., 2010a, Ground-motion modeling of Hayward Fault scenario earthquakes, part I; Construction of the suite of scenarios: Bulletin of the Seismological Society of America, v. 100, no. 6, p. 2927–2944.

Aagaard, B.T., Graves, R.W., Rodgers, A., Brocher, T.M., Simpson, R.W., Dreger, D., Petersson, N.A., Larsen, S.C., Ma, S., and Jachens, R.C., 2010b, Ground-motion modeling of Hayward Fault scenario earthquakes, part II; Simulation of long-period and broadband ground motions: Bulletin of the Seismological Society of America, v. 100, no. 6, p. 2945–2977.

Båth, M., 1965, Lateral inhomogeneities in the upper mantle: Tectonophysics, v 2, no. 6, p. 483–514.

Becker, J.S., Potter, S.H., Wein, A.M., Doyle, E.E.H., and Ratliff, J., 2015, Aftershock communication during the Canterbury earthquakes, New Zealand—Implications for response and recovery in the built environment: New Zealand Society of Earthquake Engineering proceedings, accessed at http://www.nzsee.org.nz/db/2015/Papers/O-52_Becker.pdf.

Brocher, T.M., Baltay, A.S., Hardebeck, J.L., Pollitz, F.F., Murray, J.R., Llenos, A.J., Schwartz, D.P., Blair, J.L., Ponti, D.J., Lienkaemper, J.J., Langenheim, V.E., Dawson, T.E., Hudnut, K.W., Shelly, D.R., Dreger, D.S., Boatwright, J., Aagaard, B.T., Wald, D.J., Allen, R.M., Barnhart, W.D., Knudsen, K.L., Brooks, B.A., and Scharer, K.M., 2015, The M_w 6.0 24 August 2014 South Napa earthquake: Seismological Research Letters, v. 86, no. 2A, p. 309–326.

Dietz, L.D., and Ellsworth, W.L., 1990, The October 17, 1989, Loma Prieta, California, earthquake and its aftershocks—Geometry of the sequence from high-resolution locations: Geophysical Research Letters, v. 17, no. 9, p.1417–1420.

Felzer, K.R., 2008, Simulated aftershock sequences for a M 7.8 earthquake on the southern San Andreas Fault: Seismological Research Letters, v. 80, no. 1, p. 21–25, doi:10.1785/gssrl.80.1.21.

Felzer, K.R., Abercrombie, R.E., and Ekström, G., 2003, Secondary aftershocks and their importance for aftershock prediction: Bulletin of the Seismological Society of America, v. 93, no.4, p. 1433–1448.

Felzer, K.R., Becker, T.W., Abercrombie, R.E., Ekström, G., and Rice, J.R., 2002, Triggering of the 1999 M_W 7.1 Hector Mine earthquake by aftershocks of the 1992 M_W 7.3 Landers earthquake: Journal of Geophysical Research, Solid Earth, v. 107, no. B9, p. ESE 6-1–ESE 6-13, doi:10.1029/2001JB000911.

Felzer, K.R., and Brodsky, E.E., 2006, Decay of aftershock density with distance indicates triggering by dynamic stress: Nature, v. 441, p. 735–738.

Field, E.H., Biasi, G.P., Bird, P., Dawson, T.E., Felzer, K.R., Jackson, D.D., Johnson, K.M., Jordan, T.H., Madden, C., Michael, A.J., Milner, K.R., Page, M.T., Parsons, T., Powers, P.M., Shaw, B.E., Thatcher, W.R., Weldon, R.J., II, and Zeng, Y., 2013, Uniform California earthquake rupture forecast, version 3 (UCERF3)—The time-independent model: U.S. Geological Survey Open-File Report 2013–1165, 97 p., California Geological Survey Special Report 228, and Southern California Earthquake Center Publication 1792. [Also available at https://pubs.usgs.gov/of/2013/1165/.]

Gutenberg, B., and Richter, C.F., 1944, Frequency of earthquakes in California: Bulletin of the Seismological Society of America, v. 34, p. 185–188.

Harris, R.A., and Simpson, R.W., 1998, Suppression of large earthquakes by stress shadows—A comparison of Coulomb and rate-and-state failure: Journal of Geophysical Research, v. 103, no. B10, p. 24439–24451.

Hill, D.P., Eaton, J.P., and Jones, L.N., 1990, Seismicity 1980–1989, *in* Wallace, R.E., ed., The San Andreas Fault System, California: U.S. Geological Survey Professional Paper 1515, 283 p. [Also available at https://pubs.usgs.gov/pp/1990/1515/pp1515.pdf.]

Jones, J.L., and Felzer, K.R., 2017, Point locations for earthquakes *M*2.5 and greater in a two-year aftershock sequence resulting from the HayWired scenario earthquake mainshock (4/18/2018) in the San Francisco Bay area, California: U.S. Geological Survey data release, accessed April 18, 2017, at https://doi.org/10.5066/F76H4FPH.

Jordan, T.H., Marzocchi, W., Michael, A., and Gerstenberger, M., 2014, Operational earthquake forecasting can enhance earthquake preparedness: Seismological Research Letters, v. 85, no. 5, p. 955–959.

Llenos, A.L., and Michael, A.J., 2015, Forecasting the (un) productivity of the 2014 *M*6.0 South Napa aftershock sequence [poster session abstract]: Seismological Society of America, 2015 Annual Meeting, Pasadena, Calif., 2015, accessed October 20, 2015, at http://www2.seismosoc.org/FMPro?-db=Abstract_Submission_15&-recid=554&-format=%2Fmeetings%2F2015%2Fabstracts%2Fsessionabstractdetail.html&-lay=MtgList&-find.

Lombardi, A.M., 2002, Probabilistic interpretation of Bath's Law: Annals of Geophysics, v. 45, no. 3/4, p. 455–472.

Meltzner, A.J., and Wald, D.J., 2003, Aftershocks and triggered events of the Great 1906 California earthquake: Bulletin of the Seismological Society of America, v. 93, no. 5, p. 2160–2186.

Michael, A.J., 2012. Fundamental questions of earthquake statistics, source behavior, and the estimation of earthquake probabilities from possible foreshocks: Bulletin of the Seismological Society of America, v. 103, no. 6, p. 2547–2562.

Northern California Earthquake Data Center, 2014, Northern California Earthquake Data Center dataset: University of California Berkeley Seismological Laboratory, doi: 10.7932/NCEDC.

Ogata, Y., 1988, Space-time point-process models for earthquake occurrences: Annals of the Institute of Statistical Mathematics, v. 50, no. 2, p. 379–402.

Omori, F., 1894, On the aftershocks of earthquakes: Journal of the College of Science, Imperial University of Tokyo, v. 7, p. 111–200.

Reasenberg, P.A., and Jones, L.M., 1989, Earthquake hazard after a mainshock in California: Science, v. 243, no. 4895, p. 1173–1176.

Richter, C.F., 1958, Elementary seismology: San Francisco, Freeman, 768 p.

Simpson, R.W., and Reasenberg, P.A., 1994, Earthquake-induced static stress changes on central California faults, *in* Simpson, R.W., ed., The Loma Prieta, California, earthquake of October 17, 1989—Tectonic processes and models: U.S. Geological Survey Professional Paper 1550–F, p. F55–F89. [Also available at https://pubs.usgs.gov/pp/pp1550/pp1550f/.]

Stover, C.W., and Coffman, J.L., 1993, Seismicity of the United States, 1568–1989 (revised): U.S. Geological Survey Professional Paper 1527, 418 p. [Also available at https://pubs.er.usgs.gov/publication/pp1527.]

Toppozada, T.R., Branum, D.M., Reichle, M.S., and Hallstrom, C.L., 2002, San Andreas Fault Zone, California—*M*≥5.5 earthquake history: Bulletin of the Seismological Society of America, v. 92, no. 7, p. 2555–2601.

Toppozada, T.R., and Real, C.R., 1981, Preparation of isoseismal maps and summaries of reported effects for pre-1900 California earthquakes: U.S. Geological Survey Open-File Report 81–262, 78 p., 2 appendixes. [Also available at http://pubs.er.usgs.gov/publication/ofr81262.]

U.S. Geological Survey, 2014, Earthquake planning scenario—ShakeMap for Haywired M7.05-scenario: U.S. Geological Survey Earthquake Hazards Program website, accessed August 26, 2014, at https://earthquake.usgs.gov/scenarios/eventpage/ushaywiredm7.05_se#shakemap?source=us&code=gllegacyhaywiredm7p05_se.

U.S. Geological Survey, 2015, HayWired Aftershock Planning Scenarios: U.S. Geological Survey Earthquake Hazards Program website, accessed October 21, 2015, at http://escweb.wr.usgs.gov/share/shake2/haywired/archive/scenario.html.

Utsu, T., 1961, A statistical study of the occurrence of aftershocks: Geophysical Magazine, v. 30, p. 521–605.

Utsu, T., 1971, Aftershocks and earthquake statistics (3)—Analyses of the distribution of earthquakes in magnitude, time, and space with special consideration to clustering characteristics of earthquake occurrence (1): Journal of the Faculty of Science, Hokkaido University, Series 7, Geophysics, v. 3, no. 5, p. 379–441.

Wein, A.M., Potter, S., Johal, S., Doyle, E., Becker, J., 2016, Communicating with the public during an earthquake sequence—Improving communication of geoscience by coordinating roles: Seismological Research Letters, v. 87, no. 1, 7 p., doi: 10.1785/0220150113.

The HayWired Earthquake Scenario—Earthquake Hazards
Edited by Shane T. Detweiler and Anne M. Wein
Scientific Investigations Report 2017–5013–A–H
[Also see https://doi.org/10.3133/sir20175013]

Chapter H

HayWired Scenario Three-Dimensional Numerical Ground-Motion Simulation Maps

By Keith A. Porter[1]

Abstract

The HayWired scenario examines a hypothetical earthquake (mainshock) with a moment magnitude (M_w) of 7.0 occurring on April 18, 2018, at 4:18 p.m. on the Hayward Fault in the east bay part of California's San Francisco Bay area. The HayWired scenario uses a three-dimensional (3D) numerical simulation for its ground-motion map to produce a more realistic estimate of damage and loss at both the local scale and in the aggregate. There are two common ways to create a ground-motion map for a hypothetical earthquake—(1) use ground-motion prediction equations (the more common of the two) or (2) use 3D ground-motion simulation. Each has advantages and disadvantages. The one based on ground-motion prediction equations (referred to here as a median map) usually only shows median shaking, that is, the 50th percentile. The median is a measure only of central value in a suite of many earthquakes, so a median map provides no information about real-world variability expected in a specific earthquake. Reflecting that variability can make a big difference in estimates of damage and loss, commonly increasing it over what one would estimate solely from the median. The reasons have to do with the skewed real-world distribution of shaking and with the upward-curving relation between shaking and damage at lower levels of shaking. It also has to do with spatial correlation in ground motion.

For the HayWired scenario, the 3D model deals with uncertainty by conditioning on one particular hypocenter, one realization of slip distribution, and one particular simulation of high-frequency motion using a semistochastic approach without averaging over many possible outcomes. The reader will see how using just one outcome actually does capture two important aspects of uncertainty. There are other ways to construct and use a ground-motion map for a hypothetical earthquake. This work does not address other uses, such as probabilistic seismic hazard analysis, probabilistic seismic risk analysis, or structural design, nor does it deal with assessing hazard in the sense of a probabilistic relation between ground motion and exceedance frequency. Rather, the HayWired scenario aims to provide a single outcome in terms of shaking, damage, and loss that nonetheless realistically depicts uncertainty and avoids a low bias in estimated outcomes. It is intended to explain to engineers, planners, and other non-Earth-scientist readers who may be more familiar with median maps why the 3D maps look different and why the HayWired scenario has used the 3D method rather than a median map.

Introduction—Two Valid Methods to Create a Ground-Motion Map

The HayWired scenario examines a hypothetical earthquake (mainshock) with a moment magnitude (M_w) of 7.0 occurring on April 18, 2018, at 4:18 p.m. on the Hayward Fault in the east bay part of California's San Francisco Bay area. The developers of the HayWired scenario have found that there are some unfamiliar features of three-dimensional (3D) numerical simulation that could alarm engineers and emergency managers who are familiar with a more frequently used approach.

This chapter is intended to inform engineers, emergency planners, and other consumers of earthquake-scenario ground-motion maps about the value and validity of 3D numerical simulation of ground motion for use in depicting realistic losses in a scenario earthquake. Bear in mind that a scenario (as the term is used here) depicts one realistic outcome of earthquake rupture, shaking, structural response, physical damage, and social and economic loss. It generally does not quantify and propagate uncertainties. In this way, a scenario differs from probabilistic seismic-hazard analysis or probabilistic seismic-risk analysis. As this work will show, a scenario developer still needs to account for some aspects of uncertainty, for at least two reasons—(1) to depict ground motion in a way that resembles maps of shaking in real earthquakes and (2) to minimize bias in the estimate of damage and loss.

[1]University of Colorado Boulder.

One way to create an earthquake-scenario ground-motion map is to use three-dimensional (3D) numerical simulations (as in Aagaard and others 2010a, b). This approach uses a computer model to simulate how seismic waves travel from a fault rupture through the Earth's crust and up through the surface soil to shake the base of buildings. It accounts for earthquake magnitude, the details of the rupture, the distance and path seismic waves must travel, the characteristics of the Earth's crust along that path, and the soil conditions near the surface of the Earth. Let us refer to this as the 3D method. The 3D method reflects spatial variability in ground motion, which is a real, observed effect in which some places shake much more strongly and others much more weakly than the average site at the same distance from a fault. A 3D model uses a mathematical model of the fault, the Earth's crust, and the soil near the surface of the Earth, along with laws of mechanics having to do with stress and strain, mass and acceleration, and the way waves behave to estimate earthquake shaking.

The technical reader may be curious about how the 3D model actually accounts for variability. Modelers use several approaches to address variability in ground motion conditioned on the fault segment that is assumed to rupture in an earthquake of a given magnitude. In the present case, Aagaard and others (2010a, b) produced stochastic (random) simulations of the fault-slip distribution and simulated ground motion for each of a few hypocentral locations along a fault. (Slip distribution can vary over the fault surface for a given segment and magnitude.) They simulated rupture speed and rise time, which are important parameters that affect ground motion and which vary for a given magnitude and location. The low-frequency content of ground motion (less than 1 hertz, Hz) at each grid point on a map is then a deterministic (that is, nonrandom) outcome of the simulated parameters and of the velocity model of the crust in the region. High-frequency motion is simulated using a semistochastic method proposed by Graves and Pitarka (2010) in which a source spectrum is assumed, white noise is filtered to match that spectrum with random phase, and simplified Green's functions are used to propagate the high-frequency motion from subfault segments to the ground surface at each grid point. The numerical simulation used in Aagaard and others (2010a, b) and adopted here does treat nonlinearity in site amplification; see Graves and Pitarka (2010) for details. The two processes produce a low- and a high-frequency time series at each grid point, which are then summed. The time series can then be analyzed to produce the various ground-motion parameters at each grid point—peak ground acceleration, spectral-acceleration response at any period and damping ratio of interest, and so on. Aagaard and others (2010a, b) simulated ground motion at each of 52,118 grid points spaced approximately 1.85 kilometers (km) apart.

Note that there is more than one approach to numerical simulation. The simulation used in HayWired uses a kinematic rather than dynamic calculation of the earthquake rupture. The time history of the rupture is not constrained to be physically self-consistent, so the simulation used here cannot be properly called completely physics-based. Let us henceforth refer to a map generated by 3D numerical simulation with semistochastic high-frequency motion, whether using a kinematic or dynamic rupture model, as a 3D numerical-simulation map.

Another way to create a ground-motion map is to use a mathematical model variously called an empirical ground-motion prediction equation (GMPE) or an attenuation relation. A GMPE is produced by fitting a smooth curve to ground-motion data observed in earthquakes of various magnitudes, rupture types, propagations distances, and site conditions. It accounts for magnitude, distance from a fault rupture to each site of interest, certain other features of a fault rupture and path from the rupture to the site, and the soil conditions near the surface of the Earth. It smooths out the variability by fitting a curve to past observations, typically to the natural logarithm of observed motion. Developers of GMPEs also commonly offer estimates of variability in the form of the standard deviation of the natural logarithm of the residual, usually in two parts—inter-event and intra-event variability. See for example, Abrahamson and others (2014) for a recent example of the Next Generation Attenuation Relationships for Western United States (NGA-West2) GMPEs. That uncertainty can be easy to overlook. Most scenario ground-motion maps (that is, ground-motion maps for hypothetical earthquakes) only show the median shaking. Let us refer to a map of median ground motion as a median map. Variability data are often available in addition to the median map but in a less-accessible form. For example, the U.S. Geological Survey (USGS) provides a raw grid-data download file for the M_w 7.7 1999 Chi-Chi, Taiwan, earthquake. The file contains comma-separated-values (.csv) data of estimated ground motion at 5,900 grid points. Each line in the text file contains latitude, longitude, various measures of estimated ground motion—including peak ground acceleration (PGA), peak ground velocity (PGV), Modified Mercalli Intensity (MMI)— and two measures of uncertainty—the standard deviation of PGA and the standard deviation of PGV. The uncertainty information is not presented graphically. There is no map that quantifies uncertainty in the same units as the median map, so it is less accessible than the median map. For brevity, let us refer to a scenario loss estimate that assumes shaking uniformly takes on its median ground value as estimated by ground-motion prediction equations as the median method.

The median of any variable, whether it is an estimate of the ground motion at a site or some other variable, such as the household income of an arbitrary household in the United States, measures central tendency. It refers to the value that has a 50-percent chance of being exceeded—half of the observations are above it, half below.

In this chapter, let us compare the use of a 3D numerical-simulation map with a median map generated by ground-motion prediction equations, focusing on their use in scenario loss estimation, and in particular their treatment of variability. The median by definition provides no information about variability—for example, the median map does not tell one how much higher the ground motion is with 90-percent nonexceedance probability or how much lower is the 10th percentile of motion. Average is another measure of central tendency, distinct from the median. In the case of earthquake motion, the median is generally lower than the average. Like the median, the average by definition contains no information about variability.

In the case of ground motion shown on a median map, the quantity shown at any arbitrary location is the value that has 50-percent probability of being exceeded, given an earthquake's magnitude, distance, site conditions, and various attributes of the fault rupture and direction from the rupture to the site. The quantity shown at the same location on a 3D map is not a fixed percentile—it could be near the median or it could be lower or higher, according to the probability distribution of ground motion at that site. That probability distribution is more constrained—it tends to be narrower—than if one used a GMPE. It is constrained by the additional information that a 3D simulation entails but that a GMPE does not—slip distribution, hypocenter, and other fault-rupture propagation features, along with the mechanical properties of the Earth's crust and soil along the path between rupture and the ground surface.

In a scenario, it is not particularly important to show the ground motion with a specified percentile of exceedance. A 3D map shows variability in ground motion—in some places motion is higher than the median; in others, near the median; and in still others, lower than the median. As a result, the 3D map looks blotchy, irregular, and asymmetric. Contours on median maps tend to look like concentric hot dogs aligned around a fault rupture, as shown in figure 1*A*. Contours in ground-motion maps that use 3D models tend to be more irregularly shaped, as shown in figure 1*B*, and more closely resemble observations in real earthquakes.

Both 3D and median approaches to creating earthquake-scenario maps are valid and well respected among Earth scientists. ShakeMaps (the USGS product) are intended for "post-earthquake response and recovery, public and scientific information, as well as for preparedness exercises and disaster planning," (U.S. Geological Survey, 2015). The developers of 3D maps offer them for use "in estimating the seismic hazard and the ground motions they can generate," as Aagaard and others (2010) explain in their introduction. In short, both approaches can and have been used to inform emergency preparedness. Each has advantages and disadvantages. Three-dimensional models account for knowledge of a fault's characteristics and the local geology but are computationally very demanding and have difficulty modeling high-frequency motion (the part of the earthquake motion that resonates with shorter buildings) with the same rigor as low-frequency motion (the part of the earthquake motion that resonates with taller buildings).

The median approach is based on past observations. In a sense, it considers the physics of the seismic setting, partitioning data by focal mechanism (for example, strike-slip, normal, reverse, and unspecified) and presetting some parameters such as site and anelastic coefficients, but the GMPEs on which the median approach is based are essentially regression analyses of past observations, albeit with modest constraints. The reader might assume that the closer resemblance of a 3D map to real earthquakes results from the use of site-specific averaged shear-wave velocity to a depth of 30 meters, V_{S30}, alone, which median maps can (and do) also consider. However, recall that the hypocentral location, heterogeneous slip distribution, rise time, rupture speed, and crustal velocity model that are crucial to the 3D model have nothing to do with V_{S30}, are not parameters of GMPEs, and therefore are not reflected in median maps created using GMPEs.

Skewness in Ground-Motion Intensity

Frequent users of ground-motion maps may be surprised by the difference between the outputs of the two methods. The difference is largely the result of how the 3D model reveals spatial variability, whereas the median maps do not. Maps of shaking in real earthquakes tend to look more like the 3D model. It is largely for that reason that the HayWired and ShakeOut scenarios use the 3D model (see Jones and others, 2008, for more information on the ShakeOut scenario).

There is a subtler but equally important reason for using a 3D ground-motion map for a disaster scenario—it will tend to produce estimates of damage and loss that are more realistic and higher in aggregate than if one only considers median shaking. This occurs for two reasons. First, as previously noted the average shaking tends to be higher than the median shaking. This is because the observed distribution of shaking tends to be skewed toward higher values (like a lognormal distribution) compared to the symmetric

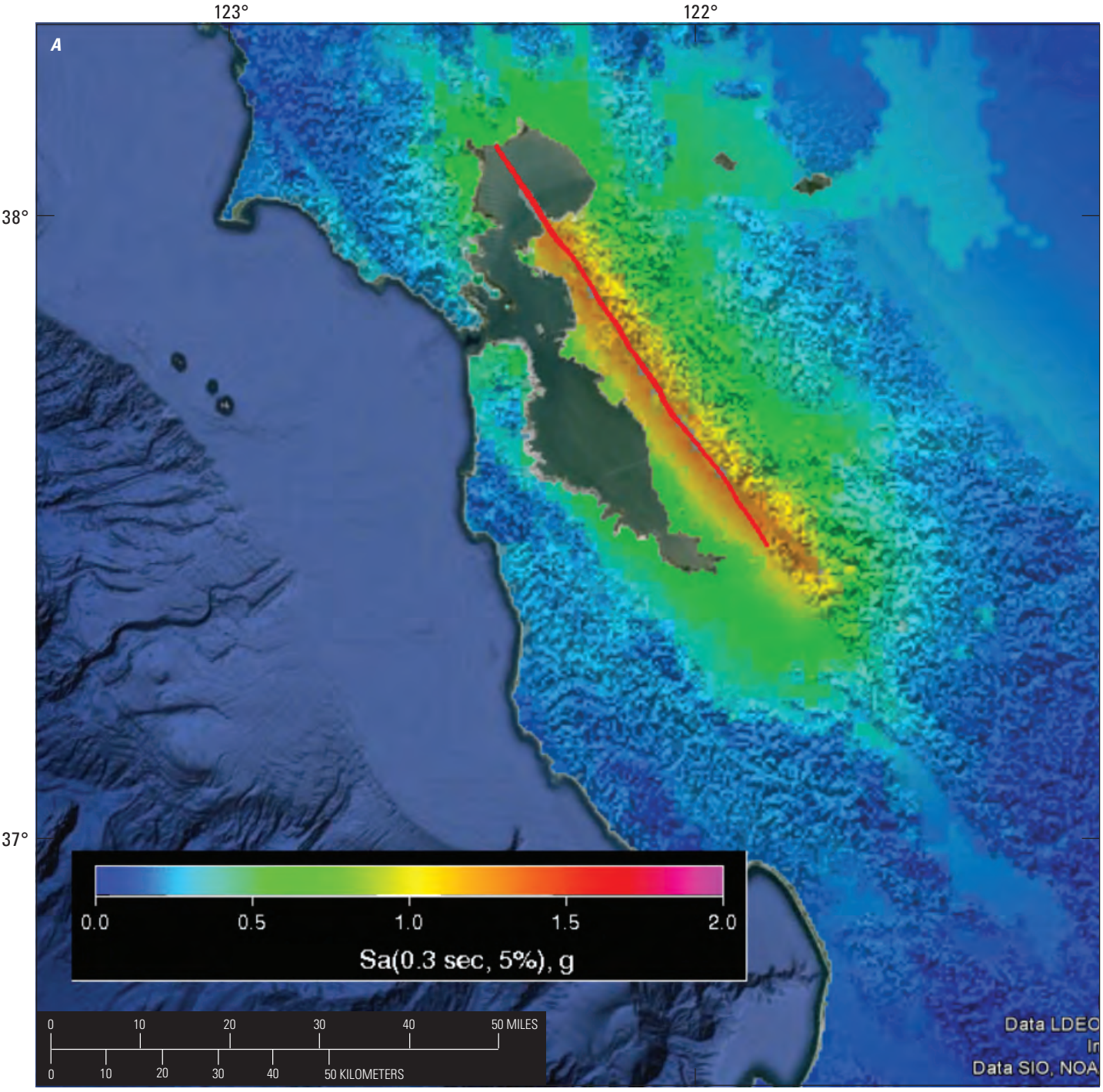

Base map from Google Earth; image Landsat/Copernicus; data LDEO-Columbia, NSF, NOAA; data SIO, NOAA, U.S., Navy, NGA, GEBCO, 2015.

Figure 1. Comparison of ground-motion maps of the San Francisco Bay region, California, for a hypothetical moment magnitude (M_w) 7.0 Hayward Fault earthquake, like that in the HayWired earthquake scenario, produced using different approaches. *A*, ground-motion map of median 0.3-second, 5-percent damped elastic spectral-acceleration response calculated using ground-motion prediction equations. *B*, ground-motion map of median 0.3-second, 5-percent damped elastic spectral-acceleration response created using a three-dimensional ground-motion simulation. Red line, HayWard Fault rupture; Sa, spectral acceleration; sec, second; %, percent; g, acceleration due to gravity. [*A* was calculated by Open Source Seismic Hazard Analysis (OpenSHA, http://www.opensha.org) Scenario ShakeMap calculator version 1.3.1, using the Uniform California Earthquake Rupture Forecast, version 3 (UCERF3, http://www.wgcep.org/ucerf3), Hayward-all rupture index 0; NGAWest2 2014 averaged attenuation relation; 50-percent exceedance probability; average horizontal motion; and the Wills and Clahan, 2006, time-averaged shear-wave velocity to a depth of 30 meters, V_{S30}, model.] Ground-motion images created by Keith A. Porter, University of Colorado Boulder.)

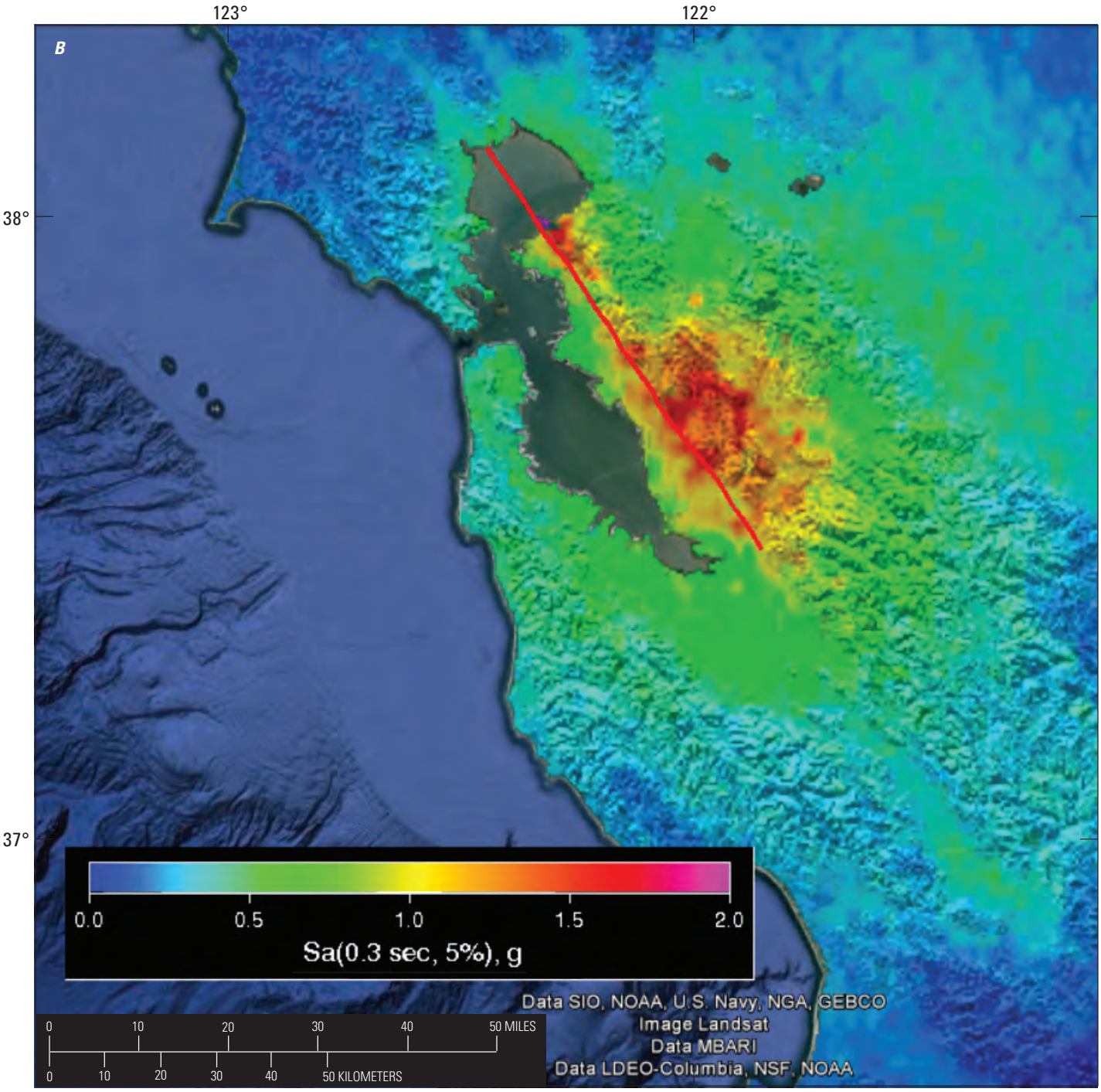

Base map from Google Earth; data SIO, NOAA, U.S., Navy, NGA, GEBCO; image Landsat; data MBARI; data LDEO-Columbia, NSF, NOAA, 2015.

Figure 1.—Continued

bell-shaped curve (called the normal distribution). That means that the probability of high shaking intensity is higher in the skewed distribution and that the probability of low shaking is smaller (fig. 2).

Nonlinearity in Damage Aggravates the Damage Estimate

The second reason that 3D maps yield higher and more realistic loss estimates is that the skewed distribution of shaking is compounded with another common feature of damageability called nonlinear fragility. Together, the skewed distribution and nonlinear fragility aggravate damage above what one would expect based solely on median shaking. By "nonlinear fragility" I mean that failure probability increases nonlinearly with shaking intensity—the failure probability curves upward when plotted against shaking intensity. Figure 3 illustrates this point, for example, where a 50-percent increase in shaking intensity results in a four-fold increase in failure probability.) Of course, there are more-fragile buildings and less-fragile buildings—this is not meant to imply that shaking is all that matters to damage—but aside from the degree of fragility, most buildings and components are modeled as having a fragility function that resembles figure 3, with its attendant nonlinearity.

Spatial Correlation

Spatial correlation in ground motion may further aggravate the damage where development is concentrated in areas of more intense shaking. Spatial correlation in ground motion means that two nearby sites tend to experience similar shaking, which means that if a building experiences shaking that is somewhat higher than average, so will a nearby building. On average, both can be expected to experience greater damage than if they both experienced average shaking, so the sum of the damage to the two buildings can be expected to be greater than if they both experienced average shaking. Similarly, if one building

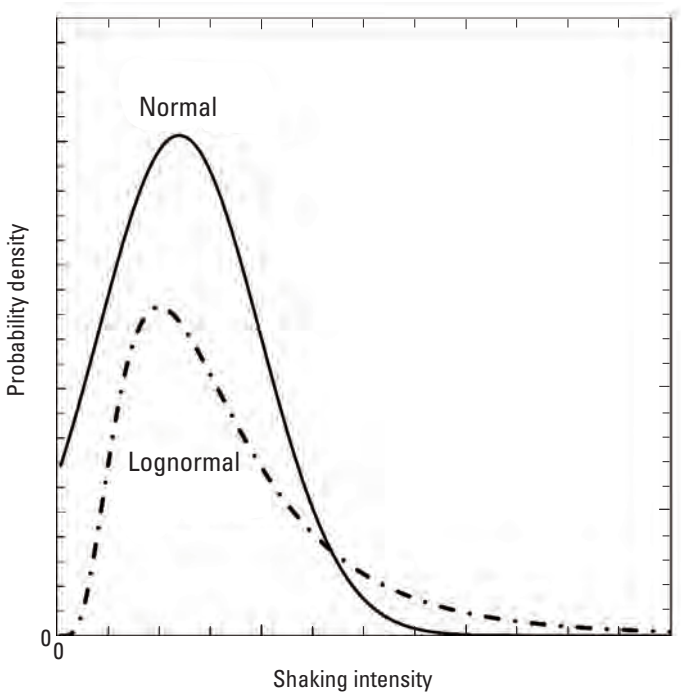

Figure 2. Graph of probability density versus earthquake-shaking intensity showing an example of normal and lognormal distributions. Both curves have the same average and standard deviation, with a ratio of standard deviation to average (the ratio is called the coefficient of variation) that is characteristic of ground-motion prediction equations. Notice how the normal distribution is symmetrical—it looks the same on the left side as on the right—but the lognormal is skewed to the right. The height of each curve measures how likely it is to produce a given shaking intensity value. Note that shaking intensity has a lower limit of zero, so the figure truncates the normal distribution below at zero, otherwise its symmetry would be even more obvious.

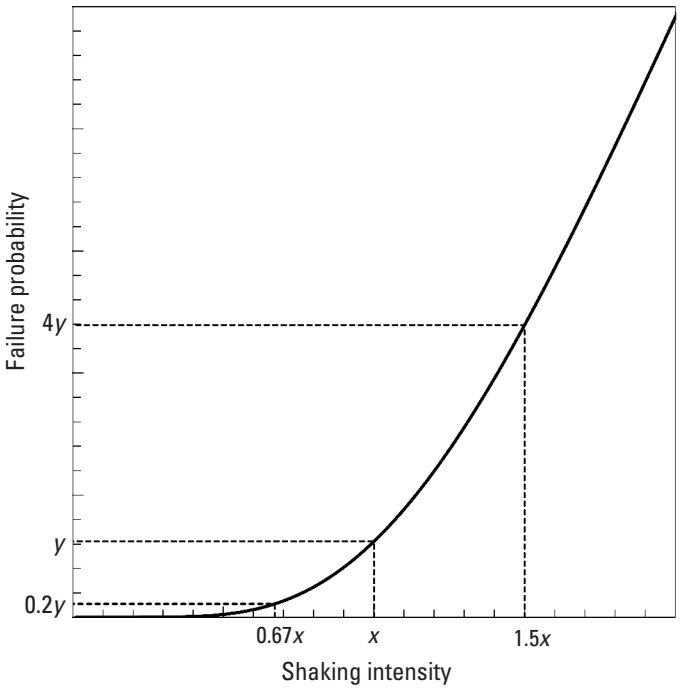

FIgure 3. Graph showing that fragility functions commonly curve upward at lower values of earthquake-shaking intensity. As a result, a little higher shaking can produce a much higher failure probability, compared with how a little lower shaking reduces a somewhat lower failure probability. The lower and higher values of shaking intensity, 0.67*x* and 1.5*x*, are about equally likely if the median shaking is *x*, which means the failure probabilities of 0.2*y* and 4*y* are equally likely, and the average or expected failure probability will tend to be higher than *y*.

experiences shaking that is somewhat lower than average, so will the other building, and both can be expected to experience lower damage (individually and in total) than if both had experienced average shaking. The closer together the two buildings are, the more similar their ground motion, and the more likely that both will experience higher than average shaking and damage or lower than average shaking and damage.

Suppose by contrast there were no spatial correlation in shaking (that is, conditioned on the median and logarithmic standard deviation of shaking at two buildings); suppose the damage at one building were independent of damage at another. If one building experienced higher shaking than average, the other could experience average shaking, higher than average shaking, or lower than average shaking. On average, with a large number of buildings, there would be as many buildings experiencing higher than average shaking and damage as buildings experiencing lower than average shaking and damage. The differences from average tend to cancel out as the number of buildings increases. This general phenomenon is called the law of large numbers. In the absence of spatially correlated ground motion, the law of large numbers guarantees that the more buildings there are, the closer and closer to average will be the total damage. However, because spatial correlation does exist, the law of large numbers does not hold. As a consequence, even with large numbers of buildings, the uncertainty in the aggregate loss does not vanish. The greater the spatial correlation, the less the aggregate loss will tend to approach the average.

Spatial correlation reaches tens of kilometers in real earthquakes, so buildings in an area larger than the City of San Francisco can all experience above-average shaking in the same earthquake. Because of spatial correlation, a community can expect to either "win" big (if one can be said to win at all in a powerful earthquake), with generally lower than expected ground motion throughout the community, or "lose" big, with generally higher than expected motion throughout the community.

Extreme Values in 3D Modeling

Three-dimensional models in general and the HayWired ground-motion map in particular can exhibit features that differ significantly from median maps. Long-period (1-second) pseudo-spectral-acceleration response (denoted PSA10 here) can exceed short-period (0.3-second) pseudo-spectral-acceleration response (denoted PSA03 here), which is contrary to what is typically observed in earthquakes. PSA10 is commonly about 40 percent as strong as PSA03, but it is possible for PSA10 to be greater than PSA03. This is a real, observable phenomenon. For example, in the 1994 Northridge, California, earthquake, that happened at 13 of the 180 ground-motion recording stations listed in a USGS ground-motion data archive for the earthquake (U.S. Geological Survey, 2009a). In the 1989 Loma Prieta, California, earthquake, it happened at 20 of the 84 stations listed at that event's ShakeMap archive (U.S. Geological Survey, 2009b). Sometimes the ratio PSA10 to PSA03 can greatly exceed 1.0. In two of the stations in the Northridge earthquake, stations LPU and PAR, the ratio reached 1.8:1, and in one station in the Loma Prieta earthquake, station A02, the ratio reached 3:1.

In the August 24, 2014, South Napa, California, earthquake (U.S. Geological Survey, 2014), station NP.1765 component HNE recorded PSA10=1.02 of the acceleration due to gravity (*g*) and PSA03=0.58 *g*, a ratio of 1.8:1. This appears to have been the highest recorded value of PSA10 of all the stations in the epicentral region. Its component HNN similarly recorded PSA10=0.99 *g* and PSA03=0.61 *g*, a ratio of 1.6:1. (Other stations in the epicentral region recorded more familiar-looking ratios; for example, the station that recorded the highest value of PSA03, station NC.N019B component 01.HNE, recorded PSA10=0.57 *g* and PSA03=1.17 *g*, a ratio of 0.49:1. The next-highest PSA03 value in the epicentral region, recorded by NC.HNC component HNN, was PSA03=1.08 *g* and PSA10=0.35 *g*, a ratio of 0.32:1. However, the point is that, although it less typical for PSA10>PSA03, it is still not very rare.)

Some of these effects may be due to a long-period pulse or another explainable phenomenon. In fact, it is likely that none of the observed motion is truly inherently random if one could know and model the focal location and mechanism, slip distribution, rupture velocity, rise time, crustal-velocity structure, surficial geology, and other physical quantities of the fault rupture and the region. That is the point of the numerical ground-motion simulation—to explicitly model and to provide insight into these issues rather than to treat them as hidden variables outside the frame of a model that uses GMPEs and treats these effects with catch-all residual variability parameters.

In addition to high ratios of PSA10 to PSA03, the absolute amplitudes of PSA10 and PSA03 can sometimes be very high, both in 3D simulations and in real earthquakes. In the HayWired 3D map, one location is estimated to experience PSA10=4.1 *g*. This is very unusual but not impossible. The site in HayWired has very soft soil, characterized by a 180 meter per second (m/s) average shear-wave velocity in the top 30 meters (m) of soil (denoted by V_{S30}). Two stations in the September 20, 1999, moment magnitude (M_w) 7.6 Chi-Chi, Taiwan, earthquake, CHY080 and TCU084, experienced 5-percent damped PSA response near 1.0-second (s) period of 4.0 *g* and 3.7 *g*, respectively, both on V_{S30}=665 m/s soil, according to Pacific Earthquake Engineering Research Center (2015). (At exactly 1.0-s period, their 5-percent damped pseudo spectral acceleration response values were 2.94 *g* and 2.70 *g*, respectively.)

It is informative to estimate what would have been the ground motion at these stations had they been on V_{S30} =180 m/s soil, as at the HayWired site just mentioned. A national standard design document used by engineers in the United States, ASCE 7-10 (American Society of Civil Engineers, 2010), offers a model to estimate the amplification. It offers a parameter called "site coefficient F_v," which relates 1-second spectral acceleration response shaking on soil with one value of V_{S30} to shaking on soil with a different value of V_{S30}. F_v varies nonlinearly with shaking but saturates at high levels of shaking—meaning that above a specified level of shaking

(PSA10≥0.65 *g* in the case of V_{S30}=600 m/s), F_v does not change. The data on which that model is based are entirely from lower levels of shaking, so to use F_v at the PSA10 values under consideration here requires one to assume that the model also applies at much higher levels of shaking. Let us assume for the moment that one can use that model (there being no apparently viable alternative). Using that model, the ASCE 7-10 model says that one would expect the softer soil to have experienced greater amplification that would have increased the motion on a site with V_{S30}=180 m/s between 15 and 85 percent compared with a site with V_{S30}=600 m/s. (The reason for the range is that ASCE 7-10 offers one amplification value for soil with 180≤V_{S30}≤360 m/s and another for soil with V_{S30}≤180 m/s, so the HayWired site of interest is on the boundary.) Taking the average of the two suggests an expected value of amplification of about 50 percent compared with 600 m/s. That suggests that had the two instruments been on soil with V_{S30}=180 m/s, an engineer using ASCE 7-10 would estimate that the peaks of the response spectra of CHY080 and TCU084 near 1.0-s period would have been 6.0 *g* and 4.4 *g*, respectively. At exactly 1.0 s, one would estimate spectral acceleration response value of 4.4 *g* and 4.0 *g*, respectively. The point is that, with a caveat arising from extrapolating F_v, the estimate of PSA10=4.1 *g* from 3D numerical simulation is consistent with two Chi-Chi earthquake records of 4 *g* and 3.7 *g* near 1.0-s period, which were recorded on stiffer soil.

Graves (written commun., July 24, 2015) offers another caveat for the HayWired ground motion map. He warns "that the value simulated in the 3D calculation is based on a very simple model for non-linear soil response, which is not well calibrated for soft soil sites at such large motions."

Close to the rupture, the South Napa earthquake produced short-period (0.3-s) spectral-acceleration response values that were much higher than the median calculated value. Farther away, motions were much lower than the median (calculated using the average of the four 2008 next-generation attenuation relations). Figure4*A* shows that some locations close to the rupture approached or reached life-safety design-level shaking for ordinary low-rise buildings (S_{DS} in the language of ASCE 7-10, which defines minimum design loads for buildings and other structures; American Society of Civil Engineers, 2010). Figure4*B* shows that within 20 km of the fault, observed 0.3-s motions were on average 1.25 to 2.25 higher than the median, and in some locations observed 0.3-s motions were as high as 5 times the median calculated value for an earthquake of this magnitude at the given distance. Farther from the fault, motions were below half the median. According to one seismologist who examined the USGS's "Did You Feel It" data, the South Napa records were not very unusual (Susan Hough, USGS, written commun., September 28, 2014). Thus, the South Napa earthquake highlights that it is not very unusual for some locations in an earthquake to experience shaking much higher than the median (fig. 4). All this is to show that real, not-very-unusual earthquakes can produce shaking more like 3D simulations than like ShakeMap medians.

These effects—high PSA10 and high ratios of PSA10 to PSA03—are unusual but as shown in figure 5 not improbable. They can be caused by constructive interference. For example, when waves from one part of the fault rupture far from the site arrive at the site and waves generated by a closer part of the rupture reach the same site at the same time. The two waves add, increasing the amplitude of ground motion at the site.

Very strong motion can also be caused by basin effects, where seismic waves traveling at high velocity through the rock of the Earth's crust refract and slow when entering a basin of soft, sedimentary soil. This increases the amplitude of the waves in the same way that water waves slow and grow to great height when they reach the shore. Furthermore, the abrupt change in density between the rock and basin soil at the basin boundary can cause seismic waves to reflect, trapping energy in the basin for a longer time and extending the duration of shaking.

The reader should also consider the nature of extreme values in large samples. Even if we do see one or two records with very strong motion, the records are very rare, which might seem to suggest that the strong motions observed in the ground-motion map are very unlikely. However, this is not necessarily the case. In any given earthquake, the records available to us number at most in the low hundreds. Close to a fault the number is even lower—the Pacific Earthquake Engineering Research Center (PEER) ground-motion database contains observed ground-motion records from only 59 stations in 8 earthquakes of *M*7 or greater and distance less than 10 km (Pacific Earthquake Engineering Research Center, 2015). By contrast, the HayWired ground-motion map contains simulated ground-motion records at 52,000 locations centered about the 83-km-long rupture and spaced every 1.8 km. That means that from this single scenario earthquake alone, the numerical ground-motion simulation provides 103×20/(1.8×1.8)=635 simulated ground-motion records within 10 km of the fault, more than 10 times the available observations from all stations within 10 km of a fault in all earthquakes of magnitude 7 or greater in the PEER database. In any population of uncertain quantities, the fewer samples or specimens one observes, the smaller the maximum value is likely to be, so it should not be surprising that the maximum ground motion in the PEER database is smaller than the maximum ground motion in the HayWired 3D ground-motion map.

More real, observed ground-motion records would be welcomed, but it is more important to note that the extreme values in the existing database of real observations will tend to give a false impression of the maximum shaking that an earthquake of *M*7 can produce. That false impression is a necessary outcome of the size of the existing database. That there is no real physical limit on the upper bound of ground motion is also a necessary outcome of the size of the existing database. However, with only 59 recordings, there is no guarantee that the maximum observed motion in the PEER database is the maximum that is physically possible; most likely the contrary is true.

Here is an analogy to illustrate the problem of judging extreme values from a limited data set. Pick 10 U.S. residents at random. Chances are the oldest will be about 72 years old. Pick 100 U.S. residents, and the oldest will be about 86 years old. Among 6,000 U.S. residents, one would find someone 100 years old. Among 6 million people one would find someone 110 years old. The same basic principle applies here—having

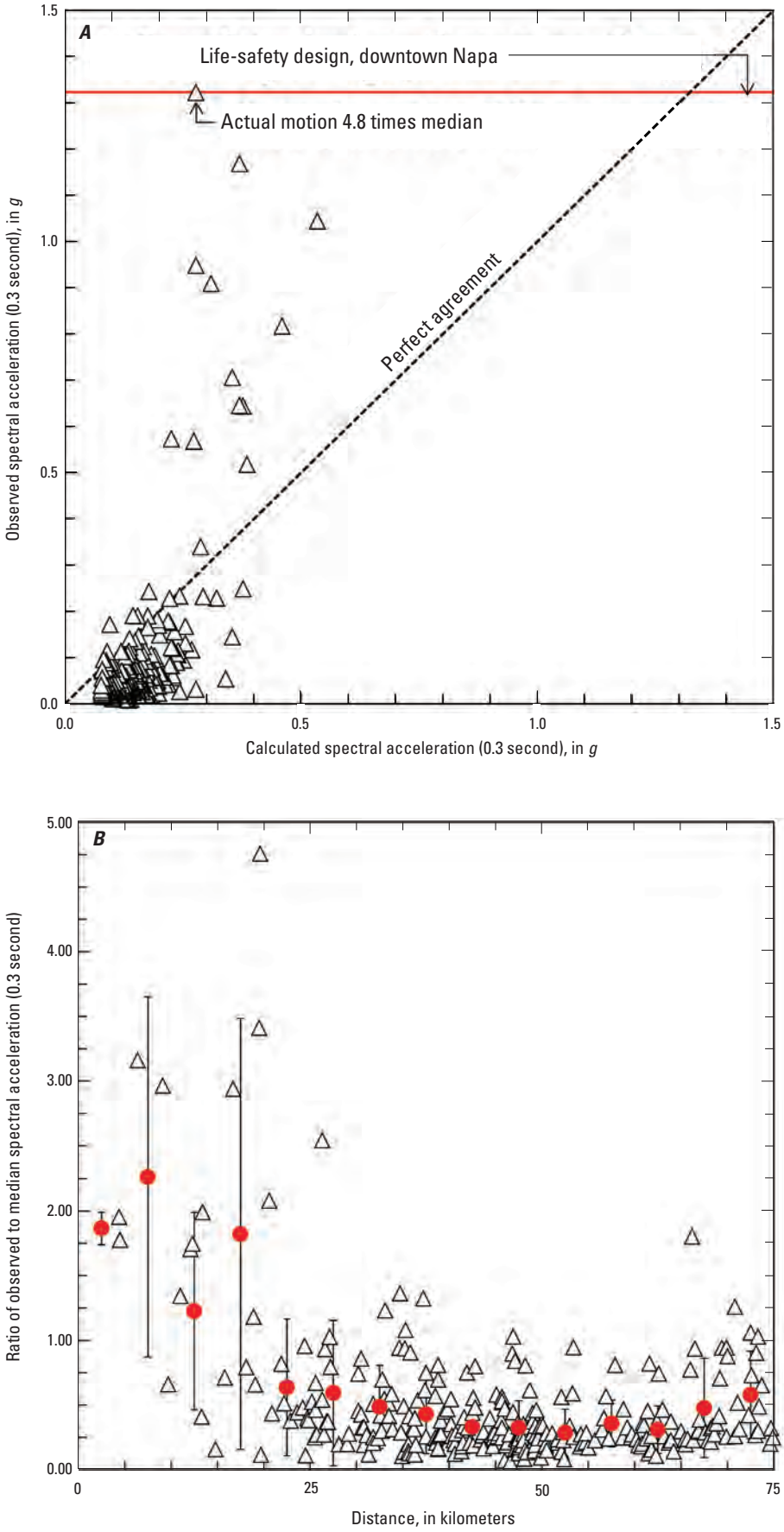

Figure 4. Graphs showing observed and calculated short-period (0.3-second) spectral-acceleration response (the part of the earthquake motion that a low-rise building would experience) in the August 2014 South Napa, California, earthquake. Triangles are observations of shaking at 315 strong-motion instruments. *A*, Observed motions were much higher than median where it matters most, close to the epicenter. Triangles above the diagonal line are higher than would be calculated. Some motions reached design-level shaking of 1.3 of the acceleration due to gravity (*g*), where the median, maximum-component calculated motion would have been 0.28 *g*. *B*, The ratio of observed to median motions plotted against distance from the rupture. Motions within 20 kilometers (km) of the epicenter were 1.25 to 2.25 times higher than the median calculated value and in some cases 3 to 5 times higher. Red dots and error bars show averages and ±1 standard deviations in 5-km distance bins. [Calculations use observations at 315 strong-motion instruments within 80 km of the fault rupture as reported by the Center for Engineering Strong Motion Data (2014), site soil information for instrument locations from the California Geological Survey (Wills and Clahan, 2006; averaged shear-wave velocity to a depth of 30 meters in American Society of Civil Engineers, 2010), and the equally weighted average of the four 2008 next-generation attenuation relations (Stewart and others, 2008; calculations were performed before the release of the 2014 relations (Bozorgnia and others, 2014)].

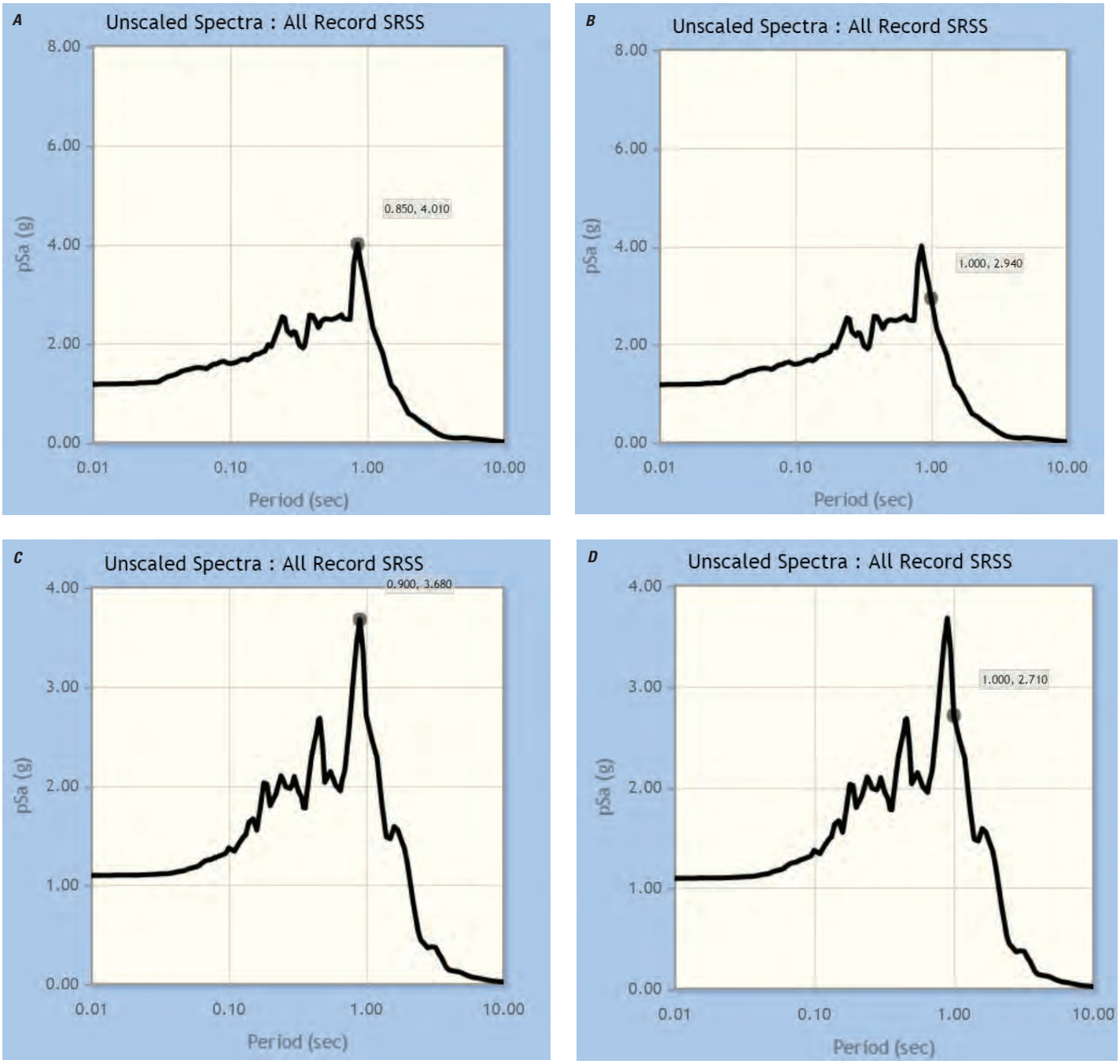

Figure 5. Graphs showing pseudo spectral acceleration (pSa) response of stations CHY080 (*A* and *B*) and TCU084 (*C* and *D*) in the 1999 Chi Chi, Taiwan, earthquake. SRSS, square root of the sum of the squares; g, acceleration due to gravity; sec, second. (From Pacific Earthquake Engineering Research Center, 2015; used with permission.)

values at each grid point in the HayWired scenario is like having a list of everybody's age in the United States. Lacking the values at each grid point is like having the ages of only 59 people. Even if the HayWired 3D ground-motion map exactly matched some past earthquake of the exact same magnitude, the maximum value on the map would almost certainly exceed the maximum we have observed by a strong-motion instrument in the same size earthquake because the number of observations by strong-motion instruments is so much smaller than the number of grid points. Comparing the maximum shaking from strong-motion instruments and the maximum shaking from a gridded 3D ground-motion map like that for the HayWired scenario is like comparing the maximum age from a sample of 100 people and the maximum age from a sample of 6,000. The maximum from the latter will generally be higher than that of the former, so if one assumes that what we have seen from strong-motion instruments is some sort of natural upper bound, one is likely to underestimate what shaking is possible. Also because the distribution of ground motion (as measured here in terms of PSA03 or PSA10) does not have an accepted, well-known upper limit (unlike human age), the maximum shaking that actually occurs (or appears on a gridded map with thousands or tens of thousands of points) is likely to be larger than the maximum observed from available strong-motion instruments.

In short, one would expect the highest values of ground motion in the HayWired 3D ground-motion map to be larger than the maximum values observed by strong-motion instruments in past earthquakes, just because we have so few actual records of strong motion near the fault in large earthquakes compared with the number of grid points in the 3D simulation.

Uncertainties

As previously noted, the HayWired scenario is not intended as a probabilistic seismic risk analysis. It depicts a single outcome of fault rupture, ground motion, and other parameters, so that emergency planners and others can more clearly see how one earthquake might turn out. Planning for that one event helps people to better prepare for the earthquake that will actually happen, but that will certainly happen differently. Why then worry about uncertainty at all? Which uncertainties should be quantified and how should they be propagated? The 3D numerical-simulation approach can capture uncertainty in fault rupture location, hypocenter, slip distribution, high-frequency motion, and other parameters. By selecting and depicting only one outcome, HayWired ignores how the ground-motion map would differ if the particular fault segments that rupture or the hypocenter, magnitude, slip distribution, or other factors were different. (Note that Aagaard and others (2010a, b), offer 39 scenarios that vary these and other parameters; HayWired uses only one for its mainshock.)

Despite that these uncertainties are ignored, I feel that the ground motion in a 3D numerical simulation map, such as that used for the HayWired scenario, more closely resembles that in a real earthquake. Contours of shaking are blotchy, asymmetrical, irregular, with locations that experience motion that is much higher than the median, near the median, and lower than the median. Its asymmetry serves an educational purpose by showing people what real maps of shaking actually look like. It also tends to reduce the bias in the damage and loss estimate that would otherwise result from the combination of nonlinear fragility or vulnerability relationships with median shaking values from a GMPE.

Make no mistake, 3D numerical simulation offers these two advantages in scenario development, relative to a median map from GMPEs. That is not to say that 3D numerical simulation is preferable in other situations. It is still fairly computationally costly, requires crustal velocity information that has not been compiled for much of the world, and lacks the built-in empirical validation that GMPEs offer.

Conclusion

Most scenario ground-motion maps depict median shaking; that is, the shaking with 50-percent exceedance probability. They are created using empirical ground-motion-prediction equations, which themselves (oversimplifying somewhat) are created by fitting smooth curves to median values of historical shaking data. Maps of median motion do not depict variability in ground motion; it is the very definition of a median that it only depicts a central value and provides no information about variability. Median maps do not resemble real earthquakes in which motion varies greatly about the median, as a consequence of natural geological heterogeneity in fault rupture and in the surrounding crust. More importantly for the purposes of the HayWired scenario, such a median map would have resulted in an underestimate of average shaking and aggregate damage (as illustrated by fig. 3). In contrast, the 3D model actually used in HayWired estimates greater damages than the median model because the distribution of shaking intensity is skewed. Above-median shaking causes disproportionately more damage than below-median shaking takes away. (GMPEs also use lognormal distributions, but the point is that a median map does not reflect a GMPE's distribution, only its median value.) The differences between the two models will be exacerbated where concentrations of manmade structures and development are exposed to the most intense shaking according to the 3D model. An emergency-planning scenario that uses only median shaking will tend to leave a community underprepared. For this reason, the USGS has opted to use a 3D numerical ground-motion simulation map for the mainshock of the HayWired scenario. (HayWired uses median maps for aftershocks out of necessity.) Three-dimensional modeling is more costly and computationally demanding than median maps but more realistically depicts real-world variability in ground motion and helps to avoid underestimation of average ground motion and aggregate damage. There are some very high values of shaking in the HayWired scenario, but they are to be expected and are consistent both with past observations of maximum shaking in the 1999 M_w 7.6 Chi-Chi, Taiwan, earthquake and with extreme-value theory when trying to draw conclusions about large populations from small datasets.

References Cited

Aagaard, B.T., Graves, R.W., Schwartz, D.P., Ponce, D.A., and Graymer, R.W., 2010a, Ground-motion modeling of Hayward Fault scenario earthquakes, part I—Construction of the suite of scenarios: Bulletin of the Seismological Society of America, v. 100, no. 6, p. 2927–2944.

Aagaard, B.T., Graves, R.W., Rodgers, A., Brocher, T.M., Simpson, R.W., Dreger, D., Petersson, N.A., Larsen, S.C., Ma, S., and Jachens, R.C., 2010b, Ground-motion modeling of Hayward Fault scenario earthquakes, part II—Simulation of long-period and broadband ground motions: Bulletin of the Seismological Society of America, v. 100, no. 6, p. 2945–2977.

Abrahamson, N.A., Silva, W.J., and Kamai, R., 2014, Summary of the ASK14 ground motion relation for active crustal regions: Earthquake Spectra, v. 30, no. 3, p. 1025–1055

American Society of Civil Engineers, 2010, Minimum Design Loads for Buildings and Other Structures: Reston, Va., American Society of Civil Engineers, ASCE/SEI 7–10, 608 p.

Bozorgnia, Y., Abrahamson, N.A., Al Atik, L., Ancheta, T.D., Atkinson, G.M., Baker, J.W., Baltay, A., Boore, D.M., Campbell, K.W., Chiou, B.S.-J., and Darragh, R., 2014, NGA-West2 research project: Earthquake Spectra, v. 30, no. 3, p. 973–987.

Center for Engineering Strong Motion Data, 2014, CESMD Internet Data Report for South Napa Earthquake of 24 Aug 2014: Center for Engineering Strong Motion Data website, accessed July 3, 2015, at https://www.strongmotioncenter.org/cgi-bin/CESMD/iqr_dist_DM2.pl?IQRID=SouthNapa_24Aug2014_72282711&SFlag=0&Flag=2.

Graves, R.W., and Pitarka, A., 2010, Broadband time history simulation using a hybrid approach: Bulletin of the Seismological Society of America, v. 100, no. 5A, p. 2095–2123.

Jones, L.M., Bernknopf, R., Cox, D., Goltz, J., Hudnut, K., Mileti, D., Perry, S., Ponti, D., Porter, K., Reichle, M., Seligson, H., Shoaf, K., Treiman, J., and Wein, A.M., 2008, The ShakeOut scenario: U.S. Geological Survey Open-File Report 2008–1150/California Geological Survey Preliminary Report 25, accessed July 3, 2015, https://pubs.usgs.gov/of/2008/1150/.

Pacific Earthquake Engineering Research Center, 2015, PEER Ground Motion Database NGA-West2: Berkeley, Calif., Pacific Earthquake Engineering Research Center accessed July 3, 2015, at http://ngawest2.berkeley.edu/.

Stewart, J.P., Archuleta, R.J., and Power, M.S., 2008, Preface: Earthquake Spectra, v. 24, no. 1, p. 1–2.

U.S. Geological Survey, 2009a, USGS ShakeMap—Northridge, California: U.S. Geological Survey website, accessed March 24, 2017, at https://earthquake.usgs.gov/earthquakes/eventpage/ci3144585#shakemap.

U.S. Geological Survey, 2009b, CISN ShakeMap for the Loma Prieta earthquake: U.S. Geological Survey website, accessed March 24, 2017, at https://earthquake.usgs.gov/earthquakes/eventpage/nc216859#shakemap.

U.S. Geological Survey, 2014, CISN ShakeMap for the South Napa earthquake: U.S. Geological Survey website, accessed November 24, 2015, at https://earthquake.usgs.gov/earthquakes/eventpage/nc72282711#shakemap.

U.S. Geological Survey, 2015, ShakeMaps: U.S. Geological Survey website, accessed June 19, 2015, at https://earthquake.usgs.gov/earthquakes/shakemap/.

Wills, C.J. and Clahan, K.B., 2006, Developing a map of geologically defined site-conditions categories for California: Bulletin of the Seismological Society of America, v. 96, no. 4A, p. 1483–1501.

Menlo Park Publishing Service Center, California
Manuscript approval date April 14, 2017
Edited by James W. Hendley II
Design and layout by Cory Hurd

ISSN 2328-0328 (online)
https://doi.org/10.3133/sir20175013v1